

**APPENDIX M**

**ALTERNATIVE MODEL DOCUMENTATION**

Rusk-Panola Attainment Demonstration State  
Implementation Plan for the 2010 Sulfur Dioxide  
National Ambient Air Quality Standard

Project Number 2020-057-SIP-NR  
SFR-122/2020-057-SIP-NR

*This page intentionally left blank*

**APPENDIX M-1: LETTER TO THE UNITED STATES ENVIRONMENTAL PROTECTION AGENCY**

Appendix M-1 includes a letter from Texas Commission on Environmental Quality (TCEQ) to the United States Environmental Protection Agency (EPA) requesting the use of the alternate model American Meteorological Society/EPA Regulatory Model - Highly Buoyant Plume (AERMOD-HBP). The letter and two attachments, Attachment 1: *AERMOD-HBP Formulation Documents from AECOM* and Attachment 2: *Modeling Protocol for Alternative Model Approval Demonstration for the Rusk-Panola Attainment Demonstration State Implementation Plan Revision for the 2010 Sulfur Dioxide (SO<sub>2</sub>) National Ambient Air Quality Standard*, was emailed by the TCEQ and to the EPA's Region Six office on May 24, 2021.

Jon Niermann, *Chairman*  
Emily Lindley, *Commissioner*  
Bobby Janecka, *Commissioner*  
Toby Baker, *Executive Director*



## TEXAS COMMISSION ON ENVIRONMENTAL QUALITY

*Protecting Texas by Reducing and Preventing Pollution*

May 24, 2021

David Garcia  
Director, Air and Radiation Division  
United States Environmental Protection Agency, Region 6  
1201 Elm Street, Suite 500  
Dallas, Texas 75270

Re: Request for Alternative Model Approval for the Rusk-Panola Attainment Demonstration (AD) State Implementation Plan (SIP) Revision for the 2010 Sulfur Dioxide (SO<sub>2</sub>) National Ambient Air Quality Standard (NAAQS)

Dear Mr. Garcia:

The Texas Commission on Environmental Quality (TCEQ) requests that the United States Environmental Protection Agency (EPA) approve an alternative model for use in the Rusk-Panola 2010 SO<sub>2</sub> NAAQS AD SIP Revision, as provided by 40 Code of Federal Regulations (CFR) Part 51, Appendix W, Section 3.2.2(b)(2).

The TCEQ requests approval of American Meteorological Society/EPA Regulatory Model - Highly Buoyant Plume (AERMOD-HBP) as the alternative model. AERMOD-HBP is an alternative formulation of the EPA's preferred model, AERMOD (40 CFR Part 51, Appendix W, Section 4.2.2.1), in which the penetrated plume component has been modified. AERMOD-HBP was developed by AECOM and its formulation is described in Attachment 1: *AERMOD-HBP Formulation Documents from AECOM*.

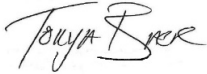
The TCEQ contracted with Ramboll US Consulting, Inc. to perform a model performance evaluation of both AERMOD and AERMOD-HBP using evaluation procedures recommended in 40 CFR Part 51, Appendix W, Section 3.2. Details of the evaluation techniques used to support the request for AERMOD-HBP's alternative model approval are provided in Attachment 2: *Modeling Protocol for Alternative Model Approval Demonstration for the Rusk-Panola Attainment Demonstration State Implementation Plan Revision for the 2010 Sulfur Dioxide (SO<sub>2</sub>) National Ambient Air Quality Standard*.

The TCEQ's statistical performance evaluation comparing modeled and monitored data shows that AERMOD-HBP performs better in estimating SO<sub>2</sub> concentration distributions at monitors in and near the Rusk-Panola nonattainment area. This supports approval of AERMOD-HBP as an alternative model for use in the Rusk-Panola 2010 SO<sub>2</sub> NAAQS AD SIP Revision.

David Garcia  
Page 2  
May 24, 2021

If you have questions or need additional information, please contact Donna F. Huff, Deputy Director of the Air Quality Division, at (512) 239-6628 or [Donna.Huff@tceq.texas.gov](mailto:Donna.Huff@tceq.texas.gov).

Sincerely,



Tonya Baer, Director  
Office of Air  
Texas Commission on Environmental Quality

Enclosures:

Attachment 1: *Formulation Documentation of AERMOD-HBP from AECOM*

Attachment 2: *Modeling Protocol for Alternative Model Approval Demonstration for Attainment Demonstration State Implementation Plan Revision for the 2010 Sulfur Dioxide (SO<sub>2</sub>) National Ambient Air Quality Standard*

cc: Guy Donaldson, EPA Region 6, U.S. Environmental Protection Agency  
Erik Snyder, EPA Region 6, U.S. Environmental Protection Agency

**ATTACHMENT 1**

**AERMOD-HBP FORMULATION DOCUMENTS FROM AECOM**

## LIST OF DOCUMENTS

- Paine, R., Szembek, C., and Warren, C., May 19, 2021, *Discussion of Penetrated Plume Treatment in AERMOD - Recommended Highly Buoyant Plume (HBP) Improvements*, AECOM
- Model Evaluation Results for Baldwin and Labadie*, Appendix A to Paine *et al.*, (2021)
- Baldwin Table and Plots*, Appendix B to Paine *et al.*, (2021)
- Labadie Tables and Plots*, Appendix C to Paine *et al.*, (2021)
- Weil, J. C., Corio, L. A., and Brower, R. P., 1997, *A PDF Dispersion Model for Buoyant Plumes in the Convective Boundary Layer*, *Journal of Applied Meteorology*. 36, 982-1003
- Moore, G.E., Milich, L.B., Liu M.K., 1988, *Plume behaviors observed using lidar and SF6 tracer at a flat and hilly site*, *Atmospheric Environment*, Volume 22, Issue 8, 1988, Pages 1673-1688
- Weil, J. C., January 2, 2020, *New Dispersion Model for Highly-Buoyant Plumes in the Convective Boundary Layer*, Preliminary Draft v4.
- Szembek, C., M. Garrison, and R. Paine, 2017, *DISTANCE-DEBUG and HRBINARY: Modeling Tools for Unpacking the AERMOD Black Box*, A&WMA Annual Conference, June 6, 2017
- Presentation by Dr. Ken Rayner on February 25, 2013, *Review of models for dispersion of tall stack plumes at Collie*. Provided to Robert Paine of AECOM on 2/25/2013, and later to Roger Brode of USEPA's Office of Air Quality Planning and Standards on June 11, 2014
- Warren, C., R. Paine, and J. Connors, 2019, *Evaluation of AERMOD SO2 Predictions for a Research-Grade Field Experiment*, Paper MO10, presented at the Air & Waste Management Association specialty conference (Guideline on Air Quality Models: Planning Ahead), March 19-21, 2019. Durham, NC

# Discussion of Penetrated Plume Treatment in AERMOD – Recommended Highly Buoyant Plume (HBP) Improvements

Robert Paine, Carlos Szembek, and Christopher Warren, AECOM

May 19, 2021

## Overview of Issue

In convective conditions, AERMOD has a three-plume treatment for stack emissions: direct, indirect and penetrated components (**Figure 1, *Three-plume Treatment by AERMOD in Convective Conditions***). For any given hour, the plume mass can be divided into as many as all three of these plume cases. As shown in **Figure 1**, the direct and indirect plumes remain within the convective mixed layer, which features vigorous vertical mixing above the surface layer (the lowest ~10% of the mixed layer). The penetrated plume is the portion of the plume that is sufficiently buoyant to break through the elevated inversion into the stable layer aloft. In this stable layer, the vertical turbulence is much lower than it is in the convective mixed layer, and the penetrated plume is observed to remain in that layer until late morning/early afternoon when the convective mixing height rises to intercept the plume due to diurnal heating. This document discusses how the current AERMOD formulation does not treat the dynamics of the penetrated plume correctly. In certain cases, AERMOD models a penetrated plume as mixing into the convective layer well before the convective mixed layer rises to the plume level. The authors propose an alternative approach, developed in conjunction with Dr. Jeffrey Weil,<sup>1</sup> that provides a more reasonable treatment of the penetrated plume. Discussions of similar findings in other databases and studies conducted by other investigators are also provided.

## Behavior of the Penetrated Plume

Dr. Weil has studied the issue of the penetrated plume for decades. A peer-reviewed paper<sup>2</sup> (provided as **Attachment 1**) that he co-authored notes that the penetrated plume rises into the stable layer above the convective boundary layer and is subsequently mixed to the ground only when the convective mixing height rises to intercept it. A conceptual diagram of the nature of the penetrated plume from the Weil et al. (1997) paper as shown in **Figure 2, *Depiction of Penetrated Plume Aloft***, indicate that the penetrated plume mixes to the ground over time, yet not necessarily during the same hour that it is emitted into the stable layer aloft.

Research-grade experiments in the 1980s were able to detect plume concentrations aloft using laser imaging, detection, and ranging (“LIDAR”) instrumentation. The methods used for the EPRI Kincaid and Bull Run field studies are described by Moore et al. (1988)<sup>3</sup> and are provided as **Attachment 2**. Remote-

---

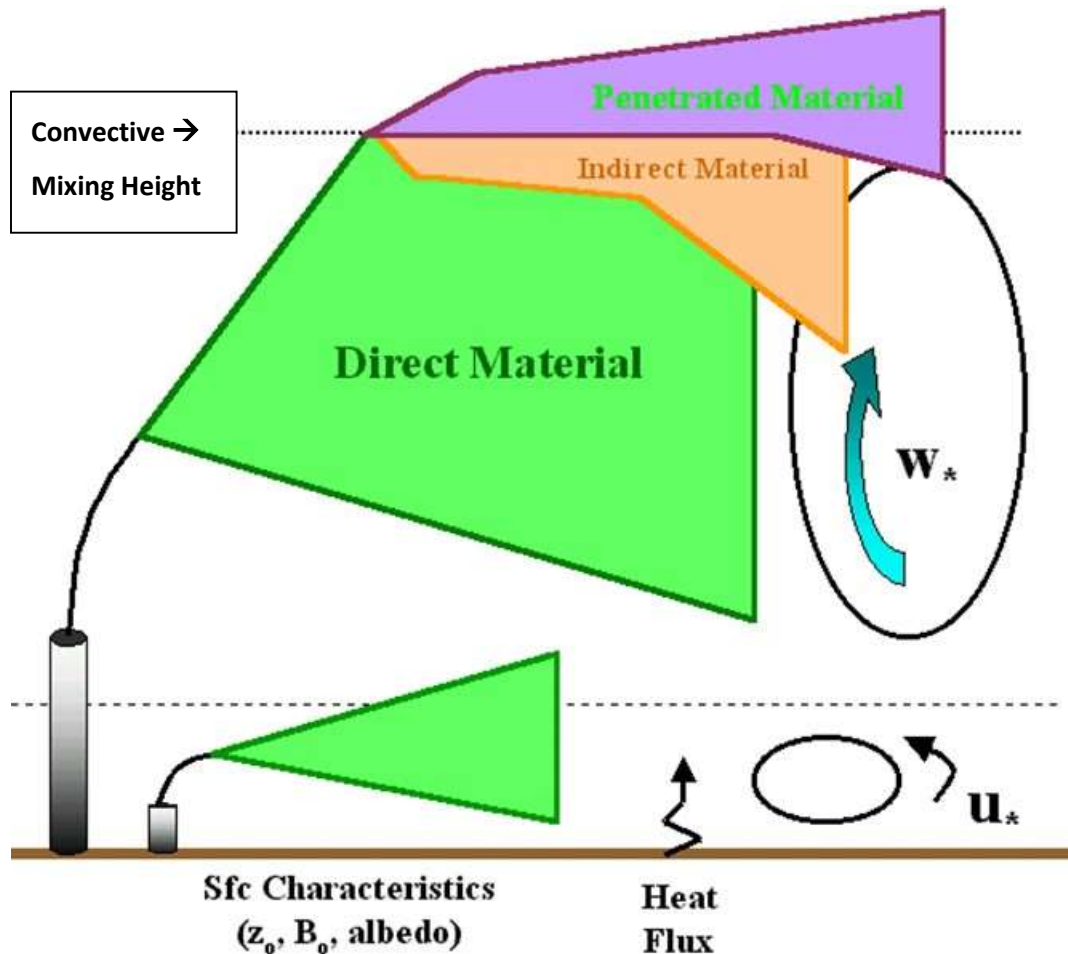
<sup>1</sup> Dr. Weil and Robert Paine (one of the AECOM authors of this document) were members of the AERMOD development team.

<sup>2</sup> Weil, J. C., Corio, L. A., and Brower, R. P.: 1997, 'A PDF Dispersion Model for Buoyant Plumes in the Convective Boundary Layer', *J. Appl. Meteorol.* 36, 982-1003.

<sup>3</sup> G.E. Moore, L.B. Milich, M.K. Liu, 1988. Plume behaviors observed using lidar and SF6 tracer at a flat and hilly site, *Atmospheric Environment*, Volume 22, Issue 8, 1988, Pages 1673-1688, ISSN 0004-6981,

sensing observations of the plume aloft were made by ground-based, mobile sulfur dioxide (SO<sub>2</sub>), differential adsorption LIDAR (“DIAL”), ground-based, mobile particle-sensing LIDAR, and airplane-based particle LIDAR known as an airborne LIDAR plume and haze analyzer (“ALPHA-I”). The SO<sub>2</sub> DIAL instrument measured the absolute SO<sub>2</sub> concentrations of the plume aloft. For the LIDAR to observe the entire plume cross-section, it had to be operated within 2 km of the stack at Kincaid and within 1 km at Bull Run. The ground-based LIDARs scanned the plume through a plane normal to the plume centerline aloft and through a plane parallel to the ground-level concentration pattern.

**Figure 1: Three-plume Treatment by AERMOD in Convective Conditions**



Inversion heights associated with the convective mixed layer height for the Kincaid and Bull Run field studies were determined throughout the daytime period from frequent tethered sonde<sup>4</sup> soundings. Vertical plume cross sections were determined from the remote sensing measurements, and plume concentrations in parts per billion (ppb) were mapped for several hourly averaging periods.

**Figures 3 through 6, LIDAR Images From Bull Run,** show an example of the time evolution of the plume behavior during one morning at Bull Run up to the time that the convective mixing height (marked in red in each figure) intercepted the plume aloft. The figures, which cover four separate hours for that day,

[https://doi.org/10.1016/0004-6981\(88\)90396-4](https://doi.org/10.1016/0004-6981(88)90396-4).

<sup>4</sup> A tethered sonde is a radiosonde attached to a fixed or tethered balloon.

show the integrated plume concentration in the X-Z plane. Basically, the compact nature of the plume was preserved until the noon hour (the last in the series, **Figure 6**) when the convective mixing height finally rose through the layer occupied by the plume. This behavior shows that prior to this time, the penetrated plume remained above the mixing height and did not mix down to the ground until it was intercepted by the rising convective mixed layer. The maximum ground-level concentrations for this case were about four times higher during the hour 1200-1300 than the preceding hours that day. The plume centerline concentrations aloft were about a factor of four lower after mixing throughout the convective boundary layer.

**Figure 2: Depiction of Penetrated Plume Aloft by Weil et al., 1997**

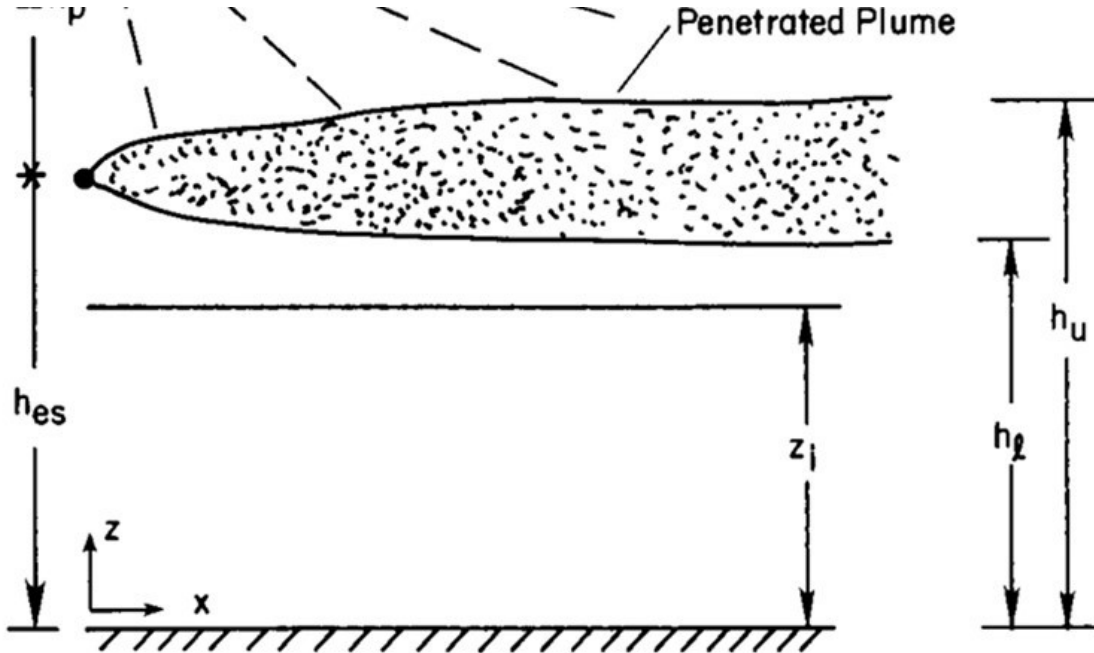


Figure 3: Lidar Image from Bull Run, October 4, 1982, 8-9 AM

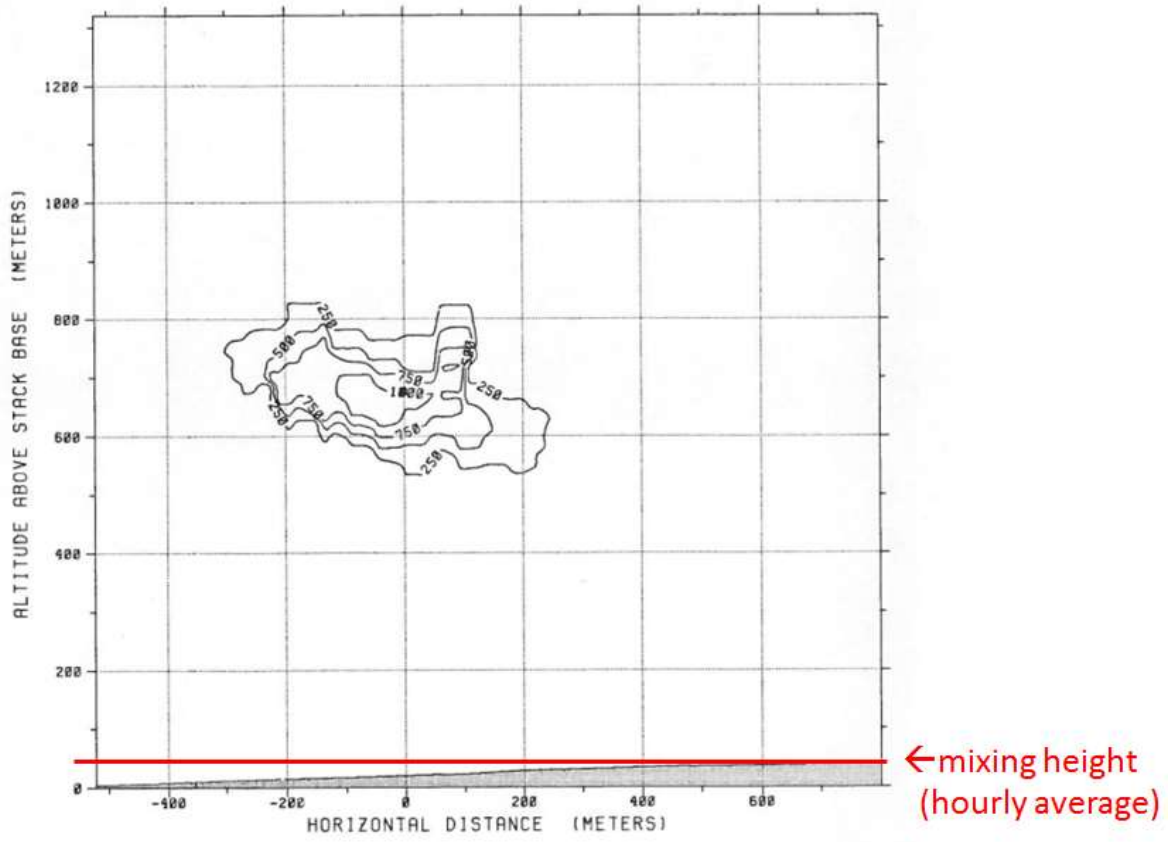


Figure 4: Lidar Images from Bull Run, October 4, 1982, 10-11 AM

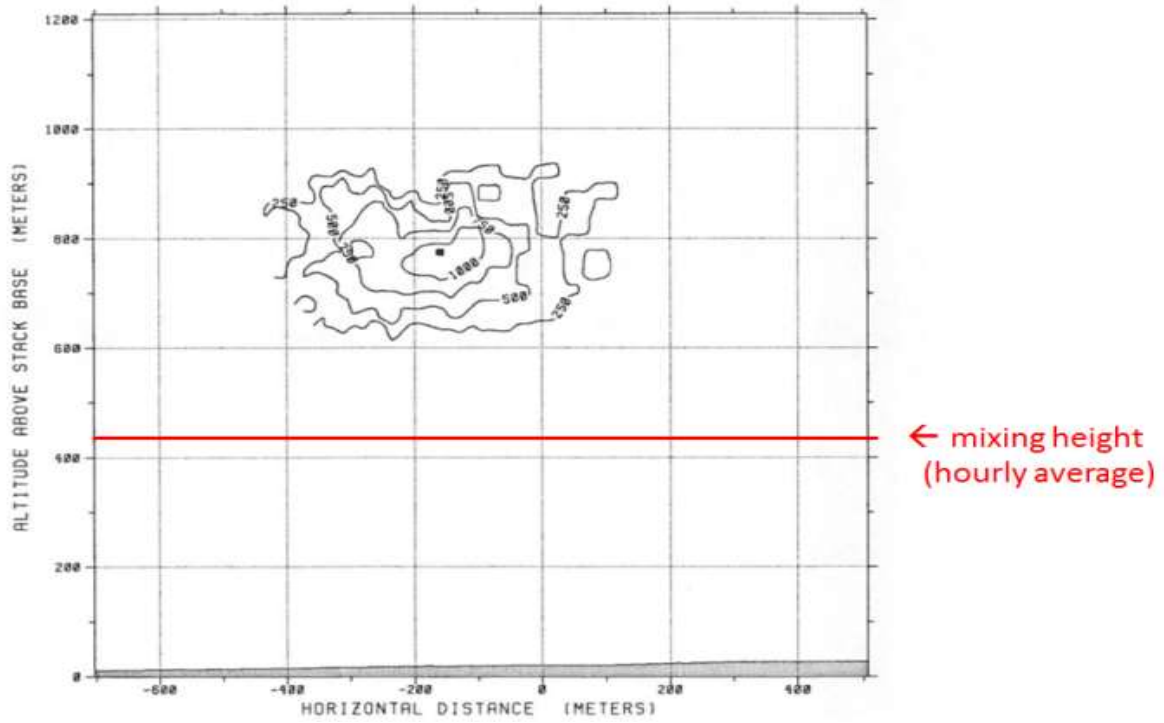


Figure 5: Lidar Image from Bull Run, October 4, 1982, 11 AM - noon

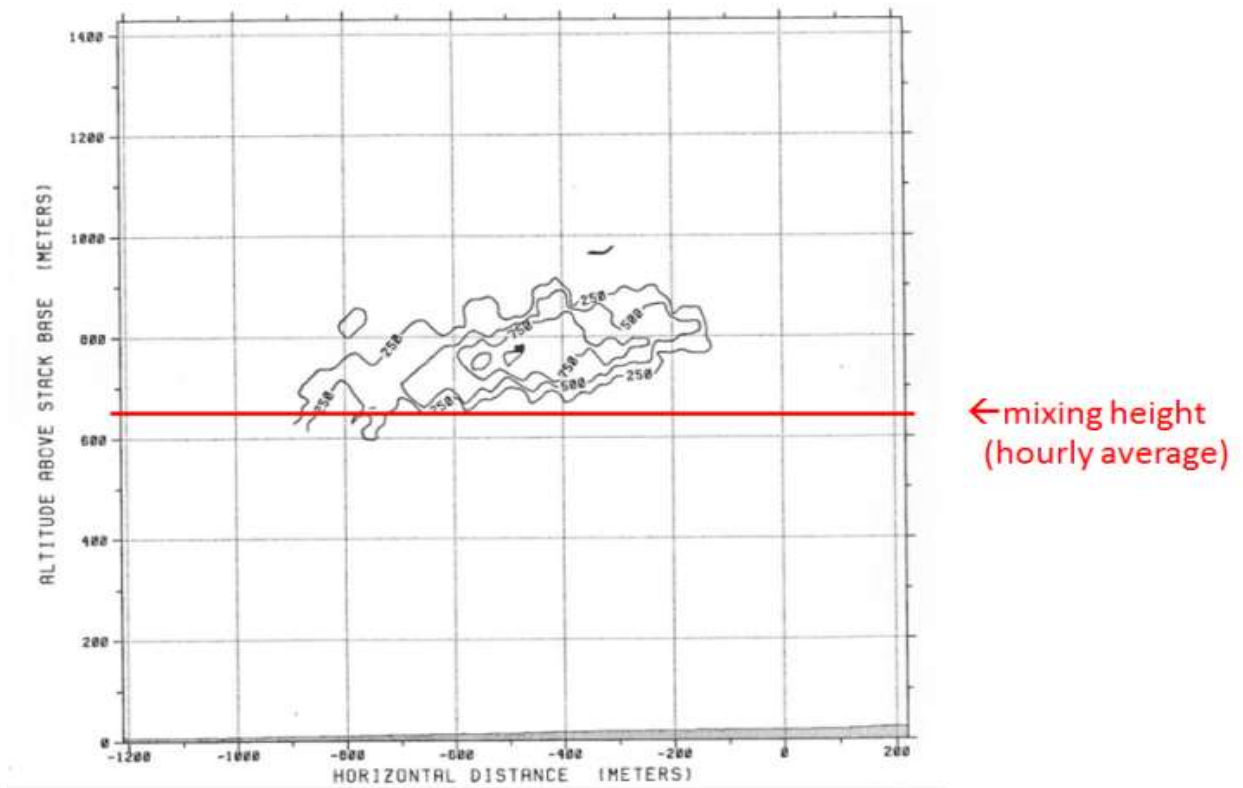
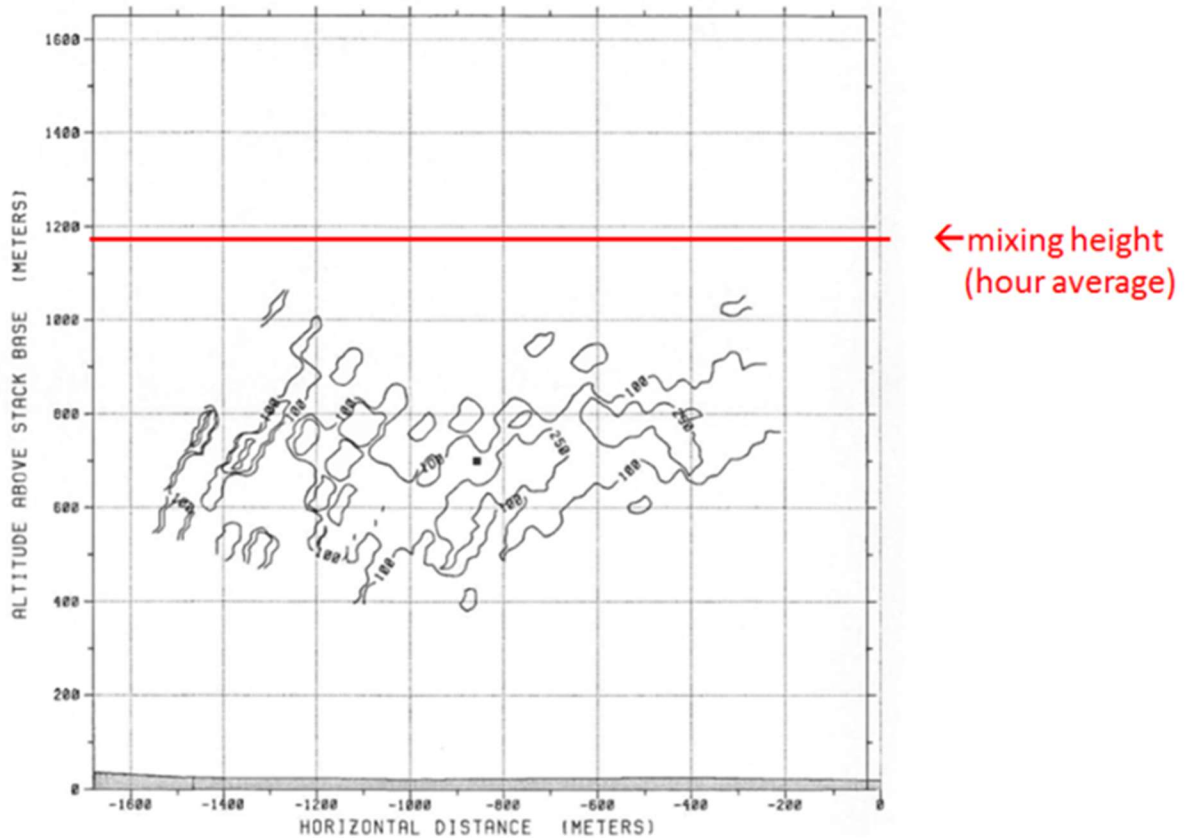


Figure 6: Lidar Image from Bull Run, October 4, 1982, noon – 1 PM



Based upon the findings noted above, the likelihood of elevated ground-level concentrations resulting from a penetrated plume is low until the convective mixed layer has risen to intercept the plume. The penetrated plume interception event, often referred to as “daytime fumigation,” typically leads to elevated concentrations only during a single hour of the day. The multiple-hour evolution of this process, as shown in Figures 3-6, presents a challenge because AERMOD is a steady-state model and has no information, absent the proposed enhancements discussed below, of the next hour’s conditions.

### Current Implementation in AERMOD

AERMOD version 21112 currently results in the mixing of the penetrated plume into the convective boundary layer during more hours than expected, resulting in a premature and repetitious mixing of the penetrated plume to the ground that only occurs once during the daytime hours. Because this premature mixing assumption is repeated for multiple hours leading up to the actual interception of the penetrated plume by the rising convective boundary layer (“CBL”), AERMOD will overstate the frequency of the plume mixing events, resulting in overpredictions. This issue with AERMOD has been observed by investigators associated with field studies where the model is found to overpredict ground-level concentration events due to the penetrated plume issue and make those predictions too often and too early, by as much as 2-4 hours, in the day compared to the timing of observed ground-level impacts.

A key area of scrutiny in the AERMOD formulation is the parameterization of the penetrated plume's vertical spreading through its calculation of "effective" dispersion parameters. AERMOD's formulation computes vertically-integrated values between the plume centerline and the higher level of the plume's bottom edge and receptor at the ground. However, this calculation can substantially overstate the vertical plume growth if the wrong vertical plume depth (a function of vertical plume dispersion,  $\sigma_z$ ) is assumed by the model.

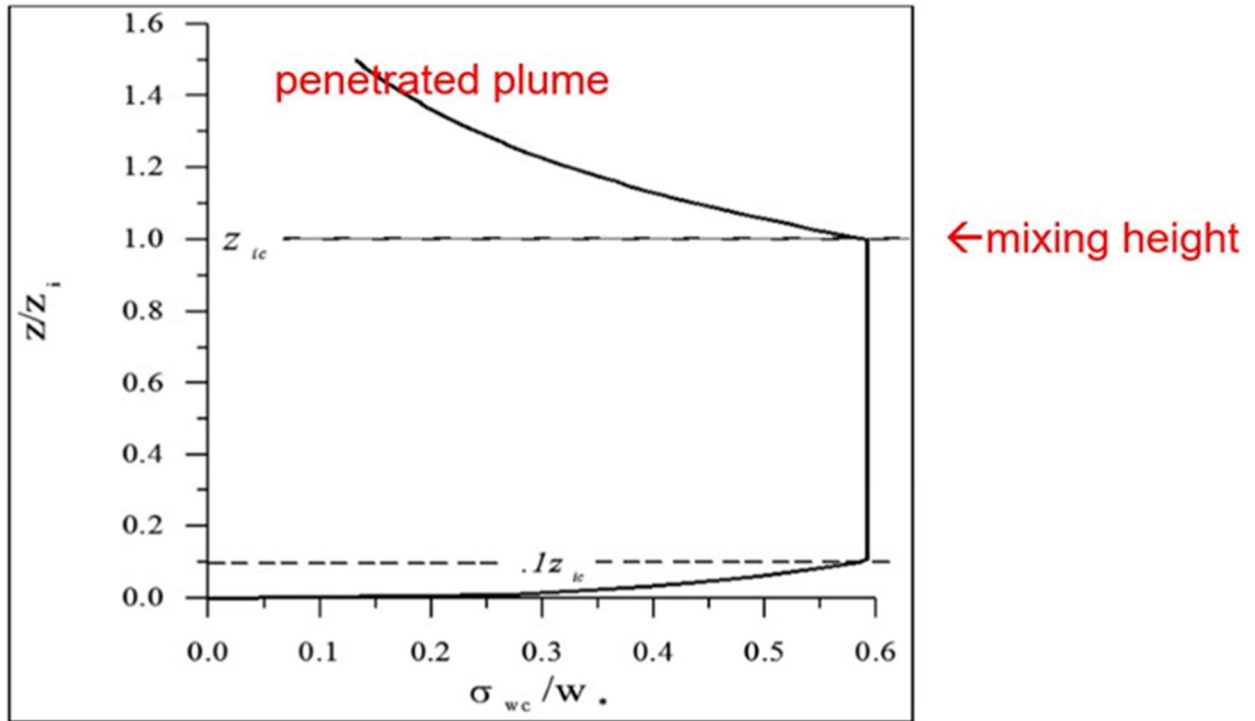
The central issue for the penetrated plume handling in AERMOD is that the computation of  $\sigma_z$  (used to determine the plume's bottom edge) is a function of the stability in the layer occupied by the plume. By definition, the penetrated plume is in a stable layer above the mixing height, but the AERMOD formulation assumes a neutral layer for computing the penetrated plume  $\sigma_z$ , which substantially and incorrectly increases the  $\sigma_z$  value. This formulation, according to the AERMOD model formulation document,<sup>5</sup> assumes that the penetrated plume mixes into the CBL and thus encounters a non-stable layer for the portion of the plume that reaches the ground. However, this assumption is only correct if the mixing height rises fast enough to capture at least a portion of the penetrated plume by the end of the current hour, according to Weil et al. 1997.<sup>2</sup> Otherwise, this assumption is incorrect as evidenced by the direct observations of the actual penetrated plume behavior not mixing down from the stable layer aloft while the CBL remains below the plume.

AERMOD computes the "effective" values for turbulence parameters (vertical turbulence,  $\sigma_w$  in particular) that involves averaging through a vertical depth between the plume centerline to the bottom of the plume, which is a distance of 2.15  $\sigma_z$  below the plume centerline. With the incorrect assumption of a large  $\sigma_z$  for a penetrated plume, AERMOD averages  $\sigma_w$  over a depth that, in reality, can involve large changes in  $\sigma_w$  with height above the mixing height (see **Figure 7, AERMOD's Treatment of Vertical Turbulence in Convective Conditions**). Hence, for hours when the actual mixing height has yet to intercept the plume, the averaged, computed value does not represent local turbulence conditions at the penetrated plume's centerline height. For many cases, where the vertical integration occurs over a significant depth within the convective boundary layer, the modeled plume spreading will be greatly exaggerated because the actual values of  $\sigma_w$  in the convective boundary layer can be an order of magnitude higher than those in the stable layer aloft.

---

<sup>5</sup> EPA, 2019. AERMOD Model Formulation and Evaluation Document. Available at [https://gaftp.epa.gov/Air/aqmg/SCRAM/models/preferred/aermod/aermod\\_mfed.pdf](https://gaftp.epa.gov/Air/aqmg/SCRAM/models/preferred/aermod/aermod_mfed.pdf).

Figure 7: AERMOD's Treatment of Vertical Turbulence in Convective Conditions



## Debugging of AERMOD to Understand the Penetrated Plume Issue

Due to AERMOD’s three-plume treatment as shown in **Figure 1**, the findings noted above for the penetrated plume were not easy to diagnose. The “Model Debug” output from AERMOD is one way to review plume behavior in AERMOD, but the file size for the output is so large that its use is impractical for routine modeling applications. This awkward debug file issue led AECOM, with funding from EPRI, to develop a more streamlined “DISTANCE DEBUG” output that lists the coherent plume statistics for only the peak impact receptor for each source and each hour, thus resulting in a manageable output size that is still useful. This tool has been documented in a conference presentation<sup>6</sup> (provided as **Attachment 4**) as well as Texas Commission on Environmental Quality’s (TCEQ’s) submittal<sup>7</sup> to EPA in 2016 for Round 2 of the SO<sub>2</sub> National Ambient Air Quality Standard (NAAQS) implementation. The TCEQ submittal notes on page 162 of 269 that,

*“the “DISTANCE DEBUG” output capability of AERMOD is documented and freely available from EPRI at <https://sourceforge.net/projects/epri-dispersion/>”, and that the “review of Sierra Club modeling results for Martin Lake [relied upon by EPA for their nonattainment designation] that were re-run with a ‘DISTANCE DEBUG’ enhanced AERMOD debugging output confirms that the Martin Lake peak AERMOD-predicted concentrations are caused by the simulated penetrated plume.”*

Two examples of how various debug output data available from AERMOD show the current problem with the penetrated plume are discussed in the following subsection.

### Examples of Martin Lake Penetrated Plume Overprediction Issues

AERMOD modeling conducted with three years of data (2018-2020) shows that the model, using default options, overpredicts the 3-year design concentration (3-year average of the 99<sup>th</sup> percentile peak daily 1-hour maximum concentration) at the monitoring site by about 30%. This overprediction tendency would result in an initial 30% penalty for Martin Lake to show NAAQS compliance with a reduced emission rate. The cause of the overprediction has been determined to be the penetrated plume and the top ten AERMOD predictions are all dominated by the penetrated plume issue, as shown in the DISTANCE-DEBUG output (**Table 1, Excerpts of DISTANCE-DEBUG Output for Top 10 Daily Maxima AERMOD Default Impacts at Martin Lake Creek Monitor**).

The combination of AERMOD’s MODEL and METEOR debug files, in addition to the DISTANCE-DEBUG output files, were used to diagnose the penetrated plume issue with the default, regulatory-approved AERMOD model. Two specific Martin Lake events are discussed below, the first occurring on June 3, 2019, at hour 11 and the second on June 29, 2019, at hour 11.

<sup>6</sup> Szembek, C., M. Garrison, and R. Paine, 2017. “DISTANCE-DEBUG and HRBINARY: Modeling Tools for Unpacking the AERMOD Black Box”, A&WMA Annual Conference; Pittsburgh, PA; June 6, 2017.

<sup>7</sup> Available at

[https://www.tceq.texas.gov/assets/public/implementation/air/sip/so2/2015RevisedRecommendation/041916\\_SO2\\_Designation\\_120-Day\\_Response.pdf](https://www.tceq.texas.gov/assets/public/implementation/air/sip/so2/2015RevisedRecommendation/041916_SO2_Designation_120-Day_Response.pdf).

**Table 1: Excerpts of DISTANCE-DEBUG Output for Top 10 Daily Maxima AERMOD Default Impacts at Martin Lake Creek Monitor**

Daily Maxima RANK	YYMMDDHH	TOTAL Conc. (µg/m <sup>3</sup> )	u* (m/s)	w* (m/s)	OBULEN (m)	Z <sub>mech</sub> (m)	Z <sub>conv</sub> (m)	SFC Z <sub>0</sub> (m)	Source ID	Actual Emissions (g/s)	Ts (K)	Vs (m/s)	Final Plume Height (FPH) (m)	Distance to FPH (m)	WDIR @ FPH (deg.)	Effective Wind Speed (m/s)	Plume Type	Meander Fraction	Partial Penetration Fraction	Effective Sigma V (m/s)	Effective Sigma W (m/s)	Hourly Conc. (µg/m <sup>3</sup> )
1	18090609	666.1	0.14	0.74	-5.2	130	285	0.032	S1	875.4	360.2	33.7	445.5	924.9	77	1.9	PEN	0.177	1.000	0.51	0.36	210.3
									S2	824.3	347.7	29.8	419.3	924.9	77	1.8	PEN	0.179	0.969	0.51	0.38	218.9
									S3	972.8	363.1	32.4	445.6	924.9	77	1.9	PEN	0.177	1.000	0.51	0.36	221.8
2	20032213	619.2	0.14	0.67	-7.3	125	322	0.025	S1	0.3	306.4	2.3	238.8	307.6	80	2.0	IND	0.147	0.075	0.48	0.42	0.1
									S2	1097.6	361.7	31.8	418.9	1227.1	80	2.0	PEN	0.141	0.769	0.48	0.38	321.8
									S3	920.6	347.7	29.1	405.6	1227.1	80	2.0	PEN	0.142	0.714	0.48	0.38	282.2
3	18022211	604.5	0.20	0.49	-42.1	213	259	0.02	S1	728.1	345.5	33.1	324.5	1656.1	82	3.5	PEN	0.052	0.779	0.48	0.31	184.2
									S2	866.0	362.0	33.4	332.1	1791.4	82	3.5	PEN	0.052	0.820	0.48	0.31	221.8
									S3	701.7	358.3	34.9	332.4	1795.8	82	3.5	PEN	0.052	0.821	0.48	0.31	183.5
4	18101910	585.8	0.13	0.43	-11.9	117	186	0.027	S1	507.0	361.2	28.8	348.7	965.2	77	1.9	PEN	0.094	1.000	0.35	0.15	167.0
									S2	585.2	348.1	27.2	334.1	965.2	77	1.9	PEN	0.095	1.000	0.35	0.17	227.6
									S3	469.4	346.8	26.9	332.1	965.2	77	1.9	PEN	0.095	1.000	0.35	0.17	176.2
5	18123011	572.2	0.13	0.45	-19.3	114	317	0.02	S1	946.6	346.2	32.4	378.2	1692.4	74	2.1	PEN	0.082	0.609	0.37	0.28	233.2
									S2	555.1	347.8	20.5	362.6	1420.6	74	2.1	PEN	0.083	0.506	0.37	0.28	126.6
									S3	998.6	343.3	31.9	376.1	1657.1	74	2.1	PEN	0.082	0.596	0.37	0.28	197.5
6	18061907	479.6	0.22	0.64	-29.6	244	303	0.032	S1	715.5	362.0	34.8	397.9	1703.9	82	3.5	PEN	0.066	0.802	0.56	0.38	132.3
									S2	935.4	366.3	31.8	395.8	1676.4	82	3.5	PEN	0.067	0.794	0.56	0.39	182.7
									S3	746.3	359.4	33.7	394.6	1660.9	82	3.5	PEN	0.067	0.789	0.56	0.39	149.5
7	18102210	468.3	0.16	0.77	-5.9	154	266	0.027	S1	599.3	351.6	27.2	363.2	957.5	85	2.2	PEN	0.150	0.904	0.55	0.42	171.9
									S2	449.5	347.5	25.5	357.4	957.5	85	2.2	PEN	0.151	0.882	0.55	0.42	138.0
									S3	459.0	345.4	27.2	359.1	957.5	85	2.2	PEN	0.151	0.888	0.548	0.42	143.4
8	20100910	464.8	0.23	0.74	-25.7	258	365	0.027	S1	913.8	349.0	28.3	435.0	1470.9	82	3.7	PEN	0.071	0.572	0.61	0.46	146.8
									S2	1068.4	368.0	33.7	456.6	1737.6	82	3.7	PEN	0.070	0.669	0.61	0.45	154.1
									S3	930.1	357.5	29.5	442.8	1568.0	82	3.7	PEN	0.071	0.610	0.61	0.46	149.0
9	18012711	459.7	0.10	0.54	-4.3	77	260	0.02	S1	791.3	346.6	31.5	438.6	867.8	75	1.4	PEN	0.172	1.000	0.37	0.23	262.4
									S2	694.5	361.9	33.9	465.9	867.8	75	1.4	PEN	0.171	1.000	0.37	0.19	182.3
									S3	0.0	--	--	<---	Source is not emitting this hour								
10	20031613	451.9	0.12	0.68	-4.3	117	360	0.025	S1	544.1	357.1	31.5	434.8	1051.4	80	1.5	PEN	0.215	0.603	0.46	0.40	156.4
									S2	625.8	367.8	33.2	442.9	1051.4	80	1.5	PEN	0.215	0.641	0.46	0.39	174.9
									S3	364.2	355.7	28.2	428.9	1051.4	80	1.5	PEN	0.216	0.574	0.46	0.40	105.6

For the hour ending 11 on June 3, 2019, AERMOD reported a penetrated plume at final heights for the three Martin Lake units averaging about 587 m, while the convective mixing height was 485 m (representing the value at the midpoint of the hour). For the following hour, the convective mixing height rose to about 658 m and as a result, the mixing height at the end of hour 11 was still below the three Martin Lake units' plume centerlines at about 572 m. AERMOD assigned large sigma-z values of about 228 – 242 m, resulting in a layer for effective parameters reaching well into the convective mixed layer, down to a level of about 107 m above the ground. **Figure 8** shows a plot of the sigma-w profile and the effective turbulence calculations in AERMOD. The sigma-w (green line) is the AERMOD internally calculated sigma-w extracted from the METEOR debug file.

The local value of sigma-w at the penetrated plume centerline shown in **Figure 8, AERMOD-Simulated Sigma-w as a Function of Height for June 3, 2019, Hour Ending 11**, is about 0.30 m/s. However, the internal AERMOD calculations of the effective sigma-w value created an average sigma-w value of more than twice the centerline value (about 0.63 m/s) in a layer between the plume centerline at ~590 m down to ~105 m. This mixing was applied to the entire mass of the penetrated plume, even though most of it remained above the mixing height even at the end of the hour. The result was an AERMOD prediction at the monitoring site of 244.0  $\mu\text{g}/\text{m}^3$ , almost twice the observed value of 123.3  $\mu\text{g}/\text{m}^3$ .

For the hour ending 11 on June 29, 2019, AERMOD reported a penetrated plume at final heights for the three Martin Lake units averaging about 390 m, while the convective mixing height was 296 m (representing the value at the midpoint of the hour). For the following hour, the convective mixing height rose only 10 m to 306 m (well under the plume centerline); hence the mixing height at the end of hour 11 was still below the three units' plume centerlines at about 301 m. AERMOD assigned large sigma-z values of about 125 m, resulting in a layer for effective parameters reaching well into the convective mixed layer, down to a level of about 120 m above the ground. **Figure 9, AERMOD-Simulated Sigma-w as a Function of Height for June 29, 2019, Hour Ending 11**, shows a plot of the sigma-w profile and the effective turbulence calculations in AERMOD.

**Figure 8: AERMOD-Simulated Sigma-w as a Function of Height for June 3, 2019, Hour Ending 11**

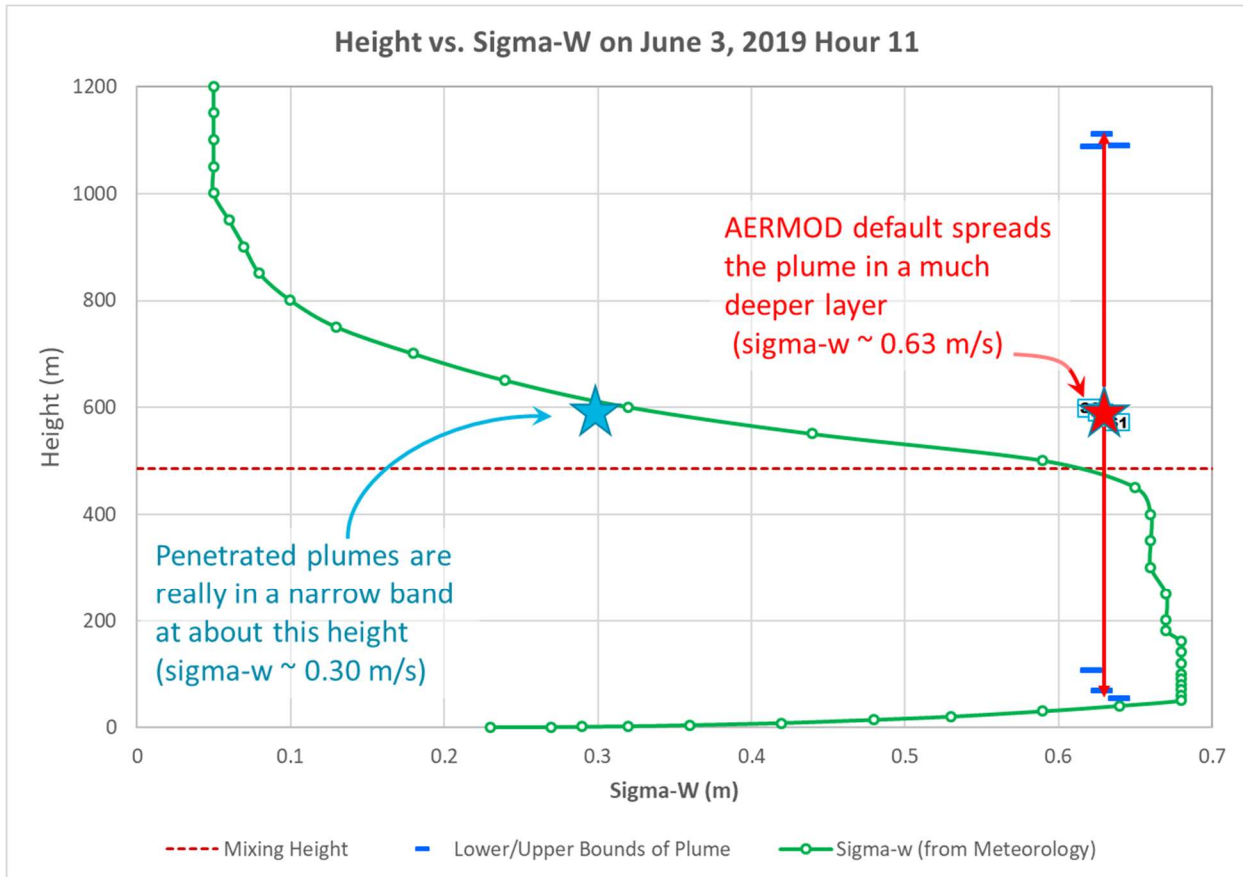
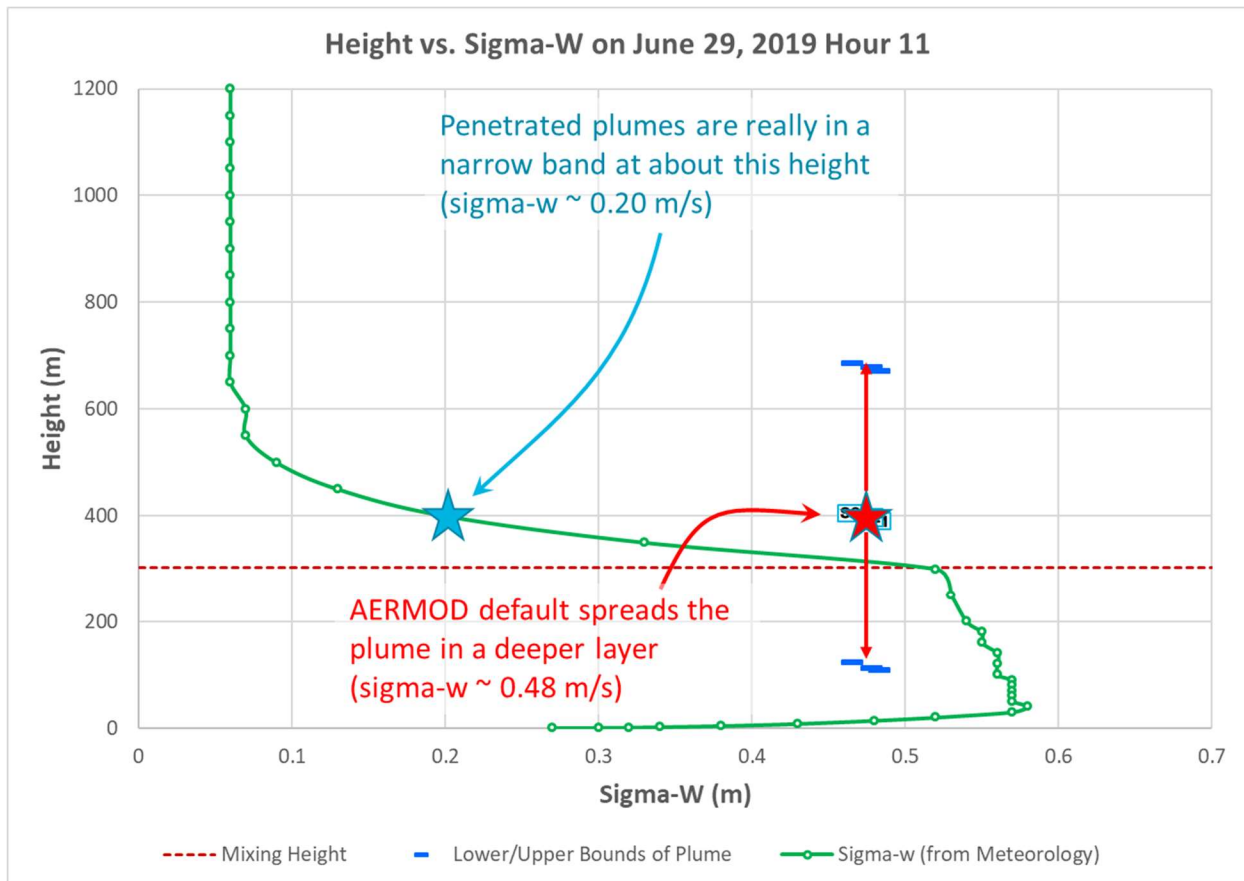


**Figure 9: AERMOD-Simulated Sigma-w as a Function of Height for June 29, 2019, Hour Ending 11**



The plot in **Figure 9** shows that the local value of sigma-w at the penetrated plume centerline is about 0.20 m/s. However, the internal AERMOD calculations of the effective sigma-w value created an average sigma-w value of 2.4 times the centerline value (about 0.48 m/s) in a layer between the plume centerline at ~395 m down to ~115 m. This mixing was applied to the entire mass of the penetrated plume, although most (if not all) of it remained above the mixing height at the end of the hour. The result was an AERMOD prediction at the monitoring site of 485.8  $\mu\text{g}/\text{m}^3$ , well above any single hour's measurement at the monitor over the 3-year period.

The key issue is the deep vertical layer over which the effective vertical mixing parameters, especially sigma-w, are calculated. The overly deep vertical layer extends the averaging well into the convective mixed layer, resulting in an exaggerated large plume depth and an associated high impact at the ground. This feature of the penetrated plume treatment was not anticipated by the AERMIC committee in designing the model.

## Other Field Databases with Penetrated Plume Overprediction Issues

To demonstrate AERMOD's overprediction tendency associated with penetrated plume events, two independent SO<sub>2</sub> modeling databases have been selected. The first is the 1982 – 83 Baldwin<sup>8</sup> database from EPA's collection of AERMOD model evaluation databases. The second is a more recent 2017 – 2019 database focusing upon the Labadie Energy Center (Labadie), owned and operated by Ameren Corporation. Both field databases focus upon coal-fueled power plants in rural areas, with Baldwin in flat terrain and Labadie surrounding by mostly flat terrain. In both datasets, the dominant SO<sub>2</sub> sources are tall stacks. These datasets are good candidates to evaluate since they are typical of many power-generating stations across the U.S. and are similar in many respects to the Martin Lake Power Plant (Midwest, tall stacks, flat terrain, rural).

### Baldwin Power Plant

The Baldwin Power Plant database is a rural flat terrain site in southwestern Illinois with ten ambient SO<sub>2</sub> monitors during the 1982 – 1983 period ranging in distance from 2 to 10 km from the facility, as shown in **Figure 10, Baldwin SO<sub>2</sub> Monitoring Network**. The plant has three 184-meter stacks aligned approximately north-south and spaced approximately 100 meters apart, as shown in **Figure 11, Google Earth View of the Baldwin Power Plant**.

Meteorological measurements were taken from an on-site 100-meter tower with measurements over a 1-year period from April 1, 1982 through March 31, 1983 as part of a model evaluation study. Hourly wind speed, wind direction, and temperature measurements were collected at 10 meters along with wind speed and direction at 100 meters. Upper air sounding data from Salem, Illinois, was used.

---

<sup>8</sup> EPA, AERMOD Model Evaluation Databases. Available at: <https://www.epa.gov/scram/air-quality-dispersion-modeling-preferred-and-recommended-models>.

**Figure 10: Baldwin SO<sub>2</sub> Monitoring Network**

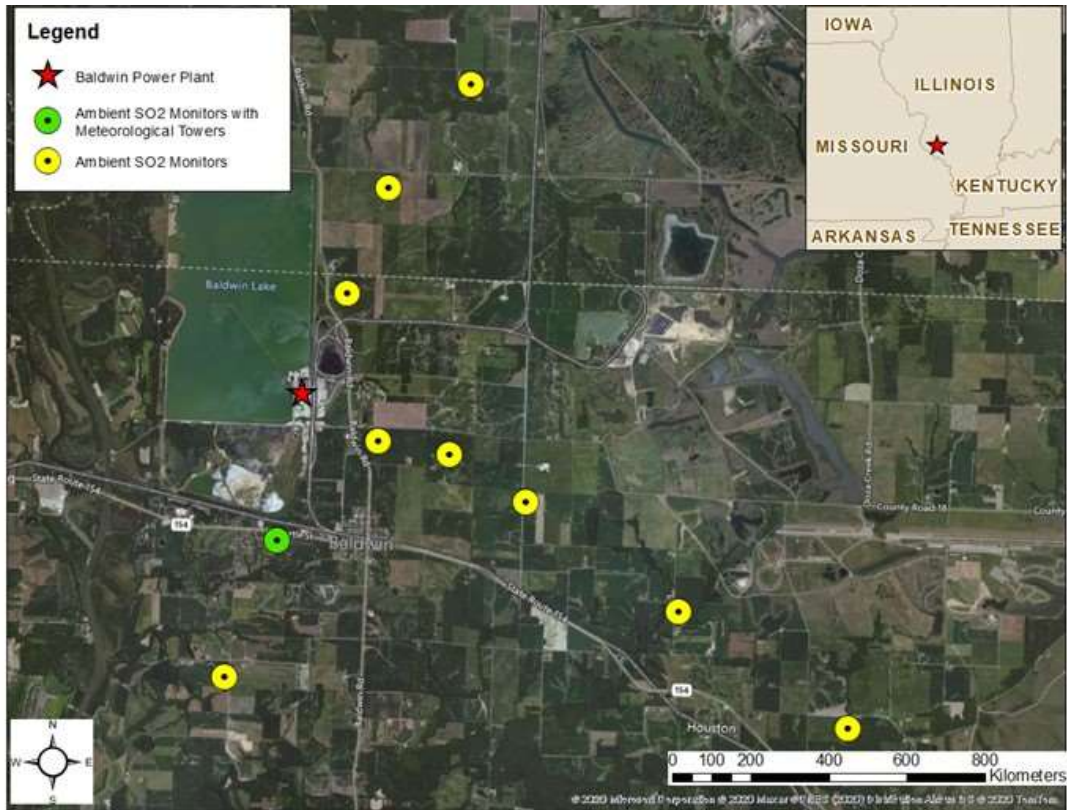


**Figure 11: Google Earth View of the Baldwin Power Plant**



Labadie Energy Center

Labadie is a 2,400-megawatt coal-fueled power plant located in Labadie, Missouri, approximately 55 kilometers west-southwest of St. Louis, Missouri. The station operates four boilers exhausting through three 213-meter tall stacks. Units 3 and 4 emit from a dual-flue stack and are modeled as a single, merged stack with EPA’s concurrence of this approach.<sup>9</sup> Hourly values of SO<sub>2</sub> emissions, stack temperatures, and stack exit velocities used in the modeling were provided by Ameren from the Continuous Emission Monitoring System (CEMS) data.

**Table 2, Labadie Stack Locations and Typical Full Load Exhaust Parameters**, lists the stack location, height and typical exhaust parameters for each source to be included in the modeling analysis. The area surrounding Labadie is rural with mostly simple terrain, as shown in **Figure 12, Labadie SO<sub>2</sub> and Meteorological Monitoring Network**. **Figure 13, Google Earth View of the Labadie Energy Center** shows a close-up of the three primary SO<sub>2</sub>-source tall stacks.

The 2016 Missouri Department of Natural Resources (DNR) monitoring plan led to the establishment of two monitoring sites for SO<sub>2</sub> located at the Valley and Northwest locations as well as one meteorological site equipped with meteorological measurements at 2 and 10 meters located at the Valley location. **Figure 13** provides a map indicating the locations of these sites. In addition to the meteorological tower, Ameren installed a doppler SODAR/RASS in October 2015 with a height sampling range set from 40 meters to 300 meters in 20-meter increments. In addition to the Missouri monitoring plan documents cited in Section 1 that have been approved by EPA, additional documentation for the Labadie monitoring program operation is available in Quality Assurance Project Plan (QAPP) documents<sup>10</sup> for that project. In early 2017, Ameren installed a second 10-meter tower at the Northwest monitoring site. Since the meteorological tower at the Northwest site was installed after the beginning of the period to be considered in this evaluation study, the Valley meteorological tower dataset is used for on-site meteorology.

**Table 2: Labadie Stack Locations and Typical Full Load Exhaust Parameters**

Source	Easting (UTM83) <sup>2</sup>	Northing (UTM83) <sup>2</sup>	Stack Height (m)	Exit Velocity (m/s)	Temperature (K)	Diameter (m)
Unit 1	688352.17	4270445.59	213.36	34.7	443.1	6.25
Unit 2	688387.01	4270400.40	213.36	35.6	442.5	6.25
Units 3 & 4	688435.47	4270332.33	213.36	34.5	433.2	8.84 <sup>(1)</sup>
(1) Equivalent diameter for merged flues (2) UTM coordinates for Zone 15.						

Penetrated Plume Model Evaluations on Baldwin and Labadie Databases

The Baldwin and Labadie databases were modeled using AERMOD with default options and compared against observed concentrations from nearby monitors. The 99<sup>th</sup> percentile daily maximum modeled SO<sub>2</sub>

<sup>9</sup> EPA (2016). Final Technical Support Document: Missouri Area Designations for the 2010 SO<sub>2</sub> Primary National Ambient Air Quality Standard. Available at: [https://www.epa.gov/sites/production/files/2016-07/documents/r7\\_mo\\_final\\_designation\\_tsd\\_07012016.pdf](https://www.epa.gov/sites/production/files/2016-07/documents/r7_mo_final_designation_tsd_07012016.pdf).

<sup>10</sup> Montrose, 2018. Labadie Sulfur Reduction Project Quality Assurance Project Plan.

concentrations were found to be 20%-50% higher than the observations for the Baldwin dataset. The 3-year averaged 99<sup>th</sup> percentile daily maximum modeled SO<sub>2</sub> concentrations were 32%-60% higher than the observed concentrations for Labadie. Other statistical measures, such as the robust highest concentration (RHC) and robust 4<sup>th</sup> highest concentration (R4HC) were about 1.5 for Baldwin and between 1.2 and 1.3 for Labadie (with 1.0 being a “perfect” and unbiased model). Therefore, indicating a 20%-50% overprediction tendency by the model.

DISTANCE-DEBUG model output from both databases indicated the dominant plume type for the top ten highest hourly SO<sub>2</sub> modeled concentrations were attributed to the penetrated plume, at each monitoring site. Additional details on the model evaluations for Baldwin and Labadie are provided in **Appendix A, Model Evaluation Results for Baldwin and Labadie**. **Appendix B, Baldwin Table and Plots**, provides DISTANCE-DEBUG data and analysis plots for Baldwin; likewise, **Appendix C, Labadie Tables and Plots**, provides similar data and plots for Labadie.

**Figure 12: Labadie SO<sub>2</sub> and Meteorological Monitoring Network**

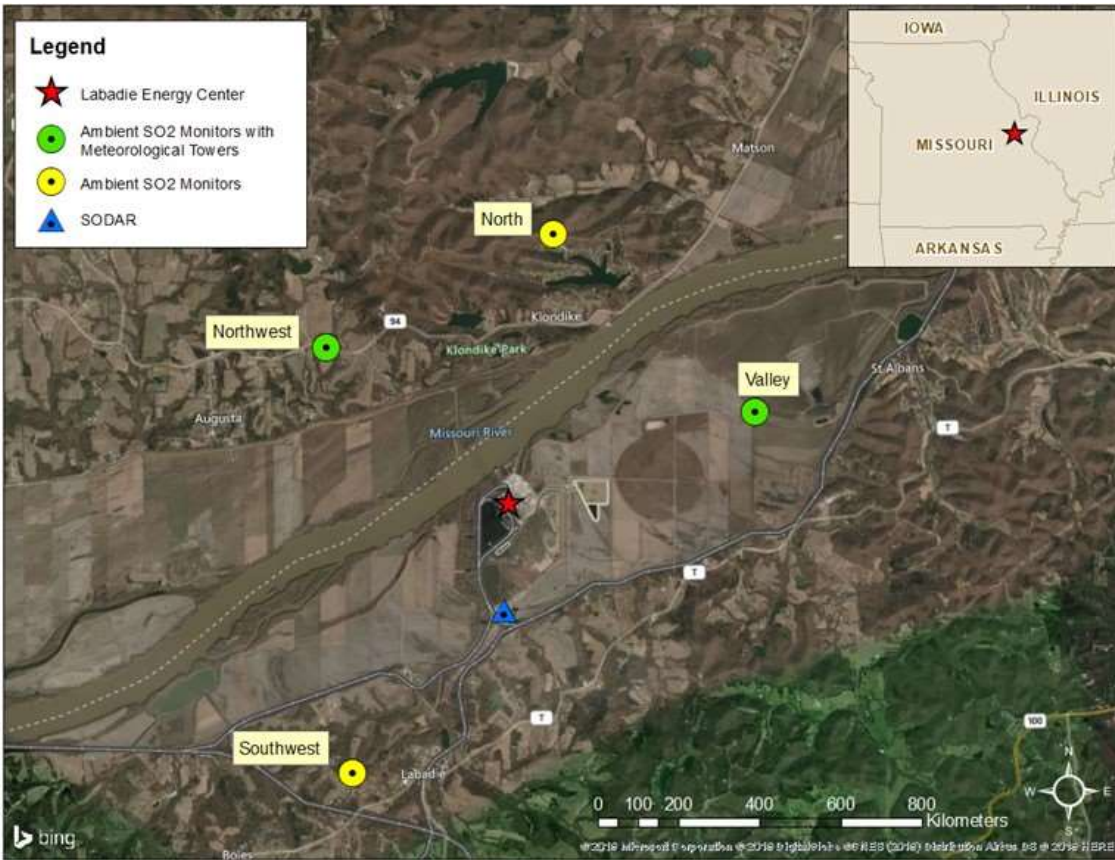


**Figure 13: Google Earth View of the Labadie Energy Center**



## Findings by Other Investigators and Notifications to EPA

The issue of the penetrated plume behavior in AERMOD was first reported by Dr. Ken Rayner of the Western Australia Department of Environment Conservation to Mr. Robert Paine (AECOM), a member of the AERMIC committee that developed AERMOD, in the 2007-2013 period. Dr. Rayner introduced his own debugging code and found<sup>11</sup> that the penetrated plume was the primary component of a 50% overprediction tendency for the Collie Airshed SO<sub>2</sub> impacts at a key monitor (“Shotts”). This information was forwarded to Roger Brode in EPA’s Office of Air Quality Planning and Standards (OAQPS) on June 11, 2014. Mr. Paine followed with a presentation<sup>12</sup> about the penetrated plume issue at the 11<sup>th</sup> EPA Modeling Conference, based upon the Western Australia experience and routine use of the DISTANCE-DEBUG tool to determine the cause of peak prediction issues with AERMOD.

The penetrated plume issue was included in a list of AERMOD areas of scientific formulation research in the AERMOD “white papers” discussion<sup>13</sup> in 2017. This issue was discussed at the 2019 Air & Waste Management Association’s Specialty Modeling Conference<sup>14</sup> in March 2019, at the annual A&WMA conference in June 2019,<sup>15</sup> and also in presentations given at the 12<sup>th</sup> EPA Modeling Conference<sup>16,17</sup> in October 2019. The second of these presentations at the 12<sup>th</sup> EPA Modeling Conference involved new findings with an SO<sub>2</sub> monitoring network near the Ameren Labadie Energy Center in eastern Missouri, as reported by Ken Anderson. Dr. Weil has been working in collaboration with Mr. Paine and Mr. Christopher Warren (AECOM) for an updated evaluation study at a site with 12 monitors located in Western Australia and has helped to refine the approach to better characterize the penetrated plume behavior in an alternative modeling approach described below.

---

<sup>11</sup> Presentation seminar by Dr. Ken Rayner on February 25, 2013: “Review of models for dispersion of tall stack plumes at Collie”; provided to Robert Paine of AECOM on 2/25/2013, and later to Roger Brode of USEPA’s Office of Air Quality Planning and Standards on June 11, 2014; provided as **Attachment 5**.

<sup>12</sup> Paine, R., 2015. “Penetrated Plume Issues”; available at [https://www3.epa.gov/ttn/scram/11thmodconf/presentations/2-4\\_Penetrated\\_Plume\\_Issues.pdf](https://www3.epa.gov/ttn/scram/11thmodconf/presentations/2-4_Penetrated_Plume_Issues.pdf).

<sup>13</sup> Available at [https://www3.epa.gov/ttn/scram/models/aermod/20170919\\_AERMOD\\_Development\\_White\\_Papers.pdf](https://www3.epa.gov/ttn/scram/models/aermod/20170919_AERMOD_Development_White_Papers.pdf).

<sup>14</sup> Warren, C., R. Paine, and J. Connors, 2019. Evaluation of AERMOD SO<sub>2</sub> Predictions for a Research-Grade Field Experiment. Paper MO10, presented at the Air & Waste Management Association specialty conference (Guideline on Air Quality Models: Planning Ahead), March 19-21, 2019. Durham, NC.; provided as **Attachment 6**.

<sup>15</sup> Paine, R., J. Connors, and C. Warren, 2019. Peak Observed and AERMOD-Predicted SO<sub>2</sub> Concentrations in Convective Conditions. Paper #593805, presented at 112th Annual Conference, Air & Waste Management Association, Quebec City, Quebec, Canada.

<sup>16</sup> Paine presentation available at: [ftp://newftp.epa.gov/Air/aqmg/SCRAM/conferences/2019\\_12th\\_Conference\\_On\\_Air\\_Quality\\_Modeling/Presentations/2-14\\_12thMC-penetrated%20plume%20presentation\\_01oct19\\_paine.pdf](ftp://newftp.epa.gov/Air/aqmg/SCRAM/conferences/2019_12th_Conference_On_Air_Quality_Modeling/Presentations/2-14_12thMC-penetrated%20plume%20presentation_01oct19_paine.pdf).

<sup>17</sup> Anderson presentation available at: [ftp://newftp.epa.gov/Air/aqmg/SCRAM/conferences/2019\\_12th\\_Conference\\_On\\_Air\\_Quality\\_Modeling/Presentations/2-15\\_12thMC-Ameren-epa%2012th%20modeling%20conf%202019.pdf](ftp://newftp.epa.gov/Air/aqmg/SCRAM/conferences/2019_12th_Conference_On_Air_Quality_Modeling/Presentations/2-15_12thMC-Ameren-epa%2012th%20modeling%20conf%202019.pdf).

## Proposed Update to AERMOD to Correct Penetrated Plume Issue: HBP modification

A proposed update to AERMOD to address the penetrated plume issue (an approach initially referred to as “HIPMOD” and now referenced as “HBP” for modifications particularly important for “highly buoyant plume”)<sup>18</sup> was prepared for testing in 2020. This revised approach, as illustrated in the flowchart shown in **Figure 14, Flowchart for AERMOD-HBP Treatment**, involves a check on the convective mixing height for the current hour as well as the next hour to determine how much of the penetrated plume has been captured by the CBL by the end of the current hour. This is the first time that AERMOD has been enhanced to look ahead to the next hour in order to improve its performance.

The amount of the penetrated plume mass that is allowed to mix to the ground in the HBP modifications depends upon the result of this calculation. There are three possible outcomes.

Case 1: No penetrated plume impact. If the average of the current and the next hour’s convective mixing height (each value represents the half-hour mark,<sup>19</sup> so the average is roughly at the end of the current hour) is below the bottom of the penetrated plume final height, then no portion of the penetrated plume is assumed to mix into the convective boundary layer. In that case, the contribution of the penetrated plume mass at the receptor is assumed to be zero. The “bottom” of the penetrated plume is 2.15 sigma-z’s below the plume centerline height, where the concentration drops to 10% of that at the plume centerline (with a Gaussian distribution assumed).

Case 2: Full penetrated plume impact. If the mixing height at the end of the current hour is above the top of the penetrated plume, then the full mass of the plume is assumed to reach the ground, and the current AERMOD formulation is used for that hour.

Case 3: Partial penetrated plume impact. For convective mixing heights (by the end of the current hour) that are in between the bottom and top of the penetrated plume, a fraction of the plume mass computed using a vertical Gaussian distribution is assumed to reach the ground using the current AERMOD formulation. For example, the captured fraction is 0.5 if the mixing height at the end of the current hour is exactly at the penetrated plume centerline. If the mixing height at the end of the hour is below (or above) the penetrated plume centerline height, then less (or more) than half of the mass of the penetrated plume will be mixed to the ground.

The approach implemented in the HBP modifications is quite simple, and the resulting plume behavior is consistent to what is seen in research-grade experiments such as EPRI’s Bull Run study in 1982. The

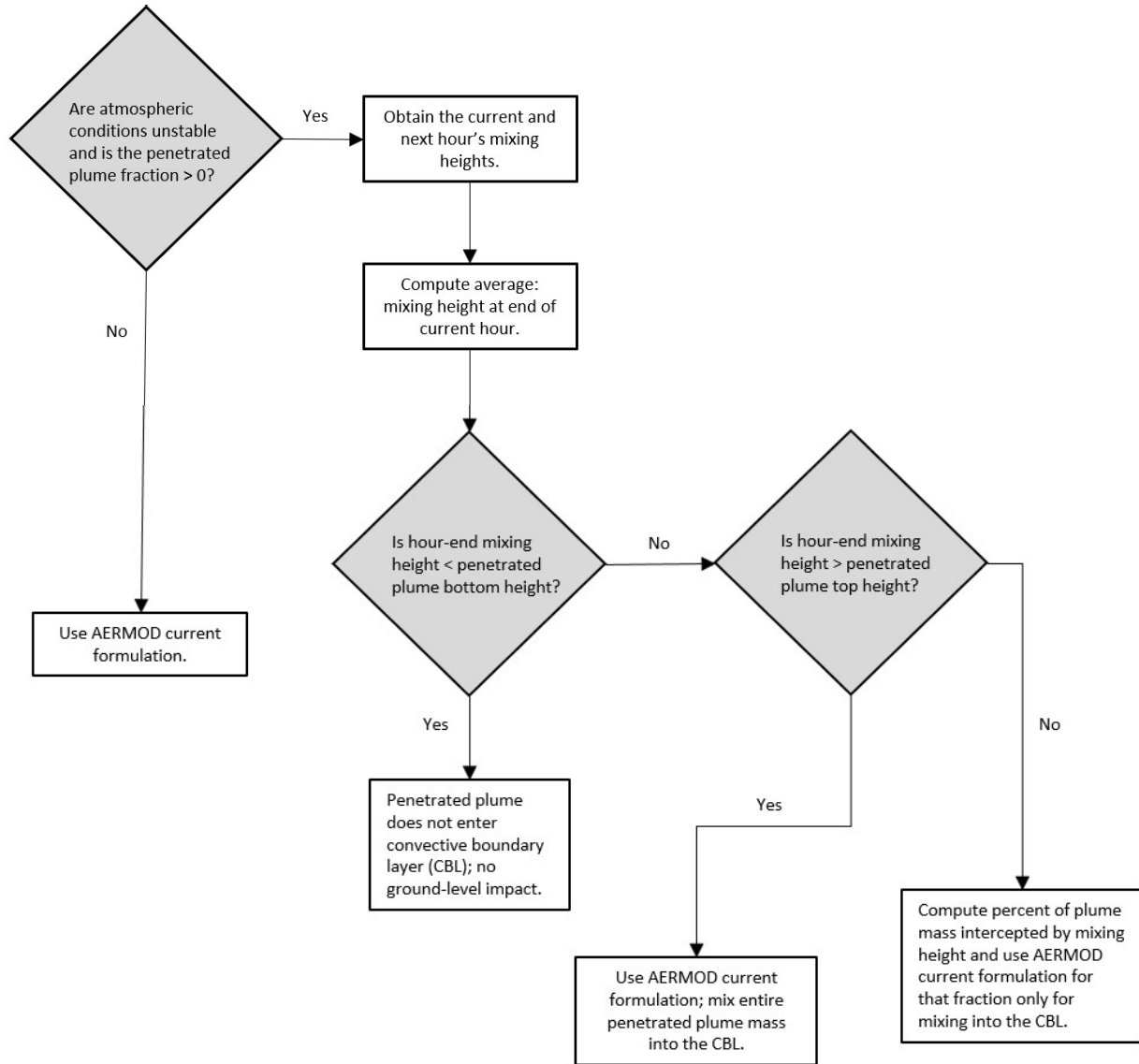
---

<sup>18</sup> The name “HIPMOD” is derived from Dr. Weil’s “Highly-buoyant Plume MODel” designation for this treatment, from his January 2, 2020 report to the Western Australia Department of Environmental Conservation: “New Dispersion Model for Highly-Buoyant Plumes in the Convective Boundary Layer” (included as **Attachment 3**). Although his report involves additional aspects of plume dispersion in the convective boundary layer, the HIPMOD application for AERMOD deals only with the interaction of the penetrated plume as currently coded in AERMOD version 21112 with the convective mixing layer, as described in this document.

<sup>19</sup> The Weil et al. (1997) paper specifically states on page 988 that “Penetrated source material is assumed to be mixed into the CBL [convective boundary layer] only when the growing, time-dependent CBL height > Zi, where Zi is the average mixed layer depth over the hour and is representative of the midpoint of the hour.”

approach also extends AERMOD's capability for dealing with only one hour at a time by enabling it to determine the rate of change for the convective mixing height, with the possibility that the rising mixing height could intercept at least part of the penetrated plume in the current hour. Additionally, the HBP modifications only affect AERMOD during the critical period of the late morning through early afternoon rise of the convective mixing height into the layer containing the penetrated plume; at all other hours, AERMOD-HBP is equivalent to AERMOD run with default options.

**Figure 14: Flowchart for AERMOD-HBP Treatment**



## Appendix A: Model Evaluation Results for Baldwin and Labadie

### Model Databases Reviewed for Penetrated Plume Issues

To demonstrate AERMOD's overprediction tendency associated with penetrated plume events, two SO<sub>2</sub> modeling databases were selected. The first is the 1982-83 Baldwin<sup>1</sup> database from EPA's collection of AERMOD model evaluation databases. The second is a more recent 2017-19 database focusing upon the Labadie Energy Center (Labadie), owned and operated by Ameren Corporation. Both field databases focus upon coal-fired power plants in rural areas, with Baldwin in flat terrain and Labadie surrounding by mostly flat terrain. In both datasets, the largest SO<sub>2</sub> sources are tall stacks.

The Baldwin data set consisted of 1-year of on-site meteorology and ambient SO<sub>2</sub> measurements from 10 nearby monitors (within 2-10 km of the plant). Labadie also contains on-site meteorological data (for a 3-year period) with 4 nearby ambient monitors.

### Model Setup and Evaluation Metrics

Both Baldwin and Labadie datasets were modeled using the regulatory version (19191) of AERMET/AERMOD with default options. Hourly SO<sub>2</sub> concentrations were extracted from the model output, via POSTFILE, and compared against the observed (measured) concentrations at each monitor location.

Quantile-Quantile (Q-Q) plots of the ranked model and observed hourly concentrations were generated for each monitor along with statistical measures of the Robust Highest Concentration (RHC) and Robust 4<sup>th</sup> Highest Concentration (R4HC)<sup>2</sup>.

To assist in identifying the dominant plume type associated with the top 10 modeled concentrations, summary tables from debug output are provided for each monitoring site. Top 10 modeled and observed concentrations are also plotted against wind speed and time of day to show any potential model biases with respect to these variables.

### AERMOD Modeling Results from Baldwin

EPA's Baldwin database was modeled with default AERMOD options. Q-Q plots (ranked model and observed values paired in space) were generated for each of the 10 monitoring sites. As shown in **Figures A-1** through **A-3**, 8 of the 10 sites exhibited model overpredictions at the highest hourly SO<sub>2</sub> concentrations, with four at or above a factor of 2 higher benchmark. For sites 1 through 7 and 9, the top few highest ranked modeled concentrations appear to stand out from the rest of the plot, suggesting a potential anomalous event or unique condition triggering these significant differences.

With the form of the 1-hour daily maximum NAAQS being the 99<sup>th</sup> percentile, the evaluation primarily focuses on this metric. The 99<sup>th</sup> percentile daily maximum modeled and observed values for monitor

<sup>1</sup> EPA, AERMOD Model Evaluation Databases. Available at: <https://www.epa.gov/scram/air-quality-dispersion-modeling-preferred-and-recommended-models>

<sup>2</sup> The Robust Highest Concentration (RHC) is a statistical estimate of the peak concentration from a ranked concentration sample as described by Cox, W. and J. Tikvart, 1990. A statistical procedure for determining the best performing air quality simulation model, *Atmospheric Environment*. Part A. General Topics, Pages 2387-2395, ISSN 0960-1686, [https://doi.org/10.1016/0960-1686\(90\)90331-G](https://doi.org/10.1016/0960-1686(90)90331-G). The "RH4C" is a variation of the RHC in which the concentrations for the top 3 days per year are discarded (consistent with days discarded for 1-hour SO<sub>2</sub> form of the ambient standard), as described by Mark Garrison at the 12<sup>th</sup> EPA modeling conference ([ftp://newftp.epa.gov/Air/aqmg/SCRAM/conferences/2019\\_12th\\_Conference\\_On\\_Air\\_Quality\\_Modeling/Presentations/2-2-2\\_12thMC-Garrison\\_ModelPerformancePanel\\_12thConference\\_03Oct2019.pdf](ftp://newftp.epa.gov/Air/aqmg/SCRAM/conferences/2019_12th_Conference_On_Air_Quality_Modeling/Presentations/2-2-2_12thMC-Garrison_ModelPerformancePanel_12thConference_03Oct2019.pdf)).

are provided in **Table A-1**. The 99<sup>th</sup> percentile daily maximum modeled concentrations are more than 20% higher than the observed at 9 of the 10 monitors, with half of the total monitors exceeding 50%.

**Table A-1: Maximum Daily 99<sup>th</sup> Percentile Concentrations for Baldwin**

Monitor	Model	Observed	Ratio Model/Observed
Site1	1266.6	730.0	1.74
Site2	1140.6	730.0	1.56
Site3	820.1	521.0	1.57
Site4	563.0	597.0	0.94
Site5	982.5	814.0	1.21
Site6	1281.6	851.0	1.51
Site7	1216.0	940.0	1.29
Site8	975.8	678.0	1.44
Site9	1238.9	782.0	1.58
Site10	1022.6	782.0	1.31

Values are in units of  $\mu\text{g}/\text{m}^3$ .

**Table A-2** summarizes the daily maximum RHC (predicted and observed) and ratio of the predicted-to-observed RHCs for each of the 10 monitoring sites. There are 9 sites that yield predicted-to-observed ratios of the RHCs of more 1.3, with 5 being greater than 1.7. Similar overprediction tendencies are seen with the R4HC (focusing on the 4<sup>th</sup> highest concentration to align with the design value of 1-hour SO<sub>2</sub>), as shown in **Table A-3**. The geometric mean across all 10 monitoring sites further showcase the overprediction tendency of this dataset with the default options of AERMOD.

The top 25 highest 1-hour SO<sub>2</sub> hourly concentrations were investigated in more detail to determine under what meteorological conditions, time of day and dominant plume type these high concentrations occur at each monitor. The predicted concentrations were also compared against the observations to evaluate whether the highest modeled and observed values occur under similar conditions.

Overall, AERMOD (with default options) tends to predict the highest concentrations earlier in the day compared to the observations. Modeled top 10 hourly concentrations generally occurred early to late morning (hours ending 09 through 12), while observed high concentrations were predominantly in the late morning to early afternoon. Six of the sites yielded a majority of the top 10 highest predicted concentrations under low wind speed conditions (less than 3 m/s), while the observations were typically higher (between 3 and 6 m/s). AERMOD missed the observed high wind events (greater than 7 m/s) at sites 4, 5 and 6. Top 10 concentration plots versus hour of day and wind speed are provided in **Appendix B (Figures B-1 through B-3)**.

**Table A-1: RHCs for Baldwin with AERMOD**

	Model Scenario	RHC <sub>pre</sub> (µg/m <sup>3</sup> )	RHC <sub>obs</sub> (µg/m <sup>3</sup> )	RHC <sub>pre</sub> /RHC <sub>obs</sub>
Site1	AERMOD (Default)	1884.02	1076.26	1.75
Site2	AERMOD (Default)	1925.66	1088.62	1.77
Site3	AERMOD (Default)	1211.10	882.08	1.37
Site4	AERMOD (Default)	1074.42	1120.76	0.96
Site5	AERMOD (Default)	1722.78	1211.65	1.42
Site6	AERMOD (Default)	2241.36	1282.80	1.75
Site7	AERMOD (Default)	2100.89	1352.74	1.55
Site8	AERMOD (Default)	1682.78	985.77	1.71
Site9	AERMOD (Default)	2158.06	1250.87	1.73
Site10	AERMOD (Default)	1639.98	1245.69	1.32
			Geometric Mean	1.51

**Table A-2: R4HCs for Baldwin with AERMOD**

Monitor	Model Scenario	R4HC <sub>pre</sub> (µg/m <sup>3</sup> )	R4HC <sub>obs</sub> (µg/m <sup>3</sup> )	R4HC <sub>pre</sub> /RHC <sub>obs</sub>
Site1	AERMOD (Default)	1497.30	855.96	1.75
Site2	AERMOD (Default)	1364.83	807.88	1.69
Site3	AERMOD (Default)	867.89	585.35	1.48
Site4	AERMOD (Default)	737.33	730.65	1.01
Site5	AERMOD (Default)	1156.13	969.43	1.19
Site6	AERMOD (Default)	1516.55	1028.13	1.48
Site7	AERMOD (Default)	1545.80	1079.24	1.43
Site8	AERMOD (Default)	1262.85	680.58	1.86
Site9	AERMOD (Default)	1747.99	817.40	2.14
Site10	AERMOD (Default)	1245.64	906.42	1.37
Geometric Mean				1.51

Another key aspect of this model evaluation is assessing the dominant plume type associated with the top 10 highest predicted SO<sub>2</sub> concentration hours. AECOM has developed debugging software that has been added to AERMOD allowing for this sort of detailed analysis to be conducted. **Table A-4** provides a summary of select meteorological parameters from the top 10 highest SO<sub>2</sub> predicted concentrations for Site 1. The maximum estimated mixing height (highest of mechanical and convective) is 476 meters. Except for 2 late afternoon hours (1 at Site 4 and 1 at Site 5), the top 10 highest predicted concentrations occurred with mixing heights less than 900 meters. Tables summarizing the meteorological parameters for the top 10 highest predicted concentrations are included in **Appendix B (Tables B-1 through B-10)**.

The debug file also contains several key source and plume information for each modeled hour. **Table A-5** provides this information for Site 1 (other sites are available in **Appendix B, Tables B-11 through B-20**). For the Baldwin database, there are 3 stacks. Plume height, distance from source, effective wind speed, plume type, meander and penetrated plume fractions, effective sigma-v and sigma-w are some of the key plume information extracted from the debugging software. The plume type helps to quickly and easily identify the dominant plume type associated with each source for a given hour. As shown in **Table A-5**, the dominant plume type associated with the top 10 highest predicted concentrations were all classified as penetrated plumes. **Tables B-11 through B-20** in **Appendix B** indicate the penetrated plume was found to be the predominant plume type across all 10 monitoring sites for the top 10 highest hourly concentrations.

Figure A-1: Q-Q Plots for Baldwin – Sites 1 through 4

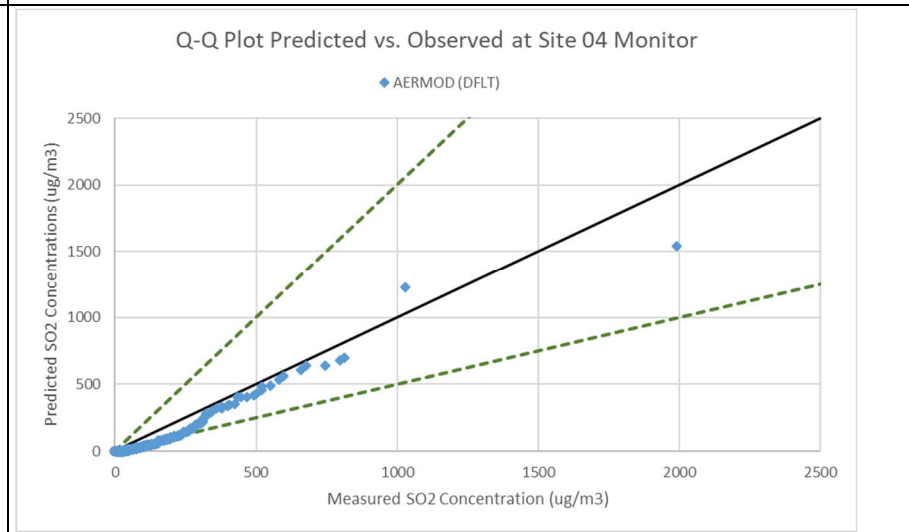
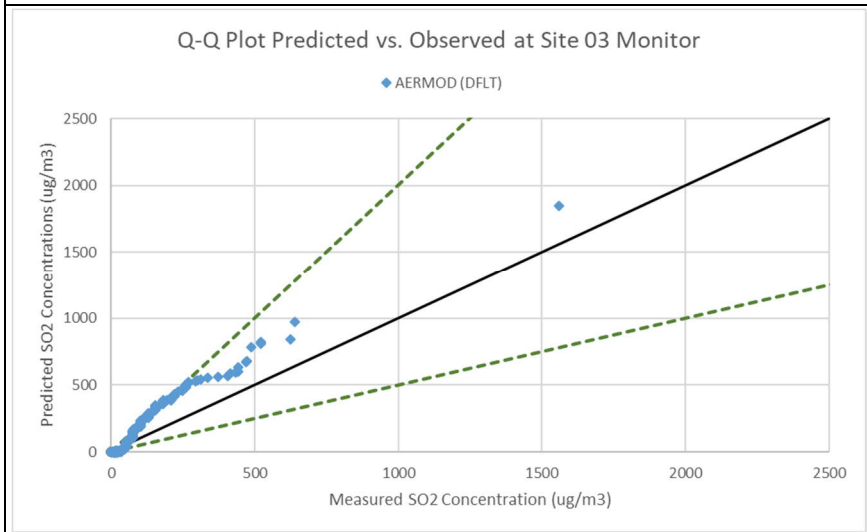
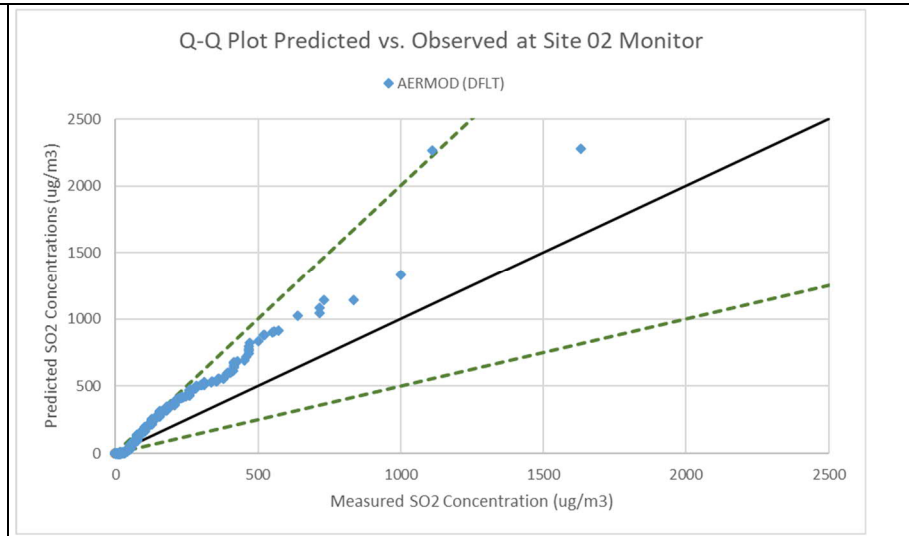
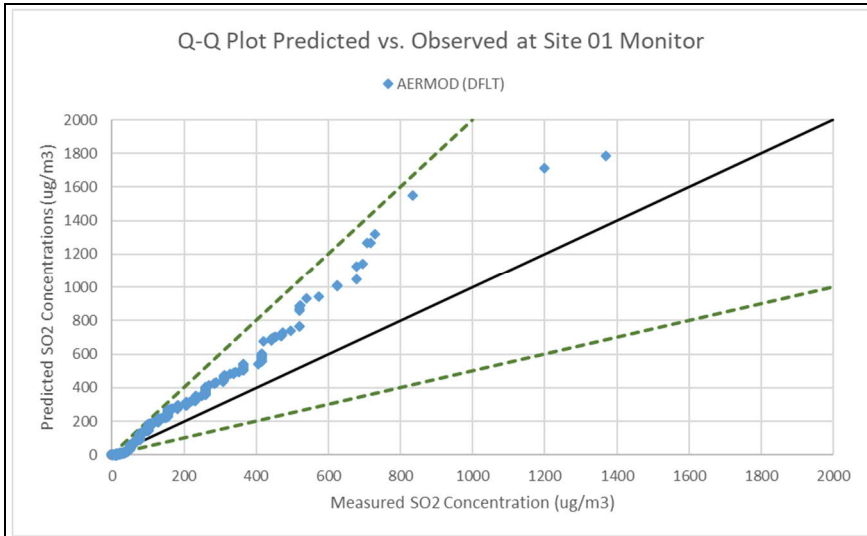
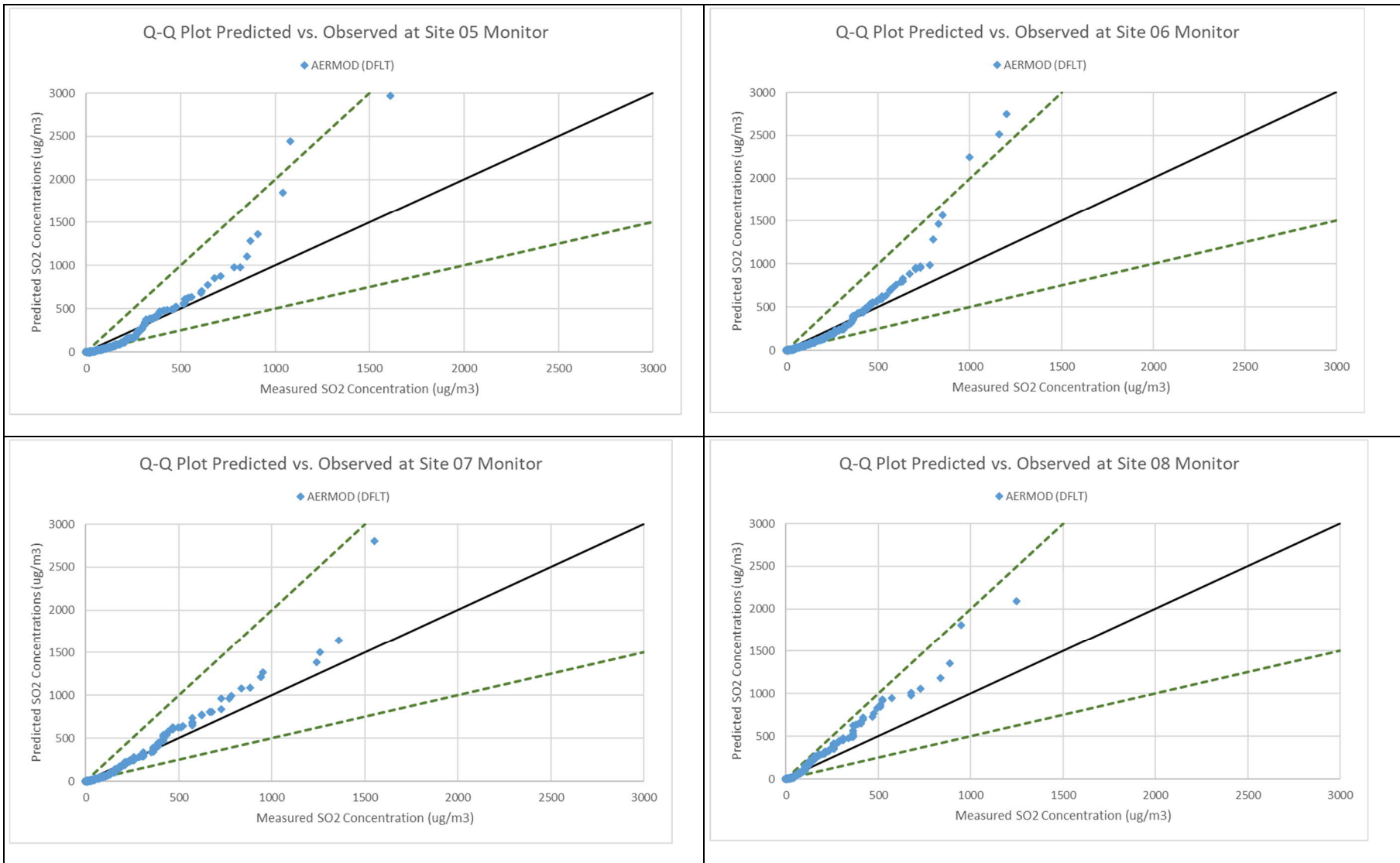
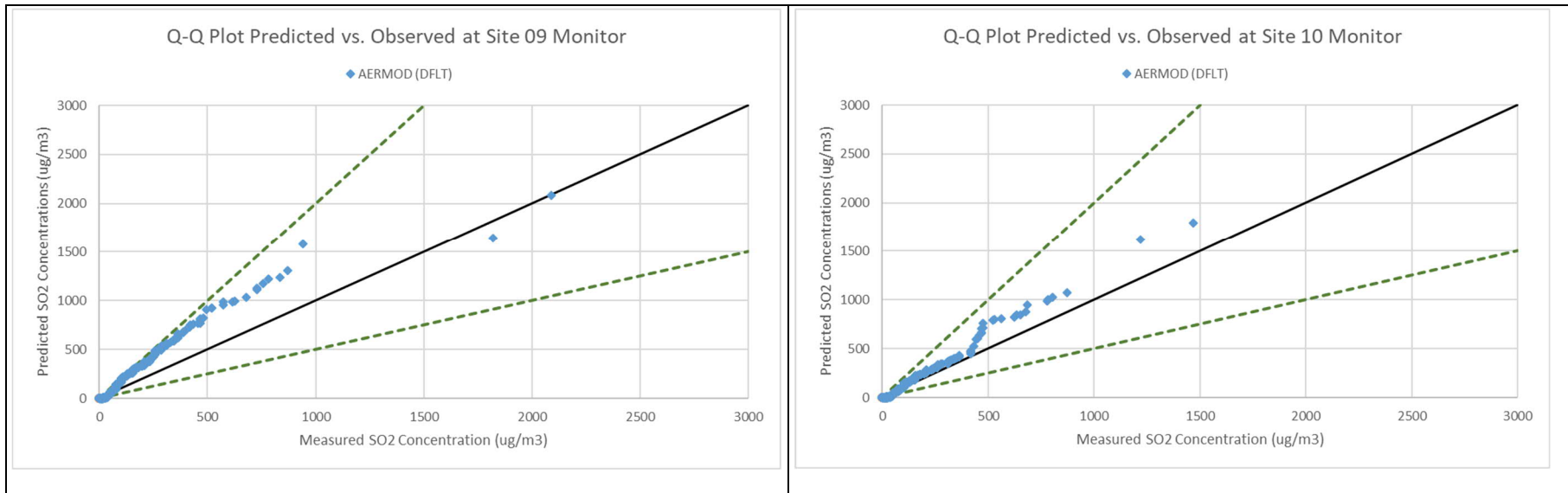


Figure A-1: Q-Q Plots for Baldwin – Sites 5 through 8



**Figure A-2: Q-Q Plots for Baldwin – Sites 9 and 10**



**Table A-3: Meteorological Parameters for Top 10 Highest SO<sub>2</sub> Predicted Concentrations – Baldwin Database Site 1**

Rank	YYMMDDHH	USTAR	WSTAR	OBULEN	URB_OBULEN	ZIMECH	ZICONV	ZI_URB	SFCZ0	THSTAR
1	83010513	0.19	0.62	-24.2	N.A.	205	315	N.A.	0.01	-9.99
2	83011313	0.17	0.61	-14.2	N.A.	165	276	N.A.	0.01	-9.99
3	83010512	0.2	0.58	-28.3	N.A.	219	263	N.A.	0.01	-9.99
4	82070318	0.21	0.67	-30.4	N.A.	238	372	N.A.	0.15	-9.99
5	82043009	0.07	0.6	-1.2	N.A.	48	262	N.A.	0.009	-9.99
6	82062811	0.25	0.83	-28.2	N.A.	303	407	N.A.	0.15	-9.99
7	83021510	0.17	0.9	-4.2	N.A.	166	255	N.A.	0.01	-9.99
8	82070317	0.27	0.75	-38.6	N.A.	333	344	N.A.	0.15	-9.99
9	82071209	0.25	1.02	-17.2	N.A.	296	476	N.A.	0.2	-9.99
10	82071710	0.33	1	-37.4	N.A.	461	403	N.A.	0.15	-9.99

**Table A-4: Source and Plume Details for Top 10 Highest SO<sub>2</sub> Predicted Concentrations – Baldwin Database Site 1**

YYMMDDHH	SOURCE TYPE	SOURCEID	RCPT NO.	FINAL PLUME HT.	DIST. FINAL PL. HT.	WDIR FINAL HT.	EFFECT. WSPD	3600* UEFF	DISTANCE TO RCPT	PLUME TYPE	MEAND. FRAC.	PART. PEN. FRAC.	EFFECT SIGMA_V	EFFECT. SIGMA_W	HOURLY CONC	AERVAL	COHERENT	PANCAKE	GAMFACT	PRMVAL	POT. TEMP. GRAD.
83010513	P	STACK1	1	418.7	1928.4	213	3.473	12502.6	5485.3	PEN	0.062	0.92	0.519	0.363	626.708	626.708	665.602	41.605	0	0	0
83010513	P	STACK2	1	416.6	1898.5	213	3.459	12451.4	5537.9	PEN	0.063	0.913	0.519	0.363	602.005	602.005	639.685	40.874	0.02	602.005	0
83010513	P	STACK3	1	414.3	1864.8	213	3.455	12439.3	5596.5	PEN	0.063	0.905	0.519	0.364	556.216	556.216	591.163	38.545	0.02	556.216	0
83011313	P	STACK1	2	412	1573.3	201	2.804	10092.7	3505.2	PEN	0.072	1	0.482	0.315	753.279	753.279	807.374	52.633	0	0	0
83011313	P	STACK2	2	399.6	1573.3	201	2.795	10060.5	3560.4	PEN	0.072	1	0.482	0.329	765.016	765.016	820.391	52.825	0.386	765.016	0
83011313	P	STACK3	2	414.8	1573.3	201	2.804	10094.6	3621.5	PEN	0.072	1	0.482	0.313	758.92	758.92	813.86	52.027	0.386	758.92	0
83010512	P	STACK1	1	387.4	1933.7	211	4.615	16614.5	5485.3	PEN	0.038	1	0.515	0.304	528.964	528.964	549.044	24.337	0	0	0
83010512	P	STACK2	1	384.7	1901.6	211	4.61	16597.1	5537.9	PEN	0.038	1	0.515	0.308	523.863	523.863	543.835	24.55	0.042	523.863	0
83010512	P	STACK3	1	382.5	1876.8	211	4.605	16578.1	5596.5	PEN	0.039	1	0.515	0.312	498.852	498.852	517.961	23.861	0.042	498.852	0
82070318	P	STACK1	1	508.9	1770.9	214	2.865	10313.2	5485.3	PEN	0.101	0.89	0.567	0.382	464.295	464.295	511.67	41.797	0	0	0
82070318	P	STACK2	1	505.9	1740.6	214	2.852	10268.6	5537.9	PEN	0.102	0.882	0.567	0.385	456.815	456.815	503.88	41.798	0.01	456.815	0
82070318	P	STACK3	1	490.6	1590.2	214	2.799	10078.1	5596.5	PEN	0.106	0.838	0.567	0.392	396.136	396.136	438.599	37.056	0.01	396.136	0
82043009	P	STACK1	1	539.7	957.2	208	1.839	6619.9	5485.3	PEN	0.118	1	0.383	0.144	389.888	389.888	438.297	27.765	0	0	0
82043009	P	STACK2	1	563.9	957.2	208	1.839	6620.9	5537.9	PEN	0.118	1	0.383	0.125	327.896	327.896	368.698	23.446	0.047	327.896	0
82043009	P	STACK3	1	471.2	957.2	208	1.835	6605.1	5596.5	PEN	0.119	1	0.383	0.22	548.835	548.835	617.849	37.797	0.047	548.835	0
82062811	P	STACK1	1	526.7	1811.2	207	3.68	13246.9	5485.3	PEN	0.089	0.777	0.684	0.491	429.667	429.667	468.371	32.839	0	0	0
82062811	P	STACK2	1	517.7	1715	207	3.655	13159.7	5537.9	PEN	0.09	0.748	0.684	0.494	409.642	409.642	447.203	31.114	0.047	409.642	0
82062811	P	STACK3	1	528.7	1832.4	207	3.675	13229.6	5596.5	PEN	0.089	0.784	0.684	0.489	426.833	426.833	465.49	32.31	0.047	426.833	0
83021510	P	STACK1	1	431.6	1514.8	209	4.554	16394.9	5485.3	PEN	0.049	1	0.606	0.366	387.318	387.318	406.14	19.731	0	0	0
83021510	P	STACK2	1	441.5	1514.8	209	4.557	16406.6	5537.9	PEN	0.049	1	0.604	0.349	388.993	388.993	407.876	19.824	0.047	388.993	0
83021510	P	STACK3	1	453.8	1514.8	209	4.56	16417.7	5596.5	PEN	0.049	1	0.603	0.329	366.375	366.375	384.138	18.715	0.047	366.375	0
82070317	P	STACK1	1	451.8	1767.5	213	4.575	16470.5	5485.3	PEN	0.059	0.862	0.672	0.45	398.481	398.481	421.753	26.68	0	0	0
82070317	P	STACK2	1	449.2	1735	213	4.551	16383.9	5537.9	PEN	0.06	0.853	0.672	0.454	390.948	390.948	414.053	26.768	0.02	390.948	0
82070317	P	STACK3	1	433.3	1540.2	213	4.379	15763.9	5596.5	PEN	0.064	0.792	0.672	0.466	337.041	337.041	358.493	23.954	0.02	337.041	0
82071209	P	STACK1	2	585.6	1559.5	209	2.614	9411.6	3505.2	PEN	0.189	0.644	0.756	0.594	408.76	408.76	490.752	56.056	0	0	0
82071209	P	STACK2	2	581.1	1559.5	209	2.613	9407.7	3560.4	PEN	0.189	0.628	0.756	0.596	390.61	390.61	469.306	53.927	0.192	390.61	0
82071209	P	STACK3	2	568.3	1537.9	209	2.61	9396.3	3621.5	PEN	0.191	0.581	0.758	0.602	341.184	341.184	410.801	47.247	0.193	341.184	0
82071710	P	STACK1	1	544.2	1753.2	205	4.796	17264.4	5485.3	PEN	0.077	0.564	0.788	0.573	337.281	337.281	363.318	25.104	0	0	0
82071710	P	STACK2	1	542.4	1730.8	205	4.788	17238.4	5537.9	PEN	0.077	0.556	0.789	0.576	341.154	341.154	367.709	25.041	0.028	341.154	0
82071710	P	STACK3	1	539.9	1698.7	205	4.777	17198.5	5596.5	PEN	0.078	0.545	0.791	0.581	333.072	333.072	359.273	24.15	0.028	333.072	0

## AERMOD Modeling Results from Labadie

The Labadie modeling database was also run with default AERMOD options. Q-Q plots (ranked model and observed values paired in space) were generated for each of the 4 monitoring sites. As shown in **Figure A-4**, 3 of the 4 sites exhibited model overpredictions at the highest hourly SO<sub>2</sub> concentrations.

With the form of the 1-hour daily maximum NAAQS being the 99<sup>th</sup> percentile, the evaluation primarily focuses on this metric. The 99<sup>th</sup> percentile daily maximum modeled and observed values for each year and 3-year average are provided in **Table A-6**. The 3-year averaged modeled concentrations are more than 60% higher than the observed at 3 of the 4 monitors, while the North monitor is 32% higher for the model versus the observed.

**Table 0-5: Maximum Daily 99<sup>th</sup> Percentile Concentrations for Labadie**

Year	Valley		NW		SW		North	
	Model	Observed	Model	Observed	Model	Observed	Model	Observed
2017	110.38	54.97	77.69	54.97	103.43	57.59	106.80	78.53
2018	94.73	99.47	80.96	44.50	99.11	52.35	97.84	57.59
2019	128.50	47.12	92.48	49.73	104.22	78.53	99.88	94.23
3-year Average	111.21	67.18	83.71	49.73	102.25	62.82	101.51	76.78

Values are in units of µg/m<sup>3</sup>.

**Table A-7** summarizes the daily maximum RHC (predicted and observed) and ratio of the predicted-to-observed RHCs for each of the 4 monitoring sites, using daily maximum predicted and observed concentrations. Two sites have predicted-to-observed ratios of the RHCs of more than 1.2, while a third is above 1.15. Similar overprediction tendencies are seen with the R4HC (focusing on the 4<sup>th</sup> highest concentration to align with the design value of 1-hour SO<sub>2</sub>), as shown in **Table A-8**. The geometric mean across all 4 monitoring sites further showcase an overprediction tendency of this dataset with the default options of AERMOD.

The top 25 highest hourly SO<sub>2</sub> concentrations were investigated in more detail to determine under what meteorological conditions, time of day and dominant plume type these high concentrations occur at each monitor. The predicted concentrations were also compared against the observations to evaluate whether the highest modeled and observed values occur under similar conditions.

Overall, AERMOD (with default options) tends to predict the highest concentrations earlier in the day compared to the observations. Modeled top 10 hourly concentrations generally occurred early to late morning (hours ending 09 through 12), while observed high concentrations were predominantly in the late morning to early afternoon. This behavioral pattern is identical to that observed in the Baldwin database. All four of the sites had all (or almost all) of the top 10 highest predicted concentrations under low wind speed conditions (less than 3 m/s), while the observations ranged from less than 2 m/s up to 4.5 m/s. Top 10 hourly concentration plots versus hour of day and wind speed are provided in **Appendix C (Figure C-1)**.

**Table A-6: Maximum Daily RHCs for Labadie with AERMOD**

Monitor	Model Scenario	RHC <sub>pre</sub> (µg/m <sup>3</sup> )	RHC <sub>obs</sub> (µg/m <sup>3</sup> )	RHC <sub>pre</sub> /RHC <sub>obs</sub>
Valley	AERMOD (Default)	198.50	147.97	1.34
NW	AERMOD (Default)	132.51	138.00	0.96
SW	AERMOD (Default)	165.42	133.68	1.24
North	AERMOD (Default)	184.21	137.91	1.34
Geometric Mean				1.21

**Table A-7: Maximum Daily R4HCs for Labadie with AERMOD**

Monitor	Model Scenario	R4HC <sub>pre</sub> (µg/m <sup>3</sup> )	R4HC <sub>obs</sub> (µg/m <sup>3</sup> )	R4HC <sub>pre</sub> /R4HC <sub>obs</sub>
Valley	AERMOD (Default)	169.87	118.21	1.44
NW	AERMOD (Default)	108.37	94.86	1.14
SW	AERMOD (Default)	146.20	98.51	1.48
North	AERMOD (Default)	147.99	113.89	1.30
Geometric Mean				1.33

**Table A-9** provides a summary of select meteorological parameters from the top 10 highest SO<sub>2</sub> predicted concentrations for the Valley monitoring site. The maximum estimated mixing height (highest of mechanical and convective) is 575 meters. At all 4 monitoring receptors, the highest mixing height value from the top 10 highest concentrations was 776 meters. Tables summarizing the meteorological parameters for the top 10 highest predicted concentrations are included in **Appendix C (Tables C-1 through C-4)**.

**Table A-10** provides modeled source and plume information for the Valley monitor (other sites are available in **Appendix C**). For the Labadie database, there are 4 stacks. Plume height, distance from source, effective wind speed, plume type, meander and penetrated plume fractions, effective sigma-v and sigma-w are some of the key plume information extracted from the debugging software. The plume type helps to quickly and easily identify the dominant plume type associated with each source for a given hour. As shown in **Table A-10**, the dominant plume type associated with the top 10 highest predicted concentrations were all classified as penetrated plumes, for the tall stack sources (Labadie1, Labadie2 and Lab34 stacks). The shorter, Labadie5, stack ended up being direct or indirect plume type, which is expected given its lower release height. **Tables C-5 through C-8 in Appendix C** indicate the penetrated plume was found to be the predominant plume type across all 4 Labadie monitoring sites for the top 10 highest concentrations.

Figure A-3: Q-Q Plots for Labadie – (a) Valley, (b) Northwest, (c) Southwest and (d) North Monitoring Sites

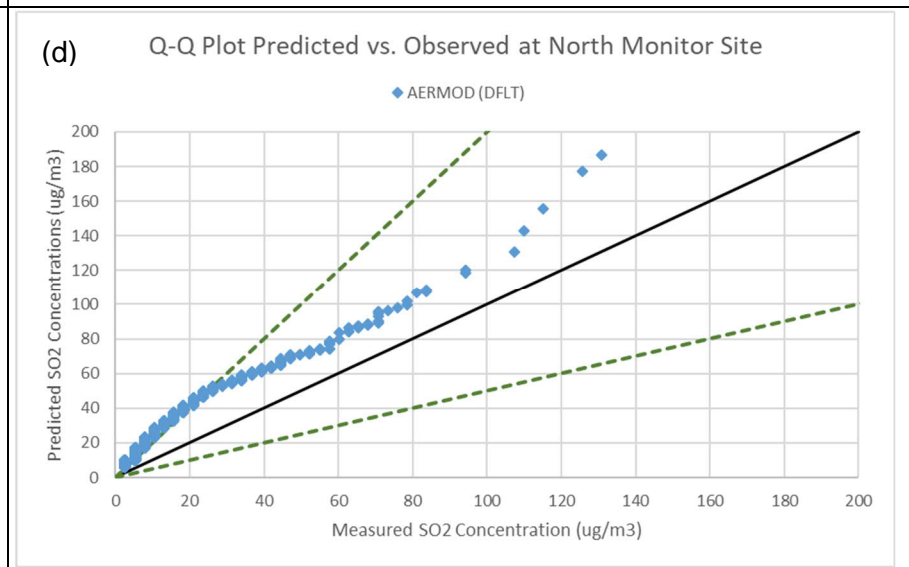
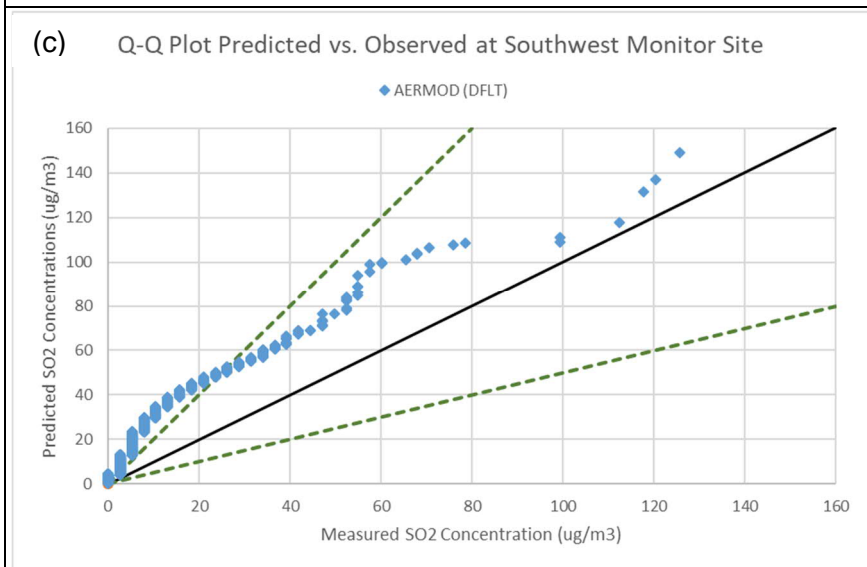
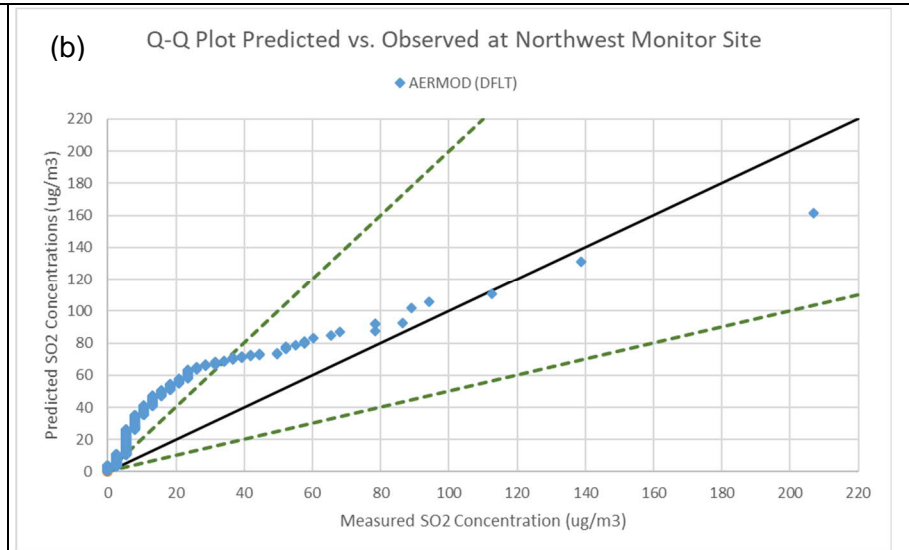
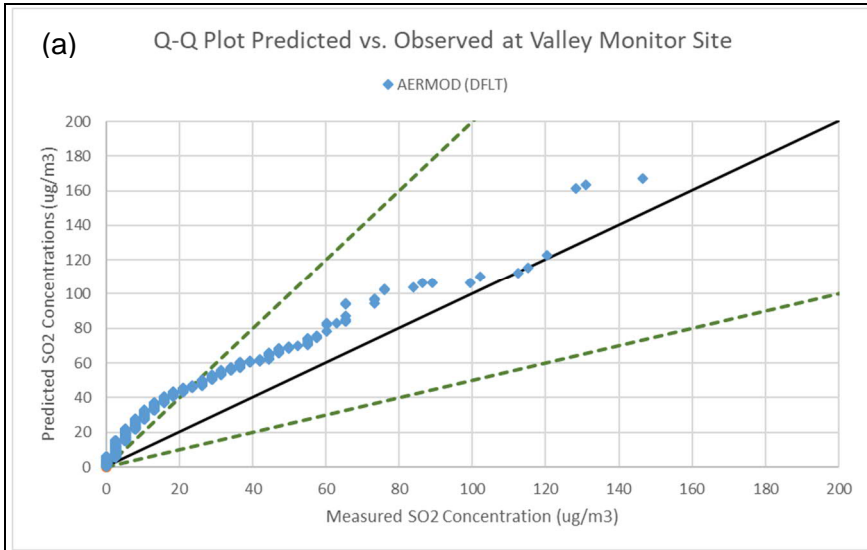


**Table A-8: Meteorological Parameters for Top 10 Highest SO<sub>2</sub> Predicted Concentrations – Labadie Database Valley Monitor**

Rank	YYMMDDHH	USTAR	WSTAR	OBULEN	URB_OBULEN	ZIMECH	ZICONV	ZI_URB	SFCZO	THSTAR
1	18121013	0.22	1.06	-7.8	N.A.	244	361	N.A.	0.03	-9.99
2	17090210	0.17	1.44	-2.5	N.A.	174	575	N.A.	0.2	-9.99
3	18060610	0.22	1.17	-7.2	N.A.	252	420	N.A.	0.2	-9.99
4	17060511	0.19	1.23	-4.3	N.A.	203	450	N.A.	0.2	-9.99
5	18121016	0.16	0.52	-31	N.A.	161	434	N.A.	0.03	-9.99
6	17092910	0.25	1.26	-9.3	N.A.	301	473	N.A.	0.2	-9.99
7	17051109	0.07	0.6	-1.5	N.A.	49	310	N.A.	0.04	-9.99
8	17050910	0.33	1.1	-24.5	N.A.	460	357	N.A.	0.04	-9.99
9	17051012	0.21	1.22	-5.3	N.A.	231	417	N.A.	0.04	-9.99
10	18060609	0.17	0.95	-4.4	N.A.	171	299	N.A.	0.2	-9.99

**Table A-9: Source and Plume Details for Top 10 Highest SO<sub>2</sub> Predicted Concentrations – Baldwin Database Valley Monitor**

YYMMDDHH	SOURCE TYPE	SOURCE ID	RCPT NO.	FINAL PLUME HT.	DIST. FINAL PL. HT.	WDIR FINAL HT.	EFFECT. WSPD	3600* UEFF	DISTANCETO RCPT	PLUMETYPE	MEAND. FRAC.	PART. PEN. FRAC.	EFFECT SIGMA_V	EFFECT. SIGMA_W	HOURLY CONC	AERVAL	COHERENT	PANCAKE	GAMFACT	PRMVAL	POT. TEMP. GRAD.
18121013	P	LAB34	1	475.3	1483.8	245	2.522	9079.9	3724.9	PEN	0.174	0.911	0.711	0.453	53.331	53.331	63.14	6.767	0.3	53.331	0
18121013	P	LABADIE1	1	467.9	1483.8	245	2.524	9086	3765.4	PEN	0.175	0.887	0.712	0.457	50.644	50.644	59.945	6.732	0.286	50.644	0
18121013	P	LABADIE2	1	475.5	1483.8	245	2.522	9079.7	3747.2	PEN	0.174	0.912	0.71	0.453	54.016	54.016	63.917	7.041	0.293	54.016	0
18121013	P	LABADIE5	1	18.8	52.2	241	2.488	8957.8	3723	DIR	0.185	0.001	0.727	0.499	0	0	0	0	0	0	0
17090210	P	LAB34	1	698.9	1073	245	1.489	5360.2	3724.9	PEN	0.433	0.61	0.594	0.587	80.84	80.84	126.836	20.557	0.214	80.84	0
17090210	P	LABADIE1	1	1380.1	1073	245	1.433	5157.1	3765.4	IND	0.492	0.405	0.613	0.633	36.269	36.269	61.533	10.209	0.183	36.269	0
17090210	P	LABADIE2	1	1446	1073	245	1.433	5157.1	3747.2	IND	0.483	0.441	0.613	0.633	41.596	41.596	69.69	11.484	0.197	41.596	0
17090210	P	LABADIE5	1	33.6	51.2	285	1.154	4155.6	3723	DIR	0.581	0	0.613	0.606	0	0	0	0	0	0	0
18060610	P	LAB34	1	596.3	852.4	236	1.537	5534.1	3724.9	PEN	0.457	0.946	0.704	0.493	74.976	74.976	118.695	22.934	0.004	74.976	0
18060610	P	LABADIE1	1	537.3	852.4	236	1.506	5422.7	3765.4	PEN	0.539	0.797	0.717	0.523	40.048	40.048	70.078	14.399	0.004	40.048	0
18060610	P	LABADIE2	1	541.6	852.4	236	1.508	5430.3	3747.2	PEN	0.533	0.811	0.716	0.521	41.303	41.303	71.865	14.479	0.004	41.303	0
18060610	P	LABADIE5	3	24.6	50.8	3	1.105	3977.3	4310.6	DIR	0.896	0.001	0.737	0.587	0	0	0	0	0	0	0
17060511	P	LAB34	1	746.9	1017.3	244	1.659	5973.9	3724.9	PEN	0.305	1	0.629	0.358	51.545	51.545	69.748	10.15	0.314	51.545	0
17060511	P	LABADIE1	1	645.1	1017.3	244	1.617	5819.6	3765.4	PEN	0.378	0.934	0.68	0.484	33.33	33.33	48.858	7.834	0.314	33.33	0
17060511	P	LABADIE2	1	647.8	1017.3	244	1.621	5834.3	3747.2	PEN	0.375	0.938	0.679	0.482	32.834	32.834	47.981	7.584	0.314	32.834	0
17060511	P	LABADIE5	1	28.6	50.8	244	1.493	5373.7	3723	DIR	0.482	0.002	0.722	0.549	0	0	0	0	0	0	0
18121016	P	LAB34	1	554.9	2020.9	255	1.579	5685.7	3724.9	PEN	0.18	0.784	0.457	0.205	35.476	35.476	42.22	4.708	0.458	35.476	0
18121016	P	LABADIE1	1	546.5	1921.8	255	1.585	5707.2	3765.4	PEN	0.178	0.757	0.457	0.209	36.478	36.478	43.371	4.601	0.452	36.478	0
18121016	P	LABADIE2	1	555.5	2027.6	255	1.579	5685.6	3747.2	PEN	0.18	0.786	0.457	0.205	37.164	37.164	44.27	4.795	0.455	37.164	0
18121016	P	LABADIE5	1	20.9	52.1	257	1.835	6607.5	3723	DIR	0.144	0.001	0.457	0.236	0	0	0	0	0	0	0
17092910	P	LAB34	1	688.8	1884.2	252	2.829	10183.8	3724.9	PEN	0.113	0.937	0.611	0.382	41.079	41.079	45.79	4.026	0.462	41.079	0
17092910	P	LABADIE1	1	608.3	1830.9	252	2.709	9753.1	3765.4	PEN	0.144	0.766	0.644	0.461	34.87	34.87	40.12	3.755	0.46	34.87	0
17092910	P	LABADIE2	1	604.4	1794.1	252	2.7	9720.6	3747.2	PEN	0.146	0.755	0.645	0.464	31.703	31.703	36.536	3.442	0.461	31.703	0
17092910	P	LABADIE5	2	22.3	51.2	217	2.202	7928.1	3346.3	DIR	0.192	0.001	0.669	0.504	0	0	0	0	0	0	0
17051109	P	LAB34	1	688.7	506.5	263	0.755	2719.6	3724.9	PEN	0.542	1	0.384	0.08	20.977	20.977	37.088	7.382	0.019	20.977	0
17051109	P	LABADIE1	1	606.4	506.5	263	0.755	2718.6	3765.4	PEN	0.543	1	0.384	0.149	44.909	44.909	81.805	13.858	0.018	44.909	0
17051109	P	LABADIE2	1	616.6	506.5	263	0.755	2719	3747.2	PEN	0.543	1	0.384	0.137	40.569	40.569	73.419	12.891	0.018	40.569	0
17051109	P	LABADIE5	1	46.2	51.2	263	0.615	2214.9	3723	IND	0.625	0.005	0.384	0.253	0	0	0	0	0	0	0
17050910	P	LAB34	1	534.8	1944.4	250	4.253	15309.5	3724.9	PEN	0.12	0.566	0.784	0.498	37.365	37.365	42.009	3.468	0.461	37.365	0
17050910	P	LABADIE1	1	533.2	1919.5	250	4.251	15303.4	3765.4	PEN	0.122	0.559	0.786	0.504	31.369	31.369	35.303	2.946	0.461	31.369	0
17050910	P	LABADIE2	1	523.5	1767.4	250	4.244	15280	3747.2	PEN	0.127	0.51	0.793	0.527	32.155	32.155	36.396	3.035	0.461	32.155	0
17050910	P	LABADIE5	1	15	50.9	258	3.086	11108.6	3723	DIR	0.177	0	0.887	0.733	0	0	0	0	0	0	0
17051012	P	LAB34	1	574.4	1644.6	244	4.533	16319.3	3724.9	PEN	0.08	0.911	0.771	0.624	39.664	39.664	42.79	3.631	0.354	39.664	0
17051012	P	LABADIE1	1	535.4	1644.6	244	4.134	14882.3	3765.4	PEN	0.108	0.806	0.793	0.68	30.389	30.389	33.666	3.454	0.339	30.389	0
17051012	P	LABADIE2	1	537.6	1644.6	244	4.16	14975.6	3747.2	PEN	0.107	0.813	0.792	0.676	32.549	32.549	36.012	3.504	0.344	32.549	0
17051012	P	LABADIE5	4	19.8	50.7	200	2.613	9407.9	3858.4	DIR	0.193	0.001	0.825	0.729	0	0	0	0	0	0	0
18060609	P	LAB34	3	706.4	336.4	68	0.532	1914.4	4312.9	PEN	1	1	0.6	0.098	40.85	40.85	65.308	40.85	PLUME OUT	OF WAKE	0
18060609	P	LABADIE1	2	598.5	336.4	68	0.542	1951.6	3203.1	PEN	1	1	0.612	0.207	36.971	36.971	7.96	36.971	PLUME OUT	OF WAKE	0
18060609	P	LABADIE2	2	605.7	336.4	68	0.539	1941.4	3259	PEN	1	1	0.611	0.195	36.188	36.188	6.502	36.188	PLUME OUT	OF WAKE	0
18060609	P	LABADIE5	2	31.1	50.9	39	0.689	2479.1	3346.3	DIR	1	0.002	0.652	0.488	0	0	0	0	0	0	0

## Key Findings and Conclusions from Baldwin and Labadie Review

A model evaluation analysis conducted on the Baldwin and Labadie databases highlight an apparent issue with AERMOD's treatment of the penetrated plume. For early morning hours, prior to the mixing height rising and intercepting a plume located in the stable layer aloft, the plume is being mixed to the ground resulting in higher than observed ground-level concentrations. In addition to the high prediction concentrations, a peak predicted impact that is 2-3 hours earlier than the timing of higher observed concentrations is also evident in both databases.

There appears to be an apparent model bias toward early to late morning hours under low wind (less than 3 m/s) conditions when the estimated-modeled mixing height is generally less than 600-800 meters. The RHC and R4HC statistics of the top 25 concentrations also indicate an overprediction tendency with AERMOD.

AECOM's debugging software helped to identify the dominant plume type associated with the modeled-overprediction events to be the penetrated plume. This situation has been captured in other database AECOM has reviewed and as a result, has helped in the development of an approach to address this issue in AERMOD.

The purpose of these model evaluations was to highlight the issue with the treatment of the penetrated plume occurs in multiple modeling databases and not unique to just Martin Lake. Both Baldwin and Labadie provide excellent insight into this issue given the on-site data, the multiple monitors, and the hourly measurements collected.

# Appendix B: Baldwin Tables and Plots

**Table B-1: Meteorological Parameters for Top 10 Highest SO<sub>2</sub> Predicted Concentrations – Baldwin Database Site 1**

Rank	YYMMDDHH	USTAR	WSTAR	OBULEN	URB_OBULEN	ZIMECH	ZICONV	ZI_URB	SFCZ0	THSTAR
1	83010513	0.19	0.62	-24.2	N.A.	205	315	N.A.	0.01	-9.99
2	83011313	0.17	0.61	-14.2	N.A.	165	276	N.A.	0.01	-9.99
3	83010512	0.2	0.58	-28.3	N.A.	219	263	N.A.	0.01	-9.99
4	82070318	0.21	0.67	-30.4	N.A.	238	372	N.A.	0.15	-9.99
5	82043009	0.07	0.6	-1.2	N.A.	48	262	N.A.	0.009	-9.99
6	82062811	0.25	0.83	-28.2	N.A.	303	407	N.A.	0.15	-9.99
7	83021510	0.17	0.9	-4.2	N.A.	166	255	N.A.	0.01	-9.99
8	82070317	0.27	0.75	-38.6	N.A.	333	344	N.A.	0.15	-9.99
9	82071209	0.25	1.02	-17.2	N.A.	296	476	N.A.	0.2	-9.99
10	82071710	0.33	1	-37.4	N.A.	461	403	N.A.	0.15	-9.99

**Table B-2: Meteorological Parameters for Top 10 Highest SO<sub>2</sub> Predicted Concentrations – Baldwin Database Site 2**

Rank	YYMMDDHH	USTAR	WSTAR	OBULEN	URB_OBULEN	ZIMECH	ZICONV	ZI_URB	SFCZ0	THSTAR
1	83011313	0.17	0.61	-14.2	N.A.	165	276	N.A.	0.01	-9.99
2	83031212	0.08	0.51	-3.8	N.A.	54	404	N.A.	0.009	-9.99
3	82062810	0.24	0.89	-19.1	N.A.	290	373	N.A.	0.2	-9.99
4	83011314	0.16	0.61	-15.1	N.A.	160	313	N.A.	0.01	-9.99
5	82071209	0.25	1.02	-17.2	N.A.	296	476	N.A.	0.2	-9.99
6	83021512	0.14	0.87	-5.7	N.A.	126	548	N.A.	0.01	-9.99
7	82053113	0.1	0.68	-4	N.A.	79	474	N.A.	0.03	-9.99
8	82062811	0.25	0.83	-28.2	N.A.	303	407	N.A.	0.15	-9.99
9	82083113	0.26	0.98	-21.2	N.A.	316	458	N.A.	0.2	-9.99
10	82061709	0.32	1	-39.4	N.A.	427	507	N.A.	0.15	-9.99

**Table B-3: Meteorological Parameters for Top 10 Highest SO<sub>2</sub> Predicted Concentrations – Baldwin Database Site 3**

Rank	YYMMDDHH	USTAR	WSTAR	OBULEN	URB_OBULEN	ZIMECH	ZICONV	ZI_URB	SFCZO	THSTAR
1	83031212	0.08	0.51	-3.8	N.A.	54	404	N.A.	0.009	-9.99
2	83021413	0.13	1.46	-1.1	N.A.	116	571	N.A.	0.01	-9.99
3	82080612	0.18	0.84	-8.6	N.A.	181	366	N.A.	0.2	-9.99
4	82071209	0.25	1.02	-17.2	N.A.	296	476	N.A.	0.2	-9.99
5	82053113	0.1	0.68	-4	N.A.	79	474	N.A.	0.03	-9.99
6	83021513	0.17	1.39	-3.3	N.A.	173	685	N.A.	0.01	-9.99
7	82072609	0.2	0.89	-9.8	N.A.	209	367	N.A.	0.19	-9.99
8	83021514	0.18	1.5	-3.7	N.A.	189	821	N.A.	0.01	-9.99
9	83020416	0.11	0.98	-2.1	N.A.	87	603	N.A.	0.01	-9.99
10	83021512	0.14	0.87	-5.7	N.A.	126	548	N.A.	0.01	-9.99

**Table B-4: Meteorological Parameters for Top 10 Highest SO<sub>2</sub> Predicted Concentrations – Baldwin Database Site 4**

Rank	YYMMDDHH	USTAR	WSTAR	OBULEN	URB_OBULEN	ZIMECH	ZICONV	ZI_URB	SFCZO	THSTAR
1	83020712	0.13	0.92	-2.4	N.A.	110	349	N.A.	0.003	-9.99
2	83020711	0.15	0.83	-4.7	N.A.	142	306	N.A.	0.003	-9.99
3	83020414	0.11	1.07	-1.6	N.A.	87	589	N.A.	0.003	-9.99
4	83010715	0.08	0.63	-2.3	N.A.	50	511	N.A.	0.003	-9.99
5	83020415	0.11	0.95	-2.3	N.A.	88	598	N.A.	0.003	-9.99
6	83010712	0.12	0.92	-2.5	N.A.	102	442	N.A.	0.01	-9.99
7	83020416	0.11	0.98	-2.1	N.A.	87	603	N.A.	0.01	-9.99
8	82090411	0.12	0.99	-2.8	N.A.	104	560	N.A.	0.06	-9.99
9	82072609	0.2	0.89	-9.8	N.A.	209	367	N.A.	0.19	-9.99
10	82080815	0.21	1.16	-16.8	N.A.	232	1128	N.A.	0.06	-9.99

**Table B-5: Meteorological Parameters for Top 10 Highest SO<sub>2</sub> Predicted Concentrations – Baldwin Database Site 5**

Rank	YYMMDDHH	USTAR	WSTAR	OBULEN	URB_OBULEN	ZIMECH	ZICONV	ZI_URB	SFCZO	THSTAR
1	83020711	0.15	0.83	-4.7	N.A.	142	306	N.A.	0.003	-9.99
2	83020712	0.13	0.92	-2.4	N.A.	110	349	N.A.	0.003	-9.99
3	83020710	0.17	0.69	-9.3	N.A.	164	265	N.A.	0.003	-9.99
4	83010712	0.12	0.92	-2.5	N.A.	102	442	N.A.	0.01	-9.99
5	83031211	0.11	0.46	-11.6	N.A.	88	336	N.A.	0.009	-9.99
6	83020713	0.14	0.97	-3.2	N.A.	131	394	N.A.	0.003	-9.99
7	82040315	0.57	1.23	-338	N.A.	1027	1375	N.A.	0.009	-9.99
8	82082317	0.12	0.53	-10.8	N.A.	102	385	N.A.	0.06	-9.99
9	83020414	0.11	1.07	-1.6	N.A.	87	589	N.A.	0.003	-9.99
10	83020415	0.11	0.95	-2.3	N.A.	88	598	N.A.	0.003	-9.99

**Table B-6: Meteorological Parameters for Top 10 Highest SO<sub>2</sub> Predicted Concentrations – Baldwin Database Site 6**

Rank	YYMMDDHH	USTAR	WSTAR	OBULEN	URB_OBULEN	ZIMECH	ZICONV	ZI_URB	SFCZO	THSTAR
1	83031211	0.11	0.46	-11.6	N.A.	88	336	N.A.	0.009	-9.99
2	83020710	0.17	0.69	-9.3	N.A.	164	265	N.A.	0.003	-9.99
3	83020711	0.15	0.83	-4.7	N.A.	142	306	N.A.	0.003	-9.99
4	83020712	0.13	0.92	-2.4	N.A.	110	349	N.A.	0.003	-9.99
5	82082317	0.12	0.53	-10.8	N.A.	102	385	N.A.	0.06	-9.99
6	82083013	0.2	0.74	-16.3	N.A.	219	321	N.A.	0.06	-9.99
7	83010715	0.08	0.63	-2.3	N.A.	50	511	N.A.	0.003	-9.99
8	83020415	0.11	0.95	-2.3	N.A.	88	598	N.A.	0.003	-9.99
9	82040516	0.61	0.39	-2661.2	N.A.	1153	279	N.A.	0.009	-9.99
10	83020414	0.11	1.07	-1.6	N.A.	87	589	N.A.	0.003	-9.99

**Table B-7: Meteorological Parameters for Top 10 Highest SO<sub>2</sub> Predicted Concentrations – Baldwin Database Site 7**

Rank	YYMMDDHH	USTAR	WSTAR	OBULEN	URB_OBULEN	ZIMECH	ZICONV	ZI_URB	SFCZO	THSTAR
1	83031211	0.11	0.46	-11.6	N.A.	88	336	N.A.	0.009	-9.99
2	83020709	0.17	0.46	-31.2	N.A.	171	234	N.A.	0.003	-9.99
3	83031210	0.14	0.39	-29.4	N.A.	122	262	N.A.	0.009	-9.99
4	83020710	0.17	0.69	-9.3	N.A.	164	265	N.A.	0.003	-9.99
5	82082317	0.12	0.53	-10.8	N.A.	102	385	N.A.	0.06	-9.99
6	83010715	0.08	0.63	-2.3	N.A.	50	511	N.A.	0.003	-9.99
7	82062910	0.14	0.83	-4.3	N.A.	132	332	N.A.	0.06	-9.99
8	82122013	0.24	0.66	-37.4	N.A.	288	298	N.A.	0.015	-9.99
9	82083013	0.2	0.74	-16.3	N.A.	219	321	N.A.	0.06	-9.99
10	82083014	0.21	0.75	-18.8	N.A.	228	357	N.A.	0.06	-9.99

**Table B-8: Meteorological Parameters for Top 10 Highest SO<sub>2</sub> Predicted Concentrations – Baldwin Database Site 8**

Rank	YYMMDDHH	USTAR	WSTAR	OBULEN	URB_OBULEN	ZIMECH	ZICONV	ZI_URB	SFCZO	THSTAR
1	83031211	0.11	0.46	-11.6	N.A.	88	336	N.A.	0.009	-9.99
2	83031210	0.14	0.39	-29.4	N.A.	122	262	N.A.	0.009	-9.99
3	83020709	0.17	0.46	-31.2	N.A.	171	234	N.A.	0.003	-9.99
4	83010711	0.11	0.38	-11.6	N.A.	86	192	N.A.	0.003	-9.99
5	83010715	0.08	0.63	-2.3	N.A.	50	511	N.A.	0.003	-9.99
6	83031209	0.15	0.28	-78.2	N.A.	147	188	N.A.	0.009	-9.99
7	82062910	0.14	0.83	-4.3	N.A.	132	332	N.A.	0.06	-9.99
8	83020409	0.2	0.48	-54.1	N.A.	219	286	N.A.	0.003	-9.99
9	82080512	0.14	0.47	-13.1	N.A.	129	187	N.A.	0.06	-9.99
10	82082317	0.12	0.53	-10.8	N.A.	102	385	N.A.	0.06	-9.99

**Table B-9: Meteorological Parameters for Top 10 Highest SO<sub>2</sub> Predicted Concentrations – Baldwin Database Site 9**

Rank	YYMMDDHH	USTAR	WSTAR	OBULEN	URB_OBULEN	ZIMECH	ZICONV	ZI_URB	SFCZO	THSTAR
1	83010310	0.16	0.79	-5.7	N.A.	153	272	N.A.	0.01	-9.99
2	83021110	0.24	1.05	-12.2	N.A.	287	392	N.A.	0.01	-9.99
3	83010311	0.14	1.11	-2	N.A.	120	453	N.A.	0.01	-9.99
4	82062209	0.27	0.92	-21.1	N.A.	330	347	N.A.	0.19	-9.99
5	83012511	0.14	0.68	-10.4	N.A.	132	425	N.A.	0.01	-9.99
6	82112113	0.27	0.88	-27.3	N.A.	343	363	N.A.	0.05	-9.99
7	83021211	0.14	1.25	-1.4	N.A.	120	420	N.A.	0.01	-9.99
8	82043012	0.15	0.69	-10.5	N.A.	142	394	N.A.	0.03	-9.99
9	82102411	0.15	0.91	-4.7	N.A.	145	385	N.A.	0.015	-9.99
10	83021212	0.18	1.37	-2.7	N.A.	184	479	N.A.	0.01	-9.99

**Table B-10: Meteorological Parameters for Top 10 Highest SO<sub>2</sub> Predicted Concentrations – Baldwin Database Site 10**

Rank	YYMMDDHH	USTAR	WSTAR	OBULEN	URB_OBULEN	ZIMECH	ZICONV	ZI_URB	SFCZO	THSTAR
1	83010311	0.14	1.11	-2	N.A.	120	453	N.A.	0.01	-9.99
2	83021211	0.14	1.25	-1.4	N.A.	120	420	N.A.	0.01	-9.99
3	82112111	0.2	0.73	-17.8	N.A.	224	315	N.A.	0.015	-9.99
4	82060511	0.19	0.86	-9.2	N.A.	203	329	N.A.	0.06	-9.99
5	82121213	0.2	0.83	-13.4	N.A.	218	366	N.A.	0.05	-9.99
6	82102411	0.15	0.91	-4.7	N.A.	145	385	N.A.	0.015	-9.99
7	83021110	0.24	1.05	-12.2	N.A.	287	392	N.A.	0.01	-9.99
8	83021212	0.18	1.37	-2.7	N.A.	184	479	N.A.	0.01	-9.99
9	83010313	0.15	1.34	-2.5	N.A.	145	655	N.A.	0.01	-9.99
10	82112113	0.27	0.88	-27.3	N.A.	343	363	N.A.	0.05	-9.99

**Table B-11: Source and Plume Details for Top 10 Highest SO<sub>2</sub> Predicted Concentrations – Baldwin Database Site 1**

YYMMDDHH	SOURCE TYPE	SOURCEID	RCPT NO.	FINAL PLUME HT.	DIST. FINAL PL. HT.	WDIR FINAL HT.	EFFECT. WSPD	3600* UEFF	DISTANCE TO RCPT	PLUMETYPE	MEAND. FRAC.	PART. PEN. FRAC.	EFFECT SIGMA_V	EFFECT. SIGMA_W	HOURLY CONC	AERVAL	COHERENT	PANCAKE	GAMFACT	PRMVAL	POT. TEMP. GRAD.
83010513	P	STACK1	1	418.7	1928.4	213	3.473	12502.6	5485.3	PEN	0.062	0.92	0.519	0.363	626.708	626.708	665.602	41.605	0	0	0
83010513	P	STACK2	1	416.6	1898.5	213	3.459	12451.4	5537.9	PEN	0.063	0.913	0.519	0.363	602.005	602.005	639.685	40.874	0.02	602.005	0
83010513	P	STACK3	1	414.3	1864.8	213	3.455	12439.3	5596.5	PEN	0.063	0.905	0.519	0.364	556.216	556.216	591.163	38.545	0.02	556.216	0
83011313	P	STACK1	2	412	1573.3	201	2.804	10092.7	3505.2	PEN	0.072	1	0.482	0.315	753.279	753.279	807.374	52.633	0	0	0
83011313	P	STACK2	2	399.6	1573.3	201	2.795	10060.5	3560.4	PEN	0.072	1	0.482	0.329	765.016	765.016	820.391	52.825	0.386	765.016	0
83011313	P	STACK3	2	414.8	1573.3	201	2.804	10094.6	3621.5	PEN	0.072	1	0.482	0.313	758.92	758.92	813.86	52.027	0.386	758.92	0
83010512	P	STACK1	1	387.4	1933.7	211	4.615	16614.5	5485.3	PEN	0.038	1	0.515	0.304	528.964	528.964	549.044	24.337	0	0	0
83010512	P	STACK2	1	384.7	1901.6	211	4.61	16597.1	5537.9	PEN	0.038	1	0.515	0.308	523.863	523.863	543.835	24.55	0.042	523.863	0
83010512	P	STACK3	1	382.5	1876.8	211	4.605	16578.1	5596.5	PEN	0.039	1	0.515	0.312	498.852	498.852	517.961	23.861	0.042	498.852	0
82070318	P	STACK1	1	508.9	1770.9	214	2.865	10313.2	5485.3	PEN	0.101	0.89	0.567	0.382	464.295	464.295	511.67	41.797	0	0	0
82070318	P	STACK2	1	505.9	1740.6	214	2.852	10268.6	5537.9	PEN	0.102	0.882	0.567	0.385	456.815	456.815	503.88	41.798	0.01	456.815	0
82070318	P	STACK3	1	490.6	1590.2	214	2.799	10078.1	5596.5	PEN	0.106	0.838	0.567	0.392	396.136	396.136	438.599	37.056	0.01	396.136	0
82043009	P	STACK1	1	539.7	957.2	208	1.839	6619.9	5485.3	PEN	0.118	1	0.383	0.144	389.888	389.888	438.297	27.765	0	0	0
82043009	P	STACK2	1	563.9	957.2	208	1.839	6620.9	5537.9	PEN	0.118	1	0.383	0.125	327.896	327.896	368.698	23.446	0.047	327.896	0
82043009	P	STACK3	1	471.2	957.2	208	1.835	6605.1	5596.5	PEN	0.119	1	0.383	0.22	548.835	548.835	617.849	37.797	0.047	548.835	0
82062811	P	STACK1	1	526.7	1811.2	207	3.68	13246.9	5485.3	PEN	0.089	0.777	0.684	0.491	429.667	429.667	468.371	32.839	0	0	0
82062811	P	STACK2	1	517.7	1715	207	3.655	13159.7	5537.9	PEN	0.09	0.748	0.684	0.494	409.642	409.642	447.203	31.114	0.047	409.642	0
82062811	P	STACK3	1	528.7	1832.4	207	3.675	13229.6	5596.5	PEN	0.089	0.784	0.684	0.489	426.833	426.833	465.49	32.31	0.047	426.833	0
83021510	P	STACK1	1	431.6	1514.8	209	4.554	16394.9	5485.3	PEN	0.049	1	0.606	0.366	387.318	387.318	406.14	19.731	0	0	0
83021510	P	STACK2	1	441.5	1514.8	209	4.557	16406.6	5537.9	PEN	0.049	1	0.604	0.349	388.993	388.993	407.876	19.824	0.047	388.993	0
83021510	P	STACK3	1	453.8	1514.8	209	4.56	16417.7	5596.5	PEN	0.049	1	0.603	0.329	366.375	366.375	384.138	18.715	0.047	366.375	0
82070317	P	STACK1	1	451.8	1767.5	213	4.575	16470.5	5485.3	PEN	0.059	0.862	0.672	0.45	398.481	398.481	421.753	26.68	0	0	0
82070317	P	STACK2	1	449.2	1735	213	4.551	16383.9	5537.9	PEN	0.06	0.853	0.672	0.454	390.948	390.948	414.053	26.768	0.02	390.948	0
82070317	P	STACK3	1	433.3	1540.2	213	4.379	15763.9	5596.5	PEN	0.064	0.792	0.672	0.466	337.041	337.041	358.493	23.954	0.02	337.041	0
82071209	P	STACK1	2	585.6	1559.5	209	2.614	9411.6	3505.2	PEN	0.189	0.644	0.756	0.594	408.76	408.76	490.752	56.056	0	0	0
82071209	P	STACK2	2	581.1	1559.5	209	2.613	9407.7	3560.4	PEN	0.189	0.628	0.756	0.596	390.61	390.61	469.306	53.927	0.192	390.61	0
82071209	P	STACK3	2	568.3	1537.9	209	2.61	9396.3	3621.5	PEN	0.191	0.581	0.758	0.602	341.184	341.184	410.801	47.247	0.193	341.184	0
82071710	P	STACK1	1	544.2	1753.2	205	4.796	17264.4	5485.3	PEN	0.077	0.564	0.788	0.573	337.281	337.281	363.318	25.104	0	0	0
82071710	P	STACK2	1	542.4	1730.8	205	4.788	17238.4	5537.9	PEN	0.077	0.556	0.789	0.576	341.154	341.154	367.709	25.041	0.028	341.154	0
82071710	P	STACK3	1	539.9	1698.7	205	4.777	17198.5	5596.5	PEN	0.078	0.545	0.791	0.581	333.072	333.072	359.273	24.15	0.028	333.072	0

**Table B-12: Source and Plume Details for Top 10 Highest SO<sub>2</sub> Predicted Concentrations – Baldwin Database Site 2**

YYMDDHH	SOURCE TYPE	SOURCEID	RCPT NO.	FINAL PLUME HT.	DIST. FINAL PL. HT.	WDIR FINAL HT.	EFFECT. WSPD	3600* UEFF	DISTANCETO RCPT	PLUME TYPE	MEAND. FRAC.	PART. PEN. FRAC.	EFFECT SIGMA_V	EFFECT. SIGMA_W	HOURLY CONC	AERVAL	COHERENT	PANCAKE	GAMFACT	PRMVAL	POT. TEMP. GRAD.
83011313	P	STACK1	2	412	1573.3	201	2.804	10092.7	3505.2	PEN	0.072	1	0.482	0.315	753.279	753.279	807.374	52.633	0	0	0
83011313	P	STACK2	2	399.6	1573.3	201	2.795	10060.5	3560.4	PEN	0.072	1	0.482	0.329	765.016	765.016	820.391	52.825	0.386	765.016	0
83011313	P	STACK3	2	414.8	1573.3	201	2.804	10094.6	3621.5	PEN	0.072	1	0.482	0.313	758.92	758.92	813.86	52.027	0.386	758.92	0
83031212	P	STACK1	2	528.4	1211	190	1.147	4130.1	3505.2	PEN	0.204	0.797	0.338	0.28	760.771	760.771	919.149	142.179	0	0	0
83031212	P	STACK2	2	526.3	1211	190	1.147	4129.9	3560.4	PEN	0.204	0.791	0.338	0.28	765.554	765.554	926.428	139.215	0	0	0
83031212	P	STACK3	2	524	1211	190	1.147	4129.5	3621.5	PEN	0.205	0.783	0.338	0.281	738.598	738.598	895.203	131.032	0	0	0
82062810	P	STACK1	2	502.9	1644.9	197	3.186	11468.4	3505.2	PEN	0.102	0.869	0.699	0.504	446.376	446.376	492.045	45.81	0	0	0
82062810	P	STACK2	2	488.3	1644.9	197	3.179	11444.4	3560.4	PEN	0.106	0.825	0.699	0.513	429.92	429.92	475.574	43.558	0.372	429.92	0
82062810	P	STACK3	2	504.6	1644.9	197	3.186	11471	3621.5	PEN	0.103	0.874	0.699	0.503	458.193	458.193	505.425	45.41	0.37	458.193	0
83011314	P	STACK1	2	423.8	1736.8	191	2.696	9704.9	3505.2	PEN	0.076	0.949	0.477	0.345	372.637	372.637	397.875	63.763	0	0	0
83011314	P	STACK2	2	412.8	1714.8	191	2.694	9699	3560.4	PEN	0.076	0.912	0.477	0.35	356.097	356.097	380.738	57.52	0	0	0
83011314	P	STACK3	2	426.4	1736.8	191	2.696	9706.2	3621.5	PEN	0.076	0.957	0.477	0.343	414.503	414.503	443.336	63.759	0	0	0
82071209	P	STACK1	2	585.6	1559.5	209	2.614	9411.6	3505.2	PEN	0.189	0.644	0.756	0.594	408.76	408.76	490.752	56.056	0	0	0
82071209	P	STACK2	2	581.1	1559.5	209	2.613	9407.7	3560.4	PEN	0.189	0.628	0.756	0.596	390.61	390.61	469.306	53.927	0.192	390.61	0
82071209	P	STACK3	2	568.3	1537.9	209	2.61	9396.3	3621.5	PEN	0.191	0.581	0.758	0.602	341.184	341.184	410.801	47.247	0.193	341.184	0
83021512	P	STACK1	2	646.7	1743.6	194	2.075	7468.8	3505.2	PEN	0.175	0.528	0.579	0.502	354.73	354.73	418.927	52.457	0	0	0
83021512	P	STACK2	2	643.8	1743.6	194	2.074	7468.1	3560.4	PEN	0.176	0.518	0.579	0.503	351.25	351.25	415.177	51.008	0	0	0
83021512	P	STACK3	2	654.9	1743.6	194	2.075	7470.8	3621.5	PEN	0.175	0.555	0.579	0.499	380.324	380.324	449.657	54.469	0	0	0
82053113	P	STACK1	2	618.9	1197.7	190	1.284	4623.3	3505.2	PEN	0.269	0.75	0.446	0.37	547.954	547.954	707.623	114.351	0	0	0
82053113	P	STACK2	<--- Source is not emitting during this hour																		
82053113	P	STACK3	2	604.8	1197.7	190	1.283	4620.1	3621.5	PEN	0.271	0.712	0.446	0.375	497.818	497.818	645.503	100.391	0	0	0
82062811	P	STACK1	1	526.7	1811.2	207	3.68	13246.9	5485.3	PEN	0.089	0.777	0.684	0.491	429.667	429.667	468.371	32.839	0	0	0
82062811	P	STACK2	1	517.7	1715	207	3.655	13159.7	5537.9	PEN	0.09	0.748	0.684	0.494	409.642	409.642	447.203	31.114	0.047	409.642	0
82062811	P	STACK3	1	528.7	1832.4	207	3.675	13229.6	5596.5	PEN	0.089	0.784	0.684	0.489	426.833	426.833	465.49	32.31	0.047	426.833	0
82083113	P	STACK1	2	541	1698.9	197	4.218	15185.4	3505.2	PEN	0.076	0.566	0.756	0.592	291.272	291.272	313.152	26.146	0	0	0
82083113	P	STACK2	2	546.3	1764.2	197	4.222	15198.3	3560.4	PEN	0.076	0.588	0.755	0.589	309.888	309.888	333.02	27.062	0.372	309.888	0
82083113	P	STACK3	2	545.4	1753.3	197	4.221	15196.1	3621.5	PEN	0.076	0.585	0.755	0.59	314.786	314.786	338.477	26.871	0.37	314.786	0
82061709	P	STACK1	2	736.4	1655.4	201	3.692	13289.5	3505.2	IND	0.11	0.469	0.816	0.679	290.022	290.022	322.701	26.687	0	0	0
82061709	P	STACK2	2	592.7	1807.8	201	3.722	13398.3	3560.4	PEN	0.108	0.52	0.797	0.625	323.212	323.212	358.882	29.491	0.386	323.212	0
82061709	P	STACK3	2	745.7	1670.7	201	3.692	13289.5	3621.5	IND	0.111	0.474	0.816	0.679	295.202	295.202	328.685	26.866	0.386	295.202	0

**Table B-13: Source and Plume Details for Top 10 Highest SO<sub>2</sub> Predicted Concentrations – Baldwin Database Site 3**

YYMMDDHH	SOURCE TYPE	SOURCE ID	RCPT NO.	FINAL PLUME HT.	DIST. FINAL PL. HT.	WDIR FINAL HT.	EFFECT. WSPD	3600* UEFF	DISTANCE TO RCPT	PLUME TYPE	MEAND. FRAC.	PART. PEN. FRAC.	EFFECT SIGMA_V	EFFECT. SIGMA_W	HOURLY CONC	AERVAL	COHERENT	PANCAKE	GAMFACT	PRMVAL	POT. TEMP. GRAD.
83031212	P	STACK1	2	528.4	1211	190	1.147	4130.1	3505.2	PEN	0.204	0.797	0.338	0.28	760.771	760.771	919.149	142.179	0	0	0
83031212	P	STACK2	2	526.3	1211	190	1.147	4129.9	3560.4	PEN	0.204	0.791	0.338	0.28	765.554	765.554	926.428	139.215	0	0	0
83031212	P	STACK3	2	524	1211	190	1.147	4129.5	3621.5	PEN	0.205	0.783	0.338	0.281	738.598	738.598	895.203	131.032	0	0	0
83021413	P	STACK1	3	1111.3	818.8	187	1.507	5426.4	1760.1	IND	0.695	0.447	0.898	0.874	331.087	331.087	687.665	174.865	0	0	0
83021413	P	STACK2	3	1088.3	818.8	187	1.507	5426.4	1814.5	IND	0.697	0.43	0.898	0.874	319.121	319.121	670.746	166.349	0	0	0
83021413	P	STACK3	3	1099.3	818.8	187	1.507	5426.4	1875	IND	0.697	0.437	0.898	0.874	319.26	319.26	675.391	164.162	0	0	0
82080612	STACK1	<--- Source is not emitting during this hour																			
82080612	P	STACK2	3	525.2	863.1	223	1.541	5547.2	1814.5	PEN	0.3	0.955	0.602	0.443	424.615	424.615	552.489	125.843	0.056	424.615	0
82080612	P	STACK3	3	541.1	863.1	223	1.543	5553.6	1875	PEN	0.297	0.988	0.602	0.433	418.773	418.773	541.286	128.987	0.054	418.773	0
82071209	P	STACK1	2	585.6	1559.5	209	2.614	9411.6	3505.2	PEN	0.189	0.644	0.756	0.594	408.76	408.76	490.752	56.056	0	0	0
82071209	P	STACK2	2	581.1	1559.5	209	2.613	9407.7	3560.4	PEN	0.189	0.628	0.756	0.596	390.61	390.61	469.306	53.927	0.192	390.61	0
82071209	P	STACK3	2	568.3	1537.9	209	2.61	9396.3	3621.5	PEN	0.191	0.581	0.758	0.602	341.184	341.184	410.801	47.247	0.193	341.184	0
82053113	P	STACK1	2	618.9	1197.7	190	1.284	4623.3	3505.2	PEN	0.269	0.75	0.446	0.37	547.954	547.954	707.623	114.351	0	0	0
82053113	STACK2	<--- Source is not emitting during this hour																			
82053113	P	STACK3	2	604.8	1197.7	190	1.283	4620.1	3621.5	PEN	0.271	0.712	0.446	0.375	497.818	497.818	645.503	100.391	0	0	0
83021513	P	STACK1	2	1034	1751.5	202	2.603	9369.8	3505.2	IND	0.247	0.252	0.884	0.843	282.34	282.34	361.102	42.784	0	0	0
83021513	P	STACK2	2	1048.1	1754.5	202	2.603	9369.8	3560.4	IND	0.247	0.26	0.884	0.843	290.895	290.895	372.092	44.004	0.385	290.895	0
83021513	P	STACK3	2	1099.2	1754.5	202	2.603	9369.8	3621.5	IND	0.247	0.291	0.884	0.843	304.958	304.958	389.844	46.305	0.386	304.958	0
82072609	P	STACK1	10	661.9	462.6	69	0.769	2766.9	2233.8	PEN	1	1	0.637	0.37	239.172	239.172	26.309	239.172	PLUME OUT O	F WAKE	0
82072609	P	STACK2	5	684.8	462.6	69	0.778	2801.3	2465.4	PEN	1	1	0.631	0.26	231.398	231.398	0	231.398	PLUME OUT	OF WAKE	0
82072609	P	STACK3	3	636.2	462.6	69	0.777	2796.4	1875	PEN	1	1	0.634	0.314	248.094	248.094	0	248.094	PLUME OUT	OF WAKE	0
83021514	P	STACK1	3	912.7	1760.5	207	3.063	11026.3	1760.1	IND	0.196	0.129	0.956	0.914	223.822	223.822	270.565	32.488	0	0	0
83021514	P	STACK2	3	922	1774.9	207	3.063	11026.3	1814.5	IND	0.197	0.131	0.956	0.914	226.994	226.994	274.511	33.081	0.987	226.994	0
83021514	P	STACK3	2	981.5	1866.8	207	3.063	11026.3	3621.5	IND	0.212	0.145	0.956	0.914	226.001	226.001	278.246	32.123	0.357	226.001	0
83020416	P	STACK1	3	1691.3	703.7	49	0.775	2789.8	1760.1	IND	0.993	0.321	0.615	0.591	194.058	194.058	0	195.461	PLUME OUT O	F WAKE	0
83020416	P	STACK2	3	1750.5	703.7	49	0.775	2789.8	1814.5	IND	0.993	0.344	0.615	0.591	210.912	210.912	0	212.399	PLUME OUT	OF WAKE	0
83020416	P	STACK3	10	1821.5	703.7	49	0.775	2789.8	2109.7	IND	0.995	0.372	0.615	0.591	228.14	228.14	380.582	227.416	PLUME OUT	OF WAKE	0
83021512	P	STACK1	2	646.7	1743.6	194	2.075	7468.8	3505.2	PEN	0.175	0.528	0.579	0.502	354.73	354.73	418.927	52.457	0	0	0
83021512	P	STACK2	2	643.8	1743.6	194	2.074	7468.1	3560.4	PEN	0.176	0.518	0.579	0.503	351.25	351.25	415.177	51.008	0	0	0
83021512	P	STACK3	2	654.9	1743.6	194	2.075	7470.8	3621.5	PEN	0.175	0.555	0.579	0.499	380.324	380.324	449.657	54.469	0	0	0

**Table B-14: Source and Plume Details for Top 10 Highest SO<sub>2</sub> Predicted Concentrations – Baldwin Database Site 4**

YYMMDDHH	SOURCE TYPE	SOURCE ID	RCPT NO.	FINAL PLUME HT.	DIST. FINAL PL. HT.	WDIR FINAL HT.	EFFECT. WSPD	3600* UEFF	DISTANCE TO RCPT	PLUME TYPE	MEAND. FRAC.	PART. PEN. FRAC.	EFFECT SIGMA_V	EFFECT. SIGMA_W	HOURLY CONC	AERVAL	COHERENT	PANCAKE	GAMFACT	PRMVAL	POT. TEMP. GRAD.
83020712	P	STACK1	5	451	928	279	1.804	6494.2	2486	PEN	0.227	0.83	0.59	0.504	788.888	788.888	977.561	144.886	0.499	788.888	0
83020712	P	STACK2	5	455.5	928	279	1.804	6493.9	2465.4	PEN	0.226	0.846	0.59	0.501	878.411	878.411	1090.514	153.323	0.5	878.411	0
83020712	P	STACK3	5	443.8	928	279	1.804	6494.8	2447.4	PEN	0.227	0.803	0.59	0.509	778.189	778.189	968.432	129.01	0.5	778.189	0
83020711	P	STACK1	5	407.8	1169.8	286	2.383	8577.9	2486	PEN	0.125	0.939	0.57	0.423	962.297	962.297	1085.643	102.228	0.926	962.297	0
83020711	P	STACK2	5	413.2	1169.8	286	2.384	8582.9	2465.4	PEN	0.126	0.957	0.57	0.413	1053.526	1053.526	1189.39	108.609	0.925	53.526	0
83020711	P	STACK3	5	405.4	1169.8	286	2.383	8578.4	2447.4	PEN	0.125	0.931	0.57	0.424	955.016	955.016	1077.986	95.765	0.924	955.016	0
83020414	P	STACK1	6	1217	1156.1	302	1.503	5411.1	3857.1	IND	0.397	0.19	0.664	0.642	290.501	290.501	438.156	65.949	0.287	290.501	0
83020414	P	STACK2	6	1251.6	1156.1	302	1.503	5411.1	3832.4	IND	0.397	0.204	0.664	0.642	302.133	302.133	454.717	69.897	0.289	302.133	0
83020414	P	STACK3	6	1373.6	1156.1	302	1.526	5493.3	3809.4	DIR	0.396	0.257	0.664	0.624	363.327	363.327	544.77	86.637	0.291	363.327	0
83010715	P	STACK1	7	1755.3	1459.8	311	1.318	4745.3	< 6720.9	DIR	0.232	0.492	0.397	0.371	436.339	436.339	545.347	75.198	0	436.339	0
83010715	P	STACK2	7	1709	1459.8	311	1.318	4745.2	< 6691.7	DIR	0.232	0.471	0.397	0.371	397.693	397.693	496.447	70.565	0	397.693	0
83010715	P	STACK3	7	1721.1	1459.8	311	1.318	4745.2	< 6663.1	DIR	0.232	0.476	0.397	0.371	381.976	381.976	475.974	70.177	0	381.976	0
83020415	P	STACK1	6	1395.6	1173	302	1.321	4756.5	3857.1	IND	0.401	0.217	0.601	0.576	305.145	305.145	461.401	71.514	0.287	5.145	0
83020415	P	STACK2	6	1416.6	1173	302	1.321	4756.5	3832.4	IND	0.401	0.225	0.601	0.576	307.797	307.797	464.564	73.325	0.289	307.797	0
83020415	P	STACK3	6	1534.4	1173	302	1.375	4951.4	3809.4	DIR	0.401	0.272	0.601	0.561	358.962	358.962	540.291	88.003	0.291	358.962	0
83010712	P	STACK1	5	532.1	1037.5	269	1.601	5762	2486	PEN	0.286	0.617	0.589	0.521	418.598	418.598	528.976	143.529	0.008	418.598	0
83010712	P	STACK2	5	531.5	1037.5	269	1.601	5761.9	2465.4	PEN	0.286	0.615	0.589	0.522	452.436	452.436	576.648	142.822	0.008	452.436	0
83010712	P	STACK3	5	535	1037.5	269	1.601	5762.6	2447.4	PEN	0.286	0.629	0.589	0.52	493.766	493.766	634.148	143.139	0.008	493.766	0
83020416	P	STACK1	3	1691.3	703.7	49	0.775	2789.8	1760.1	IND	0.993	0.321	0.615	0.591	194.058	194.058	0	195.461	PLUME OUT	OF WAKE	0
83020416	P	STACK2	3	1750.5	703.7	49	0.775	2789.8	1814.5	IND	0.993	0.344	0.615	0.591	210.912	210.912	0	212.399	PLUME OUT	OF WAKE	0
83020416	P	STACK3	10	1821.5	703.7	49	0.775	2789.8	2109.7	IND	0.995	0.372	0.615	0.591	228.14	228.14	380.582	227.416	PLUME OUT	OF WAKE	0
82090411	P	STACK1	4	689.5	1054.4	314	1.418	5104.9	1396.3	PEN	0.415	0.612	0.619	0.55	289.336	289.336	428.723	93.197	0.763	289.336	0
82090411	P	STACK2	6	697.5	1054.4	314	1.421	5114.1	3832.4	PEN	0.434	0.634	0.617	0.543	300.973	300.973	450.981	105.183	0	300.973	0
82090411	STACK3	<--- Source is not emitting during this hour																			
82072609	P	STACK1	10	661.9	462.6	69	0.769	2766.9	2233.8	PEN	1	1	0.637	0.37	239.172	239.172	26.309	239.172	PLUME	OUT OF WAKE	0
82072609	P	STACK2	5	684.8	462.6	69	0.778	2801.3	2465.4	PEN	1	1	0.631	0.26	231.398	231.398	0	231.398	PLUME	OUT OF WAKE	0
82072609	P	STACK3	3	636.2	462.6	69	0.777	2796.4	1875	PEN	1	1	0.634	0.314	248.094	248.094	0	248.094	PLUME	OUT OF WAKE	0
82080815	P	STACK1	4	410.8	811.7	292	3.051	10983.5	1396.3	DIR	0.14	0.009	0.794	0.694	223.786	223.786	255.463	28.704	1	223.786	0
82080815	P	STACK2	5	782.1	1554.7	292	3.173	11423.9	2465.4	DIR	0.135	0.041	0.794	0.714	154.494	154.494	175.807	17.599	0.924	154.494	0
82080815	P	STACK3	6	911.6	1768.2	292	3.206	11540.1	3809.4	DIR	0.139	0.056	0.794	0.718	149.58	149.58	171.177	16.226	0.497	149.58	0

**Table B-15: Source and Plume Details for Top 10 Highest SO<sub>2</sub> Predicted Concentrations – Baldwin Database Site 5**

YYMMDDHH	SOURCETYPE	SOURCE ID	RCPT NO.	FINAL PLUME HT.	DIST. FINAL PL. HT.	WDIR FINAL HT.	EFFECT. WSPD	3600 * UEFF	DISTANCE TO RCPT	PLUMETYPE	MEAND. FRAC.	PART. PEN. FRAC.	EFFECT SIGMA_V	EFFECT. SIGMA_W	HOURLY CONC	AERVAL	COHERENT	PANCAKE	GAMFACT	PRMVAL	POT. TEMP. GRAD.
83020711	P	STACK1	5	407.8	1169.8	286	2.383	8577.9	2486	PEN	0.125	0.939	0.57	0.423	962.297	962.297	1085.643	102.228	0.926	962.297	0
83020711	P	STACK2	5	413.2	1169.8	286	2.384	8582.9	2465.4	PEN	0.126	0.957	0.57	0.413	1053.526	1053.526	1189.39	108.609	0.925	1053.526	0
83020711	P	STACK3	5	405.4	1169.8	286	2.383	8578.4	2447.4	PEN	0.125	0.931	0.57	0.424	955.016	955.016	1077.986	95.765	0.924	955.016	0
83020712	P	STACK1	5	451	928	279	1.804	6494.2	2486	PEN	0.227	0.83	0.59	0.504	788.888	788.888	977.561	144.886	0.499	788.888	0
83020712	P	STACK2	5	455.5	928	279	1.804	6493.9	2465.4	PEN	0.226	0.846	0.59	0.501	878.411	878.411	1090.514	153.323	0.5	878.411	0
83020712	P	STACK3	5	443.8	928	279	1.804	6494.8	2447.4	PEN	0.227	0.803	0.59	0.509	778.189	778.189	968.432	129.01	0.5	778.189	0
83020710	P	STACK1	6	397.9	1391.7	290	2.812	10122.4	3857.1	PEN	0.083	1	0.518	0.259	824.208	824.208	892.964	67.517	0.486	824.208	0
83020710	P	STACK2	6	395.2	1391.7	290	2.812	10121.9	3832.4	PEN	0.083	1	0.518	0.263	849.679	849.679	920.776	67.051	0.486	849.679	0
83020710	P	STACK3	6	393.7	1391.7	290	2.812	10121.7	3809.4	PEN	0.083	1	0.518	0.265	840.465	840.465	910.944	64.164	0.486	840.465	0
83010712	P	STACK1	5	532.1	1037.5	269	1.601	5762	2486	PEN	0.286	0.617	0.589	0.521	418.598	418.598	528.976	143.529	0.008	418.598	0
83010712	P	STACK2	5	531.5	1037.5	269	1.601	5761.9	2465.4	PEN	0.286	0.615	0.589	0.522	452.436	452.436	576.648	142.822	0.008	452.436	0
83010712	P	STACK3	5	535	1037.5	269	1.601	5762.6	2447.4	PEN	0.286	0.629	0.589	0.52	493.766	493.766	634.148	143.139	0.008	493.766	0
83031211	P	STACK1	6	456.6	1814.9	298	2.001	7204.4	3857.1	PEN	0.082	0.921	0.343	0.216	979.745	979.745	1060.581	69.248	0.489	979.745	0
83031211	P	STACK2	7	454.8	1814.9	298	2.001	7204.4	6691.7	PEN	0.099	0.916	0.343	0.216	949.105	949.105	1046.678	60.297	0.017	949.105	0
83031211	P	STACK3	7	453.4	1814.9	298	2.001	7204.4	6663.1	PEN	0.099	0.911	0.343	0.217	907.798	907.798	1001.036	57.402	0.017	907.798	0
83020713	P	STACK1	5	466.5	1322.9	275	2.412	8684.4	2486	PEN	0.148	0.613	0.629	0.553	359.451	359.451	408.135	78.124	0.154	359.451	0
83020713	P	STACK2	5	468.8	1322.9	275	2.413	8685.1	2465.4	PEN	0.147	0.625	0.629	0.552	416.195	416.195	474.096	80.989	0.153	416.195	0
83020713	P	STACK3	5	824.4	1322.9	275	2.41	8677.8	2447.4	IND	0.149	0.476	0.633	0.588	324.798	324.798	371.682	56.427	0.153	324.798	0
82040315	P	STACK1	5	322.9	1760.3	288	16.713	60168.6	2486	DIR	0.013	0.002	1.222	0.994	453.869	104.563	105.931	3.949	0.924	482.397	0
82040315	P	STACK2	5	335	1857.1	288	16.741	60269.2	2465.4	DIR	0.013	0.002	1.22	0.993	528.62	115.084	116.559	3.742	0.924	562.594	0
82040315	STACK3	<--- Source is not emitting during this hour																			
82082317	P	ST1	6	589.9	1263.1	298	1.384	4983.4	3857.1	PEN	0.186	1	0.387	0.204	735.041	735.041	882.4	88.496	0.489	735.041	0
82082317	P	ST1	6	598.4	1263.1	298	1.385	4984.8	3832.4	PEN	0.185	1	0.387	0.196	727.478	727.478	872.341	89.013	0.489	727.478	0
82082317	STACK3	<--- Source is not emitting during this hour																			
83020414	P	STACK1	6	1217	1156.1	302	1.503	5411.1	3857.1	IND	0.397	0.19	0.664	0.642	290.501	290.501	438.156	65.949	0.287	290.501	0
83020414	P	STACK2	6	1251.6	1156.1	302	1.503	5411.1	3832.4	IND	0.397	0.204	0.664	0.642	302.133	302.133	454.717	69.897	0.289	302.133	0
83020414	P	STACK3	6	1373.6	1156.1	302	1.526	5493.3	3809.4	DIR	0.396	0.257	0.664	0.624	363.327	363.327	544.77	86.637	0.291	363.327	0
83020415	P	STACK1	6	1395.6	1173	302	1.321	4756.5	3857.1	IND	0.401	0.217	0.601	0.576	305.145	305.145	461.401	71.514	0.287	305.145	0
83020415	P	STACK2	6	1416.6	1173	302	1.321	4756.5	3832.4	IND	0.401	0.225	0.601	0.576	307.797	307.797	464.564	73.325	0.289	307.797	0
83020415	P	STACK3	6	1534.4	1173	302	1.375	4951.4	3809.4	DIR	0.401	0.272	0.601	0.561	358.962	358.962	540.291	88.003	0.291	358.962	0

**Table B-16: Source and Plume Details for Top 10 Highest SO<sub>2</sub> Predicted Concentrations – Baldwin Database Site 6**

YYMMDDHH	SOURCE TYPE	SOURCE ID	RCPT NO.	FINAL PLUME HT.	DIST. FINAL PL. HT.	WDIR FINAL HT.	EFFECT. WSPD	3600° UEFF	DISTANCE TO RCPT	PLUMETYPE	MEAND. FRAC.	PART. PEN. FRAC.	EFFECT SIGMA_V	EFFECT. SIGMA_W	HOURLY CONC	AERVAL	COHERENT	PANCAKE	GAMFACT	PRMVAL	POT. TEMP. GRAD.
83031211	P	STACK1	6	456.6	1814.9	298	2.001	7204.4	3857.1	PEN	0.082	0.921	0.343	0.216	979.745	979.745	1060.581	69.248	0.489	979.745	0
83031211	P	STACK2	7	454.8	1814.9	298	2.001	7204.4	6691.7	PEN	0.099	0.916	0.343	0.216	949.105	949.105	1046.678	60.297	0.017	949.105	0
83031211	P	STACK3	7	453.4	1814.9	298	2.001	7204.4	6663.1	PEN	0.099	0.911	0.343	0.217	907.798	907.798	1001.036	57.402	0.017	907.798	0
83020710	P	STACK1	6	397.9	1391.7	290	2.812	10122.4	3857.1	PEN	0.083	1	0.518	0.259	824.208	824.208	892.964	67.517	0.486	824.208	0
83020710	P	STACK2	6	395.2	1391.7	290	2.812	10121.9	3832.4	PEN	0.083	1	0.518	0.263	849.679	849.679	920.776	67.051	0.486	849.679	0
83020710	P	STACK3	6	393.7	1391.7	290	2.812	10121.7	3809.4	PEN	0.083	1	0.518	0.265	840.465	840.465	910.944	64.164	0.486	840.465	0
83020711	P	STACK1	5	407.8	1169.8	286	2.383	8577.9	2486	PEN	0.125	0.939	0.57	0.423	962.297	962.297	1085.643	102.228	0.926	962.297	0
83020711	P	STACK2	5	413.2	1169.8	286	2.384	8582.9	2465.4	PEN	0.126	0.957	0.57	0.413	1053.526	1053.526	1189.39	108.609	0.925	1053.526	0
83020711	P	STACK3	5	405.4	1169.8	286	2.383	8578.4	2447.4	PEN	0.125	0.931	0.57	0.424	955.016	955.016	1077.986	95.765	0.924	955.016	0
83020712	P	STACK1	5	451	928	279	1.804	6494.2	2486	PEN	0.227	0.83	0.59	0.504	788.888	788.888	977.561	144.886	0.499	788.888	0
83020712	P	STACK2	5	455.5	928	279	1.804	6493.9	2465.4	PEN	0.226	0.846	0.59	0.501	878.411	878.411	1090.514	153.323	0.5	878.411	0
83020712	P	STACK3	5	443.8	928	279	1.804	6494.8	2447.4	PEN	0.227	0.803	0.59	0.509	778.189	778.189	968.432	129.01	0.5	778.189	0
82082317	P	STACK1	6	589.9	1263.1	298	1.384	4983.4	3857.1	PEN	0.186	1	0.387	0.204	735.041	735.041	882.4	88.496	0.489	735.041	0
82082317	P	STACK2	6	598.4	1263.1	298	1.385	4984.8	3832.4	PEN	0.185	1	0.387	0.196	727.478	727.478	872.341	89.013	0.489	727.478	0
82082317	P	STACK3	<--- Source is not emitting during this hour																		
82083013	P	STACK1	6	505.5	1427.7	291	2.747	9890.8	3857.1	PEN	0.106	1	0.584	0.252	427.477	427.477	473.41	39.885	0.497	427.477	0
82083013	P	STACK2	6	508.8	1427.7	291	2.748	9891.4	3832.4	PEN	0.106	1	0.584	0.247	435.896	435.896	482.746	39.862	0.498	435.896	0
82083013	P	STACK3	6	515.5	1427.7	291	2.748	9892.4	3809.4	PEN	0.106	1	0.584	0.238	418.184	418.184	463.1	37.627	0.498	418.184	0
83010715	P	STACK1	7	1755.3	1459.8	311	1.318	4745.3	6720.9	DIR	0.232	0.492	0.397	0.371	436.339	436.339	545.347	75.198	0	436.339	0
83010715	P	STACK2	7	1709	1459.8	311	1.318	4745.2	6691.7	DIR	0.232	0.471	0.397	0.371	397.693	397.693	496.447	70.565	0	397.693	0
83010715	P	STACK3	7	1721.1	1459.8	311	1.318	4745.2	6663.1	DIR	0.232	0.476	0.397	0.371	381.976	381.976	475.974	70.177	0	381.976	0
83020415	P	STACK1	6	1395.6	1173	302	1.321	4756.5	3857.1	IND	0.401	0.217	0.601	0.576	305.145	305.145	461.401	71.514	0.287	305.145	0
83020415	P	STACK2	6	1416.6	1173	302	1.321	4756.5	3832.4	IND	0.401	0.225	0.601	0.576	307.797	307.797	464.564	73.325	0.289	307.797	0
83020415	P	STACK3	6	1534.4	1173	302	1.375	4951.4	3809.4	DIR	0.401	0.272	0.601	0.561	358.962	358.962	540.291	88.003	0.291	358.962	0
82040516	P	STACK1	6	315.8	1810.6	294	18.573	66863.6	3857.1	DIR	0.011	0.007	1.088	0.752	466.667	123.656	124.948	3.198	0.82	541.964	0
82040516	P	STACK2	6	327.6	1914	294	18.605	66979.5	3832.4	DIR	0.011	0.008	1.086	0.75	500.227	122.456	123.724	3.112	0.821	582.669	0
82040516	P	STACK3	<--- Source is not emitting during this hour																		
83020414	P	STACK1	6	1217	1156.1	302	1.503	5411.1	3857.1	IND	0.397	0.19	0.664	0.642	290.501	290.501	438.156	65.949	0.287	290.501	0
83020414	P	STACK2	6	1251.6	1156.1	302	1.503	5411.1	3832.4	IND	0.397	0.204	0.664	0.642	302.133	302.133	454.717	69.897	0.289	302.133	0
83020414	P	STACK3	6	1373.6	1156.1	302	1.526	5493.3	3809.4	DIR	0.396	0.257	0.664	0.624	363.327	363.327	544.77	86.637	0.291	363.327	0

**Table B-17: Source and Plume Details for Top 10 Highest SO<sub>2</sub> Predicted Concentrations – Baldwin Database Site 7**

YYMMDDHH	SOURCE TYPE	SOURCE ID	RCPT NO.	FINAL PLUME HT.	DIST. FINAL PL. HT.	WDIR FINAL HT.	EFFECT. WSPD	3600 * UEFF	DISTANCE TO RCPT	PLUME TYPE	MEAND. FRAC.	PART. PEN. FRAC.	EFFECT SIGMA_V	EFFECT. SIGMA_W	HOURLY CONC	AERVAL	COHERENT	PANCAKE	GAMFACT	PRMVAL	POT. TEMP. GRAD.
83031211	P	STACK1	6	456.6	1814.9	298	2.001	7204.4	3857.1	PEN	0.082	0.921	0.343	0.216	979.745	979.745	1060.581	69.248	0.489	979.745	0
83031211	P	STACK2	7	454.8	1814.9	298	2.001	7204.4	6691.7	PEN	0.099	0.916	0.343	0.216	949.105	949.105	1046.678	60.297	0.017	949.105	0
83031211	P	STACK3	7	453.4	1814.9	298	2.001	7204.4	6663.1	PEN	0.099	0.911	0.343	0.217	907.798	907.798	1001.036	57.402	0.017	907.798	0
83020709	P	STACK1	7	387.3	1964.3	296	3.74	13462.5	6720.9	PEN	0.046	1	0.424	0.136	535.807	535.807	560.451	27.271	0.015	535.807	0
83020709	P	STACK2	7	383.3	1917.9	296	3.74	13462.5	6691.7	PEN	0.046	1	0.424	0.139	553.672	553.672	579.163	27.039	0.015	553.672	0
83020709	P	STACK3	7	383.5	1919.5	296	3.74	13462.5	6663.1	PEN	0.046	1	0.424	0.138	552.422	552.422	577.852	25.947	0.015	552.422	0
83031210	P	STACK1	8	424.5	1940.7	304	2.792	10050.8	9877.5	PEN	0.072	1	0.346	0.121	626.397	626.397	672.724	32.034	0	626.397	0
83031210	P	STACK2	8	422.4	1920.3	304	2.792	10050.7	9846.7	PEN	0.072	1	0.346	0.122	606.112	606.112	650.873	31.81	0	606.112	0
83031210	P	STACK3	8	426.5	1960.1	304	2.792	10050.9	9816.2	PEN	0.072	1	0.346	0.119	575.179	575.179	617.304	31.118	0	575.179	0
83020710	P	STACK1	6	397.9	1391.7	290	2.812	10122.4	3857.1	PEN	0.083	1	0.518	0.259	824.208	824.208	892.964	67.517	0.486	824.208	0
83020710	P	STACK2	6	395.2	1391.7	290	2.812	10121.9	3832.4	PEN	0.083	1	0.518	0.263	849.679	849.679	920.776	67.051	0.486	849.679	0
83020710	P	STACK3	6	393.7	1391.7	290	2.812	10121.7	3809.4	PEN	0.083	1	0.518	0.265	840.465	840.465	910.944	64.164	0.486	840.465	0
82082317	P	STACK1	6	589.9	1263.1	298	1.384	4983.4	3857.1	PEN	0.186	1	0.387	0.204	735.041	735.041	882.4	88.496	0.489	735.041	0
82082317	P	STACK2	6	598.4	1263.1	298	1.385	4984.8	3832.4	PEN	0.185	1	0.387	0.196	727.478	727.478	872.341	89.013	0.489	727.478	0
82082317		STACK3	<--- Source is not emitting during this hour																		
83010715	P	STACK1	7	1755.3	1459.8	311	1.318	4745.3	6720.9	DIR	0.232	0.492	0.397	0.371	436.339	436.339	545.347	75.198	0	436.339	0
83010715	P	STACK2	7	1709	1459.8	311	1.318	4745.2	6691.7	DIR	0.232	0.471	0.397	0.371	397.693	397.693	496.447	70.565	0	397.693	0
83010715	P	STACK3	7	1721.1	1459.8	311	1.318	4745.2	6663.1	DIR	0.232	0.476	0.397	0.371	381.976	381.976	475.974	70.177	0	381.976	0
82062910	P	STACK1	7	521.6	1246	306	2.594	9336.7	6720.9	PEN	0.13	1	0.565	0.29	428.109	428.109	485.475	44.219	0.003	428.109	0
82062910	P	STACK2	7	518.5	1246	306	2.593	9336.3	6691.7	PEN	0.131	1	0.565	0.294	417.064	417.064	473.269	44.331	0.003	417.064	0
82062910	P	STACK3	7	500.2	1246	306	2.592	9332.3	6663.1	PEN	0.135	1	0.565	0.321	369.657	369.657	420.854	40.754	0.003	369.657	0
82122013	P	STACK1	7	432.6	1868.1	296	4.837	17412.3	6720.9	PEN	0.048	1	0.606	0.277	356.654	356.654	373.649	20.18	0.015	356.654	0
82122013	P	STACK2	7	425.7	1803.9	296	4.836	17409.7	6691.7	PEN	0.048	1	0.606	0.286	360.171	360.171	377.433	19.805	0.015	360.171	0
82122013	P	STACK3	7	434.4	1884.2	296	4.837	17413.7	6663.1	PEN	0.048	1	0.606	0.274	369.987	369.987	387.591	19.72	0.015	369.987	0
82083013	P	STACK1	6	505.5	1427.7	291	2.747	9890.8	3857.1	PEN	0.106	1	0.584	0.252	427.477	427.477	473.41	39.885	0.497	427.477	0
82083013	P	STACK2	6	508.8	1427.7	291	2.748	9891.4	3832.4	PEN	0.106	1	0.584	0.247	435.896	435.896	482.746	39.862	0.498	435.896	0
82083013	P	STACK3	6	515.5	1427.7	291	2.748	9892.4	3809.4	PEN	0.106	1	0.584	0.238	418.184	418.184	463.1	37.627	0.498	418.184	0
82083014	P	STACK1	7	506.9	1697.9	308	3.004	10815.6	6720.9	PEN	0.109	0.952	0.596	0.329	336.862	336.862	373.4	38.119	0	336.862	0
82083014	P	STACK2	7	510.1	1697.9	308	3.005	10817.1	6691.7	PEN	0.109	0.959	0.596	0.324	335.532	335.532	371.672	39.358	0	335.532	0
82083014	P	STACK3	7	513.7	1697.9	308	3.005	10818.6	6663.1	PEN	0.109	0.967	0.596	0.32	321.803	321.803	356.181	39.372	0	321.803	0

**Table B-18: Source and Plume Details for Top 10 Highest SO<sub>2</sub> Predicted Concentrations – Baldwin Database Site 8**

YYMMDDHH	SOURCE TYPE	SOURCE ID	RCPT NO.	FINAL PLUME HT.	DIST. FINAL PL. HT.	WDIR FINAL HT.	EFFECT. WSPD	3600* UEFF	DISTANCE TO RCPT	PLUME TYPE	MEAND. FRAC.	PART. PEN. FRAC.	EFFECT SIGMA_V	EFFECT. SIGMA_W	HOURLY CONC	AERIAL	COHERENT	PANCAKE	GAMFACT	PRMVAL	POT. TEMP. GRAD.
83031211	P	STACK1	6	456.6	1814.9	298	2.001	7204.4	3857.1	PEN	0.082	0.921	0.343	0.216	979.745	979.745	1060.581	69.248	0.489	979.745	0
83031211	P	STACK2	7	454.8	1814.9	298	2.001	7204.4	6691.7	PEN	0.099	0.916	0.343	0.216	949.105	949.105	1046.678	60.297	0.017	949.105	0
83031211	P	STACK3	7	453.4	1814.9	298	2.001	7204.4	6663.1	PEN	0.099	0.911	0.343	0.217	907.798	907.798	1001.036	57.402	0.017	907.798	0
83031210	P	STACK1	8	424.5	1940.7	304	2.792	10050.8	9877.5	PEN	0.072	1	0.346	0.121	626.397	626.397	672.724	32.034	0	626.397	0
83031210	P	STACK2	8	422.4	1920.3	304	2.792	10050.7	9846.7	PEN	0.072	1	0.346	0.122	606.112	606.112	650.873	31.81	0	606.112	0
83031210	P	STACK3	8	426.5	1960.1	304	2.792	10050.9	9816.2	PEN	0.072	1	0.346	0.119	575.179	575.179	617.304	31.118	0	575.179	0
83020709	P	STACK1	7	387.3	1964.3	296	3.74	13462.5	6720.9	PEN	0.046	1	0.424	0.136	535.807	535.807	560.451	27.271	0.015	535.807	0
83020709	P	STACK2	7	383.3	1917.9	296	3.74	13462.5	6691.7	PEN	0.046	1	0.424	0.139	553.672	553.672	579.163	27.039	0.015	553.672	0
83020709	P	STACK3	7	383.5	1919.5	296	3.74	13462.5	6663.1	PEN	0.046	1	0.424	0.138	552.422	552.422	577.852	25.947	0.015	552.422	0
83010711	P	STACK1	8	443.5	1365.7	294	2.238	8057.5	9877.5	PEN	0.085	1	0.304	0.052	374.966	374.966	406.837	33.7	0	374.966	0.00286
83010711	P	STACK2	8	443.7	1365.7	294	2.238	8057.5	9846.7	PEN	0.085	1	0.304	0.052	396.646	396.646	430.471	33.725	0	396.646	0.00286
83010711	P	STACK3	8	443.9	1365.7	294	2.238	8057.5	9816.2	PEN	0.085	1	0.304	0.052	407.504	407.504	442.371	32.661	0	407.504	0.00286
83010715	P	STACK1	7	1755.3	1459.8	311	1.318	4745.3	6720.9	DIR	0.232	0.492	0.397	0.371	436.339	436.339	545.347	75.198	0	436.339	0
83010715	P	STACK2	7	1709	1459.8	311	1.318	4745.2	6691.7	DIR	0.232	0.471	0.397	0.371	397.693	397.693	496.447	70.565	0	397.693	0
83010715	P	STACK3	7	1721.1	1459.8	311	1.318	4745.2	6663.1	DIR	0.232	0.476	0.397	0.371	381.976	381.976	475.974	70.177	0	381.976	0
83031209	P	STACK1	8	412.5	1939.9	297	3.422	12317.7	9877.5	PEN	0.053	1	0.338	0.073	326.599	326.599	343.797	16.597	0	326.599	0.00286
83031209	P	STACK2	8	410.4	1918.1	297	3.422	12317.7	9846.7	PEN	0.052	1	0.338	0.073	341.229	341.229	359.21	16.547	0	341.229	0.00286
83031209	P	STACK3	8	413.2	1946.9	297	3.422	12317.7	9816.2	PEN	0.052	1	0.338	0.073	344.338	344.338	362.474	15.919	0	344.338	0.00286
82062910	P	STACK1	7	521.6	1246	306	2.594	9336.7	6720.9	PEN	0.13	1	0.565	0.29	428.109	428.109	485.475	44.219	0.003	428.109	0
82062910	P	STACK2	7	518.5	1246	306	2.593	9336.3	6691.7	PEN	0.131	1	0.565	0.294	417.064	417.064	473.269	44.331	0.003	417.064	0
82062910	P	STACK3	7	500.2	1246	306	2.592	9332.3	6663.1	PEN	0.135	1	0.565	0.321	369.657	369.657	420.854	40.754	0.003	369.657	0
83020409	P	STACK1	4	222	286.5	304	4.582	16496.9	1396.3	DIR	0.025	0.084	0.479	0.353	91.73	13.307	13.627	0.852	1	91.73	0
83020409	P	STACK2	8	369.5	1920.9	304	4.888	17597	9846.7	PEN	0.044	0.933	0.479	0.249	452.707	452.707	472.703	20.893	0	452.707	0
83020409	P	STACK3	8	374.9	2019	304	4.889	17600.6	9816.2	PEN	0.044	0.954	0.479	0.243	450.783	450.783	470.567	21.732	0	450.783	0
82080512	STACK1	<--- Source is not emitting during this hour																			
82080512	P	STACK2	8	438.7	1001.8	296	2.265	8154.1	9846.7	PEN	0.106	1	0.388	0.055	449.719	449.719	499.336	33.045	0	449.719	0.0022
82080512	P	STACK3	8	455.3	1001.8	296	2.265	8154.1	9816.2	PEN	0.106	1	0.388	0.052	480.358	480.358	533.112	34.554	0	480.358	0.0022
82082317	P	STACK1	6	589.9	1263.1	298	1.384	4983.4	3857.1	PEN	0.186	1	0.387	0.204	735.041	735.041	882.4	88.496	0.489	735.041	0
82082317	P	STACK2	6	598.4	1263.1	298	1.385	4984.8	3832.4	PEN	0.185	1	0.387	0.196	727.478	727.478	872.341	89.013	0.489	727.478	0
82082317	STACK3	<--- Source is not emitting during this hour																			

**Table B-19: Source and Plume Details for Top 10 Highest SO<sub>2</sub> Predicted Concentrations – Baldwin Database Site 9**

YYMMDDHH	SOURCE TYPE	SOURCE ID	RCPT NO.	FINAL PLUME HT.	DIST. FINAL PL. HT.	WDIR FINAL HT.	EFFECT. WSPD	3600* UEFF	DISTANCE TO RCPT	PLUME TYPE	MEAND. FRAC.	PART. PEN. FRAC.	EFFECT SIGMA_V	EFFECT. SIGMA_W	HOURLY CONC	AERIAL	COHERENT	PANCAKE	GAMFACT	PRMVAL	POT. TEMP. GRAD.
83010310	P	STACK1	9	453.1	1099.4	16	2.484	8943.3	4449.8	PEN	0.119	1	0.556	0.318	708.681	708.681	795.657	63.269	0	0	0
83010310	P	STACK2	9	449.9	1099.4	16	2.484	8941.8	4391.9	PEN	0.119	1	0.556	0.321	710.674	710.674	797.736	63.385	0.143	710.674	0
83010310	P	STACK3	9	432.6	1099.4	16	2.477	8916.1	4328.4	PEN	0.119	1	0.556	0.354	662.112	662.112	743.51	58.989	0.143	662.112	0
83021110	P	STACK1	9	467.1	1827	17	3.777	13598.9	4449.8	PEN	0.096	0.63	0.765	0.619	563.402	563.402	618.535	46.317	0	0	0
83021110	P	STACK2	9	461.6	1827	17	3.777	13595.6	4391.9	PEN	0.096	0.602	0.766	0.622	530.656	530.656	582.681	43.302	0.143	530.656	0
83021110	P	STACK3	9	468.1	1827	17	3.778	13599.5	4328.4	PEN	0.096	0.634	0.765	0.619	554.475	554.475	608.508	45.468	0.143	554.475	0
83010311	P	STACK1	10	535.9	1024.5	18	1.881	6770.8	2233.8	PEN	0.299	0.573	0.697	0.643	639.636	639.636	856.123	131.893	0	0	0
83010311	P	STACK2	10	532.4	1024.5	18	1.863	6706	2174.4	PEN	0.299	0.557	0.699	0.635	617.402	617.402	826.974	126.957	0.821	617.402	0
83010311	P	STACK3	10	523.8	1024.5	18	1.862	6703.2	2109.7	PEN	0.301	0.518	0.701	0.639	533.093	533.093	715.301	109.486	0.817	533.093	0
82062209	P	STACK1	9	509.1	1290.5	17	2.846	10246.4	4449.8	PEN	0.147	0.999	0.731	0.479	443.895	443.895	512.005	49.837	0	0	0
82062209	P	STACK2	9	508.5	1290.5	17	2.847	10249.5	4391.9	PEN	0.147	0.998	0.731	0.479	447.218	447.218	515.722	50.107	0.143	447.218	0
82062209	P	STACK3	9	495.9	1290.5	17	2.833	10198.4	4328.4	PEN	0.15	0.97	0.732	0.497	416.314	416.314	481.338	46.708	0.143	416.314	0
83012511	P	STACK1	9	586.2	1689	25	2.047	7367.6	4449.8	PEN	0.134	0.859	0.484	0.364	405.787	405.787	460.022	55.264	0	0	0
83012511	P	STACK2	9	588.4	1689	25	2.046	7364.8	4391.9	PEN	0.134	0.864	0.484	0.361	417.276	417.276	473.056	56.113	0.013	417.276	0
83012511	P	STACK3	9	593.7	1689	25	2.046	7366.6	4328.4	PEN	0.133	0.876	0.484	0.356	415.833	415.833	471.335	55.314	0.014	415.833	0
82112113	P	STACK1	9	427.6	1698.8	10	4	14399.1	4449.8	PEN	0.081	0.63	0.725	0.544	437.063	437.063	472.468	35.903	0	0	0
82112113	P	STACK2	9	422.7	1617.3	10	3.997	14390.8	4391.9	PEN	0.081	0.601	0.726	0.546	398.317	398.317	430.634	32.997	0	0	0
82112113	P	STACK3	9	420.8	1585.3	10	3.997	14387.5	4328.4	PEN	0.081	0.589	0.726	0.547	382.779	382.779	413.789	32.04	0	0	0
83021211	P	STACK1	10	553.5	703	29	1.528	5502	2233.8	PEN	0.493	0.797	0.745	0.667	543.791	543.791	866.373	211.427	0	0	0
83021211	P	STACK2	10	547.2	703	29	1.528	5501.5	2174.4	PEN	0.495	0.779	0.747	0.672	525.118	525.118	840.546	203.738	0.05	525.118	0
83021211	P	STACK3	10	554.9	703	29	1.528	5502.1	2109.7	PEN	0.491	0.801	0.744	0.666	551.503	551.503	878.935	212.574	0.05	551.503	0
82043012	P	STACK1	9	526.8	1694	9	2.784	10021.3	4449.8	PEN	0.084	0.838	0.499	0.38	396.723	396.723	430.122	34.581	0	0	0
82043012	P	STACK2	9	541.3	1829.5	9	2.802	10087.8	4391.9	PEN	0.083	0.876	0.499	0.367	420.408	420.408	454.969	37.058	0	0	0
82043012	P	STACK3	9	494.1	1388.2	9	2.684	9663.6	4328.4	PEN	0.09	0.733	0.499	0.396	314.012	314.012	342.181	28.547	0	0	0
82102411	P	STACK1	9	571.3	1051.6	19	1.864	6710	4449.8	PEN	0.232	0.975	0.604	0.462	555.725	555.725	699.08	80.768	0	0	0
82102411	STACK2	<--- Source is not emitting during this hour																			
82102411	P	STACK3	9	572.3	1051.6	19	1.862	6703.2	4328.4	PEN	0.232	0.977	0.604	0.463	558.549	558.549	702.404	81.043	0.145	558.549	0
83021212	P	STACK1	9	575.2	1283.4	27	2.723	9803.6	4449.8	PEN	0.224	0.593	0.858	0.775	352.919	352.919	436.449	63.572	0	0	0
83021212	P	STACK2	9	567.5	1283.4	27	2.722	9799.7	4391.9	PEN	0.225	0.563	0.861	0.779	330.431	330.431	409.416	58.966	0.006	330.431	0
83021212	P	STACK3	9	574.5	1283.4	27	2.723	9803.3	4328.4	PEN	0.224	0.59	0.859	0.775	353.542	353.542	437.405	62.609	0.005	353.542	0

**Table B-20: Source and Plume Details for Top 10 Highest SO<sub>2</sub> Predicted Concentrations – Baldwin Database Site 10**

YYMMDDHH	SOURCE TYPE	SOURCE ID	RCPT NO.	FINAL PLUME HT.	DIST. FINAL PL. HT.	WDIR FINAL HT.	EFFECT. WSPD	3600 * UEFF	DISTANCE TO RCPT	PLUME TYPE	MEAND. FRAC.	PART. PEN. FRAC.	EFFECT SIGMA_V	EFFECT. SIGMA_W	HOURLY CONC	AERVAL	COHERENT	PANCAKE	GAMFACT	PRMVAL	POT. TEMP. GRAD.
83010311	P	STACK1	10	535.9	1024.5	18	1.881	6770.8	2233.8	PEN	0.299	0.573	0.697	0.643	639.636	639.636	856.123	131.893	0	0	0
83010311	P	STACK2	10	532.4	1024.5	18	1.863	6706	2174.4	PEN	0.299	0.557	0.699	0.635	617.402	617.402	826.974	126.957	0.821	617.402	0
83010311	P	STACK3	10	523.8	1024.5	18	1.862	6703.2	2109.7	PEN	0.301	0.518	0.701	0.639	533.093	533.093	715.301	109.486	0.817	533.093	0
83021211	P	STACK1	10	553.5	703	29	1.528	5502	2233.8	PEN	0.493	0.797	0.745	0.667	543.791	543.791	866.373	211.427	0	0	0
83021211	P	STACK2	10	547.2	703	29	1.528	5501.5	2174.4	PEN	0.495	0.779	0.747	0.672	525.118	525.118	840.546	203.738	0.05	525.118	0
83021211	P	STACK3	10	554.9	703	29	1.528	5502.1	2109.7	PEN	0.491	0.801	0.744	0.666	551.503	551.503	878.935	212.574	0.05	551.503	0
82112111	P	STACK1	10	395.4	1709.9	5	3.46	12455.6	2233.8	PEN	0.061	0.828	0.58	0.43	395.264	395.264	419.167	28.514	0	0	0
82112111	P	STACK2	10	388.6	1603.6	5	3.458	12447.3	2174.4	PEN	0.061	0.795	0.58	0.434	351.584	351.584	372.862	25.651	0	0	0
82112111	P	STACK3	10	388	1595.2	5	3.457	12446.6	2109.7	PEN	0.061	0.792	0.58	0.434	325.727	325.727	345.323	23.992	0	0	0
82060511	P	STACK1	10	471	1279	6	2.735	9845.6	2233.8	PEN	0.114	0.994	0.624	0.376	536.004	536.004	597.803	53.544	0	0	0
82060511	STACK2	<--- Source is not emitting during this hour																			
82060511	P	STACK3	10	465.3	1279	6	2.734	9844.2	2109.7	PEN	0.113	0.98	0.624	0.383	486.599	486.599	542.606	49.136	0	0	0
82121213	P	STACK1	10	510.3	1276.5	354	2.279	8203.8	2233.8	PEN	0.16	0.921	0.621	0.383	359.495	359.495	414.241	71.962	0	0	0
82121213	P	STACK2	10	501.2	1276.5	354	2.278	8200	2174.4	PEN	0.16	0.897	0.621	0.394	334.553	334.553	385.346	68.069	0	0	0
82121213	P	STACK3	10	496.6	1276.5	354	2.277	8197.8	2109.7	PEN	0.16	0.885	0.621	0.4	305.83	305.83	352.054	63.144	0	0	0
82102411	P	STACK1	9	571.3	1051.6	19	1.864	6710	4449.8	PEN	0.232	0.975	0.604	0.462	555.725	555.725	699.08	80.768	0	0	0
82102411	STACK2	<--- Source is not emitting during this hour																			
82102411	P	STACK3	9	572.3	1051.6	19	1.862	6703.2	4328.4	PEN	0.232	0.977	0.604	0.463	558.549	558.549	702.404	81.043	0.145	558.549	0
83021110	P	STACK1	9	467.1	1827	17	3.777	13598.9	4449.8	PEN	0.096	0.63	0.765	0.619	563.402	563.402	618.535	46.317	0	0	0
83021110	P	STACK2	9	461.6	1827	17	3.777	13595.6	4391.9	PEN	0.096	0.602	0.766	0.622	530.656	530.656	582.681	43.302	0.143	530.656	0
83021110	P	STACK3	9	468.1	1827	17	3.778	13599.5	4328.4	PEN	0.096	0.634	0.765	0.619	554.475	554.475	608.508	45.468	0.143	554.475	0
83021212	P	STACK1	9	575.2	1283.4	27	2.723	9803.6	4449.8	PEN	0.224	0.593	0.858	0.775	352.919	352.919	436.449	63.572	0	0	0
83021212	P	STACK2	9	567.5	1283.4	27	2.722	9799.7	4391.9	PEN	0.225	0.563	0.861	0.779	330.431	330.431	409.416	58.966	0.006	330.431	0
83021212	P	STACK3	9	574.5	1283.4	27	2.723	9803.3	4328.4	PEN	0.224	0.59	0.859	0.775	353.542	353.542	437.405	62.609	0.005	353.542	0
83010313	P	STACK1	10	1213	1264.6	3	1.894	6818.4	2233.8	DIR	0.408	0.227	0.845	0.79	315.18	315.18	477.271	79.578	0	0	0
83010313	P	STACK2	10	1122.7	1264.6	3	1.895	6823.1	2174.4	DIR	0.408	0.185	0.845	0.79	267.466	267.466	405.465	67.158	0	0	0
83010313	P	STACK3	10	1126.9	1264.6	3	1.896	6827.3	2109.7	DIR	0.408	0.186	0.845	0.79	262.624	262.624	397.7	66.357	0	0	0
82112113	P	STACK1	9	427.6	1698.8	10	4	14399.1	4449.8	PEN	0.081	0.63	0.725	0.544	437.063	437.063	472.468	35.903	0	0	0
82112113	P	STACK2	9	422.7	1617.3	10	3.997	14390.8	4391.9	PEN	0.081	0.601	0.726	0.546	398.317	398.317	430.634	32.997	0	0	0
82112113	P	STACK3	9	420.8	1585.3	10	3.997	14387.5	4328.4	PEN	0.081	0.589	0.726	0.547	382.779	382.779	413.789	32.04	0	0	0

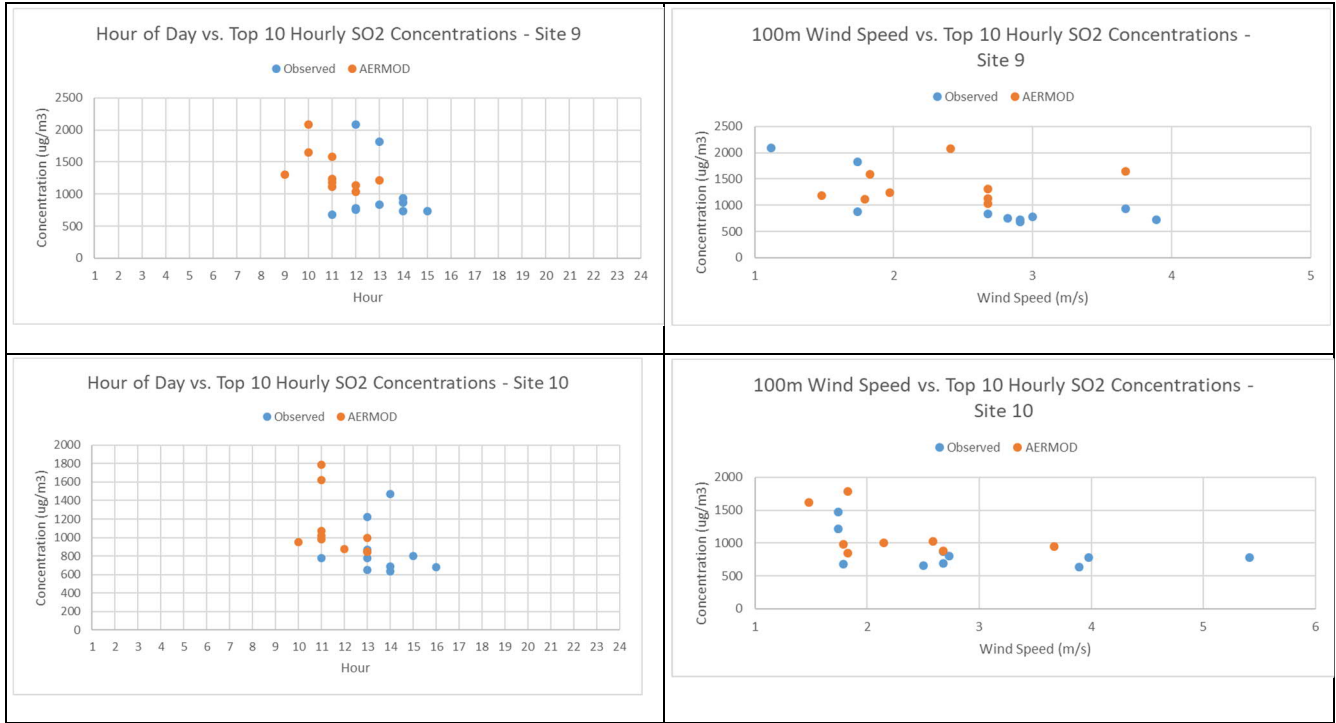
**Figure B-1: Top 10 Concentrations vs. Hour of Day and Wind Speed – Sites 1 through 4**



**Figure B-2: Top 10 Concentrations vs. Hour of Day and Wind Speed – Sites 5 through 8**



**Figure B-3: Top 10 Concentrations vs. Hour of Day and Wind Speed – Sites 9 and 10**



# APPENDIX C: Labadie Tables and Plots

**Table C-1: Meteorological Parameters for Top 10 Highest SO<sub>2</sub> Predicted Concentrations – Labadie Database Valley Site**

Rank	YYMMDDHH	USTAR	WSTAR	OBULEN	URB_OBULEN	ZIMECH	ZICONV	ZI_URB	SFCZO	THSTAR
1	18121013	0.22	1.06	-7.8	N.A.	244	361	N.A.	0.03	-9.99
2	17090210	0.17	1.44	-2.5	N.A.	174	575	N.A.	0.2	-9.99
3	18060610	0.22	1.17	-7.2	N.A.	252	420	N.A.	0.2	-9.99
4	17060511	0.19	1.23	-4.3	N.A.	203	450	N.A.	0.2	-9.99
5	18121016	0.16	0.52	-31	N.A.	161	434	N.A.	0.03	-9.99
6	17092910	0.25	1.26	-9.3	N.A.	301	473	N.A.	0.2	-9.99
7	17051109	0.07	0.6	-1.5	N.A.	49	310	N.A.	0.04	-9.99
8	17050910	0.33	1.1	-24.5	N.A.	460	357	N.A.	0.04	-9.99
9	17051012	0.21	1.22	-5.3	N.A.	231	417	N.A.	0.04	-9.99
10	18060609	0.17	0.95	-4.4	N.A.	171	299	N.A.	0.2	-9.99

**Table C-2: Meteorological Parameters for Top 10 Highest SO<sub>2</sub> Predicted Concentrations – Labadie Database Northwest Site**

Rank	YYMMDDHH	USTAR	WSTAR	OBULEN	URB_OBULEN	ZIMECH	ZICONV	ZI_URB	SFCZO	THSTAR
1	18022211	0.16	0.77	-9.1	N.A.	159	374	N.A.	0.03	-9.99
2	19062715	0.16	0.7	-15.8	N.A.	153	532	N.A.	0.2	-9.99
3	18060609	0.17	0.95	-4.4	N.A.	171	299	N.A.	0.2	-9.99
4	19111611	0.17	0.86	-6.8	N.A.	174	325	N.A.	0.2	-9.99
5	19111515	0.15	0.74	-7.1	N.A.	134	368	N.A.	0.2	-9.99
6	19061111	0.19	1.04	-6.8	N.A.	203	431	N.A.	0.2	-9.99
7	18021312	0.17	0.96	-3.6	N.A.	166	267	N.A.	0.03	-9.99
8	17111611	0.24	1.24	-10.5	N.A.	283	584	N.A.	0.176	-9.99
9	19072111	0.18	1.07	-6	N.A.	188	489	N.A.	0.2	-9.99
10	19062813	0.17	1.28	-4.3	N.A.	176	730	N.A.	0.204	-9.99

**Table C-3: Meteorological Parameters for Top 10 Highest SO<sub>2</sub> Predicted Concentrations – Labadie Database Southwest Site**

Rank	YYMMDDHH	USTAR	WSTAR	OBULEN	URB_OBULEN	ZIMECH	ZICONV	ZI_URB	SFCZO	THSTAR
1	19020112	0.22	0.92	-11.9	N.A.	247	346	N.A.	0.03	-9.99
2	19111516	0.1	0.47	-9.9	N.A.	81	370	N.A.	0.2	-9.99
3	17022310	0.13	0.95	-2.2	N.A.	117	322	N.A.	0.03	-9.99
4	19012712	0.21	0.84	-16.3	N.A.	230	422	N.A.	0.03	-9.99
5	17052708	0.12	1.04	-1.8	N.A.	97	489	N.A.	0.04	-9.99
6	17052310	0.12	0.72	-6	N.A.	104	487	N.A.	0.04	-9.99
7	17022311	0.13	1.26	-1.2	N.A.	110	451	N.A.	0.03	-9.99
8	18041709	0.16	1.26	-3.7	N.A.	153	734	N.A.	0.04	-9.99
9	18010513	0.23	0.99	-15.8	N.A.	257	544	N.A.	0.03	-9.99
10	19052610	0.21	0.93	-11.3	N.A.	226	405	N.A.	0.04	-9.99

**Table C-4: Meteorological Parameters for Top 10 Highest SO<sub>2</sub> Predicted Concentrations – Labadie Database North Site**

Rank	YYMMDDHH	USTAR	WSTAR	OBULEN	URB_OBULEN	ZIMECH	ZICONV	ZI_URB	SFCZO	THSTAR
1	19020114	0.12	0.97	-2.1	N.A.	104	414	N.A.	0.03	-9.99
2	19020115	0.13	0.9	-3.6	N.A.	117	437	N.A.	0.03	-9.99
3	18071912	0.23	1.14	-10	N.A.	271	463	N.A.	0.092	-9.99
4	17051510	0.17	1.24	-3.3	N.A.	172	504	N.A.	0.04	-9.99
5	17053010	0.09	1.44	-1	N.A.	68	776	N.A.	0.04	-9.99
6	17060410	0.16	1.21	-3.2	N.A.	152	567	N.A.	0.2	-9.99
7	19062711	0.11	1	-1.2	N.A.	83	394	N.A.	0.2	-9.99
8	18060609	0.17	0.95	-4.4	N.A.	171	299	N.A.	0.2	-9.99
9	19120713	0.14	0.9	-3.8	N.A.	129	382	N.A.	0.03	-9.99
10	17043015	0.1	0.71	-3	N.A.	77	398	N.A.	0.04	-9.99

**Table C-5: Source and Plume Details for Top 10 Highest SO<sub>2</sub> Predicted Concentrations – Labadie Database Valley Site**

YYMMDDHH	SOURCE TYPE	SOURCEID	RCPT NO.	FINAL PLUME HT.	DIST. FINAL PL. HT.	WDIR FINAL HT.	EFFECT. WSPD	3600* UEFF	DISTANCETO RCPT	PLUME TYPE	MEAND. FRAC.	PART. PEN. FRAC.	EFFECT SIGMA_V	EFFECT. SIGMA_W	HOURLY CONC	AERVAL	COHERENT	PANCAKE	GAMFACT	PRMVAL	POT. TEMP. GRAD.
18121013	P	LAB34	1	475.3	1483.8	245	2.522	9079.9	3724.9	PEN	0.174	0.911	0.711	0.453	53.331	53.331	63.14	6.767	0.3	53.331	0
18121013	P	LABADIE1	1	467.9	1483.8	245	2.524	9086	3765.4	PEN	0.175	0.887	0.712	0.457	50.644	50.644	59.945	6.732	0.286	50.644	0
18121013	P	LABADIE2	1	475.5	1483.8	245	2.522	9079.7	3747.2	PEN	0.174	0.912	0.71	0.453	54.016	54.016	63.917	7.041	0.293	54.016	0
18121013	P	LABADIE5	1	18.8	52.2	241	2.488	8957.8	3723	DIR	0.185	0.001	0.727	0.499	0	0	0	0	0	0	0
17090210	P	LAB34	1	698.9	1073	245	1.489	5360.2	3724.9	PEN	0.433	0.61	0.594	0.587	80.84	80.84	126.836	20.557	0.214	80.84	0
17090210	P	LABADIE1	1	1380.1	1073	245	1.433	5157.1	3765.4	IND	0.492	0.405	0.613	0.633	36.269	36.269	61.533	10.209	0.183	36.269	0
17090210	P	LABADIE2	1	1446	1073	245	1.433	5157.1	3747.2	IND	0.483	0.441	0.613	0.633	41.596	41.596	69.69	11.484	0.197	41.596	0
17090210	P	LABADIE5	1	33.6	51.2	285	1.154	4155.6	3723	DIR	0.581	0	0.613	0.606	0	0	0	0	0	0	0
18060610	P	LAB34	1	596.3	852.4	236	1.537	5534.1	3724.9	PEN	0.457	0.946	0.704	0.493	74.976	74.976	118.695	22.934	0.004	74.976	0
18060610	P	LABADIE1	1	537.3	852.4	236	1.506	5422.7	3765.4	PEN	0.539	0.797	0.717	0.523	40.048	40.048	70.078	14.399	0.004	40.048	0
18060610	P	LABADIE2	1	541.6	852.4	236	1.508	5430.3	3747.2	PEN	0.533	0.811	0.716	0.521	41.303	41.303	71.865	14.479	0.004	41.303	0
18060610	P	LABADIE5	3	24.6	50.8	3	1.105	3977.3	4310.6	DIR	0.896	0.001	0.737	0.587	0	0	0	0	0	0	0
17060511	P	LAB34	1	746.9	1017.3	244	1.659	5973.9	3724.9	PEN	0.305	1	0.629	0.358	51.545	51.545	69.748	10.15	0.314	51.545	0
17060511	P	LABADIE1	1	645.1	1017.3	244	1.617	5819.6	3765.4	PEN	0.378	0.934	0.68	0.484	33.33	33.33	48.858	7.834	0.314	33.33	0
17060511	P	LABADIE2	1	647.8	1017.3	244	1.621	5834.3	3747.2	PEN	0.375	0.938	0.679	0.482	32.834	32.834	47.981	7.584	0.314	32.834	0
17060511	P	LABADIE5	1	28.6	50.8	244	1.493	5373.7	3723	DIR	0.482	0.002	0.722	0.549	0	0	0	0	0	0	0
18121016	P	LAB34	1	554.9	2020.9	255	1.579	5685.7	3724.9	PEN	0.18	0.784	0.457	0.205	35.476	35.476	42.22	4.708	0.458	35.476	0
18121016	P	LABADIE1	1	546.5	1921.8	255	1.585	5707.2	3765.4	PEN	0.178	0.757	0.457	0.209	36.478	36.478	43.371	4.601	0.452	36.478	0
18121016	P	LABADIE2	1	555.5	2027.6	255	1.579	5685.6	3747.2	PEN	0.18	0.786	0.457	0.205	37.164	37.164	44.27	4.795	0.455	37.164	0
18121016	P	LABADIE5	1	20.9	52.1	257	1.835	6607.5	3723	DIR	0.144	0.001	0.457	0.236	0	0	0	0	0	0	0
17092910	P	LAB34	1	688.8	1884.2	252	2.829	10183.8	3724.9	PEN	0.113	0.937	0.611	0.382	41.079	41.079	45.79	4.026	0.462	41.079	0
17092910	P	LABADIE1	1	608.3	1830.9	252	2.709	9753.1	3765.4	PEN	0.144	0.766	0.644	0.461	34.87	34.87	40.12	3.755	0.46	34.87	0
17092910	P	LABADIE2	1	604.4	1794.1	252	2.7	9720.6	3747.2	PEN	0.146	0.755	0.645	0.464	31.703	31.703	36.536	3.442	0.461	31.703	0
17092910	P	LABADIE5	2	22.3	51.2	217	2.202	7928.1	3346.3	DIR	0.192	0.001	0.669	0.504	0	0	0	0	0	0	0
17051109	P	LAB34	1	688.7	506.5	263	0.755	2719.6	3724.9	PEN	0.542	1	0.384	0.08	20.977	20.977	37.088	7.382	0.019	20.977	0
17051109	P	LABADIE1	1	606.4	506.5	263	0.755	2718.6	3765.4	PEN	0.543	1	0.384	0.149	44.909	44.909	81.805	13.858	0.018	44.909	0
17051109	P	LABADIE2	1	616.6	506.5	263	0.755	2719	3747.2	PEN	0.543	1	0.384	0.137	40.569	40.569	73.419	12.891	0.018	40.569	0
17051109	P	LABADIE5	1	46.2	51.2	263	0.615	2214.9	3723	IND	0.625	0.005	0.384	0.253	0	0	0	0	0	0	0
17050910	P	LAB34	1	534.8	1944.4	250	4.253	15309.5	3724.9	PEN	0.12	0.566	0.784	0.498	37.365	37.365	42.009	3.468	0.461	37.365	0
17050910	P	LABADIE1	1	533.2	1919.5	250	4.251	15303.4	3765.4	PEN	0.122	0.559	0.786	0.504	31.369	31.369	35.303	2.946	0.461	31.369	0
17050910	P	LABADIE2	1	523.5	1767.4	250	4.244	15280	3747.2	PEN	0.127	0.51	0.793	0.527	32.155	32.155	36.396	3.035	0.461	32.155	0
17050910	P	LABADIE5	1	15	50.9	258	3.086	11108.6	3723	DIR	0.177	0	0.887	0.733	0	0	0	0	0	0	0
17051012	P	LAB34	1	574.4	1644.6	244	4.533	16319.3	3724.9	PEN	0.08	0.911	0.771	0.624	39.664	39.664	42.79	3.631	0.354	39.664	0
17051012	P	LABADIE1	1	535.4	1644.6	244	4.134	14882.3	3765.4	PEN	0.108	0.806	0.793	0.68	30.389	30.389	33.666	3.454	0.339	30.389	0
17051012	P	LABADIE2	1	537.6	1644.6	244	4.16	14975.6	3747.2	PEN	0.107	0.813	0.792	0.676	32.549	32.549	36.012	3.504	0.344	32.549	0
17051012	P	LABADIE5	4	19.8	50.7	200	2.613	9407.9	3858.4	DIR	0.193	0.001	0.825	0.729	0	0	0	0	0	0	0
18060609	P	LAB34	3	706.4	336.4	68	0.532	1914.4	4312.9	PEN	1	1	0.6	0.098	40.85	40.85	65.308	40.85	PLUME OUT	OF WAKE	0
18060609	P	LABADIE1	2	598.5	336.4	68	0.542	1951.6	3203.1	PEN	1	1	0.612	0.207	36.971	36.971	7.96	36.971	PLUME OUT	OF WAKE	0
18060609	P	LABADIE2	2	605.7	336.4	68	0.539	1941.4	3259	PEN	1	1	0.611	0.195	36.188	36.188	6.502	36.188	PLUME OUT	OF WAKE	0
18060609	P	LABADIE5	2	31.1	50.9	39	0.689	2479.1	3346.3	DIR	1	0.002	0.652	0.488	0	0	0	0	0	0	0

**Table C-6: Source and Plume Details for Top 10 Highest SO<sub>2</sub> Predicted Concentrations – Labadie Database Northwest Site**

YMMDDHH	SOURCE TYPE	SOURCE ID	RCPT NO.	FINAL PLUME HT.	DIST. FINAL PL HT.	WDIR FINAL HT.	EFFECT. WSPD	3600* UEFF	DISTANCE TO RCPT	PLUME TYPE	MEAND. FRAC.	PART. PEN. FRAC.	EFFECT SIGMA_V	EFFECT. SIGMA_W	HOURLY CONC	AERVAL	COHERENT	PANCAKE	GAMFACT	PRMVAL	POT. TEMP. GRAD.
18022211	P	LAB34	2	586.9	903.6	116	0.916	3298.3	3340.2	PEN	0.727	1	0.548	0.26	67.635	67.635	153.756	35.339	0.001	67.635	0
18022211	P	LABADIE1	2	510.8	903.6	116	0.952	3428.8	3203.1	PEN	0.667	0.945	0.548	0.303	44.251	44.251	92.432	20.203	0.001	44.251	0
18022211	P	LABADIE2	2	514.2	903.6	116	0.952	3425.9	3259	PEN	0.67	0.954	0.548	0.302	45.333	45.333	94.975	20.83	0.001	45.333	0
18022211	P	LABADIE5	3	21.7	52.2	31	1.012	3641.7	4310.6	DIR	0.607	0.001	0.548	0.354	0	0	0	0	0	0	0
19062715	P	LAB34	2	827.2	1431.6	142	1.358	4889.8	3340.2	PEN	0.302	0.974	0.512	0.3	50.649	50.649	67.773	11.124	PLUME OUT	OF WAKE	0
19062715	P	LABADIE1	2	724.7	1431.6	142	1.429	5146	3203.1	PEN	0.268	0.821	0.512	0.377	39.469	39.469	50.907	8.166	PLUME OUT	OF WAKE	0
19062715	P	LABADIE2	2	702.8	1431.6	142	1.433	5159.7	3259	PEN	0.265	0.776	0.512	0.392	35.835	35.835	46.109	7.318	PLUME OUT	OF WAKE	0
19062715	P	LABADIE5	2	28	50.6	157	1.569	5647.5	3346.3	DIR	0.232	0.001	0.512	0.441	0	0	0	0	0	0	0
18060609	P	LAB34	3	706.4	336.4	68	0.532	1914.4	4312.9	PEN	1	1	0.6	0.098	40.85	40.85	65.308	40.85	PLUME OUT	OF WAKE	0
18060609	P	LABADIE1	2	598.5	336.4	68	0.542	1951.6	3203.1	PEN	1	1	0.612	0.207	36.971	36.971	7.96	36.971	PLUME OUT	OF WAKE	0
18060609	P	LABADIE2	2	605.7	336.4	68	0.539	1941.4	3259	PEN	1	1	0.611	0.195	36.188	36.188	6.502	36.188	PLUME OUT	OF WAKE	0
18060609	P	LABADIE5	2	31.1	50.9	39	0.689	2479.1	3346.3	DIR	1	0.002	0.652	0.488	0	0	0	0	0	0	0
19111611	P	LAB34	2	439.9	1692.6	123	2.559	9212.4	3340.2	PEN	0.078	1	0.459	0.309	50.433	50.433	54.274	5.217	PLUME OUT	OF WAKE	0
19111611	P	LABADIE1	2	423.4	1632.4	123	2.521	9074.8	3203.1	PEN	0.081	0.957	0.459	0.324	50.252	50.252	54.252	5.011	0.046	50.252	0
19111611		LABADIE2	<--- Source is not emitting during this hour																		
19111611	P	LABADIE5	3	29.1	52	28	2.207	7944.2	4310.6	DIR	0.107	0.002	0.46	0.373	0	0	0	0	0	0	0
19111515	P	LAB34	2	602.4	685.3	135	1.484	5341.5	3340.2	PEN	0.246	1	0.499	0.237	47.729	47.729	60.871	7.504	0.18	47.729	0
19111515	P	LABADIE1	2	590	685.3	135	1.445	5200.6	3203.1	PEN	0.258	1	0.499	0.25	48.339	48.339	62.389	7.947	0.224	48.339	0
19111515		LABADIE2	<--- Source is not emitting during this hour																		
19111515	P	LABADIE5	4	33.2	51.8	54	0.699	2517.9	3858.4	DIR	0.999	0.001	0.499	0.394	0	0	0	0	0	0	0
19061111	P	LAB34	3	985.4	408.8	290	0.521	1873.9	4312.9	PEN	1	1	0.627	0.153	27.882	27.882	0	27.882	PLUME OUT	OF WAKE	0
19061111	P	LABADIE1	2	816.9	408.8	290	0.522	1879.7	3203.1	PEN	1	1	0.667	0.388	30.943	30.943	0	30.943	PLUME OUT	OF WAKE	0
19061111	P	LABADIE2	2	847.1	408.8	290	0.518	1866.5	3259	PEN	1	1	0.657	0.333	30.062	30.062	0	30.062	PLUME OUT	OF WAKE	0
19061111	P	LABADIE5	4	27	50.9	247	0.974	3506.5	3858.4	DIR	1	0.002	0.718	0.627	0	0	0	0	0	0	0
18021312	P	LAB34	3	674.1	412.9	62	0.56	2016	4312.9	PEN	1	1	0.912	0.076	32.815	32.815	47.257	32.815	PLUME OUT	OF WAKE	0
18021312	P	LABADIE1	2	566	412.9	62	0.559	2014	3203.1	PEN	1	1	0.921	0.152	32.148	32.148	0.975	32.148	PLUME OUT	OF WAKE	0
18021312	P	LABADIE2	2	569.9	412.9	62	0.559	2014.2	3259	PEN	1	1	0.92	0.148	31.06	31.06	0.816	31.06	PLUME OUT	OF WAKE	0
18021312	P	LABADIE5	2	23	52.1	158	0.918	3303.8	3346.3	DIR	1	0.002	0.998	0.515	0	0	0	0	0	0	0
17111611	P	LAB34	2	1797.1	988.7	123	1.295	4662.2	3340.2	IND	0.724	0.457	0.736	0.594	40.858	40.858	94.089	20.571	0.328	40.858	0
17111611	P	LABADIE1	2	1473.6	988.7	123	1.295	4662.2	3203.1	IND	0.721	0.308	0.736	0.594	25.873	25.873	60.324	12.538	0.263	25.873	0
17111611	P	LABADIE2	2	1311.1	988.7	123	1.295	4662.2	3259	IND	0.719	0.233	0.736	0.594	19.791	19.791	46.508	9.324	0.29	19.791	0
17111611	P	LABADIE5	2	22.5	52.1	73	1.245	4480.3	3346.3	DIR	0.709	0	0.736	0.585	0	0	0	0	0	0	0
19072111	P	LAB34	2	722.3	852.4	107	1.162	4183	3340.2	PEN	0.696	0.943	0.694	0.547	40.827	40.827	81.568	23.019	PLUME OUT	OF WAKE	0
19072111	P	LABADIE1	2	642.4	852.4	107	1.226	4412.7	3203.1	PEN	0.581	0.79	0.705	0.591	23.605	23.605	40.679	11.282	PLUME OUT	OF WAKE	0
19072111	P	LABADIE2	2	617	852.4	107	1.25	4498.4	3259	PEN	0.539	0.722	0.709	0.605	17.993	17.993	29.361	8.271	PLUME OUT	OF WAKE	0
19072111	P	LABADIE5	2	28.2	50.6	337	2.163	7786.9	3346.3	DIR	0.238	0.001	0.724	0.653	0	0	0	0	0	0	0
19062813	P	LAB34	2	878.2	1521.9	125	1.992	7171.3	3340.2	PEN	0.344	0.547	0.805	0.729	39.124	39.124	55.116	8.688	0.523	39.124	0
19062813	P	LABADIE1	2	1463.3	1521.9	125	1.696	6105.4	3203.1	IND	0.35	0.361	0.824	0.781	23.507	23.507	33.395	5.113	0.478	23.507	0
19062813	P	LABADIE2	2	1348.9	1521.9	125	1.696	6105.4	3259	IND	0.35	0.302	0.824	0.781	19.918	19.918	28.357	4.275	0.508	19.918	0
19062813	P	LABADIE5	2	31	50.5	120	2.006	7221.4	3346.3	DIR	0.35	0	0.824	0.76	0	0	0	0	0	0	0

**Table C-7: Source and Plume Details for Top 10 Highest SO<sub>2</sub> Predicted Concentrations – Labadie Database Southwest Site**

YMMDDHH	SOURCE TYPE	SOURCE ID	RCPT NO.	FINAL PLUME HT.	DIST. FINAL PL. HT.	WDIR FINAL HT.	EFFECT. WSPD	3600* UEFF	DISTANCE TO RCPT	PLUME TYPE	MEAND. FRAC.	PART. PEN. FRAC.	EFFECT SIGMA_V	EFFECT. SIGMA_W	HOURLY CONC	AERVAL	COHERENT	PANCAKE	GAMFACT	PRMVAL	POT. TEMP. GRAD.
19020112	P	LAB34	3	593.6	1121.3	24	0.865	3113.5	4312.9	PEN	0.771	1	0.532	0.227	53.665	53.665	135.778	29.213	0.208	53.665	0
19020112	P	LABADIE1	3	516.8	1121.3	24	0.981	3532.2	4371.5	PEN	0.617	1	0.536	0.269	43.356	43.356	86.75	16.421	0.182	43.356	0
19020112	P	LABADIE2	3	528.3	1121.3	24	0.973	3502.4	4348.5	PEN	0.626	1	0.535	0.264	44.103	44.103	89.217	17.122	0.192	44.103	0
19020112	P	LABADIE5	4	18.3	52.1	61	1.597	5749.9	3858.4	DIR	0.315	0.001	0.543	0.336	0	0	0	0	0	0	0
19111516	P	LAB34	3	518.7	947.1	40	1.045	3762.4	4312.9	PEN	0.441	0.983	0.472	0.271	71.335	71.335	113.691	17.599	0.008	71.335	0
19111516	P	LABADIE1	3	512.3	947.1	40	1.045	3761.7	4371.5	PEN	0.446	0.968	0.472	0.273	61.912	61.912	98.797	16.041	0.007	61.912	0
19111516	LABADIE2 <--- Source is not emitting during this hour																				
19111516	P	LABADIE5	2	41	51.8	353	0.763	2747.9	3346.3	DIR	0.776	0.002	0.472	0.319	0	0	0	0	0	0	0
17022310	P	LAB34	3	635.4	1006.6	27	1.544	5556.7	4312.9	PEN	0.196	1	0.449	0.121	26.157	26.157	31.732	3.287	0.245	26.157	0
17022310	P	LABADIE1	3	546.1	1006.6	27	1.54	5544.1	4371.5	PEN	0.209	1	0.465	0.235	50.948	50.948	62.702	6.438	0.243	50.948	0
17022310	P	LABADIE2	3	554.1	1006.6	27	1.541	5547.5	4348.5	PEN	0.207	1	0.463	0.222	51.313	51.313	63.023	6.493	0.244	51.313	0
17022310	P	LABADIE5	3	27.3	51.5	27	1.475	5309.5	4310.6	DIR	0.248	0.002	0.492	0.392	0	0	0	0	0	0	0
19012712	P	LAB34	3	520.7	2364	28	2.874	10345.7	4312.9	PEN	0.15	0.729	0.667	0.348	62.147	62.147	71.987	6.481	0.257	62.147	0
19012712	P	LABADIE1	3	492	1905.1	28	2.752	9908.9	4371.5	PEN	0.169	0.602	0.667	0.362	47.698	47.698	56.357	5.21	0.238	47.698	0
19012712	LABADIE2 <--- Source is not emitting during this hour																				
19012712	P	LABADIE5	3	18.5	52.4	35	2.087	7514.3	4310.6	DIR	0.223	0	0.667	0.39	0	0	0	0	0	0	0
17052708	P	LAB34	3	633.9	1010.7	7	1.353	4869.4	4312.9	PEN	0.307	0.769	0.446	0.453	46.505	46.505	59.013	18.326	PLUME OUT	OF WAKE	0
17052708	P	LABADIE1	3	580.1	1010.7	7	1.33	4787.2	4371.5	PEN	0.362	0.597	0.452	0.474	30.75	30.75	41.972	10.93	PLUME OUT	OF WAKE	0
17052708	P	LABADIE2	3	582.8	1010.7	7	1.331	4791.7	4348.5	PEN	0.358	0.607	0.452	0.473	30.092	30.092	40.673	11.142	PLUME OUT	OF WAKE	0
17052708	P	LABADIE5	2	31.8	51	62	0.932	3354.4	3346.3	DIR	0.504	0.001	0.458	0.488	0	0	0	0	0	0	0
17052310	P	LAB34	3	864.3	977.2	20	0.866	3117.6	4312.9	PEN	0.548	1	0.442	0.196	40.736	40.736	73.588	13.638	0.021	40.736	0
17052310	P	LABADIE1	3	728.4	977.2	20	0.854	3074.8	4371.5	PEN	0.564	0.957	0.442	0.295	30.541	30.541	56.951	10.093	0.021	30.541	0
17052310	P	LABADIE2	3	739.4	977.2	20	0.854	3072.6	4348.5	PEN	0.564	0.973	0.442	0.291	31.714	31.714	59.037	10.575	0.021	31.714	0
17052310	P	LABADIE5	1	27.4	51.3	279	0.898	3231.5	3723	DIR	0.509	0.001	0.442	0.349	0	0	0	0	0	0	0
17022311	P	LAB34	3	681.9	816.4	8	1.32	4752	4312.9	PEN	0.366	0.99	0.545	0.481	46.23	46.23	63.525	16.266	PLUME OUT	OF WAKE	0
17022311	P	LABADIE1	3	612.2	816.4	8	1.317	4742.9	4371.5	PEN	0.394	0.864	0.56	0.52	28.327	28.327	40.653	9.37	PLUME OUT	OF WAKE	0
17022311	P	LABADIE2	3	618.4	816.4	8	1.318	4743.8	4348.5	PEN	0.391	0.877	0.558	0.517	30.068	30.068	42.81	10.245	PLUME OUT	OF WAKE	0
17022311	P	LABADIE5	3	30	51.3	8	1.283	4620.1	4310.6	DIR	0.45	0.001	0.594	0.588	0	0	0	0	0	0	0
18041709	P	LAB34	3	2027.9	2261.9	32	2.032	7316	4312.9	IND	0.162	0.292	0.558	0.602	49.115	49.115	57.459	5.926	0.258	49.115	0
18041709	P	LABADIE1	3	1432.4	1891.4	32	2.032	7316	4371.5	IND	0.168	0.158	0.558	0.602	26.484	26.484	31.179	3.221	0.247	26.484	0
18041709	P	LABADIE2	3	1567.7	2029	32	2.032	7316	4348.5	IND	0.167	0.181	0.558	0.602	28.32	28.32	33.306	3.43	0.251	28.32	0
18041709	P	LABADIE5	3	24.5	52	24	2.017	7260.3	4310.6	DIR	0.174	0	0.558	0.598	0	0	0	0	0	0	0
18010513	P	LAB34	3	630.3	2250.5	33	2.916	10497.8	4312.9	PEN	0.149	0.515	0.734	0.544	44.619	44.619	51.547	5.037	0.24	44.619	0
18010513	P	LABADIE1	3	1087	1929.5	33	2.925	10528.7	4371.5	IND	0.152	0.34	0.738	0.573	25.852	25.852	29.965	2.964	0.241	25.852	0
18010513	P	LABADIE2	3	1145.3	2014.2	33	2.925	10528.7	4348.5	IND	0.152	0.363	0.738	0.573	26.984	26.984	31.27	3.052	0.241	26.984	0
18010513	P	LABADIE5	3	17.9	52.6	32	2.777	9995.9	4310.6	DIR	0.157	0	0.738	0.578	0	0	0	0	0	0	0
19052610	P	LAB34	3	551	2254.2	25	4.318	15545.2	4312.9	PEN	0.059	0.906	0.664	0.492	54.166	54.166	57.323	4.055	0.148	54.166	0
19052610	P	LABADIE1	3	433	1075.1	25	4.862	17503.1	4371.5	IND	0.067	0.411	0.674	0.58	0.036	0.036	0.038	0.002	0.163	0.036	0
19052610	P	LABADIE2	3	507.3	2023.8	25	4.162	14982.5	4348.5	PEN	0.064	0.774	0.669	0.538	44.129	44.129	46.947	3.16	0.157	44.129	0
19052610	P	LABADIE5	3	19.1	51	33	3.996	14387.2	4310.6	DIR	0.069	0.001	0.674	0.593	0	0	0	0	0	0	0

**Table C-8: Source and Plume Details for Top 10 Highest SO<sub>2</sub> Predicted Concentrations – Labadie Database North Site**

YMMDDHH	SOURCE TYPE	SOURCE ID	RCPT NO.	FINAL PLUME HT.	DIST. FINAL PL. HT.	WDIR FINAL HT.	EFFECT. WSPD	3600* UEFF	DISTANCE TO RCPT	PLUME TYPE	MEAND. FRAC.	PART. PEN. FRAC.	EFFECT SIGMA_V	EFFECT. SIGMA_W	HOURLY CONC	AERVAL	COHERENT	PANCAKE	GAMFACT	PRMVAL	POT. TEMP. GRAD.		
19020114	P	LAB34	4	722.7	852.4	188	1.483	5340.6	3854.2	PEN	0.176	1	0.407	0.19	51.968	51.968	61.739	6.121	0.37	51.968	0		
19020114	P	LABADIE1	4	629.3	852.4	188	1.305	4699	3758.4	PEN	0.234	1	0.422	0.284	64.283	64.283	81.122	9.266	0.371	64.283	0		
19020114	P	LABADIE2	4	646.8	852.4	188	1.387	4993.8	3796	PEN	0.209	1	0.419	0.266	61.637	61.637	75.78	8.159	0.371	61.637	0		
19020114	P	LABADIE5	4	29.3	51.9	340	0.625	2250.8	3858.4	DIR	0.994	0.001	0.44	0.379	0	0	0	0	0	0	0		
19020115	P	LAB34	4	702.4	956.7	189	0.663	2386.9	3854.2	PEN	0.736	1	0.402	0.222	67.144	67.144	165.026	32.1	PLUME OUT	OF WAKE	0		
19020115	P	LABADIE1	4	623.5	956.7	189	0.743	2674.6	3758.4	PEN	0.693	0.938	0.405	0.253	52.256	52.256	119.019	22.643	0.073	52.256	0		
19020115	P	LABADIE2	4	637.4	956.7	189	0.74	2664.8	3796	PEN	0.701	0.963	0.405	0.25	52.65	52.65	121.84	23.185	0.076	52.65	0		
19020115	P	LABADIE5	2	26.3	51.9	354	0.928	3340.4	3346.3	DIR	0.415	0.001	0.41	0.296	0	0	0	0	0	0	0		
18071912	P	LAB34	4	651.4	1433.3	193	2.787	10032.3	3854.2	PEN	0.169	0.902	0.768	0.589	67.012	67.012	78.91	8.433	0.371	67.012	0		
18071912	P	LABADIE1	4	581.4	1433.3	193	2.71	9757.2	3758.4	PEN	0.179	0.73	0.789	0.647	43.002	43.002	51.204	5.357	0.369	43.002	0		
18071912	P	LABADIE2	4	586.8	1433.3	193	2.711	9761	3796	PEN	0.178	0.747	0.788	0.644	42.353	42.353	50.391	5.305	0.37	42.353	0		
18071912	P	LABADIE5	4	20.1	50.8	193	2.57	9251.1	3858.4	DIR	0.193	0.001	0.806	0.694	0	0	0	0	0	0	0		
17051510	P	LAB34	4	701.2	1197.1	198	2.359	8494	3854.2	PEN	0.235	0.864	0.757	0.652	59.245	59.245	74.421	9.786	0.133	59.245	0		
17051510	P	LABADIE1	4	639.6	1197.1	198	2.261	8139	3758.4	PEN	0.263	0.724	0.778	0.688	38.707	38.707	50.186	6.472	0.142	38.707	0		
17051510	P	LABADIE2	4	643.5	1197.1	198	2.263	8145.2	3796	PEN	0.261	0.735	0.777	0.686	39.013	39.013	50.45	6.584	0.139	39.013	0		
17051510	P	LABADIE5	4	23.1	50.8	171	1.874	6746.1	3858.4	DIR	0.352	0.001	0.805	0.744	0	0	0	0	0	0	0		
17053010	P	LAB34	4	1035.4	834.2	212	0.753	2712.2	3854.2	PEN	0.516	0.72	0.356	0.514	61.059	61.059	98.403	26.095	PLUME OUT	OF WAKE	0		
17053010	P	LABADIE1	4	931.5	834.2	212	0.755	2717.9	3758.4	PEN	0.551	0.534	0.369	0.542	31.525	31.525	53.722	13.41	PLUME OUT	OF WAKE	0		
17053010	P	LABADIE2	4	934.2	834.2	212	0.755	2717.7	3796	PEN	0.55	0.54	0.369	0.542	32.259	32.259	54.698	13.908	PLUME OUT	OF WAKE	0		
17053010	P	LABADIE5	1	44.8	51.1	243	0.783	2818.1	3723	DIR	0.501	0.001	0.381	0.552	0	0	0	0	0	0	0		
17060410	P	LAB34	4	843.1	799.9	188	1.111	3999.3	3854.2	PEN	0.542	0.914	0.572	0.525	54.707	54.707	98.365	17.838	0.37	54.707	0		
17060410	P	LABADIE1	4	757.2	799.9	188	1.107	3986.1	3758.4	PEN	0.58	0.777	0.585	0.564	30.883	30.883	58.645	10.784	0.371	30.883	0		
17060410	P	LABADIE2	4	756.1	799.9	188	1.107	3986	3796	PEN	0.581	0.775	0.585	0.564	29.074	29.074	55.313	10.129	0.371	29.074	0		
17060410	P	LABADIE5	1	33.9	50.9	255	1.063	3826.7	3723	DIR	0.675	0.001	0.611	0.613	0	0	0	0	0	0	0		
19062711	P	LAB34	4	757.5	793.8	182	2.127	7656.5	3854.2	PEN	0.154	1	0.554	0.231	25.779	25.779	29.847	3.396	0.088	25.779	0		
19062711	P	LABADIE1	4	626.6	793.8	182	2.023	7283.2	3758.4	PEN	0.205	1	0.585	0.414	43.703	43.703	53.23	6.84	0.085	43.703	0		
19062711	P	LABADIE2	4	596.5	793.8	182	1.853	6669.6	3796	PEN	0.227	1	0.597	0.474	43.805	43.805	54.626	6.932	0.086	43.805	0		
19062711	P	LABADIE5	1	55	50.6	228	0.49	1763.8	3723	IND	0.519	0.004	0.627	0.385	0	0	0	0	0	0	0		
18060609	P	LAB34	3	706.4	336.4	68	0.532	1914.4	4312.9	PEN	1	1	0.6	0.098	40.85	40.85	65.308	40.85	PLUME OUT	OF WAKE	0		
18060609	P	LABADIE1	2	598.5	336.4	68	0.542	1951.6	3203.1	PEN	1	1	0.612	0.207	36.971	36.971	7.96	36.971	PLUME OUT	OF WAKE	0		
18060609	P	LABADIE2	2	605.7	336.4	68	0.539	1941.4	3259	PEN	1	1	0.611	0.195	36.188	36.188	6.502	36.188	PLUME OUT	OF WAKE	0		
18060609	P	LABADIE5	2	31.1	50.9	39	0.689	2479.1	3346.3	DIR	1	0.002	0.652	0.488	0	0	0	0	0	0	0		
19120713	P	LAB34	4	558.6	1010.4	174	1.978	7121.1	3854.2	PEN	0.199	1	0.588	0.438	64.803	64.803	77.339	14.189	PLUME OUT	OF WAKE	0		
19120713	P	LABADIE1	4	486.8	1010.4	174	1.887	6792.4	3758.4	PEN	0.219	0.831	0.593	0.503	33.647	33.647	40.758	8.23	PLUME OUT	OF WAKE	0		
19120713	P	LABADIE2	<--- Source is not emitting during this hour																				
19120713	P	LABADIE5	4	24.9	51.9	191	1.728	6221.3	3858.4	DIR	0.258	0.001	0.597	0.532	0	0	0	0	0	0	0		
17043015	P	LAB34	4	684.6	619.8	171	0.726	2614.3	3854.2	PEN	0.814	1	0.46	0.29	39.844	39.844	105.471	24.83	PLUME OUT	OF WAKE	0		
17043015	P	LABADIE1	4	614.2	619.8	171	0.784	2823.5	3758.4	PEN	0.827	1	0.46	0.344	29.003	29.003	77.842	18.775	PLUME OUT	OF WAKE	0		
17043015	P	LABADIE2	4	625.3	619.8	171	0.783	2820.1	3796	PEN	0.826	1	0.46	0.34	32.713	32.713	88.479	21.003	PLUME OUT	OF WAKE	0		
17043015	P	LABADIE5	4	33.4	51.1	166	0.907	3263.5	3858.4	DIR	0.893	0.002	0.46	0.425	0	0	0	0	0	0	0		

**Figure B-1: Top 10 Concentrations vs. Hour of Day and Wind Speed – All 4 Labadie Monitoring Sites**



## A PDF Dispersion Model for Buoyant Plumes in the Convective Boundary Layer

J. C. WEIL

*Cooperative Institute for Research in Environmental Sciences, University of Colorado, and Visiting Scientist, National Center for Atmospheric Research,\* Boulder, Colorado*

L. A. CORIO AND R. P. BROWER

*VERSAR, Incorporated, ESM Operations, Columbia, Maryland*

(Manuscript received 5 August 1996, in final form 16 December 1996)

### ABSTRACT

A probability density function (PDF) dispersion model is presented for buoyant plumes in the convective boundary layer (CBL), where the mean concentration field  $C$  is obtained from the PDFs  $p_y$  and  $p_z$  of tracer particle position in the lateral  $y$  and vertical  $z$  directions. The  $p_y$  is assumed to be Gaussian, whereas the  $p_z$  is derived from the vertical velocity PDF, which is skewed. Three primary sources contribute to the modeled  $C$  field: 1) the “direct” or real source at the stack, 2) an “indirect” source to account for the slow downward dispersion of lofting plumes from the CBL top, and 3) a “penetrated” source to treat material that initially penetrates the elevated inversion but later fumigates into the CBL. Image sources are included to satisfy the zero-flux conditions at the ground and the CBL top.

Comparisons between the modeled crosswind-integrated concentration fields  $C^x$  and convection tank data show fair to good agreement in the lower half of the CBL. In particular, the  $C^x$  profiles at the surface agree with the data over a wide range of the dimensionless buoyancy flux  $F_*$  and show a systematic decrease in  $C^x$  with  $F_*$ .

Comparisons between the modeled and observed ground-level concentrations around several power plants exhibit good agreement on average and are considerably better than those obtained with a standard Gaussian plume model. A residual analysis suggests some areas for future model development.

### 1. Introduction

Over flat terrain, the maximum ground-level concentrations (GLCs) due to tall stack releases usually occur in a convective boundary layer (CBL). The high GLCs are caused by the large-scale convective updrafts and downdrafts that lead to a “looping” plume. For buoyant releases, plume sections can be brought to the surface within a few kilometers of the source when the downdraft velocity exceeds the rise velocity due to plume buoyancy. For sufficiently high buoyancy, a plume often rises to the top of the CBL, where it “lofts,” or remains temporarily, and then mixes downward. For yet higher buoyancy, a plume can penetrate the inversion capping the CBL, but later can be reentrained by the growing CBL, or “mixed layer.”

Laboratory experiments by Willis and Deardorff (1983, 1987) demonstrated the complex dispersion pat-

terns that can be obtained and their sensitivity to the source buoyancy flux, which was characterized by the dimensionless flux  $F_*$ :

$$F_* = \frac{F_b}{Uw_*^2z_i}, \quad (1)$$

where  $F_b$  is the stack buoyancy flux [Eq. (13a) below],  $U$  is the mean wind speed in the CBL,  $w_*$  is the convective velocity scale, and  $z_i$  is the CBL depth. Here,  $w_* = (g\overline{w\theta}_o z_i/T_a)^{1/3}$ , where  $g$  is the gravitational acceleration,  $\overline{w\theta}_o$  is the surface kinematic heat flux, and  $T_a$  is the ambient absolute temperature. The laboratory experiments showed that the lofting behavior occurred for  $F_* \gtrsim 0.1$ . Field observations around power plant stacks (Hanna and Paine 1989; Weil et al. 1986) indicated that the maximum GLCs generally occurred for this  $F_*$  range, which typically existed during light and variable winds ( $\leq 2 \text{ m s}^{-1}$ ) and low CBL depths ( $\leq 500 \text{ m}$ ).

Over the past 15 years, our understanding of and modeling capability for dispersion in the CBL have improved substantially. The models that have been developed include 1) analytical–statistical approaches based on the probability density function (PDF) of the random vertical velocity  $w$ —the PDF model (Misra 1982; Venkatram 1983; Weil 1988), 2) Lagrangian sto-

\* The National Center for Atmospheric Research is sponsored by the National Science Foundation.

Corresponding author address: Dr. Jeffrey C. Weil, NCAR/MMM, P.O. Box 3000, Boulder, CO 80307-3000.  
E-mail: weil@ncar.ucar.edu

chastic models (Luhar and Britter 1989; Sawford and Guest 1987), 3) approaches based on second-order closure (Sykes et al. 1984, 1986), and 4) large-eddy simulations (Lamb 1982; Henn and Sykes 1992). The key advantages of the PDF model are its ability to capture the essential physics of dispersion and its relative simplicity, which make the model useful for air quality applications.

This paper focuses on a further development of the PDF model for the mean concentration field  $C$  due to buoyant plumes in the CBL. The concentration distribution in a plume is highly random and should be characterized not only by  $C$ , but also by the degree of randomness—for example, the root-mean-square concentration fluctuation  $\sigma_c$  (Sykes 1988). The PDF approach is amenable to the modeling of  $\sigma_c$ , but this is postponed for the future. Further information on concentration fluctuations can be found in Chatwin et al. (1995), Deardorff and Willis (1988), Hanna (1984), Henn and Sykes (1992), Mylne and Mason (1991), Sykes (1988), and Weil (1994); however, with a few exceptions, this work primarily addresses passive or nonbuoyant releases.

In the PDF approach, the mean concentration is found from the PDF of the tracer particle position, which in turn is derived from the  $w$  PDF. The model was applied first to passive scalar dispersion in the CBL (e.g., Misra 1982; Venkatram 1983; Weil 1988) and resulted in good agreement with the laboratory measurements of Willis and Deardorff (1978, 1981). In the CBL, the  $w$  PDF is positively skewed and results in a non-Gaussian vertical concentration distribution, which is included in the model. For buoyant plumes, the model was extended by superposing the displacements due to plume rise and the random  $w$  to obtain the concentration field (Weil et al. 1986). This approach worked well for weak to moderate buoyancy ( $F_* < 0.1$ ), but for high  $F_*$  ( $\geq 0.1$ ), a separate treatment was required to account for the lofting behavior (see also Hanna et al. 1986; Weil 1988). However, the above separation did not maintain continuity of the predicted concentration field with  $F_*$ .

In this paper, we introduce a new and simplified treatment of plume interaction with the elevated inversion. This includes an “indirect” source to address the lofting behavior and dispersion of “nonpenetrating” plumes, and a “penetrated” source to account for plume material that initially penetrates the inversion but subsequently fumigates into the CBL (section 2). The treatment results in a continuous variation of  $C$  with  $F_*$ , thus overcoming a limitation of the earlier PDF models. In addition, we include the effects of surface shear as well as convection in parameterizing the  $w$  PDF, so that the model is applicable in the limit of a neutral boundary layer. The model is developed and evaluated using laboratory data and is compared to GLC observations around several Maryland power plants and the Kincaid (Illinois) power plant.

## 2. PDF dispersion model

The PDF model described here applies to an elevated point source in the CBL, wherein the turbulence is idealized as homogeneous and steady. The mean wind speed  $U$  is assumed to be uniform with height, and the lateral and vertical velocity fluctuations are assumed to be statistically independent. As a result, the displacements of source-emitted particles in the lateral  $y$  and vertical  $z$  directions,  $y_p$  and  $z_p$ , respectively, are independent. Thus, the joint PDF of  $y_p$  and  $z_p$  at time  $t = x/U$  is given by  $p_{yz}(y_p, z_p; x/U) = p_y(y_p; x/U)p_z(z_p; x/U)$ , where  $x$  is the distance downwind of the source.

The ensemble-mean concentration  $C(x, y, z)$  is found from a mass balance in which the mean horizontal flux of particles through an elemental area  $\Delta y \Delta z$  normal to the mean wind is  $UC(x, y, z)\Delta y \Delta z$ . This is equal to the emission rate  $Q$  times the probability of particles lying in the intervals  $y - \Delta y/2 < y_p < y + \Delta y/2$  and  $z - \Delta z/2 < z_p < z + \Delta z/2$ ; the probability is given by  $p_y(y_p; x/U)p_z(z_p; x/U)\Delta y \Delta z$ . Thus, the mass balance can be expressed by  $UC\Delta y \Delta z = Qp_y p_z \Delta y \Delta z$ , or

$$C(x, y, z) = \frac{Q}{U} p_y\left(y; \frac{x}{U}\right) p_z\left(z; \frac{x}{U}\right), \quad (2a)$$

where we have set  $y = y_p$  and  $z = z_p$  in  $p_y$  and  $p_z$ .

In the Gaussian plume model,  $p_y$  has the familiar form

$$p_y = \frac{1}{\sqrt{2\pi}\sigma_y} \exp\left(-\frac{y^2}{2\sigma_y^2}\right), \quad (2b)$$

where  $\sigma_y(x/U)$  is the crosswind spread, or standard deviation, and  $p_z$  has a similar form.

For the PDF model, the  $p_z$  is derived from the  $w$  PDF  $p_w$ , which is skewed, as noted earlier, and results in a non-Gaussian  $p_z$ ; the  $p_y$  is assumed to be Gaussian (see Lamb 1982). In addition, the  $w$  in a downdraft or updraft is taken to be independent of  $z$ . A key assumption is that the Lagrangian timescale  $T_{Lz}$  for  $w$  is infinite, so that the particle velocity at any  $x$  downwind is uniquely determined by its initial velocity. This is an approximation that is partially justified by the large timescales ( $z_i/w_* \sim 10$  min) of the CBL convection elements; the effect of a finite  $T_{Lz}$  is discussed in section 5.

In addition to the non-Gaussian  $p_z$ , the current model has the following features. 1) For buoyant releases, no “final” plume rise is assumed. Instead, the plume trajectories are determined by the addition of a distance-dependent plume rise (e.g., as  $x^{2/3}$ ) and the random vertical displacement caused by  $w$ . GLCs appear when the downdraft velocities are sufficiently large to overcome the plume rise velocity. 2) For plume segments initially rising in updrafts, an indirect source is included above the CBL top to address the lofting behavior—that is, the plume tendency to remain near  $z_i$  and resist downward mixing. This source plays the same role as the first image source above  $z_i$  in the standard Gaussian model, but differs in the treatment of plume buoyancy.

3) A penetrated source, or plume, is included to account for material that initially penetrates the elevated inversion, but is subsequently reentrained by and disperses in the growing CBL.

Based on this discussion, there are three primary sources contributing to  $C$ : 1) the “direct” or “real” source (at the stack), 2) the indirect source, and 3) the penetrated source. In addition, image sources are included to satisfy the zero-flux conditions at  $z = 0, z_i$ . In the following, we discuss the treatment of each source including buoyancy effects as well as the concentration field. For convenience, we first obtain the crosswind-integrated concentration (CWIC)  $C^y$  and then find  $C$  from the assumed Gaussian form for  $p_y$ . The  $C^y$  is obtained by integrating Eq. (2a) over all  $y$  and gives

$$C^y(x, z) \equiv \int_{-\infty}^{\infty} C(x, y, z) dy = \frac{Q}{U} p_z. \quad (3)$$

a. Direct or real source

This source accounts for the surface CWIC and GLCs due to plume sections that reach the ground directly from the source via downdrafts.

1) CROSSWIND-INTEGRATED CONCENTRATION

The PDF  $p_z$  of the particle height  $z_p$  can be found from  $p_w$ , provided that the  $z_p$  is a monotonic function of  $w$  (see Brownlee 1965). The relationship between  $p_z$  and  $p_w$  is (Weil 1988)

$$p_z = p_w \left[ w \left( z_p; \frac{x}{U} \right) \right] \left| \frac{dw}{dz_p} \right|, \quad (4)$$

where the absolute value is taken to ensure that  $p_z$  is positive. Here,  $p_w$  represents a general form of the  $w$  PDF and will be taken below as skewed [Eq. (7)]. Writing the argument of  $p_w$  as  $w(z_p; x/U)$  means that wherever  $w$  appears in  $p_w$ , we replace it by its equivalent in terms of  $z_p$  and  $x$ . The relationship between  $z_p$  and  $w$  is found by superposing the plume rise  $\Delta h$  and the vertical displacement due to  $w$ —that is,  $wx/U$ —as

$$z_p = h_s + \Delta h + \frac{wx}{U}, \quad (5)$$

where  $h_s$  is the stack height.

In Eq. (4),  $w(z_p; x/U)$  is found by rearranging (5) as

$$w = (z_p - h_s - \Delta h) \frac{U}{x}, \quad (6)$$

from which we obtain  $|dw/dz_p| = U/x$ . This  $w$  and  $dw/dz_p$  are then substituted into Eq. (4) to obtain  $p_z$ .

In the CBL, a good approximation to the  $w$  PDF is the superposition of two Gaussian distributions (e.g., Baerentsen and Berkowicz 1984; Weil 1988),

$$p_w = \frac{\lambda_1}{\sqrt{2\pi}\sigma_{w1}} \exp \left[ -\frac{(w - \bar{w}_1)^2}{2\sigma_{w1}^2} \right] + \frac{\lambda_2}{\sqrt{2\pi}\sigma_{w2}} \exp \left[ -\frac{(w - \bar{w}_2)^2}{2\sigma_{w2}^2} \right], \quad (7)$$

where  $\lambda_1$  and  $\lambda_2$  are weighting coefficients for the distributions with  $\lambda_1 + \lambda_2 = 1$ . The  $\bar{w}_j$  and  $\sigma_{wj}$  ( $j = 1, 2$ ) are the mean vertical velocity and standard deviation for each distribution and are assumed to be proportional to  $\sigma_w$ , the “total,” or overall, root-mean-square vertical turbulence velocity; subscripts 1 and 2 denote the updraft and down-draft distributions, respectively. The  $\bar{w}_1, \bar{w}_2, \sigma_{w1}, \sigma_{w2}, \lambda_1,$  and  $\lambda_2$  are found as functions of  $\sigma_w$ , the vertical velocity skewness  $S = \bar{w}^3/\sigma_w^3$ , where  $\bar{w}^3$  is the third moment of  $w$ , and a parameter  $R = \sigma_{w1}/\bar{w}_1 = -\sigma_{w2}/\bar{w}_2$  (see appendix A). An alternative parameterization for  $\bar{w}_j$  and  $\sigma_{wj}$  is discussed in section 5.

In our analysis of laboratory data, we find that  $R = 1$  yields fair to good agreement between the modeled and measured CWIC fields (section 4a). However, for field observations, we choose  $R = 2$ , so that in the limit of a neutral boundary layer ( $w_* = 0$ ) and an assumed  $S = 0$ , the PDF approximates a Gaussian PDF (As Table 2 shows, there is little difference between the results for  $R = 1$  and 2.)

In the upper 90% of the CBL, the vertical velocity variance  $\sigma_w^2$  can be assumed to be uniform (Weil 1988), as can the skewness (Wyngaard 1988). Here, the  $\sigma_w^2$  is parameterized in terms of  $w_*$  and  $u_*$  by

$$\sigma_w^2 = 1.2u_*^2 + 0.31w_*^2, \quad (8a)$$

where the 1.2 corresponds to Hicks’s (1985) neutral limit ( $w_* = 0$ ), and the 0.31 is consistent with Weil and Brower’s (1984) convective limit ( $u_* = 0$ ), or  $\sigma_w/w_* = 0.56$ . Similarly, the lateral velocity variance  $\sigma_v^2$  can be assumed to be uniform over the CBL and parameterized by

$$\sigma_v^2 = 3.6u_*^2 + 0.31w_*^2, \quad (8b)$$

where the 3.6 is from Hicks and the 0.31 from Weil and Brower. In the convective limit, the  $S$  is taken to be 0.6, which is the vertically averaged value from the Minnesota experiments (Wyngaard 1988); the corresponding  $\bar{w}^3 = 0.6\sigma_w^3 = 0.105w_*^3$ . For arbitrary  $u_*$  and  $w_*$ , the skewness is parameterized by  $S = 0.105w_*^3/\sigma_w^3$ , with  $\sigma_w^2$  given by Eq. (8a); thus, as  $w_* \rightarrow 0, S \rightarrow 0$ , and for  $w_*/u_* \gg 1, S = 0.6$ .

Using the approach for finding  $p_z$  outlined above [Eqs. (4)–(6) and related discussion] and the  $p_w$  given by Eq. (7), we find the CWIC field for the direct plume to be

$$C^y_d(x, z) = \frac{Q}{\sqrt{2\pi}U} \left\{ \frac{\lambda_1}{\sigma_{z1}} \exp \left[ -\frac{(z - \Psi_1)^2}{2\sigma_{z1}^2} \right] + \frac{\lambda_2}{\sigma_{z2}} \exp \left[ -\frac{(z - \Psi_2)^2}{2\sigma_{z2}^2} \right] \right\}, \quad (9a)$$

or

$$C_y^j(x, z) = \frac{Q}{\sqrt{2\pi}U} \sum_{j=1}^2 \frac{\lambda_j}{\sigma_{zj}} \exp\left[-\frac{(z - \Psi_j)^2}{2\sigma_{zj}^2}\right], \quad (9b)$$

where

$$\sigma_{zj} = \frac{\sigma_{wj}x}{U} \quad \text{and} \quad \Psi_j = h_s + \Delta h + \frac{\overline{w_j}x}{U}, \quad (10)$$

with  $j = 1$  or  $2$ .

To account for the zero-flux condition at the ground, we introduce an image source at  $z = -h_s$ —that is, we assume particle reflection at  $z = 0$ . This results in a positive flux of material at  $z = z_i$ , and additional image sources are included at  $z = 2z_i + h_s$ ,  $-2z_i - h_s$ , etc., to satisfy the subsequent no-flux conditions at  $z = z_i$ ,  $0$ . The resulting CWIC due to the real and image sources is

$$C_y^j(x, z) = \frac{fQ}{\sqrt{2\pi}U} \sum_{n=0}^N \sum_{j=1}^2 \frac{\lambda_j}{\sigma_{zj}} \times \left\{ \exp\left[-\frac{(z - 2nz_i - \Psi_j)^2}{2\sigma_{zj}^2}\right] + \exp\left[-\frac{(z + 2nz_i + \Psi_j)^2}{2\sigma_{zj}^2}\right] \right\}, \quad (11)$$

where  $N$  is the number of image sources and  $f$  is the fraction of plume material that remains trapped in the CBL—that is, material that is unable to penetrate the elevated inversion. In section 4,  $N$  is taken as 50, which is more than adequate for the comparisons made there; a more computationally efficient choice for  $N$  can be made based on a series-convergence test. The expression for  $f$  is given in section 2c.

## 2) PLUME RISE

For the direct source, the plume rise is given by the superposition of the source momentum and buoyancy effects following Briggs (1975):

$$\Delta h = \left( \frac{3F_mx}{\beta_1^2 U^2} + \frac{3}{2\beta_1^2} \frac{F_b x^2}{U^3} \right)^{1/3}, \quad (12)$$

where  $F_m$  and  $F_b$  are the stack momentum and buoyancy fluxes, and  $\beta_1$  ( $=0.6$ ) is an entrainment parameter. The fluxes are defined by

$$F_m = \frac{\rho_s}{\rho_a} w_s r_s^2 \quad \text{and} \quad F_b = g w_s r_s^2 \frac{\Delta T_s}{T_s}, \quad (13a)$$

where  $w_s$ ,  $r_s$ ,  $\rho_s$ , and  $T_s$  are the stack exit velocity, radius, density, and absolute temperature;  $\rho_a$  is the ambient density; and  $\Delta T_s = T_s - T_a$ . A dimensionless momentum flux (Weil 1994)

$$F_{m^*} = \frac{F_m}{U w_* z_i^2} \quad (13b)$$

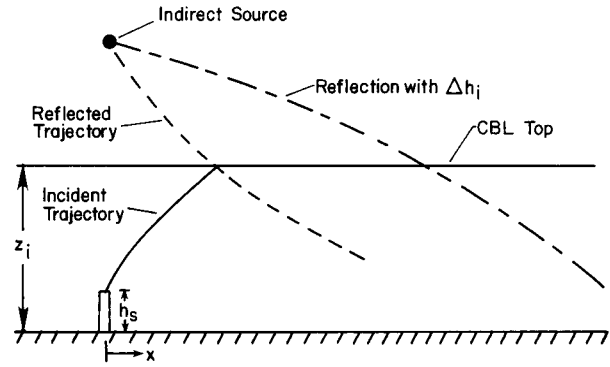


FIG. 1. Sketch of plume trajectory incident to the CBL top and reflected trajectories with and without  $\Delta h_i$ .

is used for characterizing the source momentum flux in section 4.

## b. Indirect source

The indirect source is included to treat the *first* interaction of the “updraft” plume with the elevated inversion—that is, for plume sections that initially rise to the CBL top in updrafts, but are unable to penetrate the inversion and are returned to the ground via downdrafts. Image sources are added to treat the subsequent plume interactions with the ground and inversion and to satisfy the zero-flux conditions at  $z = 0$ ,  $z_i$ . The treatment is designed to 1) provide for a continuous variation of  $C_y$  with  $F_{m^*}$  and 2) simplify computationally the analysis given in an earlier model (Hanna et al. 1986).

For the indirect source, a modified reflection approach is adopted in which the vertical velocity is reflected at  $z = z_i$ , but an “effective” plume rise  $\Delta h_i$  is added to delay the downward dispersion of plume material from the CBL top (see Fig. 1). This is intended to mimic the lofting behavior. The use of a reflection condition in the limit as  $\Delta h \rightarrow 0$  is motivated by the results of Li and Briggs (1988) and Weil (1988), which showed this approach to be satisfactory for passive releases. The  $\Delta h_i$  is derived for the limiting case of a highly buoyant plume that intercepts the plane  $z = z_i$  close to the source, but does not penetrate the inversion [section 2b(2)].

### 1) CROSSWIND-INTEGRATED CONCENTRATION

The mean CWIC due to the indirect source is found from Eq. (3), but with  $p_z$  corresponding to the reflected trajectories. In the latter, both the plume rise and the vertical velocity are reflected such that the resulting equation for  $z_p$  is

$$z_p = 2z_i - h_s - \Delta h - \frac{wx}{U} + \Delta h_i. \quad (14)$$

The corresponding  $w(z_p; x/U)$  found by rearranging the above is

$$w = -(z_p - 2z_i + h_s + \Delta h_r) \frac{U}{x}, \quad (15a)$$

where

$$\Delta h_r = \Delta h - \Delta h_i; \quad (15b)$$

the  $\Delta h_i$  is discussed in section 2b(2). The above  $w$  and the  $[dw/dz_p] = U/x$  are then substituted into Eq. (4) to obtain the  $p_z$  for the indirect plume. As  $\Delta h$  and  $\Delta h_i$  vanish, Eqs. (14) and (15a) reduce to the results for a passive release.

The CWIC due to the indirect source is found from  $p_z$  using Eqs. (4), (7), (14), and (15), and the related discussion. Image sources are included at  $z = -2z_i + h_s, 4z_i - h_s, -4z_i + h_s$ , etc., to account for the zero flux at  $z = 0, z_i$ . The total CWIC due to these sources is

$$C^y(x, z) = \frac{fQ}{\sqrt{2\pi}U} \sum_{n=1}^N \sum_{j=1}^2 \frac{\lambda_j}{\sigma_{z_j}} \times \left\{ \exp\left[-\frac{(z - 2nz_i + \Psi_j)^2}{2\sigma_{z_j}^2}\right] + \exp\left[-\frac{(z + 2nz_i - \Psi_j)^2}{2\sigma_{z_j}^2}\right] \right\}, \quad (16)$$

where

$$\Psi_j = h_s + \Delta h_r + \frac{\bar{w}_j x}{U}, \quad \text{with } j = 1 \text{ or } 2, \quad (17)$$

and  $\sigma_{z_j}$  is given by Eq. (10). Note that in the exponential terms of Eq. (16), the variables  $2nz_i$  and  $\Psi_j$  are of opposite sign, whereas they are of the same sign in Eq. (11).

2) AN EFFECTIVE PLUME RISE

For the indirect plume, an effective plume rise  $\Delta h_i$  is found using a simple energy argument governing the descent of buoyant plume elements from the CBL top. The plume is imagined to behave as a stable density interface subjected to convective mixing from below, akin to the entrainment of air above the density jump at the top of the CBL. Plume elements are assumed to be carried to the surface by downdrafts (Fig. 2a). For an element with an initial height  $z_p = z_i$ , initial vertical velocity  $-w$ , and no further entrainment of ambient air, the element's vertical velocity and trajectory are given by

$$w_p = -w + g't \quad (18a)$$

and

$$z_p = z_i - wt + \frac{1}{2}g't^2, \quad (18b)$$

where  $g' = g\Delta\rho/\rho_a$ ,  $\Delta\rho = \rho_a - \rho$ , and  $\rho$  is the plume density when an element begins its downward displacement.

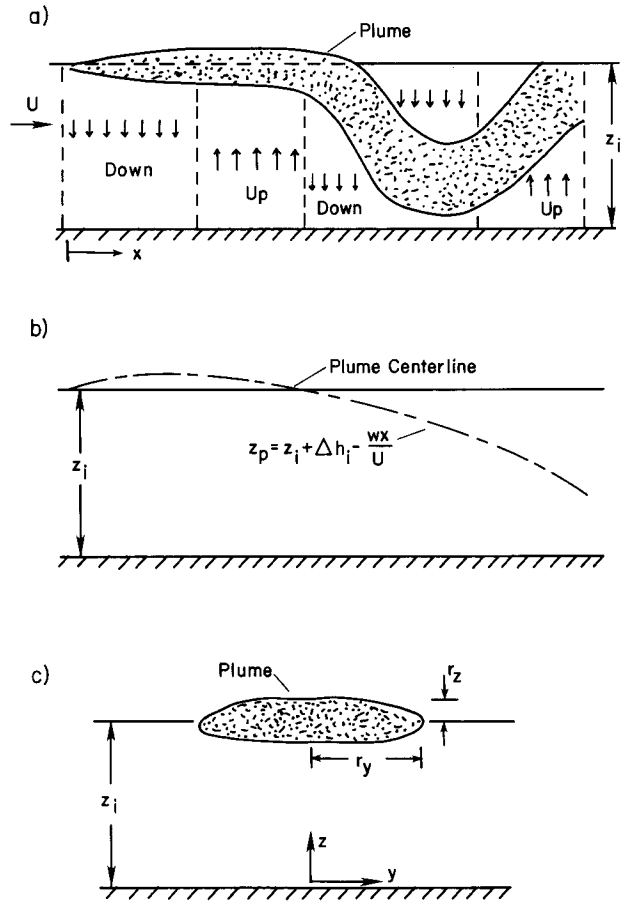


FIG. 2. Schematic showing the lofting plume: (a) behavior in the CBL, (b) trajectory for a single random velocity  $w$ , and (c) cross section at the CBL top.

If we assume that the plume element has a zero vertical velocity when it reaches the surface— $w_p = 0$  at  $z_p = 0$ —the time required for this displacement to occur is  $t = w/g'$  [see Eq. (18a)]. The corresponding  $w$  for the displacement is found by substituting this  $t$  and  $z_p = 0$  into (18b); the result is  $w^2/2 = g'z_i$ . We use the last result as the basic criterion governing the onset of the plume parcel displacement from the CBL top, but modify it by the constant  $\alpha$  as below:

$$\alpha \frac{\rho_a w^2}{2} = \Delta\rho g z_i \quad \text{or} \quad w = \left( \frac{2g'z_i}{\alpha} \right)^{1/2}. \quad (19)$$

Here,  $\Delta\rho$  is found from the buoyancy flux  $F_b$  and the relative dispersion of the elevated plume, as discussed below. A simple estimate of  $\alpha$  ( $=1.4$ ) is obtained by applying the model to the negative heat or buoyancy flux at the top of the CBL (appendix B).

The  $\Delta h_i$  can be found by requiring that a plume element enter the CBL at the distance where the criterion given by (19) is satisfied. For a plume originating at the CBL top, the trajectory for plume elements carried by downdrafts is

$$z_p = z_i + \Delta h_i - \frac{wx}{U}. \quad (20)$$

Assuming that the source buoyancy initially dominates in (20),  $z_p$  initially exceeds  $z_i$ , but becomes less than  $z_i$  some distance downwind as the downdraft speed overcomes the buoyancy effect (Fig. 2b). The trajectory intersects the height  $z = z_i$  when  $\Delta h_i = wx/U$ . Substituting  $w$  given by (19) into the  $\Delta h_i$  expression, we obtain

$$\Delta h_i = \left( \frac{2g'z_i}{\alpha} \right)^{1/2} \frac{x}{U}. \quad (21)$$

The density deficit in (21) can be estimated from the  $F_b$  and the local plume spread, or relative dispersion, which is a function of  $x$ . For this purpose, we consider a plume with an elliptical cross section having an enhanced lateral spread  $r_y$  and a diminished vertical spread  $r_z$  (Fig. 2c). For a plume trapped in the CBL, the local buoyancy flux  $F$  is conserved and given by

$$F = F_b = U r_y r_z \frac{g \Delta \rho}{\rho_a}. \quad (22)$$

Substituting Eq. (22) into Eq. (21), we have

$$\Delta h_i = \left( \frac{2F_b z_i}{\alpha U r_y r_z} \right)^{1/2} \frac{x}{U}. \quad (23)$$

The above model can be completed upon specifying the half-widths,  $r_y$  and  $r_z$ , of the plume cross section. For this, we use a modified version of an entrainment model (Weil 1991) for plumes lofting at the CBL top (see appendix C). The model gives

$$r_y r_z = r_i^2 + \frac{a_e \alpha_y^{3/2} w_*^2 x^2}{4 U^2}, \quad (24)$$

where  $r_i = \beta_2(z_i - h_s)$  is the plume radius when the plume reaches the CBL top,  $\beta_2 = 0.4$ ,  $\alpha_y = 2.3$ , and  $a_e$  is a dimensionless entrainment parameter, which is empirically estimated to be 0.1 (section 4a).

### c. Penetrated source

The penetrated source was omitted initially, but a number (14) of high-GLC cases were found at the Kincaid plant when complete penetration or  $f = 0$  was predicted, thus resulting in a zero prediction of the GLC. This typically occurred with low  $z_i$  values,  $z_i \leq 300$  m, and light winds. The following model is a simple ad hoc approach to deal with this problem, primarily at the Kincaid plant, and will be revised or generalized in the future.

#### 1) CROSSWIND-INTEGRATED CONCENTRATION

We first consider the limit of complete penetration, or  $f = 0$ . The plume is assumed to be entrained into the CBL by a growing  $z_i$ —that is, a fumigation process.

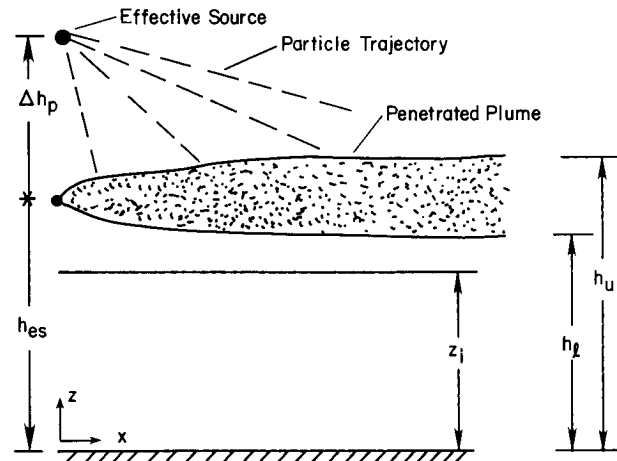


FIG. 3. Schematic of penetrated plume and treatment of its dispersion using a single effective point source.

Thus, the problem is unsteady in reality, but we treat it as steady in order to obtain a simple CWIC expression.

As shown by Deardorff and Willis (1982), plume fumigation into a growing CBL is not instantaneous, but occurs over a “fumigation period”  $t_f$  due to the horizontal variability of the entrainment layer. From their convection tank experiments, Deardorff and Willis found that the dimensionless  $t_f$ , or  $T_f$ , could be parameterized by

$$T_f = \frac{t_f w_*}{z_i} = \frac{0.42 \Delta z_i / z_i}{w_e / w_*} + 2.3, \quad (25)$$

where  $\Delta z_i$  is the variability in the mixed layer height and  $w_e$  is the entrainment velocity at  $z = z_i$ . Deardorff and Willis also found that  $\Delta z_i / z_i$  could be approximated by

$$\frac{\Delta z_i}{z_i} = 0.2 + 4 \frac{w_e}{w_*}. \quad (26)$$

Substituting Eq. (26) into Eq. (25), we find the  $T_f$  to be

$$T_f = \frac{0.084}{w_e / w_*} + 4. \quad (27)$$

In the following, we adopt a point source at height  $h_p$  as a crude representation of dispersion from the penetrated source (Fig. 3). We account for the longitudinal distance  $x_f = Ut_f$ , or spread over which a quantity of material would be entrained into the CBL, and model this spread by locating the source at a height  $\Delta h_p$  above the stabilized plume height  $h_{es}$  [section 3b(2)]; thus,  $h_p = h_{es} + \Delta h_p$ . All material dispersing from the penetrated source is assumed to be passive and to occur via downdrafts. The  $\Delta h_p$  is obtained by assuming that the mean centerline of the downdraft plume passes through the point  $(x, z) = (x_f/2, h_{es})$ . Thus, we have  $x_f/2 = Ut_f/2 = U \Delta h_p / [w_2]$ , or

$$\Delta h_p = \frac{|w_2| t_f}{2}. \tag{28}$$

Penetrated source material is assumed to be mixed into the CBL only when the growing, time-dependent CBL height  $\tilde{z}_i > z_i$ , where  $z_i$  is the average mixed layer depth over the hour and is representative of the midpoint of the hour. The  $\tilde{z}_i$  is obtained from Carson's (1973) model as

$$\tilde{z}_i^2 = z_i^2 + \frac{1 + 2A}{\partial\Theta_i/\partial z} \int_0^{t'} \frac{Q_o dt}{\rho_a c_p}, \tag{29}$$

where  $t'$  is measured from the midpoint of the hour,  $\partial\Theta_i/\partial z$  is the potential temperature gradient for  $z > z_i$ , and  $A$  ( $=0.2$ ) is the ratio of the heat flux at  $z = z_i$  to that at the surface (see Moeng and Wyngaard 1989). The penetrated plume is assumed to be dispersed in the average CBL depth over the second half of the hourly period,  $\tilde{z}_{i1} = \tilde{z}_i(t'_1)$ , with  $t'_1 = 15$  min.

With the above assumptions, the CWIC due to the penetrated source is given by

$$C_p^y(x, z) = \frac{f_p Q}{\sqrt{2\pi} U} \sum_{n=0}^N \sum_{j=1}^2 \frac{\lambda_j}{\sigma_{zj}} \times \left\{ \exp\left[-\frac{(z - 2n\tilde{z}_{i1} - \Psi_j)^2}{2\sigma_{zj}^2}\right] + \exp\left[-\frac{(z + 2n\tilde{z}_{i1} + \Psi_j)^2}{2\sigma_{zj}^2}\right] \right\}, \tag{30}$$

where

$$\Psi_j = h_p + \frac{\overline{w_1} x}{U}, \quad \text{with } j = 1 \text{ or } 2,$$

and

$$f_p = (1 - f) \frac{f_i f_q}{f_d}. \tag{31}$$

Here,  $1 - f$  is the fraction of the source material that is in the penetrated plume,  $f_d$  ( $\sim 0.6$ ) is the fraction of the  $w$  PDF comprised by downdrafts,  $f_i$  ( $=0.5$ ) is the fraction of the hourly period over which the penetrated source contributes to the GLCs, and  $f_q$  is the fraction of the penetrated plume that is captured by the growing CBL during the second half of the hour.

The  $f_q$  is given by

$$f_q = \min\left(\frac{\tilde{z}_{i2} - h_l}{h_u - h_l}, 1\right), \tag{32}$$

where  $\tilde{z}_{i2} = \tilde{z}_i$  ( $t' = 30$  min) is the CBL height at the end of the hour, and  $h_l$  and  $h_u$  are the lower and upper heights of the penetrated plume (see Fig. 3).

## 2) PLUME RISE AND INVERSION PENETRATION

The fraction of the source material that remains in the CBL is given by  $f = 1 - P$ , where  $P$  is the fraction

that penetrates the inversion. Adopting the  $P$  given by Briggs (1984), we find the  $f$  to be

$$f = \begin{cases} 0, & z'_i < 0.5\Delta h_{eq}, \\ 1, & z'_i > 1.5\Delta h_{eq}, \\ \frac{z'_i}{\Delta h_{eq}} - 0.5, & 0.5\Delta h_{eq} < z'_i < 1.5\Delta h_{eq}, \end{cases} \tag{33}$$

where

$$z'_i = z_i - h_s, \quad \Delta h_{eq} = 2.6 \left(\frac{F_b}{UN_i^2}\right)^{1/3},$$

and

$$N_i = \left(\frac{g}{\Theta_a} \frac{\partial\Theta_i}{\partial z}\right)^{1/2}. \tag{34}$$

The  $\Delta h_{eq}$  is the equilibrium plume rise in a stable environment (see Briggs 1984).

Briggs's model for  $P$  is based on a uniform rectangular plume cross section and a total vertical plume depth equal to  $\Delta h_{eq}$ . We assume that the plume height  $h_{es}$  is the centroid of the plume material above the inversion and take  $h_{es} = h_s + \Delta h_{eq}$  for  $f = 0$  or complete penetration. However, for partial penetration ( $f > 0$ ),  $h_{es}$  is taken as the average of the heights of the upper plume edge  $h_s + 1.5\Delta h_{eq}$  and  $z_i$ , or

$$h_{es} = \frac{h_s + z_i}{2} + 0.75\Delta h_{eq}. \tag{35}$$

## d. Ground-level concentrations and lateral dispersion

The mean concentration field along the plume centerline ( $y = 0$ ) can be found from the CWIC field through  $C(x, 0, z) = C^y(x, z)/\sqrt{2\pi}\sigma_y$ . For the "three-plume" contribution, we estimate the GLC along  $y = 0$  by summing the contributions from the individual plumes according to

$$C(x, 0, 0) = \frac{1}{\sqrt{2\pi}} \left(\frac{C_d^y}{\sigma_{yd}} + \frac{C_r^y}{\sigma_{yr}} + \frac{C_p^y}{\sigma_{yp}}\right). \tag{36}$$

Here,  $\sigma_{yd}$ ,  $\sigma_{yr}$ , and  $\sigma_{yp}$  are the lateral dispersion parameters for the direct, indirect, and penetrated plumes, and are discussed below.

For the direct plume, the lateral dispersion is assumed to be dominated by ambient turbulence, with  $\sigma_{yd}$  parameterized by the general form  $\sigma_{yd} = \sigma_v t (1 + 0.5t/T_{Ly})^{-1/2}$  (e.g., Venkatram 1988), which satisfies the short- and long-time limits of Taylor's (1921) theory. With the  $\sigma_v$  given by Eq. (8b), the  $\sigma_{yd}$  is

$$\sigma_{yd} = \frac{(3.6u_*^2 + 0.31w_*^2)^{1/2}(x/U)}{[1 + 0.5x(UT_{Ly})^{-1}]^{1/2}}. \tag{37}$$

We adopt  $T_{Ly} = 0.7z_i/w_*$  following Weil and Corio (1985), who found that Eq. (37), with this  $T_{Ly}$  and  $u_*$

TABLE 1. Range of stack conditions, meteorological variables, and ground-level concentrations at power plants used in model evaluation.

	Maryland plants	Midwest plants	Kincaid plant
Stack height (m)	122–213	107–305	187
Stack emission rate	0.7–4 kg s <sup>-1</sup>	3.9–10.5 kg s <sup>-1</sup>	10–25 g s <sup>-1</sup>
	SO <sub>2</sub>	SO <sub>2</sub>	SF <sub>6</sub>
Buoyancy flux per stack (m <sup>4</sup> s <sup>-3</sup> )	125–772	516–2206	500–2400
Mean wind speed (m s <sup>-1</sup> )	0.7–15.7	0.4–2.6	2–16
CBL height (m)	300–2500	1000–1300	200–2500
Ground-level concentration	4–322 ppb	150–560 ppb	1–670 ppt
	SO <sub>2</sub>	SO <sub>2</sub>	SF <sub>6</sub>
Distance to concentration (km)	1.7–33	1.3–1.8	0.5–50
Number of measurements	136	9	302

= 0, was a good average fit to the  $\sigma_y$  of buoyant plumes at Maryland power plants.

The indirect source treats plumes that rise to the CBL top in updrafts and loft. Such plumes exhibit an enhanced  $\sigma_y$  in the form of a gravity current due to the pressure difference between the plume and the local environment (Briggs 1985); the pressure difference is caused by the density difference  $\Delta\rho$ . For  $F_* > 0.06$ , Briggs found that  $\sigma_y$  was described by the following expression, which we adopt as an upper bound for  $\sigma_{yr}$ :

$$\sigma_{yr} = 1.6 \frac{F_b^{1/3}}{U} x^{2/3}. \quad (38)$$

For weakly buoyant plumes, the CBL turbulence may dominate the lateral dispersion and lead to the  $\sigma_{yr}$  given by Eq. (37). As a simple approach for determining the applicability of these two expressions, we equate them at an  $x = U z_i / w_*$  and solve for the buoyancy flux at which the expressions are equal. The dimensionless buoyancy flux  $F_{*1}$  corresponding to this equality is

$$F_{*1} = \left[ 0.07 + 0.83 \left( \frac{u_*}{w_*} \right)^2 \right]^{3/2}. \quad (39)$$

Thus, we use Eq. (37) for  $F_* < F_{*1}$ , setting  $\sigma_{yr} = \sigma_{yd}$ , and Eq. (38) for  $F_* \geq F_{*1}$ .

For the penetrated plume, we currently assume that  $\sigma_{yp} = \sigma_{yr}$  and will examine this further in the future.

### 3. Field data

#### a. Experimental description

The field data used in the model evaluation consisted of GLCs of stack effluents, meteorological variables, and stack conditions from buoyant sources—Maryland power plants and the Kincaid power plant. The Maryland plants—Chalk Point, Dickerson, and Morgantown—were in remote areas and far from other sources of SO<sub>2</sub> that the tracer monitored. Crosswind profiles of SO<sub>2</sub> were measured from a mobile instrumented van, which made repeated passes through the plume along roads transverse to the plume centerline. Typically, six profiles were measured along the same route during a 1-h interval and from them, an Eulerian-averaged profile

was constructed. The maximum concentration from the average profile was used in the model evaluation.

The meteorological variables included vertical profiles of wind from balloon tracking and vertical temperature profiles from radiosondes or instrumented aircraft. These data were supplemented by surface observations—wind speed, cloud cover, and ceiling height—from the Washington National and Dulles International Airports. In addition, insolation data were obtained from Dulles Airport for estimating the surface heat flux.

Eleven additional SO<sub>2</sub> measurements were obtained during light wind, convective conditions from fixed monitors close ( $x < 3$  km) to four power plants—Morgantown, Muskingum River (Ohio), John Sevier (Tennessee), and Cumberland (Tennessee).

The Kincaid plant is located in flat farmland near Springfield, Illinois. Continuous releases of SF<sub>6</sub> from the 187-m stack were made in approximately 30 experiments, each over a period of about 6–9 h. Hourly averaged SF<sub>6</sub> GLCs were measured at 200 sampling stations arranged on approximately five to seven arcs and ranging from 0.5 to 50 km downwind of the source.

The meteorological data included wind speed, wind direction, and temperature at four levels on a 100-m tower near the stack. These data were supplemented by vertical profiles of wind and temperature from rising instrumented balloons. In addition, hourly values of net radiation, insolation, and cloud cover were measured at the site. The SF<sub>6</sub> emission rate and other stack exit conditions were obtained either from in-stack monitors or plant operating data.

The ranges of stack conditions, meteorological variables, and GLC data from the various plants are shown in Table 1. Further experimental details can be found in Weil and Brower (1984) for the Maryland plants and in Hanna and Paine (1989) for the Kincaid plant.

#### b. Meteorological inputs and GLC data

The PDF model requires several key meteorological variables—the surface heat flux  $Q_o = \rho_a c_p w \theta_o$ , where  $c_p$  is the specific heat of air,  $z_i$ ,  $U$ , and  $u_*$ ; the  $w_*$  is determined from  $Q_o$  and  $z_i$ . The variables are given by Weil and Brower (1984) for the Maryland plants and

Hanna et al. (1986) for the Kincaid plant. The methods for determining the variables differ somewhat for the two sites and are briefly summarized below.

- For the Maryland plants,  $Q_o$  was assumed to be  $0.4Q_r$  (Weil and Brower 1984), where  $Q_r$  is the insolation. For the Kincaid plant,  $Q_o$  was estimated from the Holtslag and van Ulden (1983) model using the observed  $Q_r$  and an assumed moisture coefficient of 0.5 in their model. The Holtslag and van Ulden model generally gave similar results to  $Q_o = 0.4Q_r$ , but with slightly less variability.
- The  $z_i$  was determined from the observed temperature profiles and was subjectively chosen as the height at which the vertical temperature gradient first became isothermal above a ground-based, well-mixed layer. It was interpolated with time between the observed profiles using a modified version of Carson's (1973) model (Weil and Brower 1983), which is based on an energy balance of the CBL.
- For the Maryland plants, the  $U$  was a vertically averaged value from the balloon-tracked wind profiles. For the Kincaid plant,  $U$  was obtained by extrapolating the 10-m-level wind speed [ $\bar{u}(z = 10 \text{ m})$ ] to the height  $0.1z_i$  using the Monin–Obukhov (M–O) similarity profile (e.g., see Businger 1973):

$$\bar{u}(z) = \frac{u_*}{k} \left[ \ln\left(\frac{z}{z_o}\right) - \psi_m\left(\frac{z}{L}\right) \right], \quad (40)$$

where  $k$  is the von Kármán constant (0.4),  $z_o$  is the roughness height,  $\psi_m$  is a stability function, and  $L$  is the M–O length;  $L = -u_*^3(kg\theta_o/T_a)^{-1}$ . The  $\bar{u}(0.1z_i)$  has been shown to give good estimates of the mean wind speed in the CBL (e.g., Garrett et al. 1982; Weil and Brower 1983).

- For Kincaid, the  $u_*$  was evaluated iteratively from Eq. (40) using the observed 10-m-level wind speed,  $z_o = 0.15 \text{ m}$ , and the calculated  $Q_o$ . For the Maryland plants,  $u_*$  was estimated with less precision as  $U/16$ . The latter is a simple estimate based on the logarithmic wind profile applied at heights of 100–300 m for  $z_o = 0.3 \text{ m}$  (see Briggs 1975; his Table 6); this  $z_o$  is typical of the power plant sites that are located in rolling terrain with patches of farmland and trees. On-site surface winds were not measured at the Maryland plants.

The observed GLCs'  $C_{\text{obs}}$  used in the model evaluation were the maximum concentrations from the average crosswind profiles in the Maryland experiments and the maxima on crosswind arcs in the Kincaid experiments. The Kincaid GLC data were screened to eliminate uncertain  $\text{SF}_6$  concentrations, cases in which the plume centerline concentration was poorly defined by the sampling arc, and periods with low and ill-defined  $Q_o$ . The specific criteria that had to be satisfied were (see Hanna et al. 1986; appendix C)

- $C_{\text{obs}} > 10 \text{ ppt}$ , where the latter value is an uncertainty

in the  $\text{SF}_6$  concentration based on replicate samples and performance audits (Bowne et al. 1983);

- the observed peak concentration had to lie within an arc of  $\pm 2\sigma_v/U$  centered about the expected plume direction, which was chosen as the wind direction at the 100-m level on the Kincaid tower; and
- the  $Q_o$  had to exceed  $60 \text{ W m}^{-2}$ , and the comparisons were restricted to days without rain.

#### 4. Model comparisons with experimental data

This section focuses on the model performance using both laboratory data and field observations.

##### a. Laboratory experiments

The laboratory data were obtained from experiments conducted in a convection tank using water as the working fluid (Deardorff and Willis 1984, 1988; Willis and Deardorff 1987). A model stack was towed across the bottom of a simulated CBL, which had a mean  $z_i$  in the different experiments ranging from 19 to 23 cm and a  $w_* = 0.9 \text{ cm s}^{-1}$ . For the following data,  $h_s/z_i = 0.13$  or 0.16, and the  $F_*$  and  $F_{m*}$  were in the ranges  $0 \leq F_* \leq 0.54$  and  $0.001 \leq F_{m*} \leq 0.0058$ .

The  $\sigma_w$  and skewness  $S$  used in the model were guided by the Deardorff and Willis (1985) turbulence measurements in the same tank. Their data showed that the vertically averaged  $\sigma_w^2/w_*^2 \approx 0.29$  or  $\sigma_w/w_* \approx 0.54$ , which is close to the parameterized value 0.56 from Eq. (8a) for convective turbulence only; as a result, we used the parameterized value. The vertically averaged  $S$  was 1 for  $0 < z/z_i < 0.5$  (i.e., in the near-source region), and  $S = 1$  was used in the following calculations; this is somewhat larger than the vertically averaged  $S (=0.6)$  based on field observations (Wyngaard 1988).

To implement the model, we determine values of the entrainment parameter  $a_e$  [Eq. (24)] and the PDF variable  $R$  (appendix A) using model comparisons with the measured surface CWIC distribution. The CWIC in this and the following comparisons is shown as a function of the dimensionless distance

$$X = \frac{w_*x}{Uz_i}, \quad (41)$$

which is the ratio of travel time  $x/U$  to the eddy turnover time  $z_i/w_*$ .

Figure 4 shows the dimensionless CWIC ( $C^y U z_i / Q$ ) versus  $X$  for a low- ( $F_* = 0.03$ ) and a high- ( $F_* = 0.26$ ) buoyancy case, each for a range of  $a_e$  and two  $R$  values. In both cases, the modeled CWIC agrees well with the laboratory data for  $R = 1$  and exhibits little variation with  $a_e$  over the range  $0.05 \leq a_e \leq 0.2$ . An  $a_e = 0.1$  is an adequate fit to the data and is adopted in all of the remaining calculations. For  $F_* = 0.03$ , the results with  $R = 1$  are a better match to the measurements than with  $R = 2$ , but for  $F_* = 0.26$ , there is little

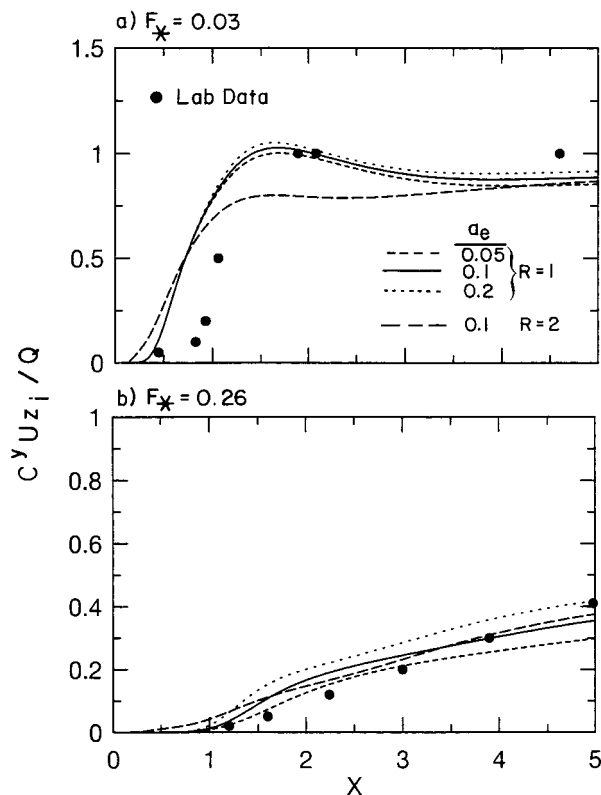


FIG. 4. Surface values of the dimensionless crosswind-integrated concentration as a function of the dimensionless downwind distance as predicted by the PDF model (lines) and measured in experiments with  $h/z_i = 0.16$ . Laboratory data are from (a) Deardorff and Willis (1988), with  $F_{m*} = 0.0014$ , and (b) Willis and Deardorff (1987), with  $F_{m*} = 0.0058$ .

difference in the results for the two  $R$  values. The comparisons for the other high-buoyancy cases ( $F_* = 0.11, 0.14,$  and  $0.54$ ) are similar to those in Fig. 4b.

Figures 5 and 6 show contours of the dimensionless CWIC as a function of  $z/z_i$  and  $X$  for  $F_* = 0.03$  and  $0.14$ . Each figure contains the modeled contours for  $R = 1$  and  $2$ , and the laboratory measurements. With  $R = 1$ , both figures (Figs. 5b and 6b) show an overall qualitatively similar pattern to the laboratory data in the near field, say  $X \leq 2$ . For example, there is an upward tilting of the contour lines due to the plume rise, and as expected, the effect is more pronounced for the higher buoyancy flux (Fig. 6b). The upward tilting differs from the behavior for passive plumes ( $F_* = F_{m*} = 0$ ), which exhibit downward-tilting contours due to the positive skewness or the higher probability (0.6) of material being released into downdrafts than into updrafts (Lamb 1982; Weil 1988). In Fig. 5b, the contours labeled “1” ( $C^y U z_i / Q = 1$ ) initially rise over the region  $X \leq 1$  and then descend to the surface in a manner similar to the 1 and 1.2 contours in the laboratory (Fig. 5c). This behavior is not found with  $R = 2$  (Fig. 5a); thus, we conclude that the results for  $R = 1$  are a better match with the laboratory data.

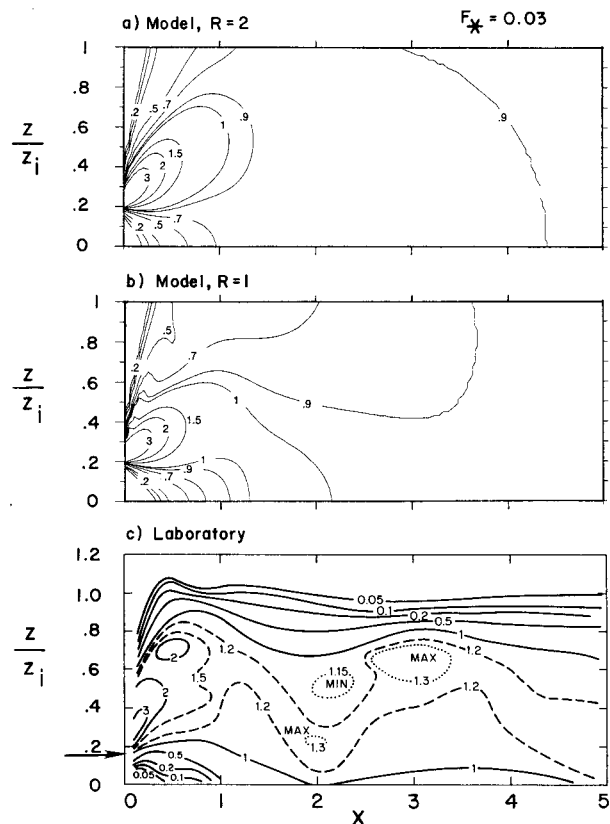


FIG. 5. Contours of the dimensionless crosswind-integrated concentration as a function of the dimensionless height and downwind distance for a buoyant source in the convective boundary layer, with  $h/z_i = 0.16$  and  $F_{m*} = 0.0014$ ; CWIC is nondimensionalized by  $Q/Uz_i$ . Laboratory results in (c) are from Deardorff and Willis (1988), and horizontal arrow denotes source height.

In contrast to the laboratory results, which show approximately horizontal contour lines near  $z/z_i = 1$ , the modeled contours are nearly normal to the lower and upper boundaries. The laboratory behavior is expected for buoyant material, which initially penetrates the inversion (near  $X \sim 0.5$  in Figs. 5 and 6) and either returns to the CBL due to insufficient buoyancy or remains penetrated. The modeled behavior differs from this due to the assumed reflection ( $z = 0$ ) or quasi reflection ( $z = z_i$ ) of particles at the boundaries; the assumption is a better approximation at the surface than at the CBL top. As a result, we consider the model to be a dispersion parameterization primarily for the lower half or so of the CBL and in particular for the ground-level distribution of  $C^y$  and  $C$ .

Figure 7 compares the modeled CWIC at the surface with the data for six  $F_*$  values. In all calculations,  $R = 1$ , and for high  $F_*$  (Figs. 7d–f), the  $f$  [see Eq. (11)] is an experimental value at  $X = 5$  taken from Willis and Deardorff (1987, their Fig. 10).

Overall, the predicted CWIC profiles are in fair to good agreement with the data, and in particular, they show a systematic reduction in the surface CWIC with

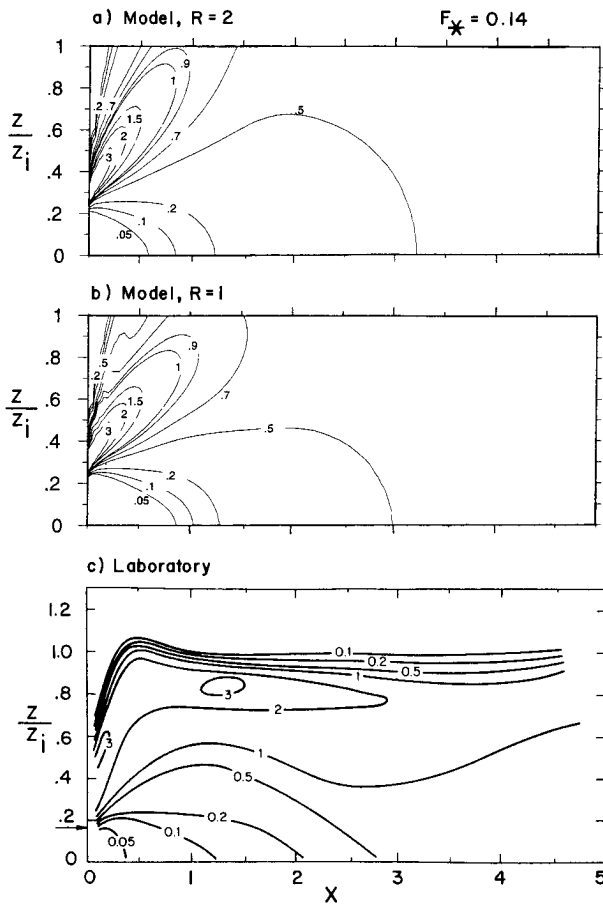


FIG. 6. Contours of the dimensionless crosswind-integrated concentration as a function of the dimensionless height and downwind distance for a buoyant source in the convective boundary layer, with  $h/z_i = 0.16$  and  $F_{m*} = 0.0058$ ; CWIC is nondimensionlized by  $Q/Uz_i$ . Laboratory results in (c) are from Willis and Deardorff (1987), and horizontal arrow denotes source height.

increasing  $F_{m*}$ , as observed. The largest discrepancies between the model and experiments occur for the non-buoyant plumes (Fig. 7a), but they are not systematic with respect to the momentum flux. For  $F_{m*} = 0.001$ , the model peaks at the correct distance, but it underestimates the magnitude of the peak, whereas for  $F_{m*} = 0.0058$ , the model overestimates the measured peak. However, in both cases, the large distance asymptote  $C^*Uz_i/Q = 1$ , characteristic of a vertically well-mixed plume, is adequately represented.

In summary, we have found that the PDF model gives a fair to good representation of the dispersion pattern in the lower half of the CBL and of the surface CWIC distribution with  $X$ . Further work is necessary to improve the modeled behavior in the upper half of the CBL, particularly near  $z = z_i$ .

*b. Field observations*

To further evaluate the model, we compare the predicted centerline GLCs with the maximum  $SF_6$  and  $SO_2$

GLCs from observed crosswind profiles near the Kincaid and Maryland power plants. The model results are based on the following parameter values:  $a_e = 0.1$ ,  $R = 2$  [see section 2a(1)],  $\sigma_w$  and  $\sigma_v$  given by Eqs. (8a) and (8b),  $S = 0.105w_*^3/\sigma_w^3$ , and a default value of  $\partial\Theta/\partial z = 0.005^\circ C m^{-1}$  in the elevated stable layer ( $z > z_i$ ). The model sensitivity to some of the parameters (Table 2) is discussed later. A total of 302 and 145 GLC observations are analyzed in the Kincaid and Maryland datasets.

Before discussing the concentration estimates, we compare the observed and predicted  $\sigma_y$  at the Maryland plants. For comparison purposes, we assume that the predicted  $\sigma_y$  can be given by Eq. (37) for  $F_* < 0.1$  and by Eq. (38) for  $F_* \geq 0.1$  (e.g., see Weil et al. 1986); this is done because the modeled  $\sigma_y$  is given separately for the direct and indirect sources. Figure 8 shows that the observations and predictions generally agree to within a factor of 2. In addition, a least squares fit to the data (dashed line) does not vary significantly from the line of equal values (solid line) over the range of the predictions.

Following the recommendations of Fox (1984), Venkatram (1982), and Weil et al. (1992), we examine the correlation between the observed ( $C_{obs}$ ) and predicted ( $C_{pred}$ ) concentrations, normalized here by  $Q$ , and then analyze the residual, or difference  $d$ , between the concentrations. The normalization by  $Q$  is included to remove the variability in  $C$  due to varying emission rates, so that the correlation plot is a test only of the transport and dispersion model. For  $d$ , we use the log transform of the concentration

$$d = \ln C_{pred} - \ln C_{obs} = \ln \left( \frac{C_{pred}}{C_{obs}} \right) \quad (42)$$

because this is close to a normal distribution for the PDF model (see Hanna et al. 1986; Weil et al. 1992). Ideally,  $C_{pred}/C_{obs}$  should be 1, or  $d = 0$ , on average.

Figure 9 shows the correlation between the observed and predicted  $C/Q$  for both datasets. Despite the significant scatter, the geometric mean (GM) and geometric standard deviation (GSD) of  $C_{pred}/C_{obs}$  are 0.89 and 2.0 for Kincaid, and 1.1 and 2.1 for Maryland; the GMs are close to the ideal value of 1. In addition, the fraction  $r^2$  of the variance explained by the model is 0.38 and 0.42 for Kincaid and Maryland, respectively, where  $r$  is the correlation coefficient between  $\ln(C_{obs}/Q)$  and  $\ln(C_{pred}/Q)$ . As shown in Table 3, the above statistics are comparable to or perhaps slightly better than those attained with the earlier model of Weil et al. (1986); in Table 3, the  $r^2$  is for  $\ln C_{obs}$  versus  $\ln C_{pred}$  (without the normalization by  $Q$ ).

The large scatter in Fig. 9 arises from 1) the natural variability in concentration due to the stochastic nature of dispersion, 2) uncertainties or errors in the model input variables, 3) errors in the model physics, and 4) errors in the concentration measurements (Fox 1984;

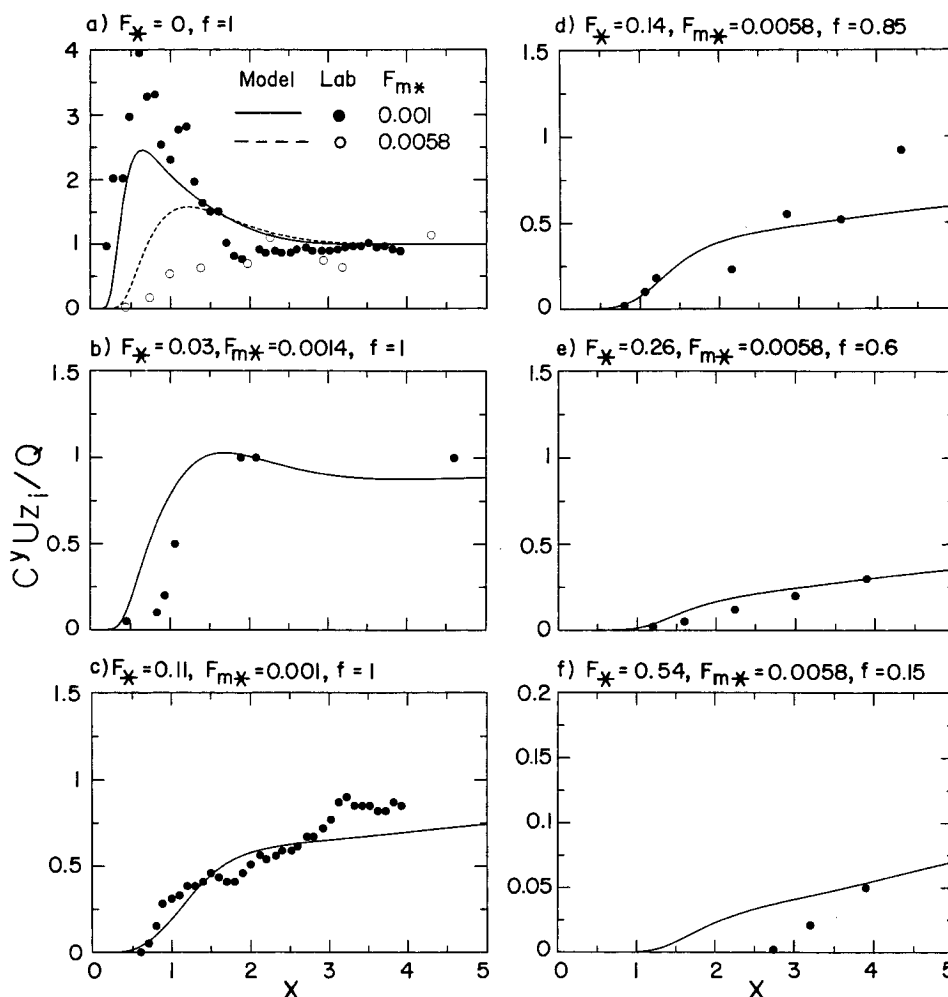


FIG. 7. Dimensionless crosswind-integrated concentration at the surface as a function of the dimensionless downwind distance for six values of  $F_*$ . Laboratory data are from (a) Deardorff and Willis (1984;  $F_{m*} = 0.001$ ) and Willis and Deardorff (1987;  $F_{m*} = 0.0058$ ), (b) Deardorff and Willis (1988), (c) Deardorff and Willis (1984), and (d)–(f) Willis and Deardorff (1987);  $h_i/z_i = 0.13$  or  $0.16$ .

Venkatram 1982; Weil et al. 1992). Here, we believe that the primary causes of the scatter are the natural variability and model input uncertainties, but there is also a contribution from model physics errors, as discussed below.

To put the above results in perspective, we show a similar plot (Fig. 10) for the Environmental Protection Agency (EPA) CRSTER model (EPA 1977), which is a standard Gaussian plume model based on the Pasquill–Gifford dispersion parameters; the plot is from an earlier analysis in which the concentrations were not normalized by  $Q$  (Weil et al. 1986). The CRSTER treatment of elevated sources is essentially the same as in the more widely used Industrial Source Complex (ISC) model (EPA 1987). As can be seen, the scatter in Fig. 10 is considerably greater than that in Fig. 9 and a significant number of zero predictions occur. The zeroes are associated with nonzero, and sometimes large, observed GLCs and are caused by predictions of complete plume

penetration of the elevated inversion with no plume–ground contact. For the nonzero predictions, the GM, GSD, and  $r^2$  are 1.0, 4.1, and 0.02, respectively; the larger GSD and smaller  $r^2$  than in Fig. 9 are consistent with the greater scatter in Fig. 10.

The residuals from Fig. 9 are divided into groups or bins of points with respect to the variables  $F_*$ ,  $U/w_*$ , and  $X$ , with the same bin widths as used in earlier work (Hanna et al. 1986; Weil et al. 1992). For each group, the GM, GSD, and uncertainty in the GM of  $C_{pred}/C_{obs}$  are determined; the uncertainty is estimated from the 95% confidence limits of a lognormal distribution using the GSD and number of points in each group. In the following, we discuss the trends of the GMs with the variables.

Figure 11 shows the residual plot for  $F_*$ , where the horizontal line corresponds to a perfect model with the GM = 1 for all  $F_*$  bins, which are denoted by the vertical bars along the horizontal line. For each bin, the

TABLE 2. Model evaluation results based on comparisons between predicted and observed ground-level concentrations.

Model parameters	Plant	Cases	$N^a$	GM <sup>b</sup>	GSD <sup>c</sup>	$r^{2d}$	Factor of 2 (%) <sup>e</sup>	Number of zero predictions <sup>f</sup>
$a_e = 0.1, R = 2$ $\partial\Theta_i/\partial z = 0.005^\circ\text{C m}^{-1}$	Kincaid	All	302	0.89	2.0	0.38	71	0
		$F_* \geq 0.1$	74	1.1	2.1		66	0
		$F_* < 0.1$	228	0.84	1.9		72	0
$a_e = 0.05, R = 2$ $\partial\Theta_i/\partial z = 0.005^\circ\text{C m}^{-1}$	Maryland	All	144	1.1	2.1	0.42	69	1
		$F_* \geq 0.1$	24	1.0	2.2		71	1
		$F_* < 0.1$	120	1.1	2.1		68	0
$a_e = 0.15, R = 2$ $\partial\Theta_i/\partial z = 0.005^\circ\text{C m}^{-1}$	Kincaid	All	302	0.86	2.0	0.37	69	0
	Maryland	All	144	1.1	2.1	0.42	69	1
$a_e = 0.1, R = 1$ $\partial\Theta_i/\partial z = 0.005^\circ\text{C m}^{-1}$	Kincaid	All	302	0.92	2.0	0.40	72	0
	Maryland	All	144	1.2	2.2	0.39	67	1
$a_e = 0.1, R = 2$ $\partial\Theta_i/\partial z = 0.01^\circ\text{C m}^{-1}$	Kincaid	All	302	0.91	2.1	0.34	69	0
	Maryland	All	144	1.1	2.1	0.42	67	1
$a_e = 0.1, R = 2$ $\partial\Theta_i/\partial z = 0.02^\circ\text{C m}^{-1}$	Kincaid	All	302	0.90	2.2	0.30	68	1
	Maryland	All	144	1.1	2.1	0.42	67	1

<sup>a</sup>  $N$ —number of comparisons exclusive of zero predictions.  
<sup>b</sup> GM—geometric mean of  $C_{\text{pred}}/C_{\text{obs}}$ .  
<sup>c</sup> GSD—geometric standard deviation of  $C_{\text{pred}}/C_{\text{obs}}$ .  
<sup>d</sup>  $r^2$ —variance between  $\ln(C_{\text{obs}}/Q)$  and  $\ln(C_{\text{pred}}/Q)$ .  
<sup>e</sup> Predictions within a factor of 2 of the observations.  
<sup>f</sup> Zero predictions not included in GM, GSD, and  $r^2$  statistics.

GM of  $C_{\text{pred}}/C_{\text{obs}}$  is denoted by the squares, and the GM uncertainty and GSD are represented by the innermost and outermost horizontal bars, respectively, on the vertical lines through the squares.

Considering both datasets, we see that the residual dependence on  $F_*$  is mixed. For Kincaid (Fig. 11a), the residuals exhibit a trend showing 1) a slight model underprediction for  $F_* < 0.1$  (GM = 0.84), 2) a modest

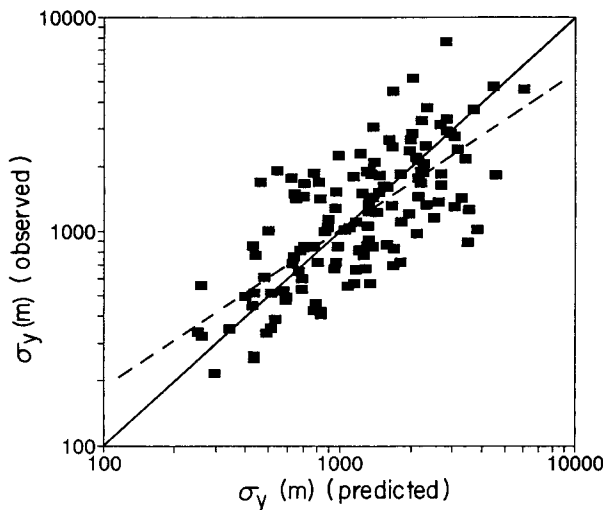


FIG. 8. Comparison between observed and predicted lateral dispersion parameter of buoyant plumes at Maryland power plants. Solid line corresponds to equal values of observations and predictions; dashed line is a least squares fit to  $\ln\sigma_{y\text{obs}}$  to  $\ln\sigma_{y\text{pred}}$ .

overprediction for  $0.1 \leq F_* < 0.4$  (GM = 1.28), and 3) a clear underprediction for  $F_* > 0.4$  (GM = 0.44). We suspect that the difference between groups 1 and 2 above is due to deficiencies in (a) the indirect source model, which depends on  $F_*$ , and (b) the penetrated plume model, which makes some GLC contributions in group 2, but none in group 1. For  $F_* > 0.4$ , the underprediction is due solely to the penetrated plume model since the predicted  $f = 0$  for all 14 cases in this group. The cases occurred in the morning, with low  $z_i$  values ( $200 \text{ m} < z_i < 300 \text{ m}$ ), generally light winds ( $U < 3 \text{ m s}^{-1}$ ), and a small  $w_*$  ( $1\text{--}1.4 \text{ m s}^{-1}$ ). The indirect source and penetrated plume models are discussed further in section 5.

In contrast to the Kincaid results, the  $C_{\text{pred}}/C_{\text{obs}}$  ratio for the Maryland plants exhibits no statistically significant trend with  $F_*$  (Fig. 11b). For the Maryland data and  $F_* \geq 0.1$ , there are probably too few observations (24) to draw firm conclusions about the performance of the penetrated plume model.

Figure 12 shows the residuals as functions of  $U/w_*$ . The Kincaid results exhibit a weak trend, with the GM differing statistically from 1 in the interval  $1.2 < U/w_* \leq 5$ . The slight overprediction for  $U/w_* \leq 1.2$  is caused by the high  $F_*$  cases; if the latter are removed, the GM falls from 1.2 to 1.0 in this interval.

Of the variables studied, the Maryland residuals exhibit their most significant variation with  $U/w_*$  (Fig. 12b). Most of this is caused by GLC observations obtained on the downwind side of wide ( $\sim 1\text{--}10 \text{ km}$ ) rivers

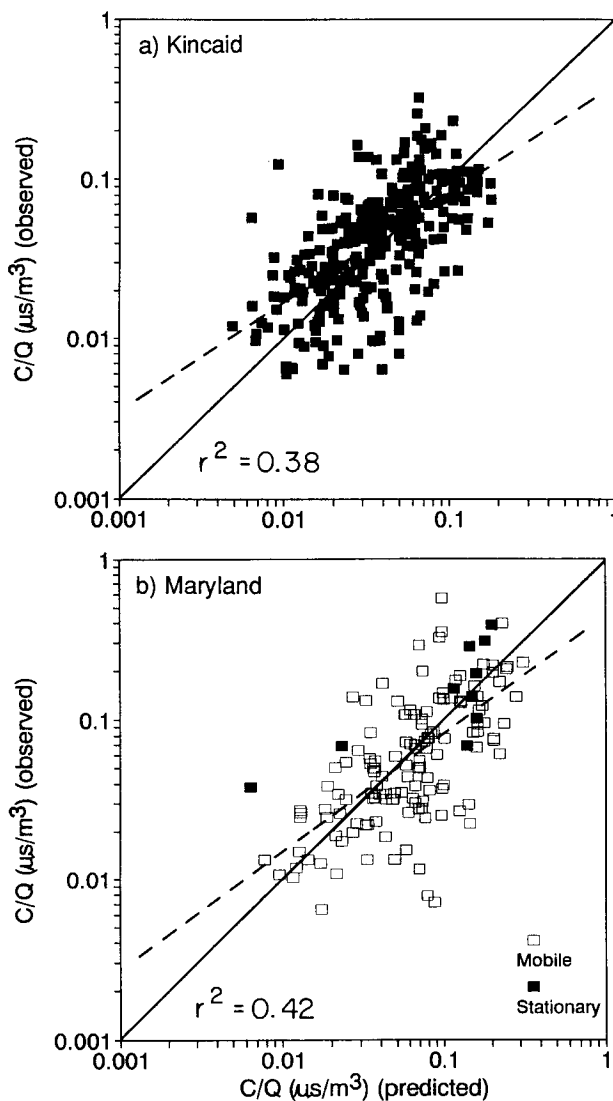


FIG. 9. Observed versus predicted ground-level concentrations for the PDF model at (a) Kincaid power plant for  $\text{SF}_6$  concentrations and (b) Maryland power plants for  $\text{SO}_2$  concentrations. Solid line corresponds to equal values of observations and predictions; dashed line is a least squares fit of  $\ln(C/Q)_{\text{obs}}$  to  $\ln(C/Q)_{\text{pred}}$ .

bordering the Chalk Point and Morgantown plants (Weil and Corio 1985). We suspect that reduced heat fluxes and turbulence levels due to the cooler water (than land) surface would induce local circulations and temporarily diminish dispersion on the downwind side of the rivers. Removal of the 25 near-river cases results in a residual, or GM behavior, given by the open circles (Fig. 12b), which show somewhat less of a trend.

Figure 13 shows the residuals as a function of  $X$ , and again, there are mixed results for the two datasets. For Kincaid, we believe that the underestimated GLCs in the interval  $2 \leq X < 5$  are caused by an overestimated vertical dispersion, particularly for wind speeds in the range  $2 \leq U/w_* < 5$  (see Fig. 12a). A good example

of the difference between the modeled and observed behavior is shown in Fig. 14a, where the dimensionless GLC  $CU_z^2/Q$  is plotted versus  $X$  for a 4-h period on 1 day. The lower observed maximum GLC and the greater distance to it than predicted (lines) imply an overestimated vertical dispersion. Figure 14b shows a similar, but less extreme, example of an underprediction bias in the  $2 \leq X < 5$  interval. A modification of the vertical dispersion formulation to correct the above bias is discussed in section 5b.

For the Maryland plants (Fig. 13b), the residuals are statistically unbiased and independent of  $X$ . The greatest departure of the GM from 1 occurs for  $X \leq 1$  and is due to the near-river observations at the Chalk Point and Morgantown plants. For  $X \leq 1$ , the GM of  $C_{\text{pred}}/C_{\text{obs}}$  is 2.0, 5.0, and 0.82 for Chalk Point, Morgantown, and Dickerson, respectively.

Overall, the above results show that the GMs of  $C_{\text{pred}}/C_{\text{obs}}$  in the various intervals range from about 0.8 to 1.25, which is considered good. Some exceptions to this and trends in the GMs were discussed in terms of model deficiencies and physical processes omitted. These include 1) limitations in the indirect source and penetrated plume models, 2) overestimated vertical dispersion for moderate winds, and 3) reduced heat fluxes and dispersion on the downwind side of wide rivers bordering two power plants.

Table 2 presents the overall statistical results for the above "base case" model, with  $a_e = 0.1$ ,  $R = 2$ , and  $\partial\Theta/\partial z = 0.005^\circ\text{C m}^{-1}$ ; note that about 70% of the predictions are within a factor of 2 of the observations. The results for other parameter values do not vary significantly from these base case results, which suggests that the model is fairly robust for the parameter ranges investigated.

As a final demonstration of model performance, we present quantile–quantile plots in Fig. 15 for the Kincaid and Maryland data. The results are obtained by ranking the  $C_{\text{pred}}$  and  $C_{\text{obs}}$  values from the lowest to highest and plotting the concentrations corresponding to the same rank in each distribution. This is not a rigorous test of model performance, but it is a useful comparison for air quality applications (e.g., Cimorelli et al. 1996). As can be seen, the results fall close to the 1:1 line, indicating good agreement between the ranked distributions. The maximum deviation from this line occurs at the high end of the distribution, where  $C_{\text{pred}} \sim 0.5C_{\text{obs}}$ . This deviation may be explained by the neglect of stochastic variability in the model and requires further investigation.

## 5. Discussion

In the following, we discuss several model features affecting the GLCs: 1) the  $w$  PDF parameterization, 2) the vertical dispersion and the effect of a finite  $T_{Lz}$ , and 3) the indirect source and penetrated plume models.

TABLE 3. Evaluation results for current and Weil et al. (1986) models based on comparisons between predicted and observed ground-level concentrations.

Model version	Plant	Cases	GM <sup>a</sup>	GSD <sup>b</sup>	r <sup>2c</sup>	Factor of 2 (%) <sup>d</sup>
Current	Kincaid	All	0.89	2.0	0.38	71
		F* ≥ 0.1	1.1	2.1	0.32	66
		F* < 0.1	0.84	1.9	0.34	72
Weil et al. (1986)	Kincaid	All	1.1	2.1	0.34	68
		F* ≥ 0.1	1.3	2.3	0.30	53
		F* < 0.1	1.0	2.0	0.32	74
Current	Maryland	All	1.1	2.1	0.50	69
		F* ≥ 0.1	1.0	2.2	0.51	71
		F* < 0.1	1.1	2.1	0.38	68
Weil et al. (1986)	Maryland	All	1.3	2.2	0.50	68
		F* ≥ 0.1	1.0	3.0	0.43	56
		F* < 0.1	1.4	2.0	0.45	70

<sup>a</sup> GM—geometric mean of C<sub>pred</sub>/C<sub>obs</sub>.  
<sup>b</sup> GSD—geometric standard deviation of C<sub>pred</sub>/C<sub>obs</sub>.  
<sup>c</sup> r<sup>2</sup>—variance between ln(C<sub>obs</sub>) and ln(C<sub>pred</sub>).  
<sup>d</sup> Predictions within a factor of 2 of the observations.

a. The w PDF parameterization

The existing p<sub>w</sub> is based on the first three moments of w—w̄, σ<sub>w</sub><sup>2</sup>, and w<sup>3</sup>—and the assumption that σ<sub>w1</sub>/w<sub>1</sub> = |σ<sub>w2</sub>/w<sub>2</sub>| = R. This is one parameterization, and alternatives should be considered. For example, Weil (1988) used the bi-Gaussian form [Eq. (7)] with an assumed λ<sub>1</sub> = 0.4 and λ<sub>2</sub> = 0.6, but empirically obtained the σ<sub>wj</sub> and w<sub>j</sub> from a fit of the modeled surface CWIC distribution to laboratory data for passive releases. Using his σ<sub>wj</sub> and w<sub>j</sub>, we find σ<sub>w1</sub>/w<sub>1</sub> = 1.2 and σ<sub>w2</sub>/w<sub>2</sub> = 0.74. The key point is that the σ<sub>wj</sub>/w<sub>j</sub> ratios are unequal, in contrast to our earlier assumption.

In a study of the bi-Gaussian PDF, Du et al. (1994) added the fourth moment of w to the input variables and specified λ<sub>1</sub> = 0.4 and λ<sub>2</sub> = 0.6 for strong convection. Using their σ<sub>wj</sub> and w<sub>j</sub> expressions, we find σ<sub>w1</sub>/w<sub>1</sub> = 2.89 and σ<sub>w2</sub>/w<sub>2</sub> = 2.08 for S = 0.1, σ<sub>w1</sub>/w<sub>1</sub> = 1.07 and σ<sub>w2</sub>/w<sub>2</sub> = 1.03 for S = 0.6, and σ<sub>w1</sub>/w<sub>1</sub> = 0.93 and σ<sub>w2</sub>/w<sub>2</sub> = 0.73 for S = 0.8. Their ratios increase as S → 0, as would be expected for a distribution approximating a Gaussian PDF in that limit, and for S = 0.8, they are close to those obtained from Weil’s (1988) empirical fit. Thus, the addition of w<sup>4</sup> to the input variables may improve the p<sub>w</sub> parameterization, and perhaps the agreement between predicted and observed GLCs.

The Du et al. (1994) approach for estimating the p<sub>w</sub> parameters should be pursued in the future. This approach could be improved further by parameterizing the λ<sub>1</sub> and λ<sub>2</sub> as functions of S such that λ<sub>1</sub>, λ<sub>2</sub> → 0.5 as S → 0. However, one must consider the uncertainty in estimates or measurements of w<sup>4</sup> and the associated uncertainty in C<sub>pred</sub> before implementing this approach in a practical model.

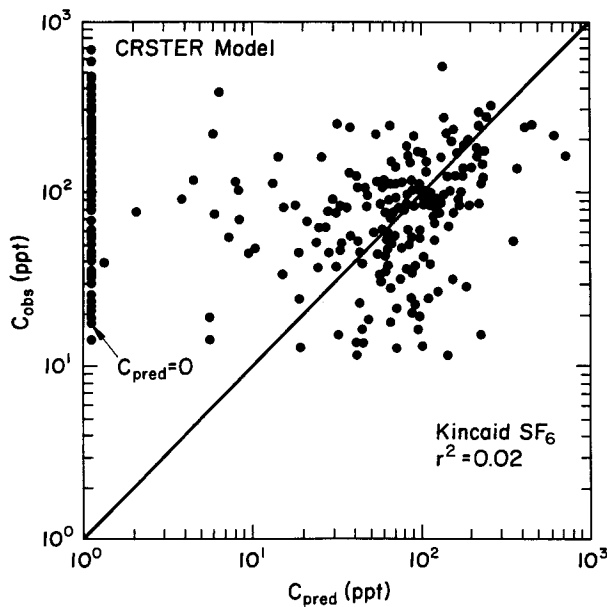


FIG. 10. Observed versus predicted ground-level SF<sub>6</sub> concentrations for the CRSTER model at the Kincaid power plant; diagonal line corresponds to C<sub>obs</sub> = C<sub>pred</sub>.

b. Vertical dispersion

The results of section 4b for the Kincaid plant suggest an apparent overestimation of the vertical dispersion during moderate winds. This may be partially caused by the infinite, rather than the finite, T<sub>Lz</sub> assumed for the CBL.

Here, we demonstrate the effect of a finite T<sub>Lz</sub> on vertical dispersion and the distance x<sub>m</sub> to the maximum GLC. We first consider a Gaussian plume model for a passive release, with the GLC along the plume centerline given by

$$C(x, 0, 0) = \frac{Q}{\pi U \sigma_y \sigma_z} \exp\left(-\frac{h_s^2}{2\sigma_z^2}\right). \quad (43)$$

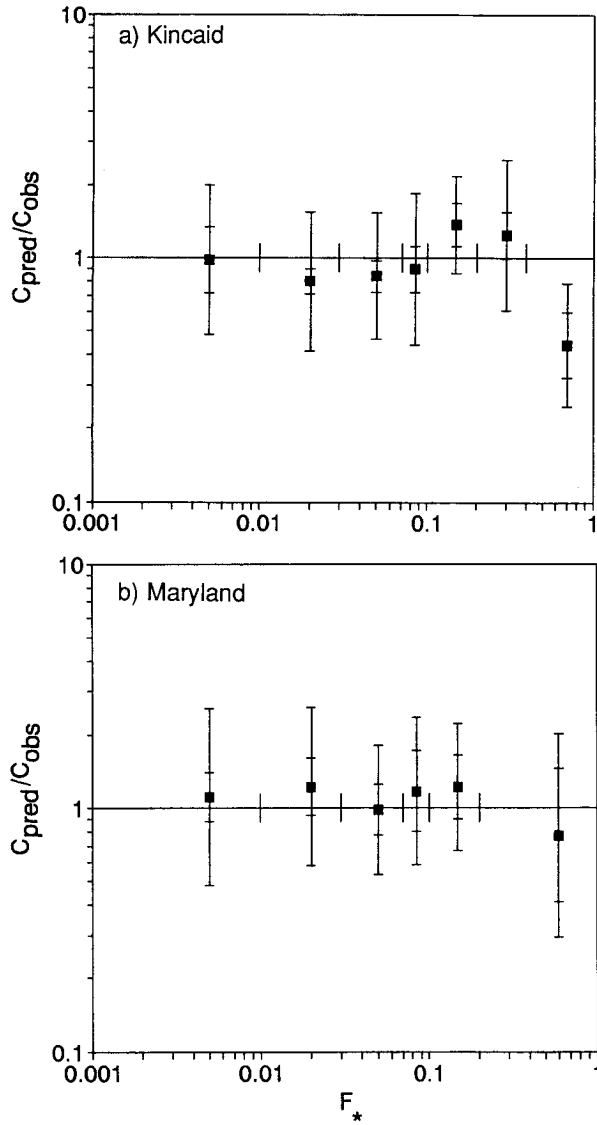


FIG. 11. Geometric mean (points) of predicted-to-observed ground-level concentration as a function of the dimensionless buoyancy flux for the PDF model. Innermost and outermost horizontal bars denote the uncertainty in the GM and the geometric standard deviation, respectively.

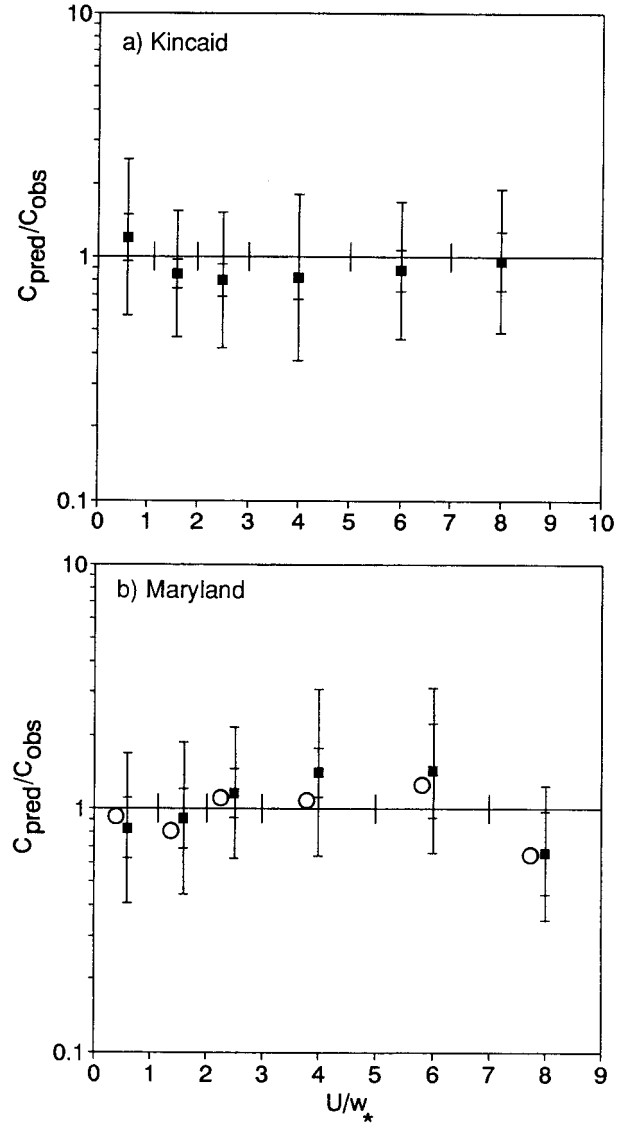


FIG. 12. Geometric mean (points) of predicted-to-observed ground-level concentration as a function of  $U/w_*$  for the PDF model. Innermost and outermost horizontal bars denote the uncertainty in the GM and the geometric standard deviation, respectively. Open circles in (b) denote GMs without near-river cases at the Chalk Point and Morgantown plants.

The  $\sigma_z$  is parameterized by  $\sigma_z = \sigma_w t(1 + 0.5t/T_{Lz})^{-1/2}$  and similarly for  $\sigma_y$ , but with  $\sigma_w$  replaced by  $\sigma_v$ ; we assume  $T_{Ly} = T_{Lz}$ . These parameterizations satisfy the short- and long-time limits of Taylor's (1921) theory.

The travel time  $t_m$  corresponding to the  $x_m$  is found by taking  $\partial C/\partial t$  in Eq. (43) and setting it equal to zero. The  $t_m$  is attained when  $2\sigma_z^2 = h_s^2$  and is

$$t_m = \frac{h_s^2}{8\sigma_w^2 T_{Lz}} \left[ 1 + \left( 1 + \frac{32\sigma_w^2 T_{Lz}^2}{h_s^2} \right)^{1/2} \right], \quad (44)$$

with  $x_m = Ut_m$ . Assuming that  $\sigma_w^2 = 0.31w_*^2$  and  $T_{Lz} = 0.7z_i/w_*$ , we find the dimensionless distance  $X_m$  corresponding to  $x_m$  to be

$$X_m = \frac{w_* x_m}{U z_i} = 0.58 h_s^{*2} \left[ 1 + \left( 1 + \frac{4.9}{h_s^{*2}} \right)^{1/2} \right], \quad (45)$$

where  $h_s^* = h_s/z_i$ . In the limit of an infinite  $T_{Lz}$ , the  $t_m$  and  $X_m$  are given by  $t_{m\infty} = h_s(\sqrt{2}\sigma_w)^{-1}$  and  $X_{m\infty} = 1.26h_s^*$ , assuming  $\sigma_w = 0.56w_*$ .

We now consider the variation of the ratio  $X_m/X_{m\infty}$  with source height. For  $h_s^* = 0.1, 0.25, 0.5$ , and  $1$ , the  $X_m = 0.13, 0.36, 0.8$ , and  $2.0$ , and the  $X_m/X_{m\infty} = 1.02, 1.13, 1.26$ , and  $1.56$ . As expected, the ratio increases with  $h_s^*$  because of the greater time required for the plume to reach the surface from a more elevated source.

With the greater time, the growth rate is reduced since  $t$  is further into the long-time or  $t^{1/2}$  regime of spread. Qualitatively, we expect the  $X_m/X_{m\infty}$  ratio to increase further with the addition of plume buoyancy because of the greater effective source height.

In the following, a simple approach is outlined for including the  $T_{Lz}$  effect for buoyant plumes and a skewed  $p_w$ . We reconsider the trajectory expression [Eq. (5)] and assume that the random vertical velocity decays from its initial value  $w$  over time according to  $w/f_L(t)$ , where  $f_L(t)$  is taken here to be  $(1 + 0.5t/T_{Lz})^{1/2}$ . With  $t = x/U$ , the new trajectory equation is

$$z_p = h_s + \Delta h + \frac{wt}{f_L(t)}, \tag{46}$$

and the  $w(z_p; t)$  found by rearranging the above is

$$w = (z_p - h_s - \Delta h) \frac{f_L(t)}{t}. \tag{47}$$

From Eq. (47), we have  $|dw/dz_p| = f_L(t)/t$ .

The above  $w$  and  $dw/dz_p$  can be substituted into Eq. (4) to obtain the  $p_z$ . Upon doing this, replacing  $t$  by  $x/U$ , and using Eq. (3), we obtain a  $C(x, z)$  expression identical to Eq. (9), but with  $\sigma_{zj}$  and  $\Psi_j$  given by

$$\sigma_{zj} = \frac{\sigma_{wj}x/U}{(1 + 0.5x/UT_{Lz})^{1/2}}$$

and

$$\Psi_j = h_s + \Delta h + \frac{\bar{w}_j x/U}{(1 + 0.5x/UT_{Lz})^{1/2}}, \tag{48}$$

with  $j = 1$  or  $2$ . For a Gaussian  $p_w$  and  $\Delta h = 0$ , this approach reproduces Eq. (43) for the GLC.

As Eq. (48) shows, the vertical dispersion ( $\sigma_{zj}$ ) at a given  $x$  becomes smaller as  $T_{Lz}$  is reduced, and thus  $x_m$  becomes larger. The  $T_{Lz}$  is expected to decrease with decreasing  $z_p/L$  because of the increased turbulence dissipation rate  $\varepsilon$  and the decreased turbulence length scale  $l$ , especially within the surface layer. The behavior of  $\varepsilon$  is shown by the observations of Guillemet et al. (1983) and that of  $l$  by the large-eddy simulations (LES) of Mason (1992). In addition, Mason's dispersion simulations using a Lagrangian model and LES fields show that a systematic reduction in vertical dispersion occurs with a decreasing  $w_*/u_*$  or  $z_p/L$  and increasing wind speed. These findings are consistent with the inferred overestimation of the vertical dispersion at the Kincaid plant (Figs. 12a and 13) for moderate winds.

The approach outlined above [Eqs. (46)–(48)] will be pursued in the future for a skewed  $p_w$ , with comparisons made between predicted and observed GLCs.

*c. Indirect source and penetrated plume models*

The Kincaid residual analysis for  $F_*$  (Fig. 11a) suggests that the indirect source model needs further development. There are two aspects that could be im-

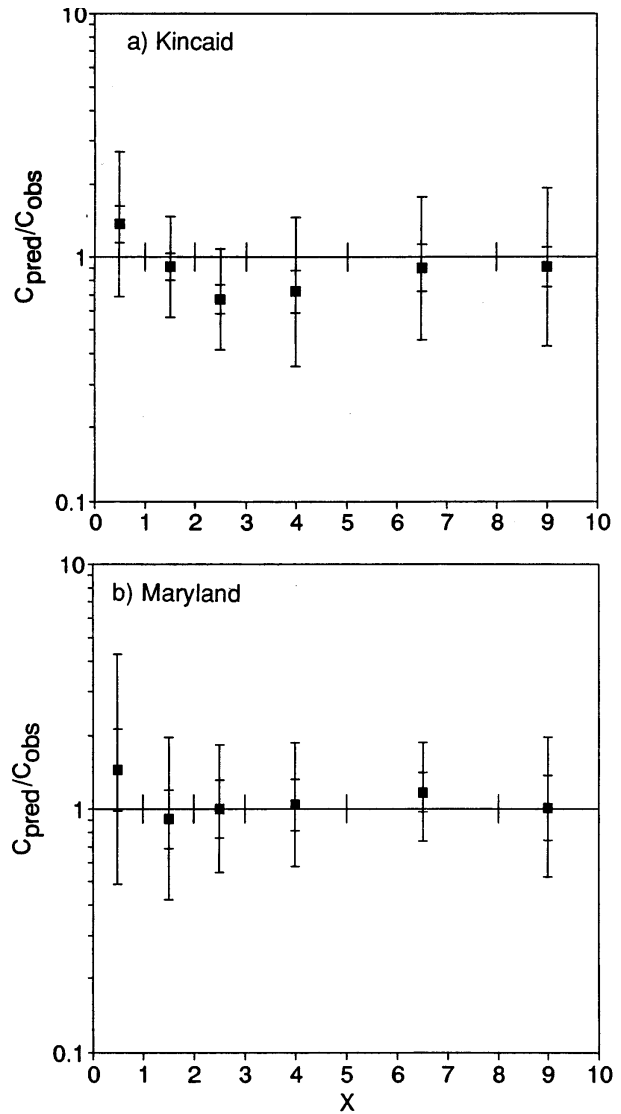


FIG. 13. Geometric mean (points) of predicted-to-observed ground-level concentration as a function of the dimensionless downwind distance for the PDF model. Innermost and outermost horizontal bars denote the uncertainty in the GM and the geometric standard deviation, respectively.

proved. The first is the inclusion of the finite  $T_{Lz}$ , which would shift the axial GLC distribution farther downwind and reduce the GLC magnitude; these changes should be more pronounced for the high- $F_*$  cases ( $0.1 \leq F_* < 0.4$ ), where model overestimation is a problem. The second is a better  $\Delta h_i$  model.

While the above improvements are worth pursuing, we must recognize the limitations of the indirect source formulation:  $\Delta h_i$  is somewhat of a “fictitious” plume rise, and the  $r_z (\propto x^{4/3})$  far downwind (appendix C) probably exhibits too rapid a growth rate. Thus, we should consider alternative treatments for the indirect source, such as a distributed source with  $x$  as originally adopted by Hanna et al. (1986). This could be expanded to in-

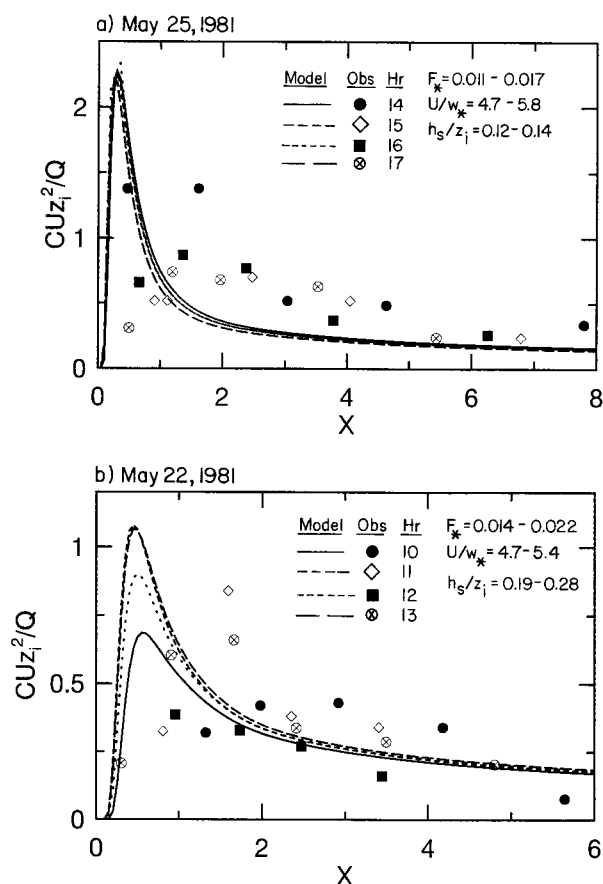


FIG. 14. Dimensionless ground-level  $SF_6$  concentration versus the dimensionless downwind distance as observed at the Kincaid power plant and predicted by the PDF model.

clude an increasing  $\tilde{z}_i$  with  $t$  over the averaging period, which is important in the morning, when many high- $F_*$  cases occur. Systematic experiments in a convection tank would be helpful for further development efforts.

The penetrated plume model is an ad hoc approach that only roughly accounts for the CBL growth and fumigation. An important feature to add is the distributed nature of the source, which is included in other fumigation models (Deardorff and Willis 1982; Luhar and Sawford 1995; Misra 1980; Venkatram 1988). This aspect, as well as the time dependence of  $\tilde{z}_i$ ,  $h_{es}$ ,  $f$ , etc., should be incorporated into a more general formulation. Although such a formulation would be more complex, it should be pursued to determine whether it leads to better predictions.

## 6. Summary and conclusions

A PDF dispersion model has been presented for buoyant releases in the CBL, where the mean concentration field  $C$  is found from the particle position PDFs,  $p_x$  and  $p_z$ . The  $p_z$  is derived from the vertical velocity ( $w$ ) PDF, which is generally skewed, whereas the  $p_y$  is assumed

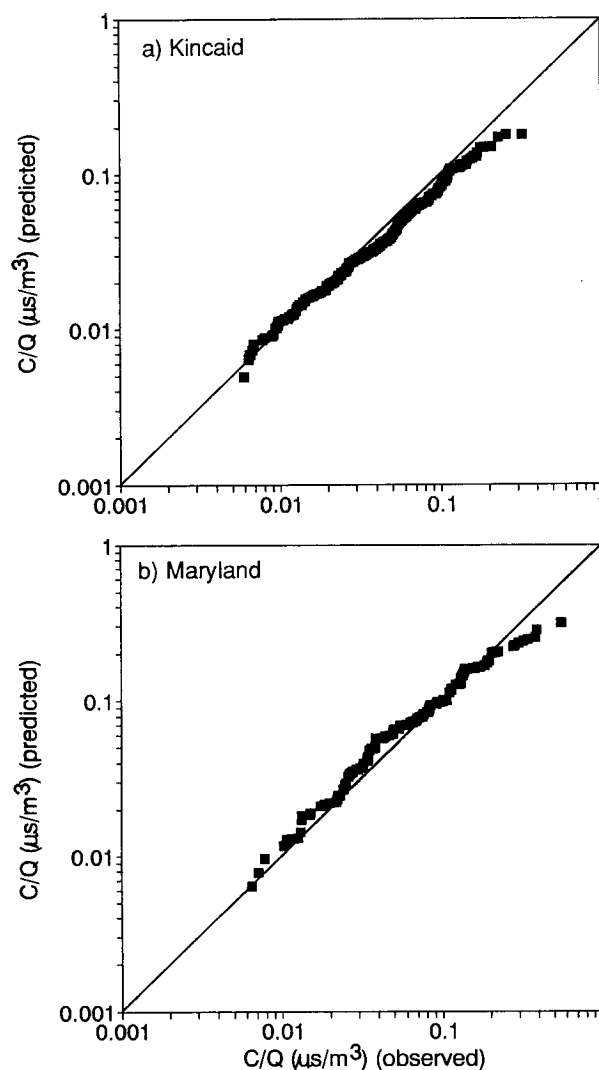


FIG. 15. Quantile-quantile plots of predicted versus observed ground-level concentration for the Kincaid and Maryland datasets.

to be Gaussian. Three primary sources contribute to the modeled  $C$  field: 1) the direct or real source (at the stack), 2) the indirect source, and 3) the penetrated source. Image sources are included to satisfy the zero-flux conditions at  $z = 0$ ,  $z_i$ . The indirect and penetrated source models are simple approaches for treating the plume interaction with the elevated inversion and lead to a continuous variation of  $C$  with the buoyancy flux.

Comparisons between modeled crosswind-integrated concentration fields ( $C$ ) and convection tank data (Deardorff and Willis 1984, 1988; Willis and Deardorff 1987) showed fair to good agreement in the lower half of the CBL. Near the source, the predicted  $C$  contours exhibited an upward tilt due to the plume rise, with the tilt increasing with the buoyancy flux. However, the predicted contour behavior near the CBL top differed from the measurements due to the assumed quasi-re-

flection at  $z = z_i$ ; improvement of this aspect is a problem for future work. Overall, the predicted  $C^y$  profiles at the surface were in agreement with the data over a wide range of the buoyancy flux and showed a progressive reduction in the  $C^y$  with increasing  $F_*$ .

The model was also evaluated with GLCs measured near several Maryland power plants and the Kincaid power plant. Correlation plots of  $C/Q$  for each dataset exhibited considerable scatter, but the  $r^2$  between predicted and observed  $\ln(C/Q)$  values was approximately 0.4 for both sets, thus demonstrating an overall consistency of model performance. In addition, the statistics of  $C_{\text{pred}}/C_{\text{obs}}$  were good, with a GM near 1 and a GSD of about 2. These results were similar to those obtained with the Weil et al. (1986) model (Table 3). Thus, in addition to maintaining a continuous variation of  $C$  with  $F_*$ , a problem with earlier PDF models, the current model yields performance results comparable to those models.

The model performance was diagnosed further using residual plots to detect model trends with the input variables; the variables included the buoyancy flux, wind speed, and downwind distance. In general, the GMs of  $C_{\text{pred}}/C_{\text{obs}}$  for grouped data ranged from 0.8 to 1.25, which is considered good. Some exceptions to this and trends in the GMs were found, suggesting some model limitations. The latter included 1) limitations in the indirect source and penetrated plume models, 2) overestimated vertical dispersion during moderate winds, and 3) reduced heat fluxes and dispersion on the downwind side of wide rivers bordering two power plants.

In summary, the PDF model is an approach that includes state-of-the-art knowledge of CBL turbulence and dispersion in a simple framework. The overall model performance is good. Future development efforts should focus on 1) improving the indirect source and penetrated plume models, and 2) incorporating a finite Lagrangian timescale ( $T_{Lz}$ ) into the model to correct the overestimated vertical dispersion during moderate winds (section 5b).

*Acknowledgments.* We wish to thank S. White and J. Walker for their assistance with the data analysis and for preparing the figures, K. Davis and T. Horst for comments on an earlier draft of this paper, and two anonymous reviewers for their comments. We also are grateful to G. A. Briggs and members of the American Meteorological Society–Environmental Protection Agency Regulatory Model Improvement Committee—A. Cimorelli, R. Lee, R. Paine, S. Perry, A. Venkatram, and R. Wilson—for helpful discussions and comments during the course of this work. This research was supported by the Maryland Department of Natural Resources and by the U.S. Environmental Protection Agency under Grant R-823419-01-0.

APPENDIX A

Parameters Defining the  $w$  PDF

The parameters of  $p_w(w)$  in Eq. (7) are obtained by equating the zeroth through third moments of that distribution,

$$\overline{w^n} = \int_{-\infty}^{\infty} w^n p_w(w) dw \tag{A1}$$

( $n = 0-3$ ), with those specified:  $\overline{w^0} = \lambda_1 + \lambda_2 = 1$ ,  $\overline{w} = 0$ ,  $\sigma_w^2$  [Eq. (8a)], and  $\overline{w^3} = S\sigma_w^3$ . The equations are given in Baerentsen and Berkowicz (1984) and Weil (1990).

Defining  $R = \sigma_{w1}/\overline{w_1} = -\sigma_{w2}/\overline{w_2}$ , Weil (1990) found the solutions for  $w_1$  and  $w_2$  to be

$$\frac{\overline{w_1}}{\sigma_w} = \frac{\gamma_1 S}{2} + \frac{1}{2} \left( \gamma_1^2 S^2 + \frac{4}{\gamma_2} \right)^{1/2} \tag{A2}$$

and

$$\frac{\overline{w_2}}{\sigma_w} = \frac{\gamma_1 S}{2} - \frac{1}{2} \left( \gamma_1^2 S^2 + \frac{4}{\gamma_2} \right)^{1/2}, \tag{A3}$$

where

$$\gamma_1 = \frac{1 + R^2}{1 + 3R^2} \tag{A4}$$

and

$$\gamma_2 = 1 + R^2. \tag{A5}$$

In addition, he obtained

$$\lambda_1 = \frac{\overline{w_2}}{w_2 - \overline{w_1}} \tag{A6}$$

and

$$\lambda_2 = -\frac{\overline{w_1}}{w_2 - \overline{w_1}}, \tag{A7}$$

as found by Baerentsen and Berkowicz.

Thus, with  $\sigma_w^2$ ,  $S$ , and  $R$  specified, the  $w_j$ ,  $\sigma_{w_j}$ , and  $\lambda_j$  ( $j = 1, 2$ ) can be found.

APPENDIX B

Estimation of the Parameter  $\alpha$  in the Energy Criterion

In the following, we apply the energy criterion of Eq. (19) to estimate the negative heat or buoyancy flux at the top of the CBL, which is assumed to be capped by a positive potential temperature jump  $\Delta\Theta = \Theta_2 - \Theta_1$ , where 2 and 1 denote conditions above and below the jump. Assuming small temperature and density ( $\Delta\rho = \rho_1 - \rho_2$ ) jumps, the two are related by  $\Delta\Theta/\Theta_a = \Delta\rho/\rho_a$ . Using the last relationship, we rewrite Eq. (19) in the form

$$g \frac{\Delta\Theta}{\theta_a} = \alpha \frac{w^2}{2z_i}. \tag{B1}$$

Within the PDF model framework, we assume that negative vertical velocities above  $z_i$  transport warm air downward into the CBL to be mixed. We estimate a

negative buoyancy flux by multiplying Eq. (B1) by  $w$  and averaging over the negative velocities as

$$\frac{1}{f_d} \int_{-\infty}^0 wg \frac{\Delta\Theta}{\Theta_a} p_w dw = \frac{1}{f_d} \int_{-\infty}^0 \frac{\alpha}{2z_i} w^3 p_w dw, \quad (\text{B2})$$

where

$$f_d = \int_{-\infty}^0 p_w dw. \quad (\text{B3})$$

The left-hand side (lhs) of (B2) is the negative buoyancy flux at the inversion,  $(g/\Theta_a)w\theta_i$ , which is generally assumed to be related to the surface buoyancy flux by

$$-\frac{g}{\Theta_a} \overline{w\theta_i} = 0.2 \frac{g}{\Theta_a} \overline{w\theta_o} \quad (\text{B4})$$

(see Moeng and Wyngaard 1989). Replacing the lhs of (B2) by the right-hand side of (B4), we have

$$0.2 \frac{g}{\Theta_a} \overline{w\theta_o} = \frac{1}{f_d} \frac{\alpha}{2z_i} \int_{-\infty}^0 w^3 p_w dw. \quad (\text{B5})$$

For simplicity in evaluating the above integral, we assume a Gaussian PDF, which leads to

$$0.2 \frac{g}{\Theta_a} \overline{w\theta_o} = \frac{2\alpha}{\sqrt{2\pi}} \frac{\sigma_w^3}{z_i}. \quad (\text{B6})$$

Using the definition of  $w_* = (\overline{gw\theta_o z_i / \Theta_a})^{1/3}$ , we have

$$0.2w_*^3 = \frac{2\alpha}{\sqrt{2\pi}} \sigma_w^3. \quad (\text{B7})$$

Evaluating (B7) with the convective limit of Eq. (8a) ( $\sigma_w = 0.56w_*$ ), we find  $\alpha = 1.4$ .

#### APPENDIX C

##### Growth of Lofting Plumes

We consider a plume of elliptical cross section trapped at the CBL top and unable to penetrate the elevated inversion. The ellipse has half-widths  $r_y$  and  $r_z$  in the lateral and vertical directions (see Fig. 2c) and a uniform density defect,  $\rho - \rho_a = -\Delta\rho$ , relative to the density in the CBL. In line with Briggs (1985), we assume that the lateral dispersion is enhanced and the vertical dispersion is constant or diminished somewhat initially. The plume is assumed to behave as a stable density interface at the CBL top with entrainment taking place on the bottom half of the plume perimeter; this is akin to entrainment across the density or temperature jump in the environment at  $z = z_i$ . With the elliptical cross section, the cross sectional area is  $\pi r_y r_z$  and the perimeter is approximated by  $\pi(r_y + r_z)$ .

Assuming that entrainment takes place only along the lower half of the plume, we use an entrainment assumption in a conservation expression for plume mass or volume, which yields

$$\frac{d}{dx}(Ur_y r_z) = \frac{w_e}{2}(r_y + r_z), \quad (\text{C1})$$

where  $w_e$  is an entrainment velocity (Weil 1991). This is analogous to the conservation expression for a circular plume. For the elliptical plume with zero penetration of the inversion, the buoyancy flux  $F$  is conserved so that

$$F = F_b = Ur_y r_z g \frac{\Delta\rho}{\rho_a}. \quad (\text{C2})$$

In line with entrainment models for turbulent mixed layers (e.g., Turner 1979; Deardorff and Willis 1985), we assume that

$$w_e = a_e \frac{w_*}{\text{Ri}^\mu}, \quad (\text{C3})$$

where  $\text{Ri}$  is a Richardson number based on the plume density defect and  $r_z$ :

$$\text{Ri} = \frac{g\Delta\rho}{\rho_a} \frac{r_z}{w_*^2}. \quad (\text{C4})$$

Using Eq. (C2), the  $\text{Ri}$  can be written as

$$\text{Ri} = \frac{F_b}{Uw_*^2 r_y}. \quad (\text{C5})$$

Equation (C3) is chosen as a simple form for  $w_e$  that results in an analytical expression for the product  $r_y r_z$ . The exponent  $\mu$  in Eq. (C3) is taken as 1/2 based on the entrainment velocity correlation with  $\text{Ri}$  from Deardorff and Willis (1985, their Fig. 20), where their  $\text{Ri}$  is defined using interfacial length and velocity scales.

Substituting Eqs. (C3) and (C5) into Eq. (C1), we have

$$\frac{d}{dx}(r_y r_z) = \frac{a_e w_*^2}{2} \left( \frac{r_y}{F_b U} \right)^{1/2} (r_y + r_z). \quad (\text{C6})$$

To complete the model, we assume that 1) the half-width  $r_y = \sqrt{2}\sigma_y$  (see Briggs 1975; Csanady 1973), 2)  $\sigma_y$  is given by Briggs's (1985) expression for lofting plumes  $\sigma_y = 1.6F_b^{1/3} x^{2/3}/U$ , and 3)  $r_z \ll r_y$  far downstream. As a result of the last assumption, we have

$$\frac{d}{dx}(r_y r_z) = \frac{a_e w_*^2}{2(F_b U)^{1/2}} r_y^{3/2}. \quad (\text{C7})$$

Substituting the expression for  $r_y$  into the above, we can integrate Eq. (C7) to obtain

$$r_y r_z = r_i^2 + \frac{a_e \alpha_y^{3/2} w_*^2}{4U^2} (x^2 - x_i^2), \quad (\text{C8})$$

where  $r_i$  is the plume radius when the rising plume reaches the inversion,  $x_i$  is the distance where this occurs, and  $\alpha_y = 1.6\sqrt{2} = 2.3$ . In the main text and model, we ignore the  $x_i$  in (C8) since our interest is primarily

for  $x \gg x_i$ . The  $a_e$  is found to be 0.1 based on comparisons with laboratory data.

Far downstream, where  $r_i^2$  and  $x_i^2$  can be neglected in Eq. (C8), we have

$$r_z \approx \frac{a_e \alpha_y^{3/2} w_*^2 x^2}{4U^2 r_y}. \quad (\text{C9})$$

Substituting the  $r_y$  expression and the value of  $\alpha_y$  into the above, we find

$$r_z \approx 0.38 a_e \frac{w_*^2 x^{4/3}}{F^{1/3} U}. \quad (\text{C10})$$

#### REFERENCES

- Baerentsen, J. H., and R. Berkowicz, 1984: Monte Carlo simulation of plume dispersion in the convective boundary layer. *Atmos. Environ.*, **18**, 701–712.
- Bowne, N. E., R. J. Londergan, D. R. Murray, and H. S. Borenstein, 1983: Overview, results and conclusions for the EPRI plume model validation and development project: Plains site. Electric Power Research Institute Rep. EA-3074, Electric Power Research Institute, Palo Alto, CA, 205 pp.
- Briggs, G. A., 1975: Plume rise predictions. *Lectures on Air Pollution and Environmental Impact Analyses*, D. A. Haugen, Ed., Amer. Meteor. Soc., 59–111.
- , 1984: Plume rise and buoyancy effects. *Atmospheric Science and Power Production*, D. Randerson, Ed., U.S. Department of Energy.
- , 1985: Analytical parameterizations of diffusion: The convective boundary layer. *J. Climate Appl. Meteor.*, **24**, 1167–1186.
- Brownlee, K. A., 1965: *Statistical Theory and Methodology*. Wiley and Sons, 550 pp.
- Businger, J. A., 1973: Turbulent transfer in the atmospheric surface layer. *Workshop on Micrometeorology*, D. A. Haugen, Ed., Amer. Meteor. Soc., 67–100.
- Carson, D. J., 1973: The development of a dry inversion-capped convectively unstable boundary layer. *Quart. J. Roy. Meteor. Soc.*, **99**, 450–467.
- Chatwin, P. C., D. M. Lewis, and P. J. Sullivan, 1995: Turbulent dispersion and the beta distribution. *Environmetrics*, **6**, 395–402.
- Cimorelli, A. J., S. G. Perry, R. F. Lee, R. J. Paine, A. Venkatram, J. C. Weil, and R. B. Wilson, 1996: Current progress in the AERMIC model development program. *Proc. 89th Annual Meeting and Exhibition of the Air and Waste Management Association*, Pittsburgh, PA, Air Waste Manage. Assoc.
- Csanady, G. T., 1973: *Turbulent Diffusion in the Environment*. Reidel, 248 pp.
- Deardorff, J. W., and G. E. Willis, 1982: Ground-level concentrations due to fumigation into an entraining mixed layer. *Atmos. Environ.*, **16**, 1159–1170.
- , and —, 1984: Groundlevel concentration fluctuations from a buoyant and a non-buoyant source within a laboratory convectively mixed layer. *Atmos. Environ.*, **18**, 1297–1309.
- , and —, 1985: Further results from a laboratory model of the convective planetary boundary layer. *Bound.-Layer Meteor.*, **32**, 205–236.
- , and —, 1988: Concentration fluctuations within a laboratory convectively mixed layer. *Lectures on Air Pollution Modeling*, A. Venkatram and J. C. Wyngaard, Eds., Amer. Meteor. Soc., 357–384.
- Du, S., J. D. Wilson, and E. Yee, 1994: Probability density functions for velocity in the convective boundary layer, and implied trajectory models. *Atmos. Environ.*, **28**, 1211–1217.
- EPA, 1977: User's manual for single source (CRSTER) model. U.S. Environmental Protection Agency Rep. EPA-450/2-77-013, U.S. EPA, OAQPS, Research Triangle Park, NC, 285 pp.
- , 1987: Industrial Source Complex (ISC) dispersion model user's guide—Second edition (revised). Vol. 1. U.S. Environmental Protection Agency Rep. EPA-450/4-88-002a, U.S. EPA, OAQPS, Research Triangle Park, NC, 240 pp.
- Fox, D. G., 1984: Uncertainty in air quality modeling. *Bull. Amer. Meteor. Soc.*, **65**, 27–36.
- Garratt, J. R., J. C. Wyngaard, and R. J. Francey, 1982: Winds in the atmospheric boundary layer—Prediction and observation. *J. Atmos. Sci.*, **39**, 1307–1316.
- Guillemet, B., H. Isaka, and P. Mascart, 1983: Molecular dissipation of turbulent fluctuations in the convective mixed layer. Part I: Height variations of dissipation rates. *Bound.-Layer Meteor.*, **27**, 141–162.
- Hanna, S. R., 1984: The exponential probability distribution function and concentration fluctuations in smoke plumes. *Bound.-Layer Meteor.*, **29**, 361–375.
- , and R. J. Paine, 1989: Hybrid plume dispersion model (HPDM) development and evaluation. *J. Appl. Meteor.*, **28**, 206–224.
- , J. C. Weil, and R. J. Paine, 1986: Plume model development and evaluation, hybrid approach. Electric Power Research Institute Rep. D034-500, Electric Power Research Institute, Palo Alto, CA, 550 pp.
- Henn, D. S., and R. I. Sykes, 1992: Large-eddy simulation of dispersion in the convective boundary layer. *Atmos. Environ.*, **26A**, 3145–3159.
- Hicks, B. B., 1985: Behavior of turbulent statistics in the convective boundary layer. *J. Climate Appl. Meteor.*, **24**, 607–614.
- Holtstag, A. A. M., and A. P. van Ulden, 1983: A simple scheme for daytime estimates of the surface fluxes from routine weather data. *J. Climate Appl. Meteor.*, **22**, 517–529.
- Lamb, R. G., 1982: Diffusion in the convective boundary layer. *Atmospheric Turbulence and Air Pollution Modelling*, F. T. M. Nieuwstadt and H. van Dop, Eds., Reidel, 159–229.
- Li, Z.-K., and G. A. Briggs, 1988: Simple pdf models for convectively driven vertical diffusion. *Atmos. Environ.*, **22**, 55–74.
- Luhar, A. K., and R. E. Britter, 1989: A random walk model for dispersion in inhomogeneous turbulence in a convective boundary layer. *Atmos. Environ.*, **23**, 1911–1924.
- , and B. L. Sawford, 1995: Lagrangian stochastic modeling of the coastal fumigation phenomenon. *J. Appl. Meteor.*, **34**, 2259–2277.
- Mason, P. J., 1992: Large-eddy simulation of dispersion in convective boundary layers with wind shear. *Atmos. Environ.*, **26A**, 1561–1571.
- Misra, P. K., 1980: Dispersion from tall stacks into a shoreline environment. *Atmos. Environ.*, **14**, 397–400.
- , 1982: Dispersion of nonbuoyant particles inside a convective boundary layer. *Atmos. Environ.*, **16**, 239–243.
- Moeng, C.-H., and J. C. Wyngaard, 1989: Evaluation of turbulent transport and dissipation closures in second-order modeling. *J. Atmos. Sci.*, **46**, 2311–2330.
- Mylne, K. R., and P. J. Mason, 1991: Concentration fluctuation measurements in a dispersing plume at a range of up to 1000 m. *Quart. J. Roy. Meteor. Soc.*, **117**, 177–206.
- Sawford, B. L., and F. M. Guest, 1987: Lagrangian stochastic analysis of flux-gradient relationships in the convective boundary layer. *J. Atmos. Sci.*, **44**, 1152–1165.
- Sykes, R. I., 1988: Concentration fluctuations in dispersing plumes. *Lectures on Air Pollution Modeling*, A. Venkatram and J. C. Wyngaard, Eds., Amer. Meteor. Soc., 325–356.
- , W. S. Lewellen, and S. F. Parker, 1984: A turbulent-transport model for concentration fluctuations and fluxes. *J. Fluid Mech.*, **139**, 193–218.
- , —, and —, 1986: A Gaussian plume model of atmospheric dispersion based on second-order closure. *J. Climate Appl. Meteor.*, **25**, 322–331.
- Taylor, G. I., 1921: Diffusion by continuous movements. *Proc. London Math. Soc., Ser. 2*, **20**, 196–212.
- Turner, J. S., 1979: *Buoyancy Effects in Fluids*. Cambridge University Press, 368 pp.

- Venkatram, A., 1982: A framework for evaluating air quality models. *Bound.-Layer Meteor.*, **24**, 371–385.
- , 1983: On dispersion in the convective boundary layer. *Atmos. Environ.*, **17**, 529–533.
- , 1988: Topics in applied dispersion modeling. *Lectures on Air Pollution Modeling*, A. Venkatram and J. C. Wyngaard, Eds., Amer. Meteor. Soc., 267–324.
- Weil, J. C., 1988: Dispersion in the convective boundary layer. *Lectures on Air Pollution Modeling*, A. Venkatram and J. C. Wyngaard, Eds., Amer. Meteor. Soc., 167–227.
- , 1991: Appendix C: Discussion of lofting model and related dispersion models. Modification of hybrid plume dispersion model (HPDM) for urban conditions and its evaluation using the Indianapolis data set. Vol. II. Electric Power Research Institute Rep. A089-1200 II, Electric Power Research Institute, Palo Alto, CA, 160 pp.
- , 1990: A diagnosis of the asymmetry in top-down and bottom-up diffusion using a Lagrangian stochastic model. *J. Atmos. Sci.*, **47**, 501–515.
- , 1994: A hybrid Lagrangian dispersion model for elevated sources in the convective boundary layer. *Atmos. Environ.*, **28**, 3433–3448.
- , and R. P. Brower, 1983: Estimating convective boundary layer parameters for diffusion applications. Maryland Power Plant Siting Program Rep. PPSP-MP-48, Dept. of Natural Resources, Annapolis, MD, 37 pp.
- , and —, 1984: An updated Gaussian plume model for tall stacks. *J. Air Pollut. Control Assoc.*, **34**, 818–827.
- , and L. A. Corio, 1985: Dispersion formulations based on convective scaling. Maryland Power Plant Siting Program Rep. PPSP-MP-60, Dept. of Natural Resources, Annapolis, MD, 39 pp.
- , —, and R. P. Brower, 1986: Dispersion of buoyant plumes in the convective boundary layer. Preprints, *Fifth Joint Conf. on Applications of Air Pollution Meteorology*, Chapel Hill, NC, Amer. Meteor. Soc., 335–338.
- , R. I. Sykes, and A. Venkatram, 1992: Evaluating air-quality models: Review and outlook. *J. Appl. Meteor.*, **31**, 1121–1145.
- Willis, G. E., and J. W. Deardorff, 1978: A laboratory study of dispersion from an elevated source within a modeled convective planetary boundary layer. *Atmos. Environ.*, **12**, 1305–1312.
- , and —, 1981: A laboratory study of dispersion from a source in the middle of the convectively mixed layer. *Atmos. Environ.*, **15**, 109–117.
- , and —, 1983: On plume rise within the convective boundary layer. *Atmos. Environ.*, **17**, 2435–2447.
- , and —, 1987: Buoyant plume dispersion and inversion entrapment in and above a laboratory mixed layer. *Atmos. Environ.*, **21**, 1725–1735.
- Wyngaard, J. C., 1988: Structure of the PBL. *Lectures on Air Pollution Modeling*, A. Venkatram and J. C. Wyngaard, Eds., Amer. Meteor. Soc., 9–61.

## PLUME BEHAVIORS OBSERVED USING LIDAR AND SF<sub>6</sub> TRACER AT A FLAT AND HILLY SITE

G. E. MOORE, L. B. MILICH and M. K. LIU

Systems Applications, Inc., 101 Lucas Valley Road, San Rafael, CA 94903, U.S.A.

(First received 6 July 1987 and in final form 19 November 1987)

**Abstract**—Two field experiments, one at Kincaid, IL, in flat terrain, the other at Bull Run, TN, in rolling terrain, were conducted under the auspices of the Electric Power Research Institute's (EPRI) Plume Model Validation and Development program. Simultaneous observations were made of ground-level SF<sub>6</sub> concentrations; plume cross-sections using light detection and ranging (lidar); turbulence; and routine meteorology at the surface and aloft. Due to terrain influences, surface wind-speeds at the Bull Run site were significantly lower than those at the Kincaid site, whereas thermal winds at Kincaid were generally larger than at Bull Run. At both sites, a reduction in turbulent intensity and an increase in atmospheric stability with height correlate with a substantial decrease in the rate of vertical plume dispersion. SF<sub>6</sub> ground-level concentration (GLC) patterns over distances of 1–50 km from the source were categorized by shape. The GLC patterns at Bull Run were frequently 'blobby', when significant GLCs occurred over an azimuth angle exceeding 90°, whereas patterns at Kincaid were generally coherent and nearly elliptical. Plume behavior was examined for 154 h during which both GLCs of SF<sub>6</sub> tracer and lidar cross-sections of the plume were of good quality. Results show that plume looping was rare at Kincaid, but occurred substantially more often at Bull Run (3%:14%), with the reverse true for meandering (11%:14%). Inversions that trapped plume material occurred much more often at Kincaid than at Bull Run (11%: <1%). Correlation of cross-wind concentration distributions of the plume aloft with those cross-wind SF<sub>6</sub> concentrations distributions at the ground were poor at both sites.

*Key word index:* Lidar, dispersion, plume, tracer.

### INTRODUCTION

Plume behavior is controlled by several dispersion processes, each of which can result in qualitatively different plume geometries and ground-level concentration (GLC) patterns. This paper summarizes the findings of a preliminary field study to relate plume trajectories and cross-sectional shapes to the meteorological parameters that control dispersion. Slade (1968) defined eight types of plume behavior: coning, meandering (fanning), looping, lofting, trapping, fumigating, bifurcation, and downwashing. These terms are useful as classifications, but are not descriptive of the dominant physical processes associated with different types of plume behavior, since a number of dispersion processes arising from either nonuniform or nonsteady meteorological conditions distort and advect the plume material.

Previous studies using lidars to examine plumes have revealed a variety of plume shapes that provide some interesting observations about dispersion. For instance, a boomerang-shaped plume cross-section has been observed under stable conditions to be accompanied by substantial directional wind shear with height (Uthe *et al.*, 1980). Under other stable conditions, such as those encountered during the STATE experiment, the plume appeared as a long, thin filament that meandered back and forth at a nearly constant height (McElroy *et al.*, 1981). Rapid

thickening of the aloft plume while entrained by the mixing layer has also been observed (Guillot, 1979). Lidar observations have been used to support recent efforts to parameterize plume dispersion under convectively unstable conditions (Weil and Altman, 1979). They have also been used to arrive at new formulations of plume spread as a function of downwind distance (e.g. Ellis *et al.*, 1984; Hoff and Froude, 1979). The following types of plume behavior were of interest in this field study:

- (1) bifurcation of the plume cross-sectional shape near the stack via stack emission-generated vortices;
- (2) plume trajectory and cross-sectional shape when affected by advection via turbulent eddies lasting 5 min to 1 h;
- (3) plume cross-sectional shape and GLC pattern when affected by nonstationarity in wind-speed and wind direction during the plume material travel time, and by directional wind shear;
- (4) plume rise and vertical spread above the ground when limited and modified by temperature inversions;
- (5) entrainment of the plume when the mixed layer rapidly brings plume material to the ground.

In this paper we compare the meteorological characteristics and plume behavior patterns observed by both lidar and ground-based SF<sub>6</sub> or SO<sub>2</sub> measurements at the Kincaid and Bull Run sites, and examine

in detail cases of plume bifurcation, meandering, looping, trapping, and fumigation to clarify the processes by which such plumes are dispersed.

#### DESCRIPTION OF THE FIELD STUDY

Field measurements of plume dispersion from elevated, buoyant point sources were conducted at two sites, one in flat terrain at Kincaid, IL, and one in moderately complex terrain at Bull Run, TN, as part of the Electric Power Research Institute (EPRI) Plume Model Validation and Development program (Hilst, 1978). Plume dispersion was measured using (1) SF<sub>6</sub> tracer and SO<sub>2</sub> concentration patterns at the ground, (2) lidar observations of plume cross-sections of SO<sub>2</sub> concentrations and particle mass aloft, and (3) meteorological measurements of winds, temperature, and turbulence at the surface and aloft (Bowne *et al.*, 1983, 1985) to study the behavior of plumes from an elevated point sources under various atmospheric conditions.

The Kincaid experiment consisted of 34 weeks of routine observations between 14 April 1980 and 7 June 1981. Within this period three measurement programs also collected both tracer and remote-sensing observations and hourly upper-air soundings. Approximately 5000 h of routine observations and 370 h of tracer test observations are available for this site. The Bull Run experiment extended over a much shorter period of time and consisted of two 5-week intensive measurement periods during which 326 h of tracer tests were made.

#### Terrain

The Kincaid power plant is located in central Illinois in a flat area extensively cultivated for corn. The Bull Run power plant is located approx. 20 km southeast of the Cumberland Mountains in Tennessee in a valley whose axis is oriented northeast-southwest. This valley contains parallel ridges that are generally less than 100 m above the stack base. The surface cover in the vicinity of the Bull Run power plant is a mix of forest and suburban buildings. Both the Kincaid and Bull Run power plant stacks are tall (180 and 244 m, respectively) with effluent temperatures of approx. 400 K and exit velocities of 15–25 m s<sup>-1</sup>.

#### Meteorological measurements

The experimental programs conducted at the two sites were quite similar. Meteorological measurements included horizontal wind-speed and wind direction at 10, 30, 50, and 100 m; vertical wind-speed at 10 and 100 m; and temperature at 2, 10, 50, and 100 m. Meteorological observations were collected every 10 s and stored as 5-min averages. The variables observed and archived during the two experiments are described in data catalogs compiled by Reynolds *et al.* (1984) and Hudischewsky and Reynolds (1984). Qual-

ity assurance and estimates of measurement uncertainty for the instruments at both sites are provided in Smith *et al.* (1983), and Smith and Decker (1983).

Upper-air soundings were made remotely with two bistatic (Doppler) acoustic sounders and directly by T-sondes. The sounders collected 15-min average wind-speeds and directions for 30-m-thick layers over an effective range of 0–400 m. The T-sondes were released hourly during the intensive measurement periods. Wind speed and direction, and temperatures aloft at both sites were measured for air layers 60–90 m thick.

#### Tracer measurements

Samples of SF<sub>6</sub> tracer were collected at 2 m above ground at over 1500 total sites 0–50 km from the stack, either by additive bag 'gulp' sampling or by slowly increasing syringe volume sampling over a period of 1 h.

#### Remote sensing measurements

Remote-sensing observations of the plume aloft were made by

ground-based, mobile SO<sub>2</sub> differential adsorption lidar (DIAL) operated by SRI (Hawley *et al.*, 1982), ground-based, mobile particle-sensing lidar operated by the computer Genetic Corp (CGC), and airplane-based particle lidar known as an airborne lidar plume and haze analyzer (ALPHA-1) operated by SRI (Uthe *et al.*, 1980).

The SO<sub>2</sub> DIAL measures the absolute SO<sub>2</sub> concentrations of the plume aloft. For the lidar to observe the entire plume cross-section, it had to be operated within 2 km of the stack at Kincaid and within 1 km at Bull Run. The CGC particle lidar, available only at Kincaid, was typically operated 2–4 km downwind of the stack. The ALPHA-1 instrument observed the plume at distances out to 20 km from the stack. The ground-based lidars scanned the plume through a plane normal to the plume centerline aloft and through a plane parallel to the GLC pattern. The only lidar measurements used in the analysis reported here are those taken when the lidar was operated with a fixed azimuth angle to make a series of line-of-sight observations for various elevation angles and distances from the instrument. Both the CGC particle lidar and SO<sub>2</sub> DIAL made a complete scan of the plume cross-section in approx. 5-min. The ALPHA-1 instrument traversed the plume at least four or five times during the course of an hour. Lidar observations were generally made during the hours when SF<sub>6</sub> tracer tests were conducted.

#### TYPICAL DISPERSION METEOROLOGIES AT THE TWO EXPERIMENTAL SITES

Meteorological variables important to dispersion processes include wind-speed, turbulence, and atmospheric stability. Local dispersion meteorology is in-

fluenced by factors such as terrain and surface roughness and synoptic flow patterns. One of the greatest differences between the Kincaid and Bull Run sites is the moderately complex terrain and greater surface roughness at Bull Run. Kincaid has flat terrain and an average roughness length of 0.20 m. The roughness length at Bull Run is much larger ( $\sim 2$  m) because of forests and small ( $< 200$  m) hills. Wind-tunnel modeling and field experiments at the Kingston steam plant roughly 30 km to the west-southwest of Bull Run suggest that the terrain significantly enhances vertical plume spread even at 600 m above the ground under light winds (Graham *et al.*, 1979).

The average wind-speed profile at Kincaid closely resembled a power law relationship with height. In contrast, wind-speeds at Bull Run were unusually low (average  $\sim 1$   $\text{m s}^{-1}$  at 10 m, vs  $\sim 3.5$   $\text{m s}^{-1}$  at 10 m at Kincaid) and accompanied by large fluctuations in direction. Measurements made by Oak Ridge National Laboratory near Bull Run revealed anomalously low wind-speeds up to a height of 1 km (Holland, 1953). Moore and Liu (1984) found that the Cumberland Mountains 20 km northwest of the Bull Run plant often influence winds at the site through downwind wake-phenomena such as vortices and lee wind deceleration. Smaller wind-speeds at Bull Run give rise to greater observed plume rises ( $\Delta h = 326$  m vs 175 m at Kincaid) and large displacements of the plume centerline from linearity.

Significant differences between the sites in the horizontal component of turbulence intensity are evident in the standard deviation of horizontal wind direction,  $\sigma_\theta$ . Hourly averaged  $\sigma_\theta$  in the first 100 m at Bull Run are generally a factor of three larger than those at Kincaid. The standard deviation of the vertical component of the 100-m wind velocity,  $\sigma_w$ , is on average a factor of two larger at Bull Run than at Kincaid. Because of the large  $\sigma_\theta$  observed at Bull Run, the GLC patterns of SF<sub>6</sub> and cross-sections of the plume aloft are substantially wider than at Kincaid. The increased  $\sigma_w$  and lower horizontal average wind-speeds lead to more frequent plume looping at Bull Run.

The similarity theory relationship between the non-dimensionalized height ( $z/L$ ) and wind shear ( $\phi_m$ ) at Kincaid resembled the empirical relation suggested by Businger *et al.* (1971); however, no systematic relationship between  $\phi_m$  and  $z/L$  was found at Bull Run. The average friction velocity ( $u_*$ ), computed from  $U'W'$  observations at 100 m was 0.25  $\text{m s}^{-1}$  at Kincaid and 0.13  $\text{m s}^{-1}$  at Bull Run.

The average mixing height at Kincaid was 544 m, with a median of 360 m, vs 500 and 310 m, respectively, at Bull Run. However, the 10–100-m temperature gradients for the two sites were quite different. At Kincaid, extreme positive temperature lapses ( $> 5^\circ\text{C}$  over the layer) occurred for 1.4% of the cases, but were almost nonexistent at Bull Run. Positive temperature lapses within layers were larger at Kincaid ( $\sim 2^\circ\text{C}$  vs

$\sim 1^\circ\text{C}$ ) and occurred more often than at Bull Run ( $\sim 32\%$  of cases vs  $\sim 22\%$ ). The Richardson number over the 10–100-m layer was computed on an hourly basis using a geometric gradient method recommended by McBean *et al.* (1979). A comparison of Richardson numbers revealed a peak in the frequency of occurrence near zero for both sites; however, the Richardson number varied over a substantially wider range at Kincaid ( $-5$ – $2.5$ ) than at Bull Run ( $-0.4$ – $0.6$ ). Vertical wind direction shears ( $\Delta W/D/\Delta Z$ ) were comparable at both sites,  $\sim 20$ – $90^\circ$  over a 150-m layer for 40% of the cases.

In summary, there appear to be substantial differences in the vertical structure of the atmosphere at the two sites. Kincaid has greater vertical gradients of wind-speed and temperature than Bull Run. However, during unstable conditions, Bull Run has greater turbulent intensity since the wind-speeds that provide directional organization to the turbulence are substantially lower. As a result, vertical gradients of meteorological quantities are smaller at Bull Run because of a greater degree of mixing.

#### CHARACTERIZATION OF PLUME BEHAVIOR AT THE TWO EXPERIMENTAL SITES

Plume dispersion can be characterized in several ways that include (1) the pattern of ground-level concentrations, as determined from SF<sub>6</sub> tracer observations; (2) the shape of the plume cross-section aloft, as determined from remote-sensing observations; and (3) trajectories of plume material, determined either indirectly from wind observations or directly from the movement of the plume centerline (if estimates of the centerline exist).

Most kinematic models adopt a simplified view of plume behavior and use an averaging period of 1 h (Liu *et al.*, 1982). An hourly 'time exposure' of the plume is assumed to show a straight, level centerline much like those shown by Slade (1968). The plume cross-section is assumed to follow a bivariate Gaussian distribution, although the series of instantaneous plume dimensions seen in the time exposures may be quite irregular and fluctuate a great deal.

To determine the degree of steady state of the plume during an hour for this study, hourly trajectories were constructed from 5-min averages of wind-speed and wind direction at the 100-m level (Fig. 1). Assuming that the winds measured at 100 m are both horizontally homogeneous and are representative of those causing plume transport, the trajectories shown in Fig. 1 should provide good estimates of the plume centerline position for 45 h of data at Kincaid and 93 h at Bull Run. The trajectories for Kincaid (Fig. 1a) indicate that during the first hour of travel the plume material follows a relatively straight line between 10 and 40 km from the stack, and that the wind-speeds are relatively constant during any hour. At Bull Run, the trajectories have a substantial number of 'kinks'

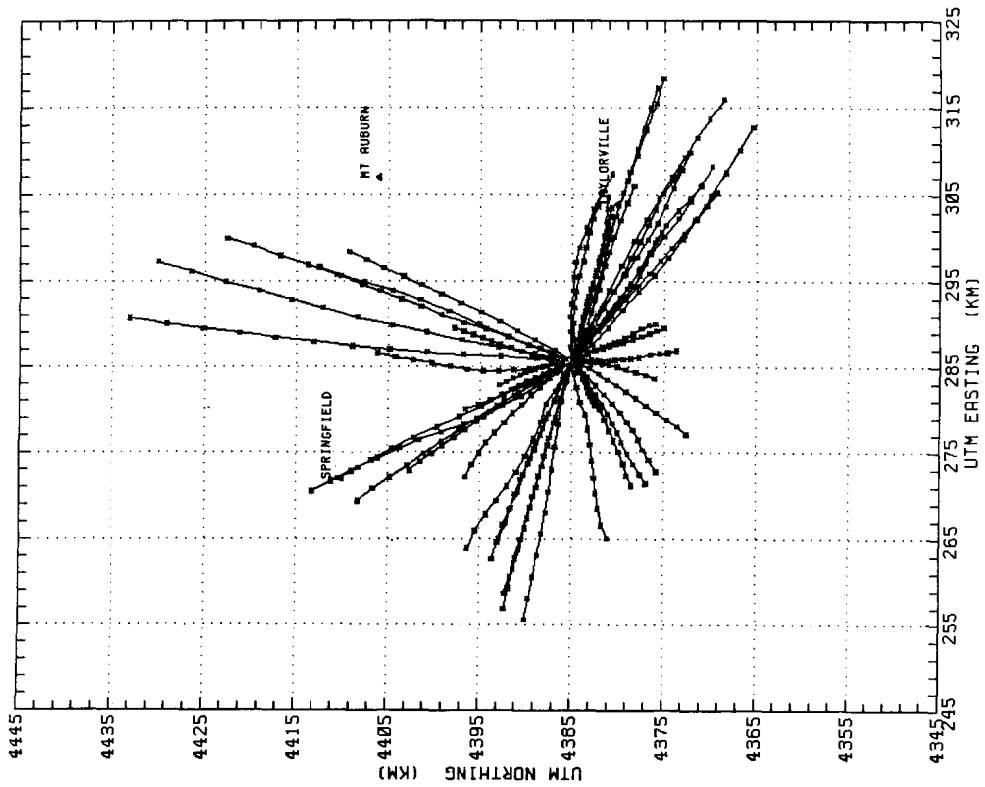


Fig. 1a. Hourly trajectory plots based on 5-min wind statistics measured at 100 m for 45-h of lidar data collected around the Kincaid power plant.

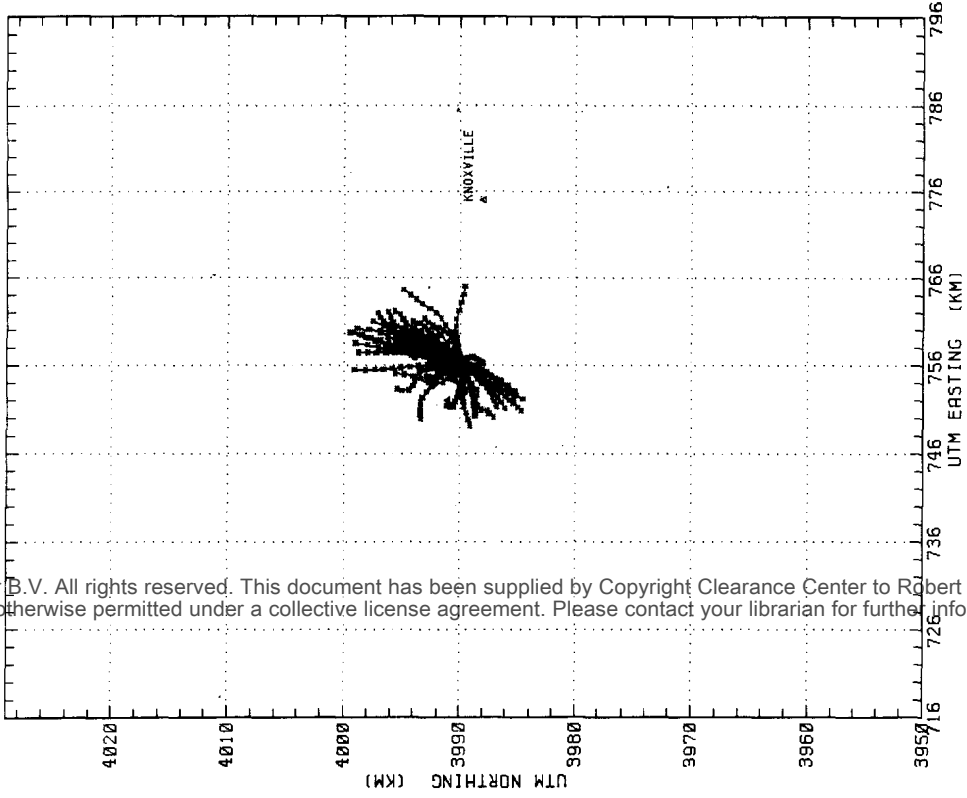


Fig. 1b. Hourly trajectory plots based on 5-min wind statistics measured at 100 m for 93-h of lidar data collected around the Bull Run power plant.

© Elsevier B.V. All rights reserved. This document has been supplied by Copyright Clearance Center to Robert P. Taylor. Any reproduction or otherwise permitted under a collective license agreement. Please contact your librarian for further information. 12/23/2020.

and the distances covered by 5-min travel segments are typically unequal and only half the distance of the Kincaid trajectories (Fig. 1b). The results suggest that at Bull Run the plume meanders over a larger range of azimuthal angles.

A number of dispersion phenomena arising from either nonuniform or nonsteady meteorological conditions act to distort and advect the plume material. These processes are summarized in Table 1. In addition to these processes, the source itself affects plume behavior through momentum- and buoyancy-induced dispersion at 'small' downwind distances from the stack, i.e. distances  $< 10$  stack heights (Briggs, 1975).

Many of the dispersion processes given in Table 1 widen or increase the GLC pattern while maintaining the elliptical shape expected of a Gaussian plume. Because hourly averaging of data tends to smooth out irregular instantaneous plumes (Slade, 1968), Gaussian-shaped distributions of cross-wind concentration might occur on the tracer arcs more often than expected from instantaneous distributions. To test this possibility, cross-wind concentration distributions for selected tracer experiment hours were surveyed. Roughly 35% of the arcs and hours at Kincaid were sufficiently free of odd distribution moments and multiple peaks to be judged Gaussian in shape. At Bull Run only 20% of such arc-hours were judged to be Gaussian-shaped.

Setting aside the issue of subjectivity in the classification, the analysis makes two important points: (1) Gaussian-shaped concentration distributions both at the ground and aloft are a minority at both sites, and (2) they occur substantially less often at the site in moderately complex terrain (Bull Run), which typically has larger turbulent intensities, than at the site in flat terrain (Kincaid). A third notable finding is that no significant association between occurrences of Gaussian plume cross-sections aloft and Gaussian-shaped cross-wind distributions of concentration at the ground was evident from a two-way classification of GLC patterns and plume cross-sections. The lack of correlation was significant at the 90% confidence level.

A number of different types of plume behavior were seen at each site. Plume behavior was classified using successive 5-min lidar scans of cross-sections of the plume aloft. The cross-sectional shape and location of the plume mass centroid were noted for each scan. Plume looping and meandering were tracked by following the plume mass centroids on successive scans. Plume lofting and trapping were examined by using the vertical gradients of concentration and the thermal structure as observed by T-sondes. Other plume behaviors were examined using such factors as plume center of mass locations, wind-speed (downwashing), or cross-sectional shape (bifurcation).

The frequency of occurrence of common plume behaviors at the two experimental sites is summarized in Table 2. Reduced inversion strengths at Bull Run make lofting or trapped plumes quite rare. Low wind-

speeds at Bull Run lead to more occurrences of looping than at Kincaid, and an absence of plume downwash. A combination of lower wind-speeds and the operation of the DIAL at a location less than five stack heights ( $\sim 1$  km) downwind of the plant contribute to a dramatically larger number of observed bifurcated plume cross-sections at Bull Run than at Kincaid. Coning is the most common behavior at both sites.

## EXAMPLES OF PLUME BEHAVIOR

### *Bifurcation*

Bifurcation has often been used to describe the persistence of vortex pairs that initially develop within the plume near the source. The definition of bifurcation is often a matter of degree of persistence of the vortex pair normally formed by plume rise. To some, bifurcation is said to only occur if the vortices diverge and never combine again. To others, the plume is said to bifurcate if the vortex pairs are separate at downwind distances where the plume has bent over and its internal velocity profile resembles that of the ambient wind. In this section we will use the less restrictive definition where bifurcation is said to occur when vortex pairs persist, but may at some later time rejoin due to diffusive intermingling.

DIAL  $\text{SO}_2$  observations at Bull Run reveal frequent cases in which two distinct concentration maxima aloft persist for several hours. Such was the case during 1800–1900 h LDT on 9 October 1982 when the 100-m wind-speed was  $3.6 \text{ m s}^{-1}$  and the plume cross-section was observed 1 km downwind of the stack. The ensemble of successive plume scans in Fig. 2 shows that two distinct concentration maxima persist throughout the entire hour, with both maxima occurring at roughly the same height ( $\sim 460$  m). The shape of the DIAL cross-section is similar to observations of a bifurcated plume undergoing complete centerline separation that were made by Fanaki (1975) at a Sudbury, Ontario, nickel smelter. The upper-air meteorological structure for 1800–1900 h on 9 October 1982 is displayed in Fig. 3. Fanaki (1975) distinguished two characteristics of this sounding type: (1) the wind-speed begins to decrease with height immediately above the stack, and (2) the wind direction changes direction sharply somewhere between the stack and the plume centerline height. The change in wind direction with elevation heights results in a lateral shear ( $\partial \bar{v} / \partial z \approx \bar{u} \Delta WD / \Delta z$ ) that at some point downwind begins to assist one vortex and inhibit the other by increasing its entrainment of ambient air that possesses no circulation of its own. A change in the entrainment rate in one branch would tend to cause the centerlines to separate, with the branch experiencing enhanced entrainment having a lower plume centerline.

Turner (1960) suggested that if the vortex circulation remains relatively constant with time as the plume bends over, the entrained ambient air will not

Table 1. A summary of several plume behavior characteristics.  $(\bar{\quad})$ —1-h average,  $S$ —standard deviation of 5-min averages over 1-h,  $\sigma$ —5-min standard deviation. The  $\approx$  indicates that the dispersive phenomenon is large enough to make a significant addition to  $\sigma$  estimated without such a dispersive phenomenon

Meteorological condition	Behavior of plume aloft	Behavior of GLC pattern	Reference
<i>Nonsteady conditions</i>			
$S_w/\bar{u} \sim 0(1)$	Varying plume rise—different plume segments have different rise heights and dilution rates	Radial distribution of ground-level centerline concentrations contains several maxima with irregular width	Pasquill and Smith (1983)
$S_w \Delta X \gtrsim \sigma_y$ $\Delta X$ is downwind travel in 5 min	Horizontal displacement of plume by turbulent eddies—'kinky' or 'meandering' trajectory	Azimuthal angle of ground-level centerline varies with radial distance	Hilst (1957)
$S_w \Delta t \gtrsim \sigma_z$ $\Delta t = 5$ min	Vertical displacement of plume by turbulent eddies—'looping' plume trajectory	Radial distribution of ground-level centerline concentrations contains several maxima with irregular width	Hilst (1957)
$S(\sigma_\theta)/\bar{\sigma}_\theta \sim 0(1)$ $\theta$ is azimuthal angle	Trend or intermittency in the horizontal diffusive spread	Ground-level width of plume varies with time; the GLC pattern width may pulse, grow, or shrink with time	
$S(\sigma_\phi)/\bar{\sigma}_\phi \sim 0(1)$ $\phi$ is elevation angle	Trend or intermittency in the vertical diffusive spread	Ground-level radial position of GLC mass centroid may move back and forth	
<i>Nonhomogeneous conditions</i>			
$\frac{\Delta \bar{u}}{\Delta z} > 0$	Skew in vertical distribution of concentration—the mass centroid moves downward	Ground-level centerline maximum concentrations are increased	Csanady (1973)
$\frac{\Delta \lambda_z}{\Delta z} > 0$	Plume cross-section is stretched upward—the mass centroid moves upward	Ground-level centerline maximum concentrations are decreased	Csanady (1973)
$\lambda_z$ is dominant vertical length scale of eddies	Major axis of plume cross-section is tilted (rotated)	The GLC is widened by some added azimuthal angle and skewed	Pasquill (1969) Howroyd and Slawson (1979)
$\frac{\Delta W D}{\Delta z} \gtrsim 0(\sigma_y)$ $X$ is downwind distance $H_{cent}$ is height of plume mass centroid	Skew in vertically integrated cross-wind distribution of concentration toward higher wind-speeds	Centerline is increasingly displaced toward higher wind-speeds as horizontal size of plume grows; the GLC pattern is skewed	Okubo and Karweit (1969)
$\frac{\Delta \bar{u}}{\Delta y} > 0$			

$\frac{\Delta\sigma_{\theta}}{\Delta z} < 0$	Plume parcel diffuses more rapidly as it is displaced towards the ground. Plume cross-section increases in width along bottom edge	GLC pattern becomes wider	
$\frac{\Delta\sigma_w}{\Delta z} < 0$	Plume vertical spread is skewed downward, the mass centroid descends, i.e. plume trapping	GLCs are increased	
$\frac{\Delta\sigma_w}{\Delta z} > 0$	Plume vertical spread is skewed upward, the mass centroid ascends, i.e. plume lofting	GLCs are reduced (usually are zero)	
Probability of $W \uparrow$ less than $W \downarrow$ when $1.5 W_* < U < 6W_*$ ( $W_*$ is convective scaling velocity)	Plume centerline descends to the ground	The GLC pattern widens, moves toward source, and higher concentrations occur	Willis and Deardorff (1981)
<i>Conditions varying in both space and time</i> $h_{end} > H_{cent} > h_{beg}$ ( $h_{beg}$ , mixing height at beginning time)	Plume is entrained into the mixed layer due to increasing mixing height	GLC CWICs* at certain radii increase dramatically over a short time-span, i.e. $\sim H_{cent}/\sigma_w$	Briggs (1975)
$h_{beg} > h_{end} \sim 0.1u_*/f$	Plume diffusive mixing to the surface decreases abruptly	GLC CWIC at all arcs decrease dramatically	
$KU > V_s$ $K = 1.5$ $V_s$ is stack exit velocity	Plume centroid drops (down-washes) due to $\Delta u/\Delta z > 0$ and $\Delta \sigma_w/\Delta z < 0$ . Also, near-stack wake effects can displace plume vertically and horizontally	GLC pattern is wider and has larger centerline concentrations; sometimes GLC is broken into several distinct GLC maxima varying both radially and azimuthally	Davies and Moore (1964)

\* Cross-wind integrated concentration.

mix across the plume centerline and the vortex pairs will remain separate. The vortex circulation depends on how much noncirculating air is entrained, which in turn is expected to depend on the intensity of the ambient turbulence. Teske and Lewellen (1980) performed several numerical experiments which confirm the fact that the degree of vortex separation for buoyant plumes depends strongly on the amount of ambient turbulence.

The normal separation of the vortex pairs at the point of final rise is expected to be about  $\Delta h/2$ . For the plume depicted in Fig. 2 this is about 120 m. The separation of the plume concentration maxima in Fig. 2 is in excess of 200 m for most lidar scans. Thus it can be seen that the angular separation is somewhat abnormal. If one treats each vortex as a separate

plume and applies the Pasquill relationship  $\sigma_y = f(x)\sigma_\theta$  the  $\sigma_y$  from turbulent dispersion is  $\sim 55$  m since  $\sigma_\theta$  at 100 m is only  $5^\circ$ . The separation of the two vortices creates a much wider combined and averaged plume than that expected for a plume with no buoyancy-enhanced dispersion or plume vortex pairs.

In some cases the separation caused by wind direction shear outstrips the turbulent diffusion of each branch of the plume and this effects a complete separation of the vortices. In most cases, the vortices will entrain enough ambient air with little or no circulation so that (1) one of the vortices rapidly decays due to entrainment and disappears or (2) the rate of turbulent diffusion of each vortex is faster than the rate of separation and at some point downwind the two vortices completely intermingle.

#### Meandering

Plume meandering (fanning) generally occurs under strongly stable conditions and low wind-speed at the surface, e.g. within a surface-based inversion during early morning hours. However, meandering can also occur under moderate wind-speeds. An example of such meandering occurred at 0300–0400 h LDT on 15 May 1981 at the Kincaid site. The wind-speed was  $10.5 \text{ m s}^{-1}$  at the stack height, and the 100-m hourly arithmetic average of the 5-minute  $\sigma_\theta$  observations ( $\bar{\sigma}_{\theta(\text{high})}$ ) is only  $1.5^\circ$ . The standard deviation of the wind direction between the 5-minute segments  $\bar{\sigma}_{\theta(\text{low})}$  is nearly  $4^\circ$ . While the fluctuation in wind direction is not that large, the lateral displacements due to the

Table 2. Frequency of occurrence of plume types at the Kincaid and Bull Run sites

Plume type	% total cases identified	
	Kincaid	Bull Run
Coining	60	52
Meandering	11	4
Looping	3	14
Bifurcated	2	28
Trapped	11	—
Lofting	11	2
Downwash	1	—

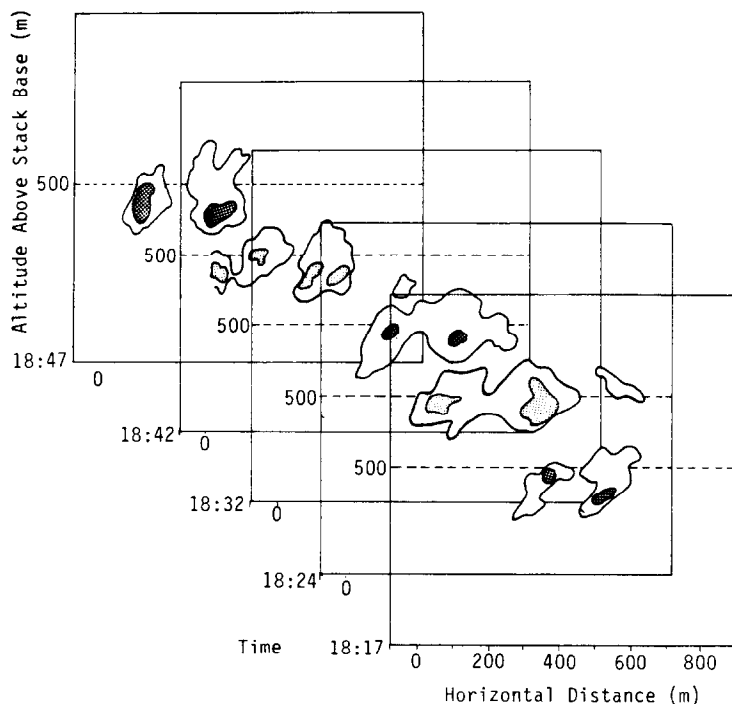


Fig. 2. Cross-sections illustrating the multiple islands of elevated  $\text{SO}_2$  concentrations typical of a bifurcated plume measured at Bull Run by DIAL  $\text{SO}_2$  lidar on 9 October 1982, 1800–1900 h LDT at 1 km downwind.

large horizontal wind-speeds are greater than the lateral diffusive growth.

The hourly average cross-section observed by the DIAL SO<sub>2</sub> lidar at 2.3 km downwind shows two separate concentration maxima (Fig. 4). At a wind speed of 10.5 m s<sup>-1</sup>, the plume takes less than one 5-minute averaging period to travel from the stack to the

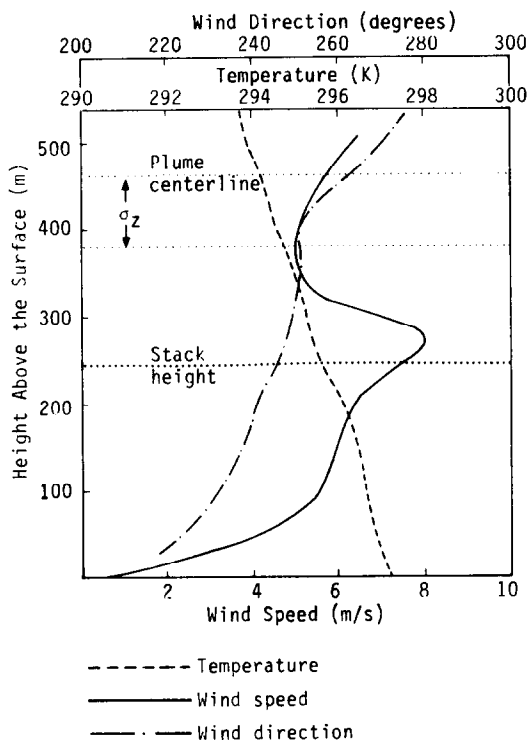


Fig. 3. Vertical profiles of wind-speed, wind direction, and temperature from the 1821 h LDT T-sonde at Bull Run on 9 October 1982.

point where the cross-section is observed. According to  $\bar{\sigma}_{\theta(\text{low})}$ , the horizontal displacements of the plume mass centroid would be expected to be  $\sim 2.5$  times greater than the growth of the plume cross-section via the wind direction fluctuations contained in  $\bar{\sigma}_{\theta(\text{high})}$ . The hourly averaged plume width as measured by the standard deviation of the cross-wind distribution of concentration  $\bar{\sigma}_y$  is 300 m, or more than three times the 5-min averaged plume width as measured by individual lidar scans. It is movement of the plume over several individual scans which produces the double concentration maximum pattern that is illustrated in the successive scans shown in Fig. 4. The air mass between 200 and 400 m above the ground (where most of the plume mass is) has relatively little wind directional shear ( $\sim 7^\circ$ ) and a lapse rate of  $4.2^\circ\text{C km}^{-1}$ . The only substantial gradient is one of wind-speed shear, which increases to  $17\text{ m s}^{-1}$  at 450 m.

Despite the fact that the wind-speed may be large and the lapse rate is only slightly stable, the gradient Richardson number of the 200–400-m layer is about 0.80, so that mechanical turbulence is suppressed. The 5-min average lateral plume width of  $\sigma_y \sim 90\text{ m}$ , supports a Pasquill–Gifford stability class of F. However, surface observations support a classification of D or E, depending on which of several methods is used. This case illustrates that meandering can occur under conditions other than light wind-speeds and extremely stable air layers aloft. In fact, meandering should in principle be able to occur whenever the Richardson number is positive and  $> 0.5$  so that the mechanical interlayer coupling is completely suppressed.

#### Looping

The phenomenon known as plume looping can occur when the standard deviations between 5-min

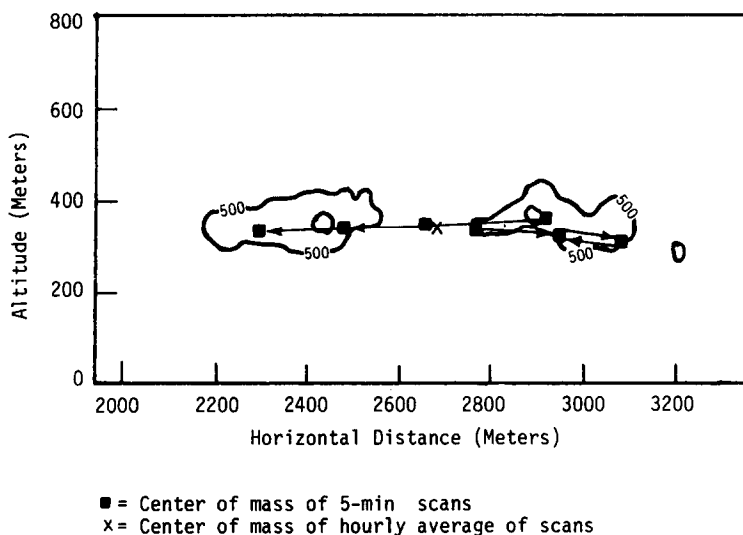


Fig. 4. Center of mass trajectory for a meandering plume based on DIAL SO<sub>2</sub> lidar scans at Kincaid at 0300–0400 h LST, 15 May 1981, 2.3 km downwind of the stack.

Averages of either  $S_u$  or  $S_w$  are comparable with  $\bar{u}$  and  $\bar{\sigma}_w$ , respectively. The effect of  $S_u$  is to vary the plume rise and dilution between 5-min plume segments. The effects of updrafts and downdrafts (measured by  $S_w$ ), such as those noted by Taconet and Weill (1983), will result in plume material being wafted upward or downward. The looping behavior was identified using successive 5-min lidar scans from which a plume mass centroid aloft could be estimated and consequently tracked from scan to scan. Looping behavior was observed more frequently at Bull Run than at Kincaid. A notable example of plume looping occurred on 20 August 1982 from 1600 to 1700 h LDT at Bull Run.

Figure 5 displays seven scans of the plume cross-section measured by the DIAL  $\text{SO}_2$  lidar 730 m downwind of the stack from 1600 to 1700 h LDT. In this figure, the progressive motion of the plume mass centroids is indicated by arrows. The looping displacement of the plume results in an hourly averaged  $\sigma_z$  of 155 m, while the arithmetic mean of  $\sigma_z$  for the seven individual scans is only 96 m. The increased spread due to plume displacement is a substantial 122 m, which is confirmed by taking the standard deviation of the mass centroid height of each scan. The plume also significantly wanders laterally, as Fig. 5 demonstrates.

The hourly average cross-wind spread as estimated by  $\sigma_y$  is 165 m, while the arithmetic average of the  $\sigma_y$  of the seven scans is only 109 m. Two of the most noticeable features of Fig. 5 are that the plume boundary is quite irregularly shaped, even for an hourly average, and that a cellular structure exists inside the plume.

The mixed-layer thickness,  $Z_i$  (from ALPHA-1 observations), is  $\sim 1900$  m. The convective scaling velocity (from 100-m data) is  $1.3 \text{ m s}^{-1}$ ; the 100-m wind-speed is only  $3.1 \text{ m s}^{-1}$ . According to Deardorff and Willis (1975), the relative magnitudes of the velocities imply convective conditions, a conclusion supported by 0.028 calculated for  $-L/Z_i$ . Wind direction changes with height are less than  $5^\circ$  of the azimuthal angle between 250 and 750 m. Wind-speed neither increases nor decreases systematically and averages only  $3.1 \text{ m s}^{-1}$  over the first 1000 m above the surface.

The hourly standard deviation of 5-min averaged wind-speed,  $S_w$ , at 100 m is  $0.82 \text{ m s}^{-1}$ , which would result in a final plume rise fluctuation of  $\sim 25\%$  if a  $1/u$  relationship for rise is assumed. With the average height of the mass centroid at 635 m, this represents a fluctuation of 96 m. The hourly standard deviation of

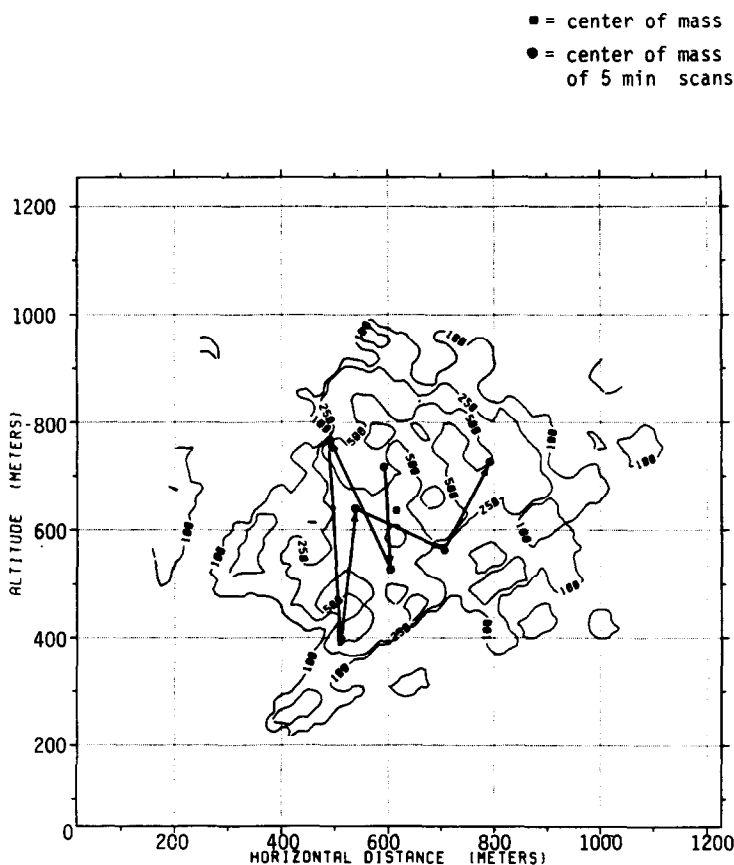


Fig. 5. An example of plume looping, based on DIAL  $\text{SO}_2$  lidar scans at Bull Run at 1600–1700 h LST, 20 August 1982. The centers of mass of successive 5-min scans are tracked for 1 h. Contours of  $\text{SO}_2$  are in ppb.

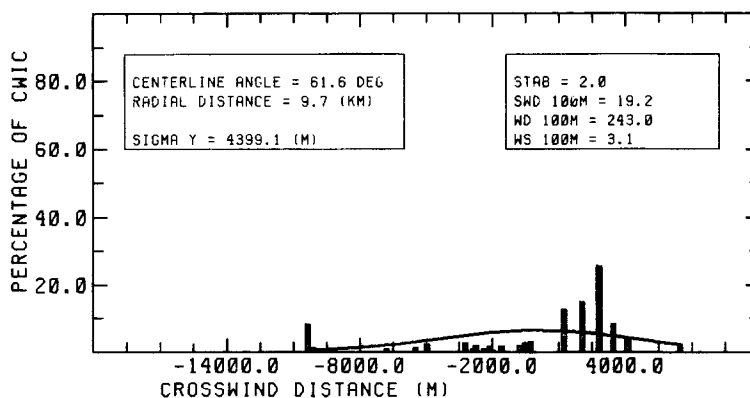
5-min-average vertical wind velocity,  $S_w$ , is  $0.30 \text{ m s}^{-1}$ . The travel time to the 730-m downwind distance is approx. 230 s. Such fluctuations in the vertical velocity would result in fluctuations of 70 m in the height of the plume mass centroid. The horizontal wind-speed and the vertical component of wind velocity are negatively correlated ( $\rho \sim -0.2$ ), so that the larger upward velocities occur when the wind-speed is small and the rise is higher. Thus, it is no surprise that the two dispersive processes can interact to achieve a plume displacement (measured by the standard deviation of mass centroid height) of 122 m.

The irregularity of the plume shape extends to the ground. Figure 6a displays the cross-wind distribution of concentration on the 9.7-km arc. The maximum ground-level concentration ( $C_{\text{max}} = 68 \text{ ppt}$ ) occurs on this arc. The cross-wind distribution of concentrations is quite skewed. At 1.3 km (Fig. 6b) the GLC distribution shows multiple maxima over lateral distances;  $\sigma_y$  is larger (753 m) than typically observed aloft, where

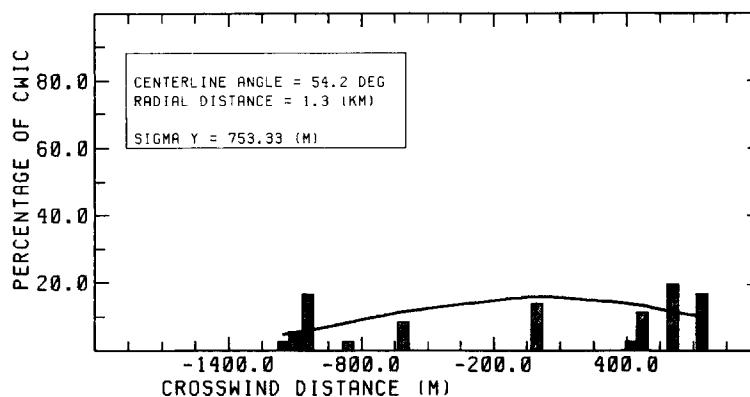
$\sigma_y$ , estimated from lidar data is 158 m at about the same downwind distance. The vertical variation of  $\sigma_\theta$  is quite large. At 100 m, the hourly averaged  $\sigma_\theta$  is already a relatively large  $27^\circ$ , but at 10 m it rapidly increases to an extremely large value of  $73^\circ$ . The difference between the small  $\sigma_\theta$  aloft (100 m) and the large value at the ground (10 m), is consistent with the substantially wider GLC pattern compared with the plume width aloft.

*Trapping*

The effects of inversion trapping and directional wind shear on plume behavior have been observationally examined by Hoff and Froude (1979), who found skewing in the cross-wind and vertical distributions of plume particulates using lidar observations. Similarly, Uthe *et al.* (1980) observed a boomerang-shaped plume cross-section created by the effects of changes in wind direction with height. During 1000–1100 h LST on 15 May 1981 at Kincaid, an inversion limited the



(a) 9.7 km maximum SF<sub>6</sub> GLC arc



(b) 1.3 km arc

Fig. 6. Looping plume at Bull Run, 20 August 1982, 1600–1700 h LST. The observations at specific tracer sampling sites are shown as shaded bars; the solid line is the fitted Gaussian horizontal concentration profile. The stability is the numerical PGT.

dispersion of the plume aloft, while directional wind shear skewed the concentration cross-section. These combined effects are seen most clearly in Fig. 7, measured at 4.2 km downwind by a ground-based CGC particle lidar. This particular shape predominated throughout the hour, so the hourly averaged scan closely resembles the scan at 1021 LST, with the exception that the concentrations are not as large, and less detail can be seen in the hourly average. In addition to plume trapping, there is some indication of bifurcation (two separate concentration maxima), where one branch of the plume is being mixed to the ground and the other is not.

The most useful meteorological observation for this case of plume behavior is the T-sonde at 1030 h LST shown in Fig. 8, where the salient features are the inversion base at 588 m and the wind-speed minimum and sharp directional shear ( $\sim 30^\circ$ ) over the 270–590-m layer. This large wind direction shear was not spurious since it was observed in previous hours. The lidar was located so that larger wind azimuthal angles, such as those associated with the 270–590-m layer, blow the plume further away from the instrument, as seen in Fig. 7. If the plume is divided into a number of layers and the lateral position of the mass centroid for each layer is computed, the average lateral displacement over the 270–450-m layer is  $\sim \arctan[100$

$m(\Delta y)/180 m(\Delta z)]$ , or roughly  $30^\circ$ , which corresponds to the amount of wind direction shear observed.

The turbulence intensity, ( $\bar{\sigma}_{\theta(\text{high})}$ ) is  $12.0^\circ$  at 100 m. The variations in the 5-min averages of wind-speed and wind direction at 100 m as measured by  $S_u$  and  $S_\theta$  are  $0.5 \text{ m s}^{-1}$  (10% of  $\bar{u}$ ) and  $7.4^\circ$ , respectively. The locations of the plume mass centroids indicate that the plume does not move about very much during the hour, as the meteorological observations suggest. Gill UVW observations at 100 m were missing; however, using the algorithm of Holtslag and Van Ulden (1983), the friction velocity, temperature flux, and Monin–Obukhov length were estimated from wind-speed, temperature, temperature lapse, and net radiation. The mixing height,  $Z_i$  was approx. 490 m. The ratio  $-L/Z_i$  was 0.13 and the convective scaling velocity,  $W_*$ , was  $1.7 \text{ m s}^{-1}$ . These results, when viewed collectively, suggest that the PBL is convectively unstable.

Appreciable amounts of tracer were dispersed to the ground; the GLC pattern of SF<sub>6</sub> in Fig. 9 shows that the maximum concentration was over 200 ppt at  $\sim 5$  km downwind. The cross-wind concentration distributions for each arc indicate that the entire GLC pattern is skewed. This skew is consistent with that expected from theoretical considerations, such as those of Saffman (1962), for a plume whose major

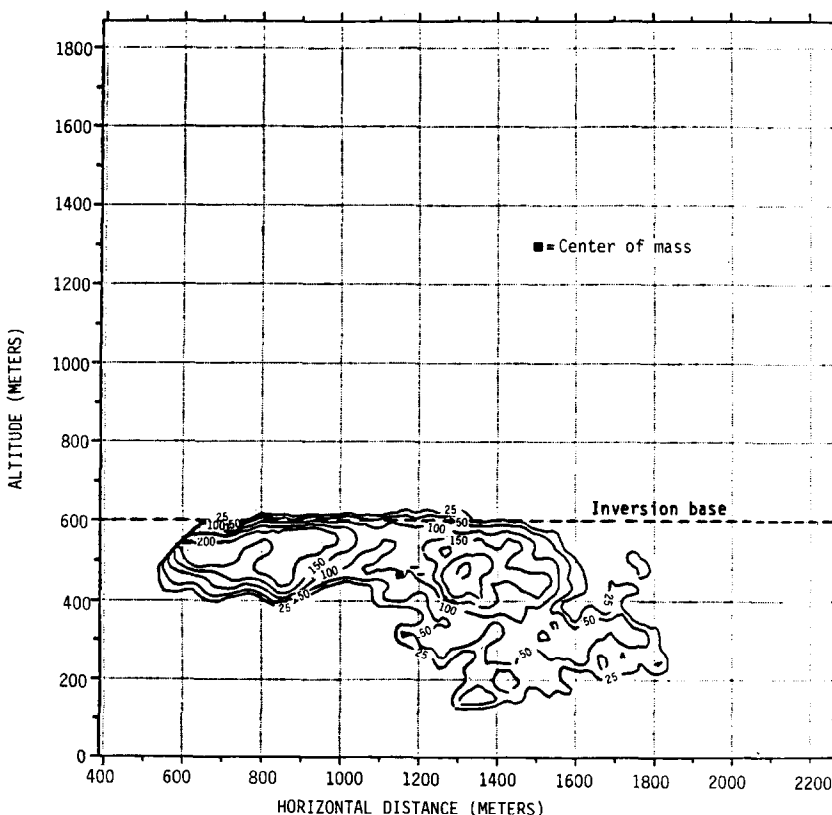


Fig. 7. An example of plume reflection near the base of an inversion at Kincaid observed 4.2 km downwind by the CGC particle lidar vertical scan at 1021 h LST on 15 May 1981; concentrations are relative.

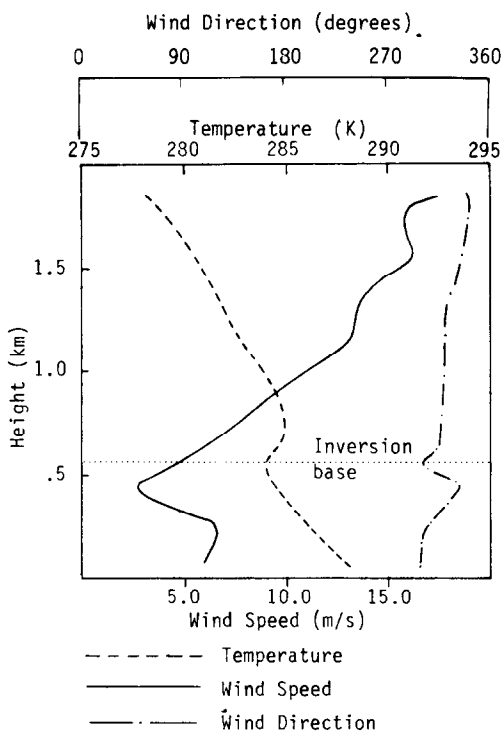


Fig. 8. Vertical profiles of wind-speed, wind direction, and temperature from the 1032 h LST T-sonde at Kincaid on 15 May 1981.

cross-wind axis is rotated and its width is stretched by the directional shear.

### Fumigation

Fumigation can cause some of the highest ground-level concentrations. A short-lived phenomenon, it occurs when the plume aloft is suddenly eroded from beneath by eddies driven at the surface. A rapid and dramatic case of plume mixing to the ground was observed by the CGC particle lidar 5 km downwind from the Kincaid plant during 0900–1000 h LST on 20 July 1980 (Fig. 10). In about 6-min, the plume spilled to the ground and the plume mass centroid dropped from 314 to 173 m.

The CGC particle lidar data reveal that the initial vertical thickness of the plume as measured by  $\sigma_z$  during the 5-min lidar scans was  $\sim 40$  m before fumigation, but expanded to over 80 m during fumigation. The plume cross-wind width also increased slightly. The decrease in the height of the plume mass centroid (from 314 to 173 m) resulted in a larger hourly averaged vertical spread of the plume cross-sections (119 m) around the hourly averaged mass centroid (at 250 m) than would be expected from the Pasquill–Gifford curves.

The most dominant meteorological feature of the 0928 h LST T-sonde profiles is the very large wind-speed at stack height ( $10.0 \text{ m s}^{-1}$ ). Briggs' criterion

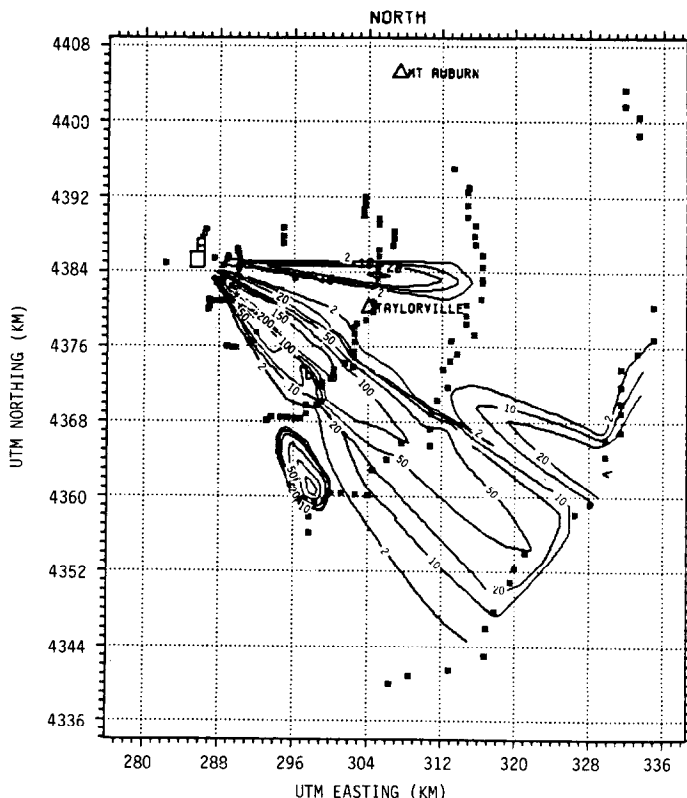


Fig. 9. GLC pattern of  $\text{SF}_6$  at Kincaid on 15 May 1981, 1000–1100 h LST. Units are in ppt; solid squares represent receptor sites.

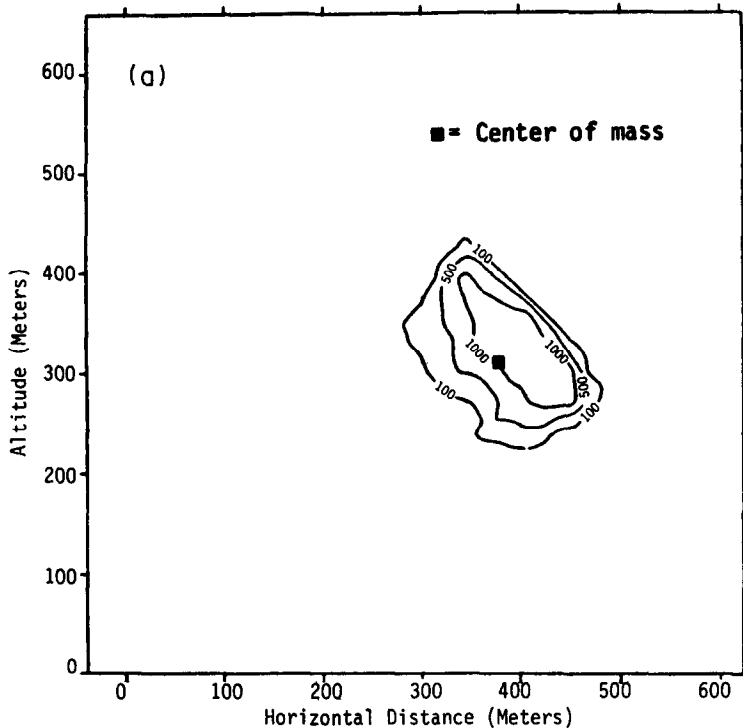


Fig. 10a. An example of plume fumigation at Kincaid observed 5 km downwind on 20 July 1981, 0900–1000 h LST, by the CGC particle lidar; before mixing to the ground at 0929 h LST (concentrations are relative).

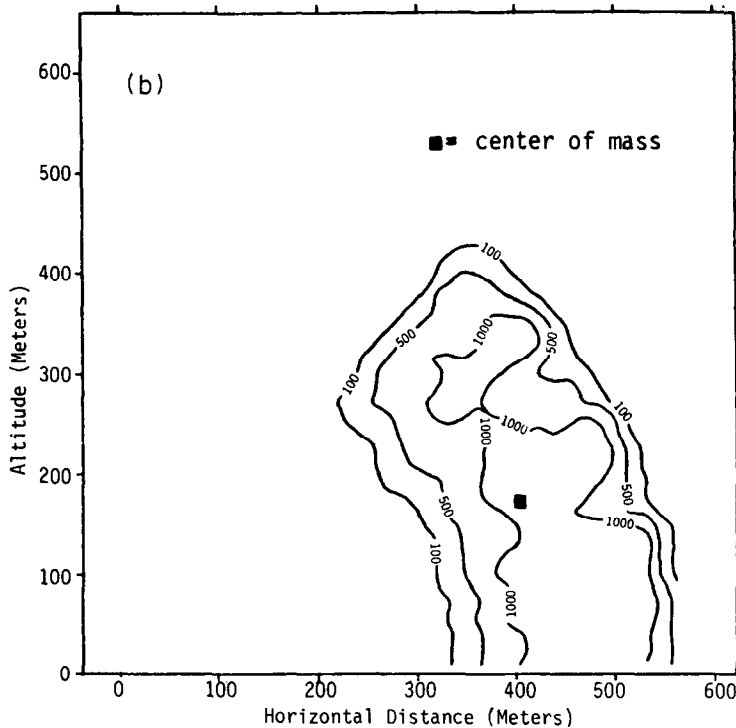


Fig. 10b. After mixing to the ground at 0935 h LST.

(1975) for stack downdraft for large Froude number sources is that the ratio of stack velocity to mean wind-speed be less than 1.5. In this case, the stack gas

exit velocity is  $21 \text{ m s}^{-1}$ ; thus downdraft would not be expected to occur. The T-sonde and acoustic sounder put the mixing height,  $Z_i$ , at approx. 340 m. The

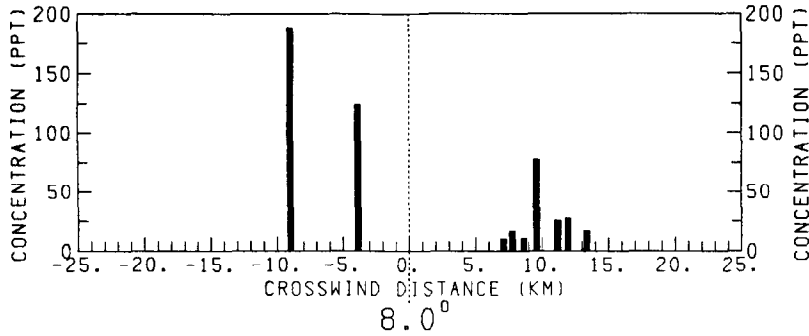


Fig. 11. A bar plot of  $\text{SF}_6$  tracer concentrations as a function of distance from the center of mass of the cross-wind concentration distribution. The dotted line and angle denote the position and azimuthal angle of the center of mass from the stack.

horizontal turbulence intensity at 100 m is only  $5^\circ$  and the vertical turbulence intensity is  $4^\circ$ . The gradient Richardson number in the 10–100-m layer is  $-0.05$ , which indicates that the boundary layer is unstable. However, it is not convectively unstable since  $-L/Z$  is of the order of one and the convective scaling velocity is quite small ( $W_* = 0.56 \text{ m s}^{-1}$ ). The friction velocity of  $0.4 \text{ m s}^{-1}$  is relatively large. The Townsend number estimated for the 0–340-m layer was nearly 500, which, according to Tennekes (1973), suggests that the mean wind-speed gradient is large enough to sustain eddies of the scale of the mixed layer height,  $Z_i$ .

The ground-level cross-wind distributions of  $\text{SF}_6$  reveal two separate concentration maxima on the 20-km arc (Fig. 11). The larger peak is due to the fumigation of the plume abruptly to the ground. A directional shear produces the separation. Figure 10 shows the plume slightly tilted near the source; at 20 km the fumigated plume material descends directly to the ground, substantially to one side of the original plume footprint. A wind shear of  $25^\circ$  was observed between the ground and 350 m. This translates into an approximate separation of 9 km at 20 km downwind, which explains in large part the separation of the concentration maxima seen in Fig. 11.

#### SUMMARY AND CONCLUSIONS

The effects of local meteorology on plume behavior were found to vary greatly for a flat terrain site (Kincaid, IL) and a moderately complex terrain site (Bull Run, TN). The most notable differences are the wind-speed and the degree of wind direction fluctuations. The much lower wind-speeds and larger wind direction fluctuations measured at the ground and aloft at Bull Run are due to the terrain and the degree of surface roughness. These two meteorological differences produce larger plume rises and plume widths, and more frequent plume meandering and plume looping at Bull Run than at Kincaid. Relatively strong capping inversions limited plume mixing more often at Kincaid than at Bull Run. Thus, there were more

occurrences of plume lofting, trapping, and fumigation at Kincaid than at Bull Run.

Some of the meteorological phenomena that give rise to particular plume behaviors and patterns of dispersion were reviewed. Several specific cases of plume behavior were studied using both meteorology and lidar observations of plume cross-sections aloft. Cases of plume bifurcation, meandering, looping, trapping, and fumigation were analyzed to identify the effects of various dispersion processes on the shape, center of mass location, and size of the plume cross-section. The effects of 5-min to 1-h eddies on plume transport and dispersion were examined closely because they are important in producing transient or nonstationary variations in the plume location and size under certain dispersion conditions such as plume looping and fumigation. Vertical changes in atmospheric stability and in the wind field were examined because these kinds of vertical variations are quite important in such dispersion processes as plume trapping and bifurcation. The most gratifying finding is that when such variables as fluctuation in wind-speed and direction are measured appropriately, these measurements can frequently be used to estimate short-term (5-min) plume segment displacements. These displacements, in turn, can be used to account for increases in hourly averaged plume spread aloft and at the ground.

*Acknowledgements*—This research was supported by the Electric Power Research Institute with Dr Glenn Hilst as project monitor. The authors also recognize and appreciate the helpful suggestions made by one of the reviewers which greatly improved the discussion of plume bifurcation.

#### REFERENCES

- Bowne N. E., Londergan R. J., Murray D. R. and Borenstein H. (1983) Overview, results and conclusion for the EPRI plume model and development project: plains site. EA-3074, Electric Power Research Institute, Palo Alto, CA.
- Bowne N. E., Londergan R. J. and Murray D. R. (1985) Summary of results and conclusions for the EPRI plume model validation project: moderately complex site. EA-3755, Electric Power Research Institute, Palo Alto, CA.

- Briggs G. A. (1975) Plume rise predictions. In *Lectures on Air Pollution and Environmental Impact Analysis* (edited by D. A. Haugen), American Meteorological Society, Boston.
- Businger J. A., Wyngaard J. C., Izumi T. and Bradley E. F. (1971) Flux profile relationships in the atmospheric surface layer. *J. Atmos. Sci.* **28**, 181–189.
- Csanady G. T. (1973) *Turbulent Diffusion in the Environment*. D. Riedel, Dordrecht.
- Davis P. O. A. L. and Moore D. J. (1964) Experiments on the behavior of effluent emitted from stacks at or near the roof level of tall reactor buildings. *Int. J. Air Water Pollut.* **8**, 515–523.
- Deardorff J. W. and Willis G. E. (1975) A parameterization of diffusion in the mixed layer. *J. appl. Met.* **14**, 1451–1458.
- Ellis H. M., Logan M. and Chiu C. (1984) Investigation of plume dispersion using lidar plume measurements. 77th annual meeting of the Air Pollution Control Association, San Francisco, CA.
- Fanaki F. H. (1975) Experimental observations of a bifurcated buoyant plume. *Boundary-Layer Met.* **9**, 479–495.
- Graham N. E., Taylor G. H., Petersen R. L., Sinclair P. C., Frey J. W. and Koss T. C. (1979) An analysis of terrain-induced aerodynamic effects near the Kingston steam plant, Kingston, Tennessee. In *Proc. 4th Symp. Turbulence, Diffusion, and Air Pollution*. Am. Met. Soc., Boston, pp. 113–116.
- Guillot P. (1979) Dispersion of pollutants from tall stacks studied by remote sensing techniques during EEC joint campaigns. In *Proc. 10th Int. Tech. Mg Air Pollut. Modeling and Its Applications*. NATO Committee on the Challenges to Modern Society, Brussels.
- Hilst G. R. (1957) The dispersion of stack gases in stable atmospheres. *J. Air Pollut. Control Ass.* **7**, 205.
- Hilst G. R. (1978) Plume model validation. EA-917-SY, Electric Power Research Institute, Palo Alto, CA.
- Hoff R. M. and Froude F. A. (1979) Lidar observations of plume dispersion in northern Alberta. *Atmospheric Environment* **13**, 35–43.
- Holland J. Z. (1953) *A Meteorological Survey of the Oak Ridge Area*. ORO-99, U.S. Atomic Energy Commission Technical Information Service, Oak Ridge, TN.
- Holtslag A. A. M. and Van Ulden A. P. (1983) A simple scheme for daytime estimates of surface fluxes from routine weather data. *J. Clim. appl. Meteorol.* **22**, 517–529.
- Howroyd G. C. and Slawson P. R. (1979) The effects of cross-wind shear on plumes released from elevated sources. In *Proc. 4th Symp. Turbulence, Diffusion, and Air Pollution*, Am. Met. Soc., Boston, pp. 56–61.
- Hudischewskij A. B. and Reynolds S. D. (1984) A catalog of data for the EPRI plume model validation data base: Kincaid site. EA-3080, Electric Power Research Institute, Palo Alto, CA.
- Liu M. K., Moore G. E. and Holman H. Y. (1982) A survey of plume models for atmospheric applications. EA-2243, Electric Power Research Institute, Palo Alto, CA.
- McElroy J. L., Eckert J. A. and Hagen C. J. (1981) Airborne downlooking lidar measurements during State 78. *Atmospheric Environment* **15**, 2223–2230.
- Moore G. E. and Liu M. K. (1984) Diagnostic evaluation of Gaussian and first-order plume models at a moderately complex terrain site. EA-3760, Electric Power Research Institute, Palo Alto, CA.
- Okubo A. and Karweit M. J. (1969) Diffusion from a continuous source in a uniform shear flow. *Limnol. Oceanogr.* **14**, 516–520.
- Pasquill F. (1969) The influence of the turning of wind with height on crosswind diffusion. *Phil. Trans. R. Soc.* **265**, 173.
- Pasquill F. and Smith F. B. (1983) *Atmospheric Diffusion*, 3rd edn. Ellis Horwood Series in Environmental Science, Chichester.
- Reynolds S. D., Seigneur C., Stoekenius T. E., Moore G. E. and Johnson R. G. (1984) Operational validation of Gaussian plume models at a plains site. EA-3076, Electric Power Research Institute, Palo Alto, CA.
- Saffman P. C. (1962) The effect of wind shear on horizontal spread from an instantaneous ground source. *Q. Jl R. met. Soc.* **88**, 382.
- Slade D. H. (1968) *Meteorology and atomic energy*. U.S. Atomic Energy Commission, Division of Technical Information, Oak Ridge, TN.
- Smith F., Decker C. E., Strong R. B., White J. H., Arey F. K. and Bach W. D. (1983) Estimates of uncertainty for the plume model validation and development project field measurements—plains site. EA-3081, Electric Power Research Institute, Palo Alto, CA.
- Smith F. and Decker C. E. (1983) External Quality Assurance for the PMV&D project—moderately complex terrain site. RTI/1877, Research Triangle Institute, Research Triangle Park, NC.
- Taconet O. and Weill A. (1983) Convective plumes in the atmospheric boundary layer as observed with an acoustic Doppler sodar. *Boundary-Layer Met.* **25**, 143–158.
- Tennekes H. (1973) Similarity laws and scale relations in planetary boundary layers. In *Workshop on Micrometeorology* (edited by D. A. Haugen). Am. Met. Soc., Boston.
- Teske M. E. and Lewellen W. S. (1980) Example calculations of atmospheric dispersion using second-order closure modeling. Aeronautical Research Associates of Princeton, NJ.
- Turner J. S. (1960) *Buoyancy Effects In Fluids*. Cambridge University Press, Cambridge.
- Ute E. E., Ludwig F. L. and Pooler F. (1980) Lidar observations of diurnal behavior of the Cumberland Plateau power plant plume. *J. Air Pollut. Control Ass.* **30**, 889–893.
- Weil J. C. and Altman J. L. (1979) Stack plume characterization and model assessment with lidar data. Martin Marietta Environmental Center, Baltimore, MD.
- Willis G. E. and Deardorff J. W. (1981) A laboratory study of dispersion from a source in the middle of a convectively mixed layer. *Atmospheric Environment* **15**, 109–117.

# **New Dispersion Model for Highly-Buoyant Plumes in the Convective Boundary Layer**

by  
Jeffrey C. Weil

January 2, 2020

**Preliminary Draft V4**

## 1. Introduction

Dispersion of buoyant plumes in the convective boundary layer (CBL) is assumed to take place in a random field of convective elements—updrafts and downdrafts—that travel with the mean wind. The vertical velocity in each element is assumed to be a random variable prescribed by a probability distribution. The dispersion process can be divided into two main components: 1) plume segments in strong downdrafts which carry the segments to the surface (downdraft fraction), and 2) plume segments in updrafts, which transport material all the way to the CBL top (updraft fraction), where they either penetrate the elevated inversion capping the CBL or are “entrapped” by it. For sufficiently high buoyancy, a fraction of the updraft plume can penetrate the inversion depending on the buoyancy and the degree of stratification (air potential temperature gradient) aloft. The fraction that is entrapped by the inversion remains temporarily at the CBL top or “lofts” and is slowly entrained into the main region or “mixed layer” of the CBL.

The dispersion model AERMOD (Cimorelli et al., 2005; Perry et al., 2005) treats the above components separately and has a dispersion prediction for each process or source: 1) the “real stack” source which contributes mainly to the downdraft fraction, 2) the “indirect source” which handles the entrapped material, and 3) the “penetrated source” dealing with material rising above the inversion. The contributions to the concentration are then summed. Historically, the main issues or problems arising with AERMOD have been with the indirect and penetrated sources, e.g., see Ken Rayner’s discussion (email Feb. 25, 2013), which are the focus of this work.

The modeling project for the Collie Airshed Study has two main goals or tasks: 1) Task A: to modify and further develop the “lofting plume” (LP) dispersion model for the indirect source or entrapped material, and 2) Task B: to further develop the AERMOD dispersion treatment for moderate-to-strong winds and weak convection.

This document highlights the main results for Task A, which has made key use of the convection tank experimental data of Weil et al. (WEA, 2002) on buoyant plume dispersion in the CBL. We present the new LP dispersion model derivation, changes from the AERMOD formulation, and a comparison of results with the convection tank data of Weil et al. (2002).

## 2. Dispersion Model for Highly Buoyant Plumes

The degree of plume buoyancy from sources in the CBL is usually measured by the dimensionless buoyancy flux,  $F_* = F_b / (U w_*^2 z_i)$ , where  $F_b$  is the stack buoyancy flux (proportional

to the stack heat flux),  $U$  is the mean (vertically-averaged) wind speed,  $w_*$  is the convective velocity scale that characterizes the turbulent velocities in the CBL, and  $z_i$  is the CBL height. Highly-buoyant plumes generally are considered as those with  $F_* \geq 0.1$  and typically occur in light winds ( $U < 3$  m/s) with low  $z_i$  values; here, we consider highly-buoyant cases as those with  $F_* \geq 0.07$ . The WEA (2002) tank experiments covered  $F_*$  values of 0.1, 0.2, and 0.4, a useful range for developing and testing the LP model.

In the PDF approach, the mean crosswind-integrated concentration CWIC,  $C^y$ , is given by

$$C^y(x, z) = \frac{Q}{U} p_z, \quad (1)$$

where  $x$  is the downwind distance,  $z$  is the height above ground,  $Q$  is the source strength or emission rate,  $U$  is the mean (vertically-averaged) wind speed in the CBL, and  $p_z$  is the probability density function (PDF) of the plume or particle height (see Weil et al., 1997). This expression is based on a mass flux balance (Weil, 1988a), where  $p_z \Delta z$  is the probability of finding the plume or particle height in the interval  $z - \Delta z/2 < z < z + \Delta z/2$ , and  $\Delta z$  is a small height increment.

The  $p_z$  is found from the PDF of the (random) vertical velocity  $w$  in the CBL as

$$p_z = p_w[w(z_p; x/U)] |dw/dz_p|, \quad (2)$$

where  $z_p$  is the plume height, and the absolute value is taken to ensure that the  $p_z$  is positive. Here,  $p_w$  represents a general form of the  $w$  PDF and will be taken below as skewed (Eq. 5). Writing the argument of  $p_w$  as  $w(z_p; x/U)$  means that wherever  $w$  appears in  $p_w$ , we replace it by its equivalent in terms of  $z_p$  and  $x$ . The relationship between  $z_p$  and  $w$  is found by superposing the plume rise  $\Delta h$  and the vertical displacement due to  $w$ , i.e.,  $wx/U$ , as:

$$z_p = h_s + \Delta h + \frac{wx}{U}, \quad (3)$$

where  $z_s$  is the stack height.

In Eq. (2),  $w(z_p; x/U)$  is found by rearranging (3) as

$$w = (z_p - h_s - \Delta h) \frac{U}{x} \quad (4)$$

from which we obtain  $|dw/dz_p| = U/x$ . This  $w$  and  $dw/dz_p$  are then substituted into Eq. (4) to obtain  $p_z$ .

In the CBL, a good approximation to the  $w$  PDF is the superposition of two Gaussian distributions (e.g., Baerentsen and Berkowicz, 1984; Weil, 1988a)

$$p_w = \frac{\lambda_1}{\sqrt{2\pi}\sigma_{w1}} \exp\left(-\frac{(w - \overline{w}_1)^2}{2\sigma_{w1}^2}\right) + \frac{\lambda_2}{\sqrt{2\pi}\sigma_{w2}} \exp\left(-\frac{(w - \overline{w}_2)^2}{2\sigma_{w2}^2}\right), \quad (5)$$

where  $\lambda_1$  and  $\lambda_2$  are weighting coefficients for the distributions with  $\lambda_1 + \lambda_2 = 1$ . The  $\overline{w}_j$  and  $\sigma_{wj}$  ( $j = 1, 2$ ) are the mean vertical velocity and standard deviation for each distribution and are assumed to be proportional to  $\sigma_w$ , the “total” or overall root-mean-square vertical turbulence velocity; subscripts 1 and 2 denote the updraft and downdraft distributions, respectively. The  $\overline{w}_1, \overline{w}_2, \sigma_{w1}, \sigma_{w2}, \lambda_1, \lambda_2$  are found as a function of  $\sigma_w$ , the vertical velocity skewness  $S = \overline{w^3}/\sigma_w^3$  where  $\overline{w^3}$  is the third moment of  $w$ , and a parameter  $R = \sigma_{w1}/\overline{w}_1 = -\sigma_{w2}/\overline{w}_2$  (see Weil et al., 1997).

In their analysis of laboratory data, Weil et al. (1997) found that  $R = 1$  produced fair-to-good agreement between the modeled and measured CWIC fields. However, for field observations, they used  $R = 2$  so that in the limit of a neutral boundary layer ( $w_* = 0$ ) and an assumed  $S = 0$ , the  $w$  PDF approximated that of a Gaussian PDF. They also found that there was little difference between the results for  $R = 1$  and 2 in the case of field data (see their Table 2).

In the upper 90% of the CBL, the vertical velocity variance  $\sigma_w^2$  can be assumed to be uniform (Weil, 1988a) as can the skewness (Wyngaard, 1988). Here, the  $\sigma_w^2$  is parameterized in terms of  $w_*$  and the surface friction velocity  $u_*$  by

$$\sigma_w^2 = 1.2u_*^2 + 0.35w_*^2, \quad (6a)$$

where the coefficients 1.2 and 0.35 are taken from Hicks (1985). Similarly, the lateral velocity variance  $\sigma_v^2$  can be assumed to be uniform over the CBL and parameterized by

$$\sigma_v^2 = 3.6u_*^2 + 0.35w_*^2, \quad (6b)$$

where the coefficients 3.6 and 0.35 are also from Hicks (1985). The convective contribution to the variances,  $0.35w_*^2$  in Eqs. (6a, 6b), are consistent with AERMOD (Cimorelli et al., 2005). In the convective limit, the  $S$  is taken as 0.6 which is the vertically-averaged value from the Minnesota experiments (Wyngaard, 1988); the corresponding  $\overline{w^3} = 0.6\sigma_w^3 = 0.124w_*^3$ . For arbitrary  $u_*$  and  $w_*$ , the skewness is parameterized by  $S = 0.124w_*^3/\sigma_w^3$  with  $\sigma_w^2$  given by Eq. (8a); thus as  $w_* \rightarrow 0$ ,  $S \rightarrow 0$  and for  $w_*/u_* \gg 1$ ,  $S = 0.6$ .

Using the approach for finding  $p_z$  outlined above (Eqs. 2 - 4 and related discussion) and the  $p_w$  given by Eq. (5), Weil et al. (1997) obtained the CWIC field for the direct plume as

$$C_d^y(x, z) = \frac{Q}{\sqrt{2\pi}U} \left[ \frac{\lambda_1}{\sigma_{z1}} \exp\left(-\frac{(z - \Psi_1)^2}{2\sigma_{z1}^2}\right) + \frac{\lambda_2}{\sigma_{z2}} \exp\left(-\frac{(z - \Psi_2)^2}{2\sigma_{z2}^2}\right) \right] \quad (7a)$$

or

$$C_d^y(x, z) = \frac{Q}{\sqrt{2\pi}U} \sum_{j=1}^2 \frac{\lambda_j}{\sigma_{zj}} \exp\left(-\frac{(z - \Psi_j)^2}{2\sigma_{zj}^2}\right), \quad (7b)$$

where

$$\sigma_{zj} = \frac{\sigma_{wj}x}{U}, \quad \Psi_j = h_s + \Delta h + \frac{\overline{w_j}x}{U} \quad \text{with } j = 1 \text{ or } 2. \quad (8)$$

To account for the zero-flux condition at the ground, Weil et al. introduced an image source at  $z = -h_s$ , i.e., assumed particle reflection at  $z = 0$ . This resulted in a positive flux of material at  $z = z_i$ , and additional image sources were included at  $z = 2z_i + h_s$ ,  $-2z_i - h_s$ , etc. to satisfy the subsequent no-flux conditions at  $z = z_i, 0$ . The resulting CWIC due to the real and image sources was

$$C_d^y(x, z) = \frac{Q}{\sqrt{2\pi}U} \sum_{n=0}^N \sum_{j=1}^2 \frac{\lambda_j}{\sigma_{zj}} \left[ \exp\left(-\frac{(z - 2nz_i - \Psi_j)^2}{2\sigma_{zj}^2}\right) + \exp\left(-\frac{(z + 2nz_i + \Psi_j)^2}{2\sigma_{zj}^2}\right) \right], \quad (9)$$

where  $N$  is the number of image sources. A value of  $N = 50$  is used here and also by Weil et al., which is more than adequate for the comparisons made here. A more computationally-efficient choice for  $N$  can be made based on a series-convergence test.

In AERMOD and many other dispersion models (e.g., Weil et al., 1997), the strength of the real and image sources is corrected for the degree of plume penetration of the elevated inversion by multiplying  $Q$  by  $f = 1 - P$ , where  $P$  is the penetration fraction and  $f$  is the plume fraction trapped in the CBL. However, in the new dispersion model here, the real stack source term is left as  $Q$  since the plume segments carried from the stack to the surface are not affected by the penetration. The  $P$  only affects the indirect or entrapped model source term and the penetrated source term; the latter is given by  $PQ$ .

### 3. Model Components for Highly Buoyant Plume Dispersion

#### 3.1. Entrapment and Entrainment Models

Following Willis and Deardorff (1987) and Weil et al. (2002), we use the term “entrapment” to describe the plume mass that rises to the CBL top, penetrates into the inversion

layer, and becomes temporarily trapped there. We refer to the average inversion layer as the region  $1 \leq z/z_i \leq 1.2$  and over which a temperature jump or inversion  $\Delta\Theta_i$ , occurs due to mixed-layer entrainment of the overlying fluid; the inversion layer is the upper part of the interfacial or entrainment zone and is capped by an upper stable layer. The trapped buoyant material has a local concentration maximum within the inversion layer (see WEA, 2002) and is slowly entrained into the mixed layer by the large CBL eddies; this is similar to plume fumigation (Deardorff and Willis, 1982). Non-buoyant plumes also have a portion of their mass within the inversion layer but do not exhibit a local elevated maximum (WEA, 2002).

The entrapped plume acts as an elevated reservoir of pollutants for the mixed layer, and therefore it is important to describe the entrapment process as accurately as possible since it will indeed contribute to surface concentrations.

As in WEA (2002), we define the mean entrapment  $E(x)$  at distance  $x$  as the fraction of the plume mass lying above  $z_i$

$$E(x) = \frac{\int_{z_i}^{\infty} C^y(x, z) dz}{\int_0^{\infty} C^y(x, z) dz}, \quad (10)$$

where  $C^y$  is the CWIC. Entrapment is viewed as a two-part process consisting of: 1) initial entrapment due to highly-buoyant plume segments that rise above  $z_i$  into the inversion layer ( $z > z_i$ ), and 2) entrainment of the entrapped material back into the mixed layer by the CBL turbulence. The initial entrapment is due to plume segments caught in updrafts or weak downdrafts, where the weak downdrafts are defined as those in which the maximum plume height  $z_{max} \geq z_i$ ; for strong downdrafts, the plume does not escape the mixed layer and  $z_{max} < z_i$ .

The initial entrapment is found using the plume trajectory (Eq. 3) by including the rise for a buoyant plume

$$\Delta h = 1.6 \frac{F_b^{1/3}}{U} x^{2/3} \quad (11)$$

(Briggs, 1975; Weil, 1988b). The resulting equation can then be rearranged to find the vertical velocity that produces a particular plume rise  $z' = z_p - z_s$  for the given  $x$ ,  $U$ , and  $F_b$ :

$$w = \frac{z'U}{x} - 1.6 \frac{F_b^{1/3}}{x^{1/3}}. \quad (12)$$

With  $z' = z'_i$ , the  $w$  is

$$w(x; z'_i) = \frac{z'_i U}{x} - 1.6 \frac{F_b^{1/3}}{x^{1/3}} . \quad (13)$$

The initial entrainment,  $E_{in}$ , can be obtained by integrating the  $w$  PDF (Eq. 5) over all possible velocities leading to  $w(x; z'_i)$  and this yields

$$E_{in} = \frac{\lambda_1}{2} [1 - \text{erf}(\phi_{1m})] + \frac{\lambda_2}{2} [1 - \text{erf}(\phi_{2m})] , \quad (14)$$

where  $\lambda_i$ ,  $\bar{w}_i$  and  $\sigma_i$  are the PDF parameters discussed in Section 2 (i.e., from Weil et al., 1997), and erf is the error function. The  $\phi_{im}$  are

$$\phi_{1m} = \frac{w - \bar{w}_1}{\sqrt{2}\sigma_1} , \quad \phi_{2m} = \frac{w - \bar{w}_2}{\sqrt{2}\sigma_2} , \quad (15)$$

where  $w$  is replaced by Eq. (13) to obtain  $\phi_{1m}$ ,  $\phi_{2m}$ , and  $E_{in}$  as functions distance  $x$ .

The net entrainment,  $E(x)$ , at  $x$  due to the initial value,  $E_{in}(x)$ , and the change  $\Delta E(x)$  caused by mixed-layer entrainment can be found from a simple mass flux balance in the lofting plume. By multiplying the numerator and denominator of Eq. (10) by the mean wind speed  $U$ , we can introduce the mass flux  $\dot{m}$  in the entrainment zone as

$$\dot{m} = \int_{z_i}^{\infty} U c^y(x, y) dz = QE(x) . \quad (16a)$$

The third part of the equality holds because  $U$  times the denominator of Eq. (10) is the total pollutant flux  $Q$  from the source. A flux balance over the distance interval,  $x$  to  $x + \Delta x$ , is given by

$$\Delta \dot{m} = \dot{m}_{in}(x + \Delta x) - \dot{m}_{in}(x) - w_e C_1^y \Delta x , \quad (16b)$$

where  $C_1^y$  is the CWIC in the inversion layer, taken here to be a uniform distribution over the depth  $\Delta z_1$ , and  $w_e$  is the entrainment velocity for entrainment of plume material into the CBL mixed layer. In addition, we have

$$\dot{m} = UC_1^y \Delta z_1 = QE \quad \text{or} \quad C_1^y = \frac{QE}{U\Delta z_1} . \quad (16c)$$

By substituting the  $C_1^y$  from Eq. (16c) into (16b) and taking the limit as  $\Delta x \rightarrow dx$ , we obtain the following differential equation for  $E(x)$ :

$$\frac{dE}{dx} + \frac{w_e}{U\Delta z_1} E = \frac{dE_{in}}{dx} . \quad (17)$$

Provided that  $w_e(x)$  and  $E_{in}$  are known, the  $E(x)$  can be found by numerical integration. This integration may be done in the future, but for now we seek a simpler approximate method for obtaining  $E$ .

In the approximate method, we assume that the net entrainment is given by the superposition of the initial value,  $E_{in}(x)$ , and the net change or loss in entrainment from an “instantaneously-placed” entrapped plume having an initial value  $E_h(0) = E_\infty$ , where  $E_\infty$  is the large-distance limit of Eq. (14); this is the entrainment after all penetrated plume segments have crossed the plane  $z = z_i$ . We now find the entrainment,  $E_h(x)$ , for this plume, which satisfies the “homogeneous” case of Eq. (17), i.e., with the right-hand-side (rhs) set to zero. The  $E_h(x)$  is found to be

$$E_h = E_\infty \left[ \exp \left( - \int_0^x \frac{w_e}{U \Delta z_1} dx' \right) \right], \quad (18)$$

and the net change (loss) in  $E_h$ ,  $\Delta E_h$ , due to entrainment of plume material by the mixed layer is

$$\Delta E_h = E_\infty \left[ \exp \left( - \int_0^x \frac{w_e}{U \Delta z_1} dx' \right) - 1 \right]. \quad (19)$$

Thus, the approximate solution to  $E(x)$  is

$$E(x) = E_{in}(x) + \Delta E_h(x). \quad (20)$$

We note that the loss in the entrainment given by Eq. (19) is a gain or source of pollution for the mixed layer and is used in Section 3.2 for that purpose.

The above model can be completed upon specifying the entrainment velocity. Following earlier entrainment models (e.g., Turner, 1979; Deardorff and Willis, 1985), we assume that

$$w_e = a_e \frac{w_*}{Ri}, \quad (21)$$

where  $Ri$  is a Richardson number characterizing buoyancy and turbulence effects. Here,  $Ri$  is based on the plume fractional density defect,  $\Delta\rho/\rho_a$ , and the vertical plume thickness,  $\Delta z_1$ , and can be written as

$$Ri = \frac{F_b}{U w_*^2 r_y}, \quad (22)$$

where  $r_y$  is the lateral half-width. The  $r_y$  is given by

$$r_y = C_1 \frac{F_b^{1/3}}{U} x^{2/3} \quad (23)$$

(Briggs, 1985; WEA, 2002) with  $C_1 = 2.26$  and  $1.13$  for field observations and laboratory experiments, respectively (WEA, 2002).

By substituting the above results (Eqs. 21 - 23) into Eq. (19), we find the net change  $\Delta E_h$  to be given by

$$\Delta E_h = E_\infty \left[ \exp\left( - \frac{a'_e X^{5/3}}{F_*^{2/3}} \right) - 1 \right], \quad (24)$$

where

$$X = \frac{w_* x}{U z_i}, \quad (25)$$

and  $a'_e$  is a net entrainment coefficient determined empirically using the WEA (2002) data.  $X$  is the usual dimensionless distance in convective dispersion problems (Willis and Deardorff, 1976; Briggs, 1985; Weil, 1988a) and is the ratio of plume travel time  $x/U$  to the large-eddy turnover time  $z_i/w_*$ .

Figure 1 compares the approximate entrainment model (Eqs. 20, 24) with the WEA (2002) laboratory data for  $F_* = 0.1, 0.2$  and  $0.4$ , which exhibit a monotonic increase in  $E$  with buoyancy, i.e.,  $F_*$ , as would be expected. Overall, the model shows the correct qualitative behavior of  $E$  with the dimensionless distance ( $X$ ) and buoyancy flux ( $F_*$ ) and produces a maximum value,  $E_{max}$ , near  $X = 1.5$ . Following the maximum, the measured and modeled  $E$  decrease due to CBL entrainment of the entrapped plume. The model decreases to an imposed long-distance limit,  $E_L = 0.17 + P_t$ , where  $P_t$  is the measured plume fraction penetrating the inversion top ( $z = 1.2z_i$ ) and thus does not participate in the entrainment/entrainment process; the coefficient  $0.17$  is the entrainment for a non-buoyant plume and serves as a lower limit.

The model results are given for two  $a'_e$  values,  $0.03$  (solid lines) and  $0.035$  (dashed lines), with those for  $0.03$  perhaps agreeing slightly better with the highest buoyancy case ( $F_* = 0.4$ ) for which the approximate model assumptions may be most appropriate. For the lowest two buoyancy fluxes ( $F_* = 0.1, 0.2$ ), the model curves appear to be shifted downstream relative to the measurements and generally overestimate them; this could be due to assumptions in the approximate model. It is possible that the solution to Eq. (17) with the  $dE_{in}/dx$  forcing included would correct this aspect and that solution should be pursued. Overall, however, we believe that the approximate model is reasonable and sufficiently good for dispersion predictions.

### 3.2. Crosswind-Integrated and Point Concentration Models

As discussed earlier, the pollutant concentration in the CBL is the sum of contributions from the three modeled sources: the downdraft plume (subscript  $d$  below), the entrapped plume (subscript  $e$ ), and the penetrated plume (subscript  $p$ ). Thus, the total surface CWIC due to the three sources is

$$C^y = C_d^y + C_e^y + C_p^y . \quad (26)$$

The downdraft model accounts for the initial and subsequent plume reflections at the surface and CBL top from a series summation (Eq. 9; Section 2) as done in Weil et al. (1997) and AERMOD (Cimorelli et al., 2005).

For the entrapped plume, an elemental plume segment entrained at some distance downwind by the CBL turbulence is assumed to mix rapidly, i.e., instantaneously, such that it is uniformly mixed in the vertical once it is entrained. This is guided by the WEA (2002) tank data (see also Weil, 2000), which show uniform CWIC profiles in the mixed layer,  $z \leq z_i$ , at dimensionless downstream distances of  $X \geq 2.5$  or 3 and for  $F_* = 0.1 - 0.4$ . The contribution from the penetrated plume also is assumed to occur by entrainment, but this happens as a result of mixed-layer growth,  $dz_i/dt$ ; it behaves much like the mixing and dispersion of the entrapped material except that it is driven by  $dz_i/dt$  and is akin to the fumigation process. In the WEA (2002) experiments, the  $z_i$  growth was quite slow due to the strong inversion, and for now such growth is ignored for the experimental data. Thus, the  $C_p^y$  is assumed to be zero in the model comparisons with the data (Fig. 2).

The dimensionless CWIC for the downdraft and entrapped plumes uses the standard CBL scaling (e.g., Deardorff and Willis, 1976; Weil, 1988a) and is given by

$$\frac{C^y U z_i}{Q} = \frac{C_d^y U z_i}{Q} + |\Delta E_h(X)| , \quad (27)$$

where the entrapped plume contribution  $|\Delta E_h(X)|$  is due to the entrained plume mass; the absolute value is taken since the  $\Delta E_h(X)$  is negative in Eq. (24). This term is a loss for the entrapped plume but a source and CWIC gain for the mixed layer.

Figure 2 compares the modeled surface CWIC in dimensionless form with the WEA (2002) data and shows that modeled and data trends are in general agreement. Here, results are shown for the same two  $a'_e$  values as in Fig. 1, which somewhat bracket the data with those for  $a'_e = 0.035$  yielding larger CWICs as would be expected. The model exhibits the correct distance ( $X$ ) and buoyancy flux ( $F_*$ ) variation and tends to a limiting CWIC

value (horizontal line) far downstream due to the entrainment limit,  $E_L$ , discussed earlier and shown in Fig. 1. The data overshoot of the model at  $X = 2.5$  ( $F_* = 0.1$ ) and 3 ( $F_* = 0.2$ ) by  $\sim 20\%$  to  $30\%$  could be due to initial non-uniform (non-instantaneous) vertical mixing as a result of turbulence vertical inhomogeneity. If necessary and important, this behavior could be addressed by a source distribution with  $x$  at the mixed-layer top as used in some fumigation models (e.g., Luhar and Sawford, 1996). However, this would require a more detailed dispersion model; an advantage of the assumed instantaneous vertical mixing is the model simplicity.

The plume centerline (or arc-maximum) surface concentration  $C$  can be found from the total  $C^y$  as  $C(x) = C^y(x)/(\sqrt{2\pi}\sigma_y(x))$ , where  $\sigma_y$  is the lateral root-mean-square spread or dispersion. The dimensionless surface concentration is given by the following standard form for the CBL:

$$\frac{CUz_i^2}{Q} = \frac{(C^yUz_i/Q)}{\sqrt{2\pi}\sigma_y/z_i}. \quad (28)$$

With the laboratory plumes, the dimensionless spread,  $\sigma_y/z_i$ , for highly-buoyant plumes was found to be

$$\frac{\sigma_y}{z_i} = a_y F_*^{1/3} X^{2/3} \quad (29a)$$

with  $a_y = 0.8$ , and in the case of non-buoyant plumes ( $F_* = 0$ ), it was given by

$$\frac{\sigma_y}{z_i} = \frac{0.51X}{(1 + 0.8X)^{1/2}}; \quad (29b)$$

see Weil et al. (2002).

Figure 3 presents the dimensionless surface concentration versus  $X$  for the model and tank data, where results are shown for the same two  $a'_e$  values used earlier. Here, as in Fig. 2, the results for the larger  $a'_e$  (0.035) are slightly higher and closer to the data. The model generally predicts the correct trends with  $X$  and  $F_*$  although the underestimates of the concentration for  $F_* = 0.1$  and  $0.2$  occur at the same location as in Fig. 2 for the CWIC and likely for the same reason, i.e., initial non-uniform and non-instantaneous vertical mixing. In all cases, the lateral dispersion used was the maximum of Eqs. (29a) (with  $a_y = 0.8$ ) and (29b). Due to the small underestimation of the concentrations in the higher  $F_*$  cases (0.2, 0.4), a second estimate of  $\sigma_y$  was made with a coefficient in Eq. (29a) of 0.7 rather than 0.8. These results are shown in Fig. 4, where one can see a modest improvement to the model results for  $a_y = 0.7$ .

#### 4. Plume Inversion Penetration

In earlier work, Weil (1988b) reviewed models and observations of plume penetration of thin and thick elevated temperature inversions, where the latter case also applied to elevated stable layers (not necessarily an inversion). A more relevant case is a combination of the thin and thick inversions, which is the more common situation and is considered here. Thus, our model daytime CBL potential temperature profile consists of a well-mixed layer with  $\partial\Theta/\partial z = 0$  ( $z \leq z_i$ ) capped by a thin temperature inversion or jump,  $\Delta\Theta_i$ , over a layer thickness  $\Delta z_i$  (i.e., for  $z_i < z \leq z_i + \Delta z_i$ ); the jump is followed by a deeper stable layer or inversion characterized by its potential temperature gradient (PTG),  $\partial\Theta_a/\partial z$  (for  $z > z_i + \Delta z_i$ ).

In the following, we present the new inversion penetration model and compare it with observations and an earlier model by Berkowicz et al. (1986), which is used in AERMOD.

Briggs (1975) assumed that a plume rising into an elevated inversion or stable layer would attain an equilibrium height,  $z'_e$ , when its buoyancy flux was completely depleted, i.e.,  $F = 0$ . Weil (1988b) used the same approach to investigate plume penetration of elevated inversions, thin and thick, or stable layers. The buoyancy depletion equation is

$$\frac{dF}{dz'} = -\frac{U}{\pi} \frac{g}{\Theta_a} \int \int_{A_i} \frac{d\Theta}{dz} dy dz, \quad (30)$$

where  $A_i$  is the plume area in the inversion or stable layer,  $z'$  ( $= z_i - z_s$ ) is the height above the source,  $U$  is the mean wind speed,  $g$  is the gravitation acceleration, and  $\Theta$  is the ambient potential temperature; Eq. (30) follows from a slight simplification of Eq. (3.31) in Weil (1988b). To integrate Eq. (30), we must assume a plume cross-sectional shape, which is taken as a square of edge length  $W$ , i.e.,  $A_i = W^2$ . The square is akin to the more realistic circular shape adopted in most plume rise models (Briggs, 1975, 1984; Weil, 1988b) but it (square) facilitates the integration of Eq. (30).

In contrast to the square geometry, Briggs (1984) assumed a rectangular cross section in his simple penetration model with a ratio of depth  $Z$  to width  $W$ ,  $Z/W$ , equal to 2. This asymmetric shape differed significantly from the usual round (or symmetric) plume assumption.

The plume is assumed to grow by buoyancy-induced turbulence using the usual entrainment assumption wherein the width increases in proportion to the rise  $z'$  or  $W = \beta_p z'$ , where  $\beta_p$  is an entrainment coefficient. The plume depth  $H$  within the inversion is given

by  $H = z'_u - z'_i$ , where  $z'_u$  is the height of the plume upper edge, and the prime ( $'$ ) denotes heights above the stack or source. The  $\beta_p$  is taken as 0.7 to ensure that the plume area,  $A_i = 0.5z'^2$ , is the same as that for a round plume of radius  $r$ :  $\pi r^2 = \pi\beta'z'^2$  with  $\beta' \simeq 0.4$  (Weil, 1988b).

By substituting  $W$  and  $H$  into Eq. (30) and integrating, we obtain

$$F - F_b = -\frac{U}{\pi} \frac{g}{\Theta_a} \int_{z'_i}^{z'_u} \frac{d\Theta}{dz} \beta_p z' (z'_u - z'_i) dz' , \quad (31)$$

where  $z_1 = z'_i/(1 + \beta_h)$  and is the plume centroid height when the plume upper edge is at the inversion base ( $z'_i$ ), and  $\beta_h = \beta_p/2$ . It is convenient to express  $z'$  in terms of the upper edge height or  $z'_u = (1 + \beta_h)z'$ . With this substitution, Eq. (31) can be written as

$$F - F_b = -a_1 U N_i^2 \int_{z'_i}^{z'_u} z'_u (z'_u - z'_i) dz'_u , \quad (32)$$

where  $a_1 = \beta_p/[\pi(1 + \beta_h)^2]$ ,  $N_i^2 = (g/\Theta)(d\Theta_i/dz)$ , and  $d\Theta_i/dz (= \Delta\Theta_i/\Delta z_i)$  is the potential temperature gradient (PTG) in the thin inversion.  $N$  is the Brunt-Vaissala frequency (BVF) or the oscillation frequency of a fluid parcel in a stratified fluid; hence,  $N_i$  is the BVF in the inversion. Equation (32) is valid as long as the plume geometry expressed in Eqs. (31, 32) is valid, and this holds for  $z'_u \leq z'_{is}$ , where

$$z'_{is} = z_i + \Delta z_i - z_s \quad \text{or} \quad z'_{is} = z'_i + \Delta z_i . \quad (33)$$

For  $z'_u \leq z'_{is}$ , Eq. (32) can be integrated to yield

$$F - F_b = -a_1 U N_i^2 z_i'^3 \left( \frac{z_u'^3}{3} - \frac{z_u'^2}{2} - \frac{1}{6} \right) , \quad (34)$$

which is written in terms of the dimensionless height  $z_u^*$ :

$$z_u^* = \frac{z'_u}{z'_i} . \quad (35)$$

To maintain consistency with earlier models, we determine the upper plume edge  $z'_u$  and penetration in terms of a dimensionless buoyancy flux  $P_s$  based on ‘‘penetration conditions’’ and given by

$$P_s = \frac{F_b}{U N_a^2 z_i'^3} , \quad (36)$$

(see Briggs, 1984; Weil, 1988b), where  $N_a^2 = (g/\Theta)(d\Theta_a/dz)$  and is the squared BVF for the elevated stable layer above the inversion. Thus, for the equilibrium plume height with  $F = 0$ , Eq. (34) is given by the dimensionless form

$$P_s = a_1 R_n \left( \frac{z_u^{*3}}{3} - \frac{z_u^{*2}}{2} - \frac{1}{6} \right), \quad (37)$$

where  $R_n = N_i^2/N_a^2$ , the ratio of the PTG's or BVF squared in the inversion to that in the elevated stable layer. The  $z_u^*$  versus  $P_s$  can be found either from the solution to the cubic equation (37) or by a simple iterative method; we have adopted the iterative method.

The degree of plume penetration  $P$  is defined by the ratio of the plume cross-sectional area  $WH$  above the inversion to that of the overall cross-section,  $W^2$ , or

$$P = \frac{H}{W} = \frac{1 + \beta_h}{\beta_p} \left( 1 - \frac{1}{z_u^*} \right), \quad (38)$$

and the plume fraction trapped by the inversion is

$$f = 1 - P. \quad (39)$$

From Eq. (37), the dimensionless buoyancy flux,  $P_{s1}$ , can be found where the upper plume edge  $z'_u = z'_{is}$ . With greater buoyancy, the plume top exceeds the inversion top and moves into the elevated stable layer. Equations (30) and (31) still describe the buoyancy depletion, but must be modified to account for the change in the temperature gradient between the inversion ( $d\Theta_i/dz$ ) and the upper stable layer ( $d\Theta_a/dz$ ). This modification results in the following equation for  $P_s$  as a function of  $z_u^*$ :

$$P_s = P_{s1} + \frac{a_1 R_n}{2} \frac{\Delta z_i}{z'_i} \lambda_s^2 (z_u^{*2} - 1) + a_1 \lambda_s^3 \left( \frac{z_u^{*3}}{3} - \frac{z_u^{*2}}{2} + \frac{1}{6} \right) \quad \text{if } z'_u > z'_{is}, \quad (40)$$

where  $P_{s1} = a_1 R_n (\lambda_s^3/3 - \lambda_s^2/2 + 1/6)$ , and  $\lambda_s = z'_{is}/z'_i$ . The solution for  $z_u^*$  as a function of  $P_s$  is obtained using a simple iterative method.

Figure 5 shows results for the plume fraction trapped  $f$  as a function of  $P_s$  as well as observations from two power plant studies. The buoyancy depletion model with or without a strong elevated inversion but with a deep stable layer shows a wide range of potential behavior given by the solid lines. The red line is the result for the case of no elevated inversion, only a deep stable layer, and with  $z_s/z_i = 0.15$ . This shows that the plume fraction trapped is only non-zero over a narrow range of  $P_s$  ( $P_s < 0.125$ ) and is zero for larger  $P_s$  values; that

is, all of the plume penetrates the elevated inversion for a sufficiently large  $P_s$ ,  $P_s > 0.125$ . This is quite consistent with the behavior for a round plume, where the fraction trapped is only non-zero over the range  $P_s < 0.15$  (see Weil, 1988b; Fig. 3.10).

The blue line gives the fraction trapped for the case of a thin elevated inversion ( $\Delta z_i/z_i = 0.05$ ), with a strong inversion temperature gradient ( $R_n = 7$ ), capped by a deep stable layer and  $z_s/z_i = 0.5$ ; this relative stack height ratio ( $z_s/z_i$ ) matches some of the Morgantown data below. The black line corresponds to the same inversion conditions as case 2 (blue line) but for a relatively high release height,  $z_s/z_i = 0.98$ ; i.e., a source very close to but below the inversion.

The buoyancy depletion model generalized to include a sharp elevated inversion as well as a deeper stable layer gives a broad range of range of results for the trapped plume fraction,  $f$ , versus the buoyancy parameter,  $P_s$ , depending especially on the stack height ratio,  $z_s/z_i$ , but also on  $\Delta z_i/z_i$  and  $R_n$ . However, the Berkowicz et al. (1986) model (dashed line, Fig. 4), which is used in AERMOD, gives only a single curve and is independent of  $z_s/z_i$  (see Weil, 1988b). It does account for the stability ( $\partial\Theta_i/\partial z$ ) of the deep stable layer but does not include a sharp elevated inversion at  $z_i$  and its stability.

Figure 5 shows that for both models, the  $f \rightarrow 1$  as  $P_s \rightarrow 0$ , which makes sense physically since for a small amount of buoyancy some portion of a plume should be able to penetrate the base of an inversion having a finite  $d\Theta_i/dz$ . The Morgantown data support this behavior. We place more significance on this data in general because  $f$  was numerically calculated from horizontal integrals of the plume aerosol distribution measured via lidar, and the variation of the integrals with height. For the Keystone data,  $f$  was estimated (Briggs, 1984) with more difficulty from hardcopy isopleths of aerosol content given in a report by Johnson and Uthe (1969).

One of the limitations of the earlier analysis of the  $f$  versus  $P_s$  data by Weil (1988b) was absence of an explanation and model calculation for the Morgantown data over the range  $0.05 < P_s < 0.11$ , where  $f$  ranges from 0.22 to 0.33 (solid squares, Fig. 5). The new buoyancy depletion model with a thin elevated inversion at  $z_i$  and inclusion of  $z_s/z_i$  approximately matches the  $f$  for these data. The flexibility of the new model is especially necessary to address early morning dispersion scenarios when the mixed layer is shallow and the stack height can be a significant fraction,  $\sim 0.5$  or greater, of  $z_i$ . These conditions in concert with light winds typically lead to high  $F_*$  values and sometimes high surface

concentrations.

## 5. Dispersion of Penetrated Plume

As with the other sources or contributions to the total concentration (Eq. 20), the concentrations in the CBL due to the penetrated plume satisfy the turbulent diffusion equation:

$$\frac{\partial C_p}{\partial t} + \mathbf{U} \cdot \nabla C_p + \nabla \cdot (\overline{\mathbf{u}'c'}) = 0, \quad (41)$$

where the third term on the left-hand-side (lhs) is the turbulent species flux. Here, the upper case symbols denote the mean wind ( $U$ ) and concentration ( $C$ ), the primes denote the turbulent fluctuations, and a bold symbol represents a vector. Under quasi-steady conditions as assumed here, the  $\partial C_p / \partial t$  is neglected. Applying the divergence theorem to Eq. (41) (Weil, 1988b), we obtain

$$\frac{d}{dx} \int_{-\infty}^{z_i} U C_p dy dz = - \int_{-\infty}^{\infty} (\overline{w'c'})_p(x, z_i) dy, \quad (42)$$

which states that the change in the mean species flux in the CBL (lhs) is equal to the turbulent flux at  $x$  through the plume top boundary at  $z_i$  (rhs). **Note that the  $C_p$  is zero at the beginning of the penetration process, but increases as the mixed-layer or CBL grows and entrains the elevated plume material at later times or downwind distances.**

We adopt the usual entrainment assumption for mixed layers which assumes that the turbulent flux can be parameterized as  $(\overline{w'c'})_p = C_{ep} w_{ep}$ , where  $C_{ep}$  and  $w_{ep}$  are the mean concentration in the elevated (penetrated) plume and the entrainment velocity for that material into the CBL. Additionally, for entrainment by mixed layer growth,  $w_{ep} = dz_i / dt$ , the change in the CBL height with time. We can now replace the integral on the rhs of Eq. (42) by

$$\int_{-\infty}^{\infty} (\overline{w'c'})_p(x, z_i) dy = C_{ep} \cdot dz_i / dt = C_{ep} \cdot U dz_i / dx, \quad (43)$$

where the last term results from assuming that the plume is advected by the mean wind.

The lhs of Eq. (42) is simplified further by our assumption that the mean concentration in the CBL is uniformly mixed such that

$$\int_0^{z_i} \int_{-\infty}^{\infty} C_p^y dy dz = C_p^y z_i. \quad (44)$$

By combining Eqs. (42 - 44), we have

$$\frac{d}{dx} (C_p^y z_i) = C_{ep}^y \frac{dz_i}{dx}, \quad (45)$$

which can be integrated to yield

$$C_p^y z_i(x) - C_p^y z_i(x_o) = C_{ep}^y (z_i(x) - z_i(x_o)) \quad (46)$$

where  $x_o$  is the distance where entrainment of the penetrated plume commences. Since  $C_p(x_o) = 0$ , Eq. (46) simplifies to

$$C_p^y = C_{ep}^y (1 - z_i(x_o)/z_i(x)) . \quad (47)$$

For now, we assume that the time  $t_o$  and distance  $x_o$  are those values where the mean CBL height  $\bar{z}_i = z_i(x_o)$  is attained since the penetration fraction  $P$  is based on that height; this will be explored further.

There are two additional variables needed to complete the penetrated plume dispersion model:  $C_{ep}^y$  and the  $z_i(t)$  or  $z_i(x)$ . The  $C_{ep}^y$  is found from a mass flux balance for the penetrated plume:

$$\int_{\bar{z}_i}^{z_t} U C_{ep}^y dz = U C_{ep}^y (z_t - \bar{z}_i) = PQ , \quad (48)$$

where the vertical concentration distribution in the penetrated plume is assumed to be uniform consistent with the penetration model (Section 4),  $z_t$  is the height of the plume top found from that model, and  $P$  is the penetration fraction. Equation (48) yields

$$C_{pe}^y = \frac{PQ}{U(z_t - z_i(x_o))} , \quad (49)$$

and substitution of this into Eq. (47) gives a prediction for the penetrated plume contribution,  $C_p^y(x)$ , to the CWIC in the CBL as

$$C_p^y(x) = \frac{PQ}{U\bar{z}_i} \frac{z_i(x) - \bar{z}_i}{z_t - \bar{z}_i} , \quad (50)$$

where we have replaced  $z_i(x_o)$  by  $\bar{z}_i$ . **This expression states that the increase in the penetrated plume concentration in the CBL or mixed layer increases linearly with the amount or fraction of the elevated plume entrained into the mixed layer.**

The CBL height  $z_i$  as a function of time  $t$  or distance ( $x = Ut$ ) is found from Carson's (1973) model as used by Weil et al. (1997) and discussed further in Section 6.

## 6. Model Comparisons with Field Observations

The field data for the model comparisons included ground-level concentrations of stack effluents, meteorological variables, and stack conditions from Maryland power plants and the

Kincaid (Illinois) power plant. The source and measurement conditions are discussed below for the two data sets. Briefly, the boundary layer and meteorological variables were found as follows: 1) the surface heat flux was assumed proportional to the measured insolation, 2) the mean wind speed  $U$  was obtained from balloon-tracked wind profiles (Maryland) or extrapolated upwards from the 10-m level wind using Monin-Obukhov (MO) similarity theory (Kincaid), and 3) the friction velocity was found from MO theory using the 10-m wind speed (Kincaid) or evaluated with less precision assuming  $u_* = U/16$  (Maryland). Further details are given in Weil et al. (1997).

The CBL height,  $z_i$ , was determined from observed temperature profiles either at the sites or from radiosondes at nearby weather stations. It was chosen subjectively as the height at which the vertical temperature gradient first became isothermal ( $\partial\Theta/\partial z = 0.01^\circ\text{C}/\text{m}$ ) above a ground-based, well-mixed layer. The  $z_i$  was interpolated with time between the observed profiles using a modified version of the Carson (1973) model (Weil and Brower, 1983), which is based on an energy balance of the CBL. The modified model accounts for an arbitrary-shaped  $\Theta(z)$  profile from an early morning sounding. However, the soundings from the original work (Weil et al., 1997) were not readily available for this study, but the  $\partial\Theta_a/\partial z$  above the CBL was important and necessary for estimating plume penetration of the CBL.

A default value of  $\partial\Theta_a/\partial z = 0.01^\circ\text{C}/\text{m}$  was used for most of the cases at the Maryland plants based on an average value found at the Morgantown plant (Weil, 1980). However, in early morning situations when  $z_i$  was low ( $< 500$  m), an explicit calculation of  $\partial\Theta_a/\partial z$  was adopted. In these cases, the  $\partial\Theta_a/\partial z$  between reported  $z_i$  values was found from the original Carson (1973) model for an assumed constant  $\partial\Theta/\partial z$ :

$$z_{i2}^2 = z_{i1}^2 + \frac{1 + 2A}{\partial\Theta/\partial z} \int_{t_1}^{t_2} \frac{Q_o(t)dt}{\rho c_p}, \quad (51)$$

where  $Q_o(t)$  is the surface heat flux at time  $t$ ,  $\rho$  and  $c_p$  are the density and specific heat of air, and subscripts “1” and “2” denote the reported  $z_i$  at two times  $t_1$  and  $t_2$ . Given  $Q_o(t)$ ,  $z_{i1}$ , and  $z_{i2}$ , one can estimate the potential temperature gradient. It is especially important to know the  $\partial\Theta_a/\partial z$  for low  $z_i$  values when plume penetration can be significant.

## 6.1. Maryland Power Plants

### 6.1.1. Source and measurement conditions

The Maryland power plants—Chalk Point, Dickerson, and Morgantown—were in remote areas and far from other sources of  $\text{SO}_2$ , the tracer monitored. Crosswind profiles of  $\text{SO}_2$

were measured from a mobile instrumented van that made repeated passes through the plume along roads transverse to the plume centerline. Typically, six profiles were measured along the same route during a 1-h interval and from them, an average crosswind ( $y$ ) profile was constructed. The maximum concentration from the average profile was used in the model evaluation.

In addition, ten additional high hourly-averaged concentrations from fixed monitors were obtained during light-wind convective conditions close to the sources ( $x < 3$  km). Two of the measurements were from the Morgantown plant and eight were from three midwest plants: Muskingham River (Ohio), John Sevier (Tennessee), and Cumberland (Tennessee). The Maryland plants had stacks ranging from 122-213 m tall and SO<sub>2</sub> emission rates varying from 0.7 to 4 kg/s; for the midwest plants, the stack heights ranged from 107-305 m and the SO<sub>2</sub> emission rates from 3.9 to 10.5 kg/s. Other details are given in Weil et al. (1997).

### 6.1.2. Evaluation results

To assess the improvement of the new model over previous models, we compared the new model results with those from the earlier PDF model (Weil et al., 1997). The PDF model served as the basis and starting point of the AERMOD convective dispersion formulation. For the Maryland plants, it was expected that the new model would perform about the same as the PDF model because there were not a large number ( $N$ ) of very high  $F_*$  cases;  $N = 11$  for  $0.2 \leq F_* < 0.4$  and  $N = 3$  for  $F_* \geq 0.4$ . In addition, the data scatter was typically large such that the uncertainty in the mean or geometric mean of the predicted-to-observed concentration ratio,  $C_{pred}/C_{obs}$ , was large.

For this evaluation, there were a total of 38 high  $F_*$  cases: 30 from the Maryland plants and 8 from the midwest plants with the meteorology better documented for the Maryland sites. High  $F_*$  was defined as  $F_* \geq 0.07$  as noted earlier.

Figure 6 compares the predicted arc-maximum SO<sub>2</sub> concentrations from the new and PDF models with the observed concentrations at a number of distances. As can be seen, the agreement between  $C_{pred}$  and  $C_{obs}$  appear reasonable and similar for the two models, where the solid lines indicate equal values of  $C_{pred}$  and  $C_{obs}$  and the dashed lines denote predictions within a factor of 2 of the observations. The visual results (Fig. 6) are supported by the statistics of the comparisons for which we obtain the geometric mean ( $GM$ ) and geometric standard deviation ( $GSD$ ) of  $C_{pred}/C_{obs}$  and the number of predictions within a factor of 2 of the observations,  $Fac2$ . Over all comparisons, the  $GM$ ,  $GSD$ , and  $Fac2$  were 0.90, 2.12,

and 68% for the new model and 1.13, 2.15, and 66% for the PDF model.

The uncertainty in the  $GM$  can be estimated from the 95% confidence limits of a log-normal distribution using the above  $GSD$  and number of comparisons (see Weil et al., 1997). With  $N = 38$ , this yields an uncertainty factor of 1.27 leading to an uncertainty range about the  $GM$  of  $1/1.27 GM$  to  $1.27 GM$ . This leads to no statistically significant difference between the new model and PDF model results, i.e., the uncertainty ranges of the two models overlap.

For the total number of comparisons ( $N = 38$ ), the default  $\partial\Theta_a/\partial z$  and the explicit value (from Eq. 51) were adopted in 33 and 5 cases, respectively. For the 5 cases, the predicted concentrations led to a  $GM = 1.13$ , a  $GSD = 1.68$ , and a  $Fac2$  of 80%. In contrast, predictions based on the default  $\partial\Theta_a/\partial z$  for the 5 cases produced somewhat poorer results: a  $GM = 0.79$ ,  $GSD = 2.49$ , and  $Fac2$  of 60%. The latter results were almost entirely attributed to one case with a  $z_i = 190$  m, a predicted penetration fraction  $P$  of  $\simeq 1$ , and a very low  $C_{pred}$ ,  $C_{pred}/C_{obs} = 0.19$ . In contrast, the explicitly calculated  $\partial\Theta_a/\partial z$  ( $= 0.048^\circ\text{C}/\text{m}$ ) led to a  $P = 0.72$  and  $C_{pred}/C_{obs} = 0.74$ . Thus, the larger temperature gradient produced better results—less plume penetration and a higher concentration, which was more in line with the observed concentration.

As noted earlier, the meteorological conditions were better known for the Maryland plants than the midwest plants, and thus the statistics were computed for the Maryland cases only. For the Maryland runs ( $N = 30$ ), the new model statistics were  $GM = 1.07$ ,  $GSD = 2.00$ , and  $Fac2 = 70\%$ ; for the PDF model, they were  $GM = 1.30$ ,  $GSD = 2.02$ , and  $Fac2 = 67\%$ . Hence, there was a slight improvement in the results for the Maryland only runs.

## 6.2. Kincaid Power Plant

### 6.2.1. Source and measurement conditions

The Kincaid is located in a flat rural area near Springfield, Illinois. Continuous releases of  $\text{SF}_6$  from the 187-stack were conducted over about 30 experiments, each lasting typically 6-9 hr. Hourly averaged  $\text{SF}_6$  ground-level concentrations (GLCs) were made at 200 monitors distributed on five to seven arcs at distances of 0.5 to 50 km downstream of the source. The concentration maxima were used for comparison to the modeled plume centerline values.

### 6.2.2. Model evaluation

For Kincaid, our focus was on concentrations in the highest  $F_*$  category of  $F_* \geq 0.5$  since

there were only 2 cases of such values from the Maryland data set.

## 7. References

- Baerentsen, J.H., and R. Berkowicz, 1984: Monte Carlo simulation of plume dispersion in the convective boundary layer. *Atmos. Environ.*, **18**, 701–712.
- Berkowicz, R., H.R. Oleson, and U. Torp, 1986: The Danish Gaussian air pollution model (OML); Description, test and sensitivity analysis in view of regulatory applications. *Air Pollution Modeling and Its Application V*, C. De Wispelaere, F.A. Schiermier, and N.V. Gillani, Eds., Plenum, New York, 453–481.
- Briggs, G.A., 1975: Plume rise predictions. *Lectures on Air Pollution and Environmental Impact Analyses*, D.A. Haugen, Ed., Amer. Meteor. Soc., Boston, 59–111.
- Briggs, G.A., 1984: Plume rise and buoyancy effects. *Atmospheric Science and Power Production*, D. Randerson, Ed., U.S. Dept. of Energy DOE/TIC-27601, available from NTIS as DE84005177, 327–366.
- Briggs, G.A., 1985: Analytical parameterizations of diffusion: the convective boundary layer. *J. Climate Appl. Meteor.*, **24**, 1167–1186.
- Carson, D.J., 1973: The development of a dry inversion-capped convectively unstable boundary layer. *Quart J. Roy. Meteor. Soc.*, **90**, 450–467.
- Cimorelli, A., S.G. Perry, A. Venkatram, J.C. Weil, R.J. Paine, R.B. Wilson, R.F. Lee, W.D. Peters, and R.W. Brode, 2005: AERMOD: A dispersion model for industrial source applications. Part 1. General model formulation and boundary layer characterization. *J. Appl. Meteorol.*, **44**, 682–693.
- Deardorff, J.W., and G.E. Willis, 1982: Ground-level concentrations due to fumigation into an entraining mixed layer. *Atmos. Environ.*, **16**, 1159–1170.
- Deardorff, J.W., and G.E. Willis, 1985: Further results from a laboratory model of the convective planetary boundary layer. *Bound.-Layer Meteor.*, **32**, 205–236.
- Hicks, B.B., 1985: Behavior of turbulent statistics in the convective boundary layer. *J. Clim. Appl. Meteorol.*, **24**, 607–614.
- Johnson, W.B., and E.E. Uthe, 1969: Lidar study of stack plumes. Stanford Research Institute, Palo Alto, Final report, SRI Project 7289 for Dept. Health, Education, and Welfare, National Air Pollution Control Administration, 116 pp.
- Perry, S.G., A.J. Cimorelli, R.J. Paine, R.W. Brode, J.C. Weil, A. Venkatram, R.B. Wilson,

- R.F. Lee, and W.D. Peters, 2005: AERMOD: A dispersion model for industrial source applications. Part II: Model performance against 17 field study databases. *J. Appl. Meteorol.*, **44**, 694–708.
- Turner, J.S., 1978: *Buoyancy effects in fluids*. Cambridge University Press, 367 pp.
- Weil, J.C., 1980: Performance of simple models for stack plume dispersion during convective conditions. Revision 1. Martin Marietta Environmental Center, Baltimore, Report No. PPSP-MP-30, 34 pp.
- Weil, J.C., 1988a: Dispersion in the convective boundary layer. *Lectures on Air Pollution Modeling*, A. Venkatram and J.C. Wyngaard, Eds., Amer. Meteor. Soc., Boston, 167–165.
- Weil, J.C., 1988b: Plume rise. *Lectures on Air Pollution Modeling*, A. Venkatram and J.C. Wyngaard, Eds., Amer. Meteor. Soc., Boston, 119–166.
- Weil, J.C., and R.P. Brower, 1983: Estimating convective boundary layer parameters for diffusion applications. Martin Marietta Environmental Center, Columbia, MD, Report No. PPSP-MP-48, 37 pp.
- Weil, J.C., and R.P. Brower, 1984: An updated Gaussian plume model for tall stacks. *J. Air Pollut. Control Assoc.*, **34**, 818–827.
- Weil, J.C., L.A. Corio, and R.P. Brower, 1997: A PDF dispersion model for buoyant plumes in the convective boundary layer. *J. Appl. Meteor.*, **36**, 982–1003.
- Weil, J.C., W.H. Snyder, R.E. Lawson, and M.S. Shipman, 2002: Experiments on buoyant plume dispersion in a laboratory convection tank. *Bound.-Layer Meteorol.*, **102**, 367–414.
- Willis, G.E., and J.W. Deardorff, 1976: A laboratory model of diffusion into the convective planetary layer. *Quart. J. Roy. Meteor. Soc.*, **102**, 427–445.
- Willis, G.E., and J.W. Deardorff, 1987: Buoyant plume dispersion and inversion entrapment in and above a laboratory mixed layer. *Atmos. Environ.*, **21**, 1725–1735.
- Wyngaard, J.C., 1988: Structure of the PBL. *Lectures on Air Pollution Modeling*, A. Venkatram and J.C. Wyngaard, Eds., Amer. Meteor. Soc., Boston, 9–61.

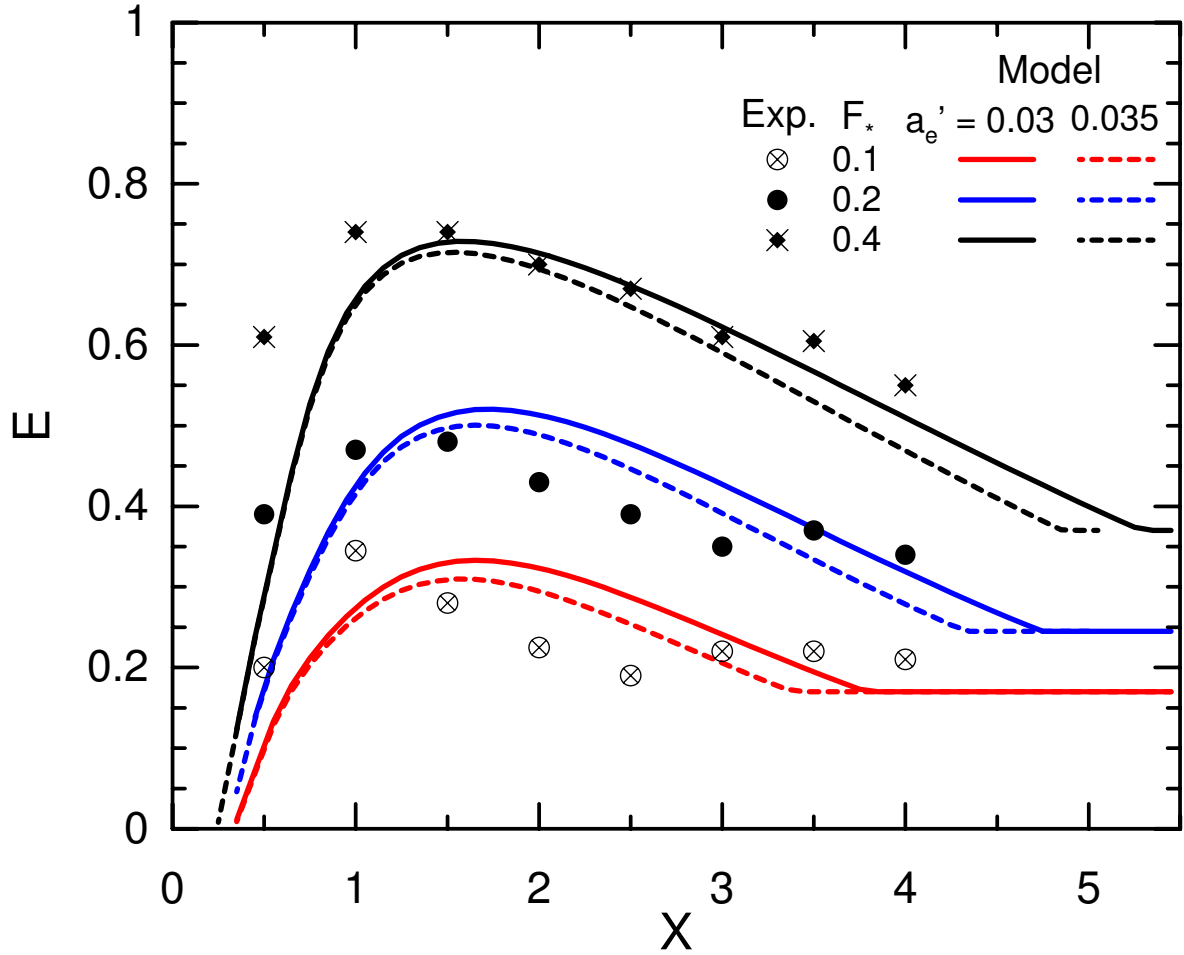


Figure 1: Plume entrainment as a function of dimensionless distance for highly buoyant plumes in the convective boundary layer; points are from the convection tank experiments of Weil et al. (2002).

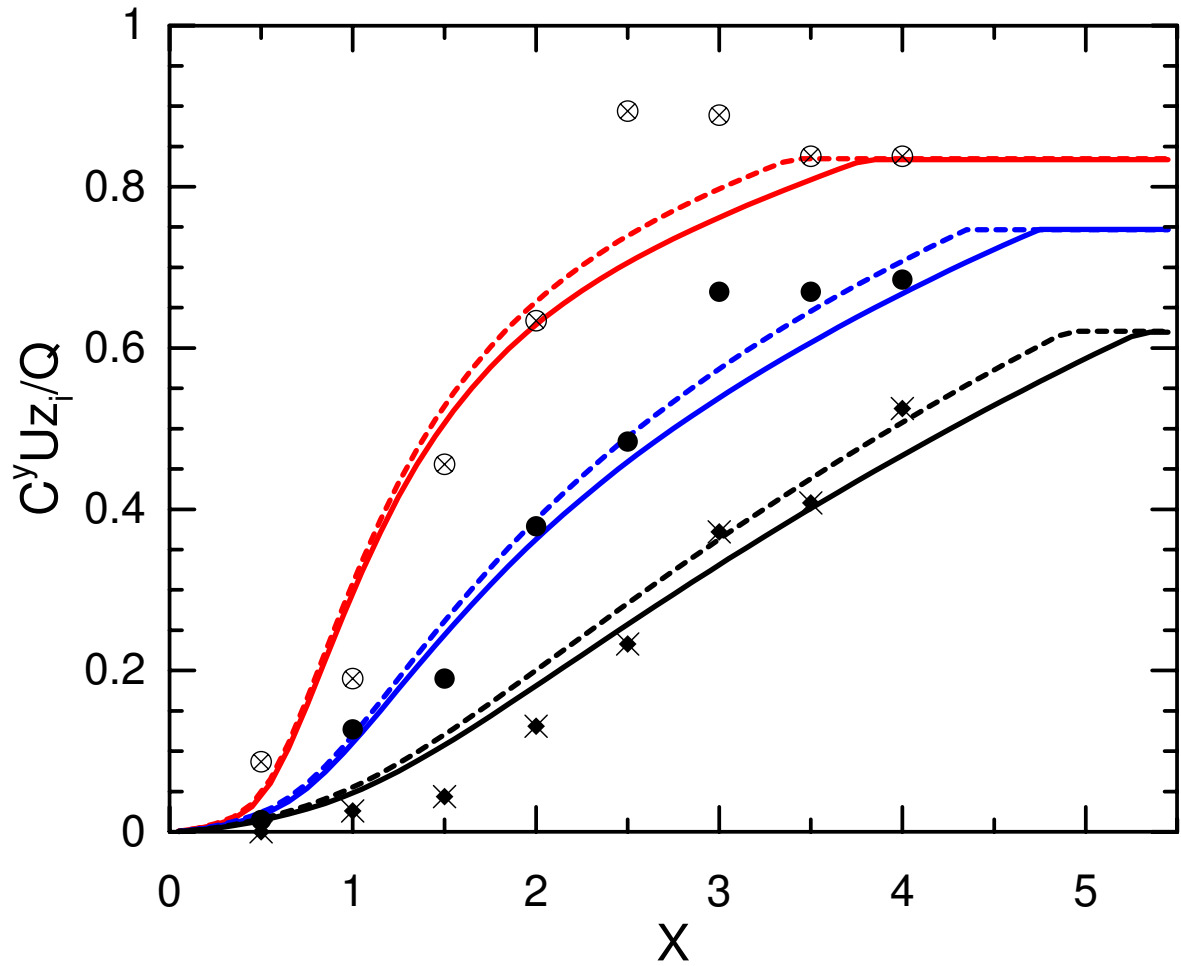


Figure 2: Dimensionless CWIC surface concentration as a function of dimensionless distance for highly buoyant plumes in the convective boundary layer; for key to lines (model) and points (convection tank data) see Fig. 1.

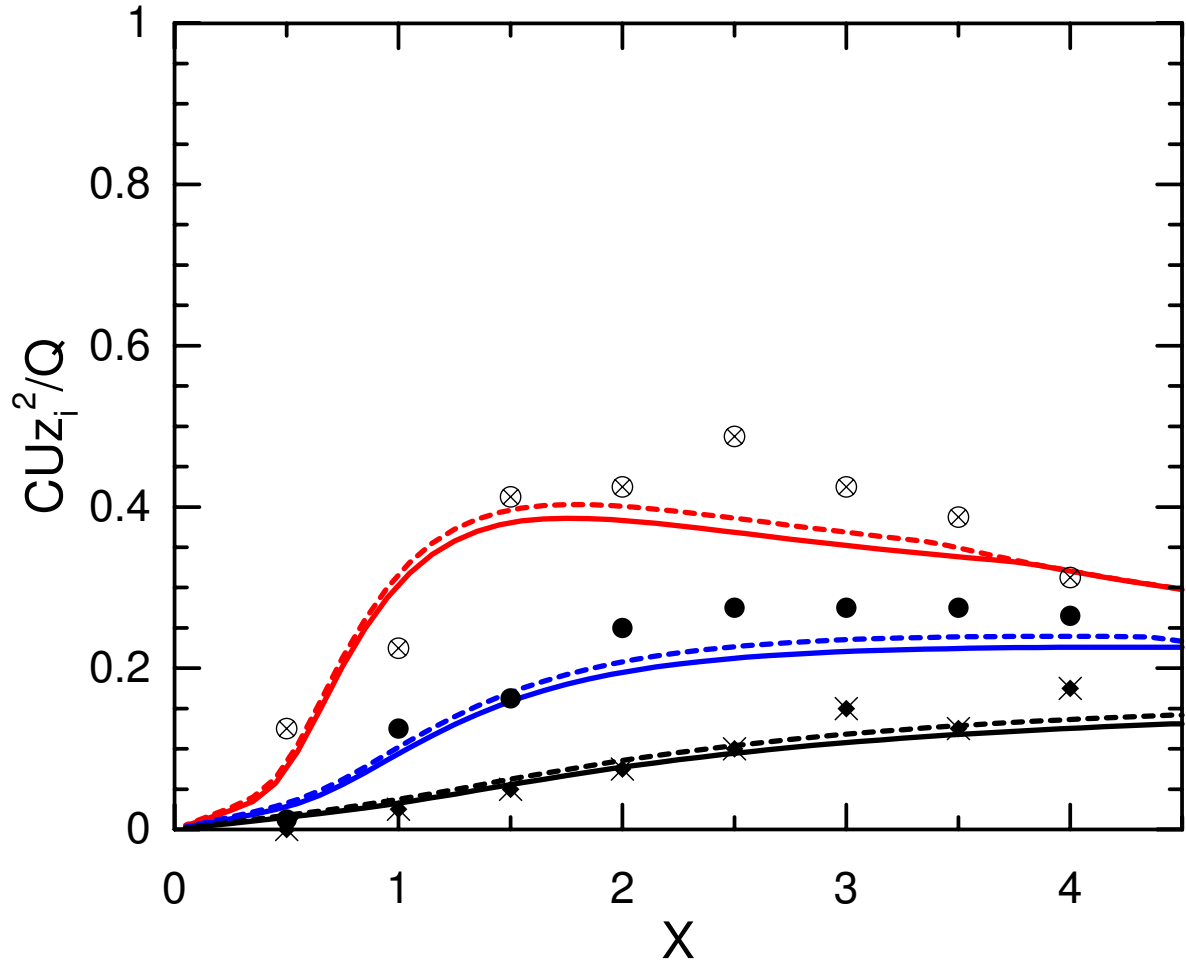


Figure 3: Dimensionless surface concentration along plume centerline as a function of dimensionless distance for highly buoyant plumes in the convective boundary layer, where  $a_y = 0.8$  for lateral dispersion in Eq. (29a); for key to lines (model) and points (convection tank data) see Fig. 1.

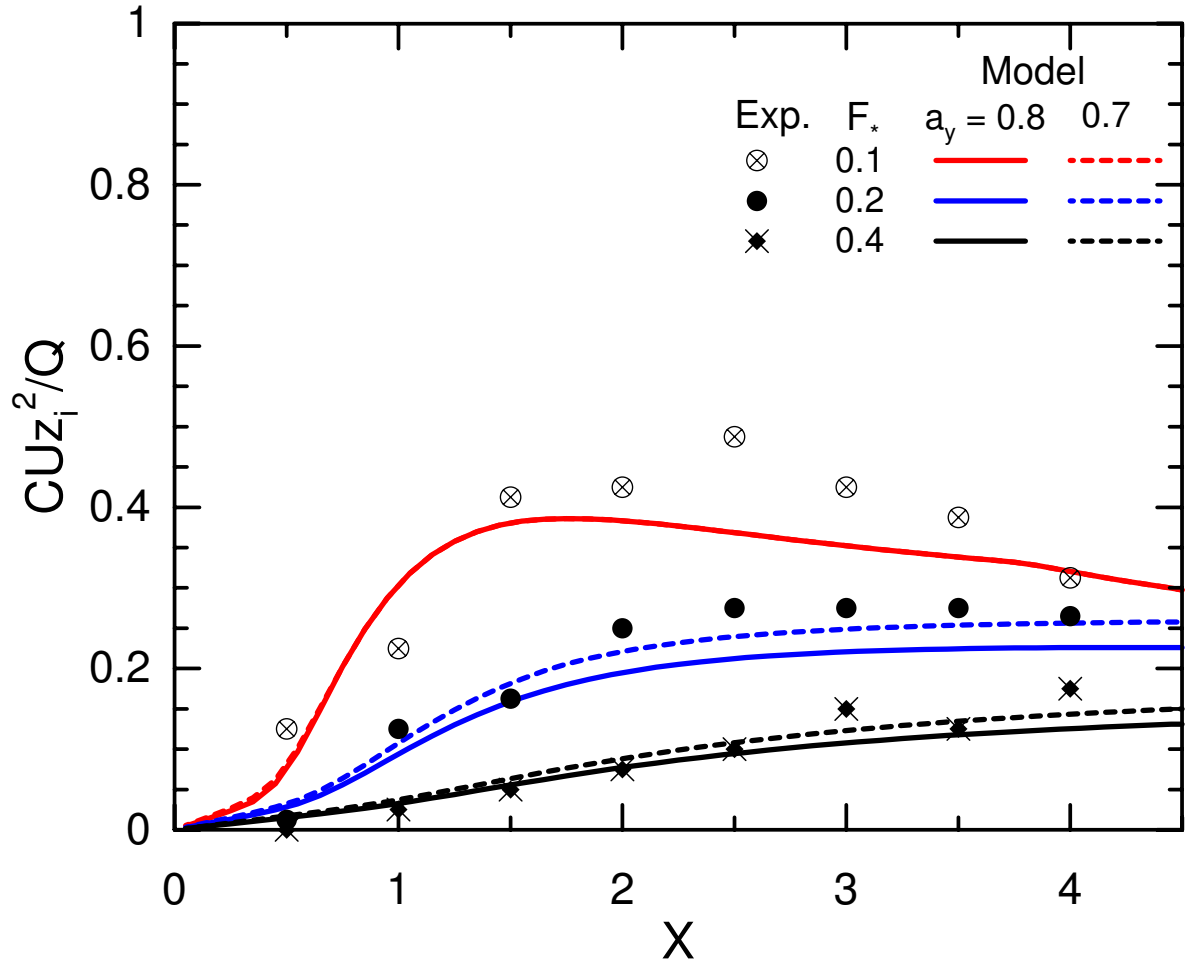


Figure 4: Dimensionless surface concentration along plume centerline as a function of dimensionless distance for highly buoyant plumes in the convective boundary layer, where  $a'_e = 0.03$  and  $a_y$  is coefficient for lateral dispersion in Eq. (29a); points are from the convection tank experiments of Weil et al. (2002).

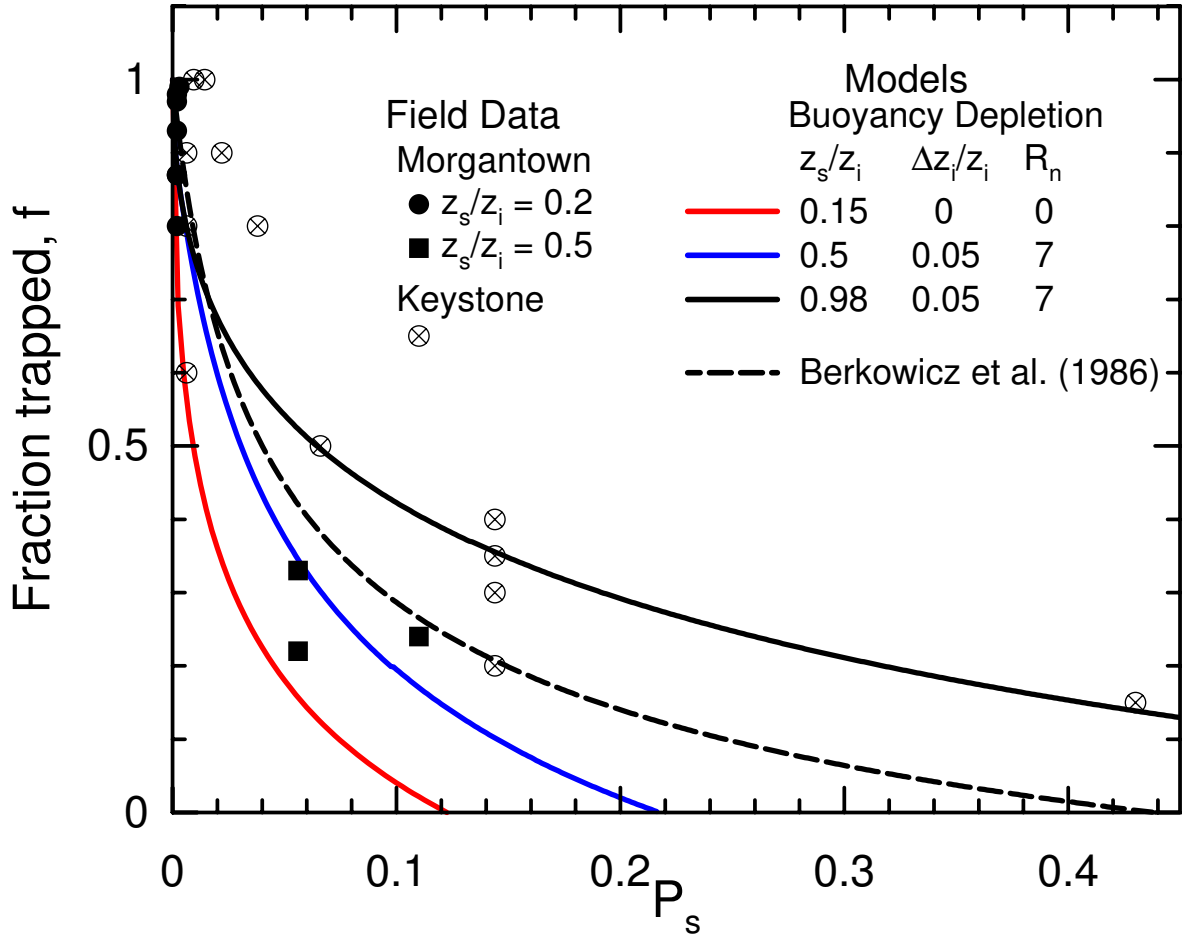


Figure 5: Fraction of plume trapped beneath an elevated inversion capping the convective boundary layer as a function of dimensionless buoyancy flux based on penetration conditions. Comparison between models and field observations from two power plants—Morgantown (Weil, 1980) and Keystone (Briggs, 1984; Johnson and Uthe, 1969).

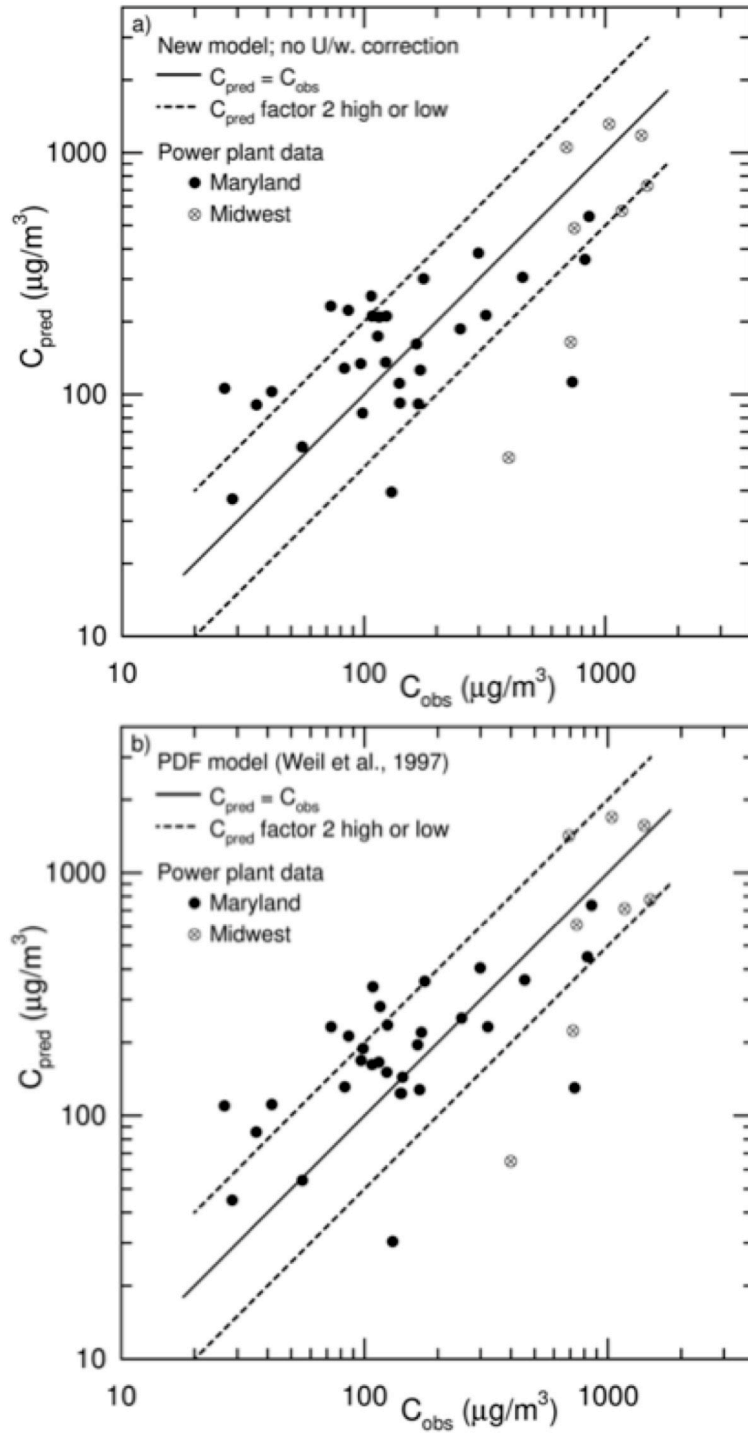


Figure 6: Comparison of new model and earlier PDF model (Weil et al., 1997) with ground-level SO<sub>2</sub> concentrations downwind of Maryland and midwest power plants; results for high  $F_*$  ( $\geq 0.07$ ) and no  $U/w_*$  correction to the lateral dispersion.

# DISTANCE-DEBUG and HRBINARY: Modeling Tools for Unpacking the AERMOD BlackBox

A&WMA Annual Conference and Exhibition

Pittsburgh, PA

June 5-8, 2017

Abstract # 298000

Carlos Szembek<sup>1</sup>,  
Robert Paine<sup>2</sup>, Mark Garrison<sup>1</sup>

<sup>1</sup> ERM, <sup>2</sup> AECOM

*The business of sustainability*



# DISTANCE-DEBUG and HRBINARY: Modeling Tools for Unpacking the AERMOD BlackBox

AERMOD, the U.S. Environmental Protection Agency preferred air dispersion model, is a steady-state model that incorporates concepts of planetary boundary layer turbulence with plume dispersion dynamics. The model statistically approximates horizontal and vertical plume transport interacting with hourly meteorology, terrain and any identified impact from building downwash and urban enhanced buoyancy. An array of pre-processors generates meteorological, topographic and building downwash inputs for AERMOD. These inputs allow AERMOD to calculate hourly ground level concentration gradients.

Despite the quality of the inputs, assumptions or faulty implementation within a model's formulation can potentially generate questionable or even erroneous results. While there are several debugging options for investigating AERMOD's intermediary calculations, these current options produce massive cumbersome output files unless run on a single receptor or single hour. The Electric Power Research Institute (EPRI) sponsored a study to develop a model tool, "DISTANCE-DEBUG" that would efficiently diagnose causes for predicted high concentrations. DISTANCE-DEBUG generates a streamlined hourly file echoing key meteorology and tabulating AERMOD-calculated plume dynamics for each point, volume and area source. Hourly intermediary concentration calculations are also reported for the coherent plume. Example cases will be presented that highlight the DISTANCE-DEBUG features, particularly its legibility and ease of use.

A separate EPRI-funded tool, "HRBINARY", in conjunction with a concentration processor ("BINMERGE-2017") will be discussed that allows for binary output from multiple AERMOD runs to be post-processed, including an example case of two buoyant line sources using different buoyancy parameters, an option not currently available in AERMOD version 16216r.

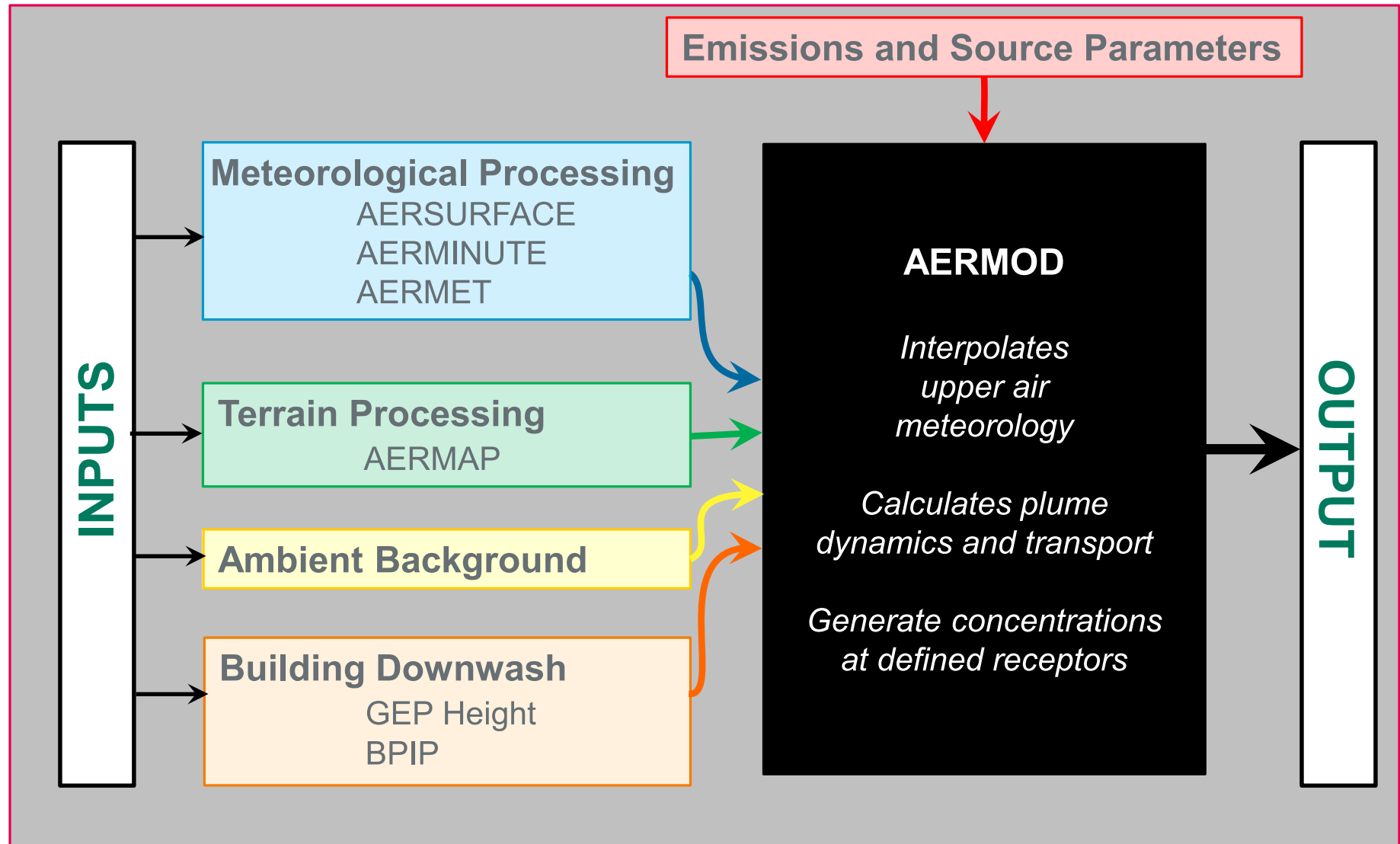
# Overview

---

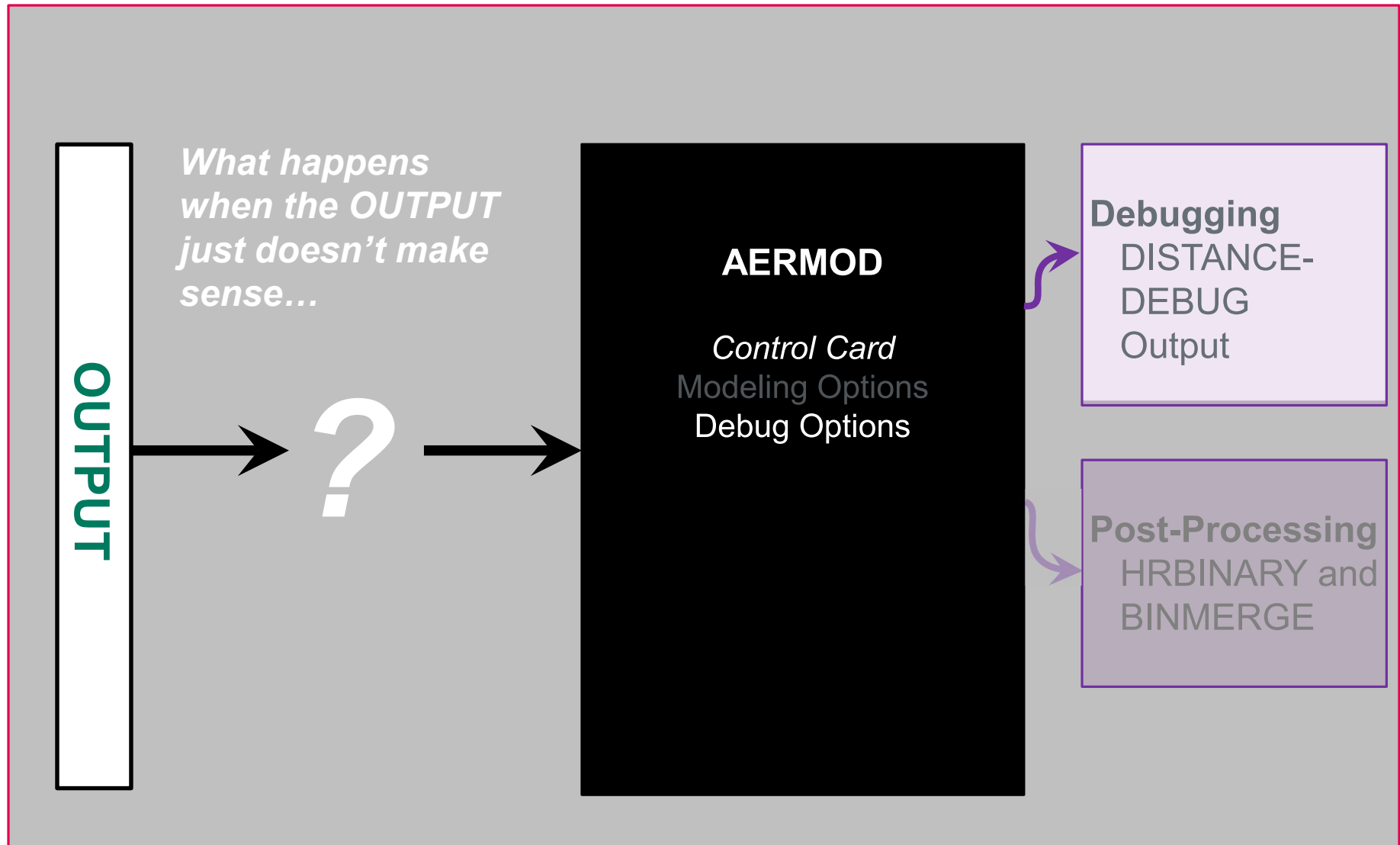
In 2012, the Electric Power Research Institute (EPRI) sponsored two modeling tools:

- **DISTANCE-DEBUG** an AERMOD debugging tool intended to streamline the diagnostics associated with predicted high concentrations.
- **HRBINARY**, a post-processing option in AERMOD that (in conjunction with another post-processor, “BINMERGE”) allows for merged output from multiple (but separately performed) AERMOD runs to be analyzed to generate NAAQS-ranked design value output.

# The AERMOD BlackBox



# The AERMOD BlackBox



# Debugging...so many options

---

- **MODEL:** General modeling debug file
- **METEOR:** General meteorological
- **PRIME:** PRIME downwash
- **DEPOS:** Deposition (for both gas & particle)
- **AREA or LINE:** Area, Line and Open Pit
- **PVMRM or OLM or ARM or ARM2:** NO<sub>x</sub>-to-NO<sub>2</sub> conversion

*So why the need for another debug file?*

# ...can be overwhelming

## Excerpt from 60,000 line PRIME Debug file

PRIME Module Results for Current Source and Hour  
(all lengths in meters)

```
-----  
      XB      X      Z  Hwake  Hcav   Sz    Sy    Ufac  dUfac  R->Sz  dRdx  Pos  Szcav  Sycav  
      48.5     0.0    42.7   74.9   49.6    0.0   0.0   0.639  0.000    0.0  0.000   1   14.2   34.5  
      48.5     0.0    43.7   74.9   49.6    0.3   0.3   0.638  0.000    1.6  0.000   1   14.2   34.5  
.  
.  
.  
      970.2  921.8   47.0  182.7    0.0   66.8   86.9   0.832  0.001   47.2  0.038   3   65.1  109.4  
     1008.2  959.8   46.6  185.0    0.0   67.8   88.3   0.835  0.001   47.2  0.003   3   66.2  111.1  
  
YR/MN/DY/HR:          10070101  ISRC:          1  IREC:          1  
  
GAMFACT = 6.940565230893733E-004  
AERVAL  = 5.69810811953800  
PRMVAL  = 121.518405396800  
HRVAL   = 5.77849395236943  
  
YR/MN/DY/HR:          10070101  
  
WAKE_SCALES inputs:  
  HB    = 49.6200000000000    (m)  
  WB    = 86.5100000000000    (m)  
  LB    = 112.9400000000000    (m)  
  
WAKE_SCALES output:  
  Scale length (R)          = 59.7209366698920  
  Max. cavity height (HR)   = 62.7586060673762  
  Length of downwind cavity (LR) = 85.7776606883091  
  Length of roof cavity (LC) = 53.7488430029028  
  
PRIME Effective Parameters:  
ZLO, ZHI    = 0.500000000000000    178.035578770569  
SWEFF, SVEFF = 0.168846389190163    0.343228206052833  
UEFF, TGEFF = 6.86456412105667    5.997118404810090E-002
```

7

*The business of sustainability*

# ...can be overwhelming (cont'd.)

## Excerpt from 60,000 line PRIME Debug file

NNP	X	Y	Z	R	U	V	W	USC	PHI	DEN	TP	UA	RA	TA	DUDZ	DPDZ	DZDS	DYDS	IPOS	DELTAZ
1	0.08	0.00	47.62	2.61	1.78	0.00	9.65	9.82	1.3887	1.090	312.02	5.57	1.180	288.37	0.057	0.070	0.000	0.000	1	0.994
2	0.35	0.00	48.58	3.47	2.84	0.00	7.02	7.58	1.1862	1.114	305.41	5.63	1.179	288.42	0.056	0.070	0.000	0.000	1	1.953
3	0.80	0.00	49.47	4.27	3.50	0.00	5.42	6.45	0.9974	1.129	301.38	5.67	1.179	288.48	0.056	0.069	0.000	0.000	1	2.839
4	1.40	0.00	50.27	4.97	3.93	0.00	4.41	5.91	0.8423	1.138	298.83	5.73	1.179	288.53	0.102	0.069	0.000	0.000	3	3.635
5	2.11	0.00	51.36	5.54	4.25	0.00	3.73	5.66	0.7212	1.144	297.15	5.81	1.178	288.59	0.103	0.069	0.387	0.000	3	4.730
6	2.88	0.00	52.39	6.01	4.48	0.00	3.27	5.54	0.6300	1.149	295.99	5.89	1.178	288.65	0.105	0.069	0.399	0.000	3	5.759
7	3.71	0.00	53.35	6.41	4.66	0.00	2.93	5.50	0.5609	1.152	295.16	5.96	1.178	288.71	0.106	0.069	0.393	0.000	3	6.716
8	4.57	0.00	54.23	6.76	4.80	0.00	2.67	5.49	0.5074	1.154	294.53	6.02	1.177	288.76	0.107	0.069	0.376	0.000	3	7.604
9	5.45	0.00	55.06	7.07	4.91	0.00	2.46	5.50	0.4649	1.156	294.03	6.08	1.177	288.81	0.109	0.069	0.354	0.000	3	8.429
10	6.35	0.00	55.83	7.35	5.01	0.00	2.30	5.51	0.4304	1.157	293.64	6.13	1.177	288.85	0.110	0.069	0.331	0.000	3	9.196
11	7.26	0.00	56.54	7.61	5.09	0.00	2.16	5.53	0.4016	1.159	293.31	6.17	1.176	288.90	0.111	0.069	0.307	0.000	3	9.910
12	8.19	0.00	57.21	7.86	5.16	0.00	2.04	5.55	0.3773	1.160	293.03	6.21	1.176	288.94	0.113	0.069	0.283	0.000	3	10.575
13	9.12	0.00	57.83	8.10	5.21	0.00	1.94	5.56	0.3565	1.160	292.79	6.24	1.176	288.97	0.114	0.069	0.260	0.000	3	11.196
14	10.06	0.00	58.41	8.32	5.27	0.00	1.85	5.58	0.3385	1.161	292.58	6.27	1.176	289.01	0.115	0.069	0.237	0.000	3	11.776

NUMRISE call to WAKE\_DFSN

x,y,z,z+zcum: 10.05785 0.00000 55.07828 58.40623  
ds,u,w : 1.00000 5.26501 1.85351  
xb,phi : 18.14785 0.33849  
szi,syi : 2.42068 2.46556

WAKE\_XA Calculations:

ambiz, ambiy = 2.459681142350115E-002 5.0000000000000001E-002  
farizt, fariyt = 3.197585485055150E-002 6.5000000000000002E-002  
xaz, xay = 1008.75405004838 1008.75405004838

----- WAKE\_DFSN: NWAK = 50  
Z-dispersion reaches ambient at: 1000.66405004838  
Y-dispersion reaches ambient at: 1000.66405004838  
xadj, yadj, xi (m) = -8.09000 -3.10000 18.14785  
xbc, distc, xdc (m) = 112.94000 104.85000 198.71766  
lwak, nws, npw = T 0 497  
lcav, ncs, npc = T 48

# DISTANCE-DEBUG: Focus on Clarity

\*\*\*\*\* AERMOD DISTANCE DEBUG FILE \*\*\*\*\*

## PLUME TYPES:

- GAUSSIAN:** Idealized plume under stable conditions or when the stack height > the mixing height under unstable conditions
- DIRECT:** Direct transport of plume material to the ground within the mixed layer
- INDIRECT:** Portion of the plume caught in convective updrafts but does not penetrate elevated inversions. The indirect plume material eventually is reflected down to the ground.
- PENETRATED:** Portion of the plume that penetrates the elevated inversion and is eventually re-entrained into the CBL (Convective Boundary Layer)

## OTHER TERMS USED:

- MEAND FRAC:** Meander fraction (m.f.); the fraction of the total concentration component associated with the meander component. The remaining fraction is assigned to the coherent component.
- PART PEN FRAC:** Partial penetration fraction
- HRVAL:** Overall calculated hourly concentration;  $HRVAL = (1-GAMFACT)*AERVAL + (GAMFACT*PRMVAL)$   
where  $AERVAL = m.f.*PANCake + (1 - m.f.)*COHERENT$   
For volume sources:  $HRVAL = (1-m.f.)*AERVAL + (m.f.)*PANCake$   
For area sources:  $HRVAL = AbsoluteValue (VAL)*QTK*EMIFAC$
- AERVAL:** Portion of hourly concentration not associated with downwash
- PRMVAL:** Portion of hourly concentration associated with downwash
- GAMFACT:** Gamma Factor; scaling factor associated with the PRMVAL
- PANCake:** Value from calculating a \*pancak-ing\* plume
- COHERENT:** The coherent portion of the plume NOT associated with downwash
- VAL:** Iterated integral hourly concentration for an area source
- QTK:** Adjusted emission rate factor
- EMIFAC:** Emission rate unit factor

\*\*\*\*\*

- NOTES:
- [1] The urban Monin-Obukhov length, URB\_OBULEN, and the urban mechanical mixing height, ZI\_URB, are displayed for only the first urban source group.
  - [2] GAMFACT & PRMVAL marked with:  
PLUME OUT OF WAKE designates no downwash due to the plume being outside the wake zone  
RCPTR OUT OF WAKE designates no downwash affect at the maximum receptor
  - [3] Hourly values and receptor numbers listed are for the MAXIMUM CONCENTRATION calculated for each source.
  - [4] The potential temperature gradient listed is at the stack height.
  - [5] Final plume height, effective windspeed (ueff), and the effective sigma v and w values are provided for only the COHERENT portion of the plume.  
The values associated with the MEANDER component are not listed.
  - [6] A less-than sign, <, is inserted at column 62 for events when ueff would not transport the plume for a given source in one hour to the distance of the maximum receptor.

## DISTANCE-DEBUG:

Each file begins with a legend of the extracted parameters

Some parameters are only reported for the **coherent plume** (versus the meander component of the plume)

# DISTANCE-DEBUG Output

## Basic met hourly met data

OBSERVED MET CONDITIONS FOR:	USTAR	WSTAR	OBULEN	URB_OBULEN	ZIMECH	ZICONV	ZI_URB	SFCZ0	THSTAR
YYMDDHH: 12040102	(m/s)	(m/s)	(m)	(m)	(m)	(m)	(m)	(m)	(K)
	0.13	-9.00	12.90	N.A.	103.00	-999.00	N.A.	0.4280	0.090

## Followed by point source data

### POINT SOURCES:

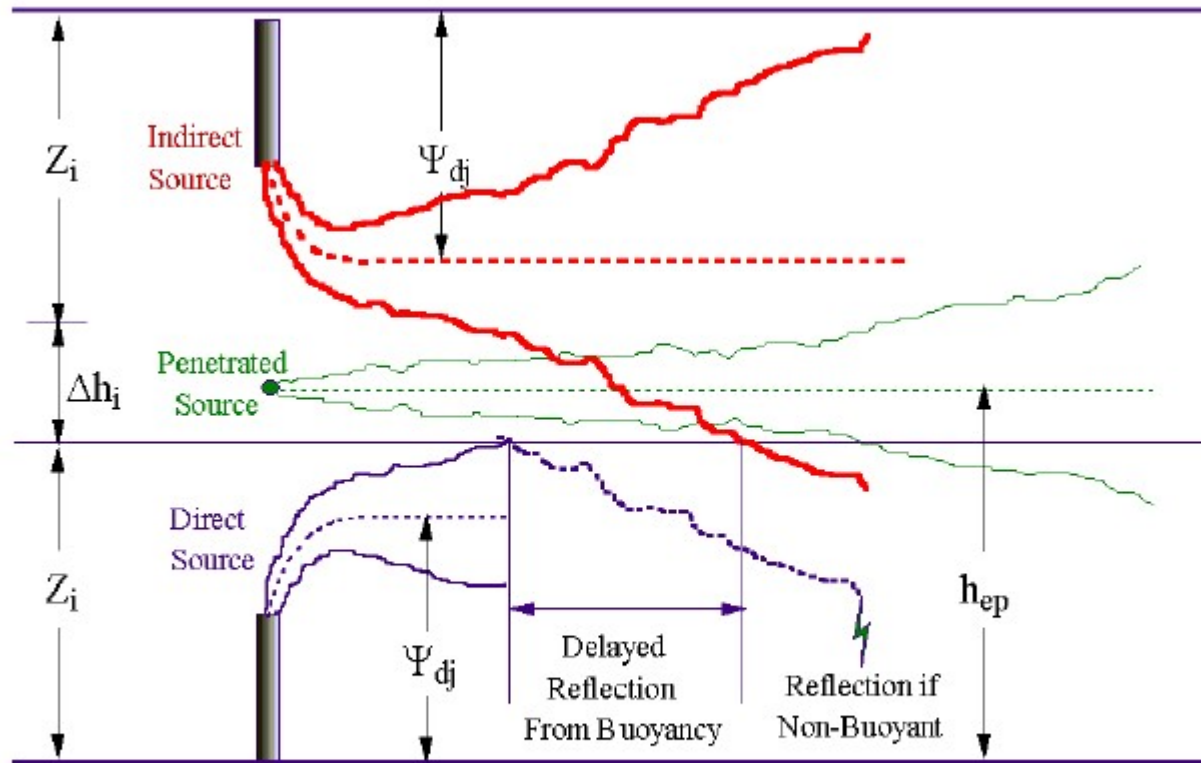
SOURCE ID	RCPT NO.	FINAL PLUME HT. (m)	DIST. FINAL PL. HT (m)	WDIR HT. (deg)	Effect. FINAL WSPD (m/s)	3600* ueff (m/s)	DISTANCE TO RECEIPT (m)	MEAND. PLUME TYPE	PART. PEN. FRAC.	EFFECT. SIGMA_V (m/s)	EFFECT. SIGMA_W (m/s)	HOURLY CONC. (µg/m3)	AERVAL (µg/m3)	COHERENT (µg/m3)	PANCAKE (µg/m3)	GAMFACT	PRMVAL (µg/m3)	POT. TEMP. GRAD. (K/m)	
P MERGE001	329	153.1	269.4	273.	2.669	9610.1	3242.0	GAU	0.025	0.000	0.200	0.052	35.017	0.000	0.000	0.000	PLUME OUT OF WAKE	0.01637	
MERGE001	<--- Source is not emitting during this hour																		
P POINT002	1130	31.5	172.3	273.	1.347	4848.7	9157.9	GAU	0.090	0.000	0.200	0.074	2.209	2.209	2.422	0.066	PLUME OUT OF WAKE	0.01637	
P POINT003	329	14.4	158.4	273.	1.347	4848.7	3202.3	GAU	0.073	0.000	0.200	0.074	13.187	13.019	14.021	0.330	1.000	13.187	0.01278
P POINT004	1099	30.6	172.3	273.	1.347	4848.7	8260.8	GAU	0.085	0.000	0.200	0.074	2.880	2.880	3.141	0.055	0.000	6.682	0.01278
P POINT005	325	16.2	158.4	273.	1.347	4848.7	2779.5	GAU	0.070	0.000	0.200	0.074	15.001	15.001	16.095	0.397	0.000	39.017	0.01278
P POINT006	332	14.6	158.4	273.	1.347	4848.7	3637.3	GAU	0.077	0.000	0.200	0.074	14.365	14.365	15.528	0.358	0.000	24.576	0.01278
P POINT007	333	15.6	158.4	273.	1.347	4848.7	3690.4	GAU	0.077	0.000	0.200	0.074	14.284	14.284	15.448	0.354	0.000	23.986	0.00781

For each source DISTANCE-DEBUG marks predicted max impacts too distant to be reached by the effective wind speed

### VOLUME AND AREA SOURCES:

SOURCE ID	RCPT NO.	FINAL PLUME HT. (m)	DIST. FINAL PL. HT (m)	WDIR HT. (deg)	Effect. FINAL WSPD (m/s)	3600* ueff (m/s)	DISTANCE TO RECEIPT (m)	MEAND. PLUME TYPE	PART. PEN. FRAC.	EFFECT. SIGMA_V (m/s)	EFFECT. SIGMA_W (m/s)	HOURLY CONC. (µg/m3)	AERVAL (µg/m3)	COHERENT (µg/m3)	PANCAKE (µg/m3)	GAMFACT	PRMVAL (µg/m3)	POT. TEMP. GRAD. (K/m)	
VOLUME01	<--- Source is not emitting during this hour																		
V VOLUME02	1105	45.0	0.0	273.	2.669	9610.1	14473.7	DIR	0.083	0.200	0.052	0.002	0.002	0.000	N.A.	N.A.			
VOLUME03	<--- Source is not emitting during this hour																		
V VOLUME04	1105	45.0	0.0	273.	2.669	9610.1	14255.1	DIR	0.082	0.200	0.052	0.002	0.002	0.000	N.A.	N.A.			
VOLUME05	<--- Source is not emitting during this hour																		
V VOLUME06	328	5.0	0.0	273.	0.929	3344.9	3055.8	DIR	0.222	0.200	0.079	0.507	0.648	0.017	N.A.	N.A.			
VOLUME07	<--- Source is not emitting during this hour																		
V VOLUME08	1090	35.0	0.0	273.	2.539	9141.4	14347.0	DIR	0.114	0.200	0.054	0.025	0.029	0.001	N.A.	N.A.			
VOLUME09	<--- Source is not emitting during this hour																		
V VOLUME10	324	5.0	0.0	273.	0.929	3344.9	2681.8	DIR	0.217	0.200	0.079	0.634	0.804	0.021	N.A.	N.A.			
A AREA01	325	10.0	0.0	273.	1.347	4848.7	3427.0	DIR	N.A.	0.200	0.074	236.915	0.237E+00	N.A.	0.1E-02	0.1E+07			

# Example of Reported Point Source Parameters



← *Mixing Height,  $z_i$*   
 $Z_{conv}$ ,  $Z_{mech}$  Or  $Z_{urb}$

*Final plume height (centerline)*  
 $\Psi_{dj} = H_s + H_p$

*Not shown:*

*Gaussian plume: idealized plume under stable conditions or during unstable conditions when stack height > mixing height*

# DISTANCE-DEBUG Output

OBSERVED MET CONDITIONS FOR: USTAR WSTAR OBULEN URB\_OBULEN ZLIMECH ZICONV ZI\_URB SFCZ0 THSTAR  
 YYMMDDHH: 12040102 (m/s) (m/s) (m) (m) (m) (m) (m) (m) (K)  
 0.13 -9.00 12.90 N.A. 103.00 -999.00 N.A. 0.4280 0.090

POINT SOURCES:

SOURCE ID	RCPT NO.	FINAL PLUME HT. (m)	DIST. FINAL PL. HT (m)	WDIR HT. (deg)	Effect. FINAL WSPD (m/s)	3600* ueff (m/s)	<----- DISTANCE TO RECEIPT (m)	-----> MEAND. PLUME TYPE	PEN. FRAC.	EFFECT. SIGMA_V (m/s)	EFFECT. SIGMA_W (m/s)	HOURLY CONC. (µg/m3)	AERVAL (µg/m3)	COHERENT (µg/m3)	PANCAKE (µg/m3)	GAMFACT	PRMVAL (µg/m3)	POT. TEMP. GRAD. (K/m)
P MERGE001	329	153.1	269.4	273.	2.669	9610.1	3242.0	GAU	0.025	0.200	0.052	35.017	0.000	0.000	0.000	PLUME OUT OF WAKE		0.01637
MERGE001	<--- Source is not emitting during this hour																	
P POINT002	1130	31.5	172.3	273.	1.347	4848.7	9157.9	GAU	0.090	0.200	0.074	2.209	2.209	2.422	0.066	PLUME OUT OF WAKE		0.01637
P POINT003	329	14.4	158.4	273.	1.347	4848.7	3202.3	GAU	0.073	0.200	0.074	13.187	13.019	14.021	0.330	1.000	13.187	0.01278
P POINT004	1099	30.6	172.3	273.	1.347	4848.7	8260.8	GAU	0.085	0.200	0.074	2.880	2.880	3.141	0.055	0.000	6.682	0.01278
P POINT005	325	16.2	158.4	273.	1.347	4848.7	2779.5	GAU	0.070	0.200	0.074	15.001	15.001	16.095	0.397	0.000	39.017	0.01278
P POINT006	332	14.6	158.4	273.	1.347	4848.7	3637.3	GAU	0.077	0.200	0.074	14.365	14.365	15.528	0.358	0.000	24.576	0.01278
P POINT007	333	15.6	158.4	273.	1.347	4848.7	3690.4	GAU	0.077	0.200	0.074	14.284	14.284	15.448	0.354	0.000	23.986	0.00781

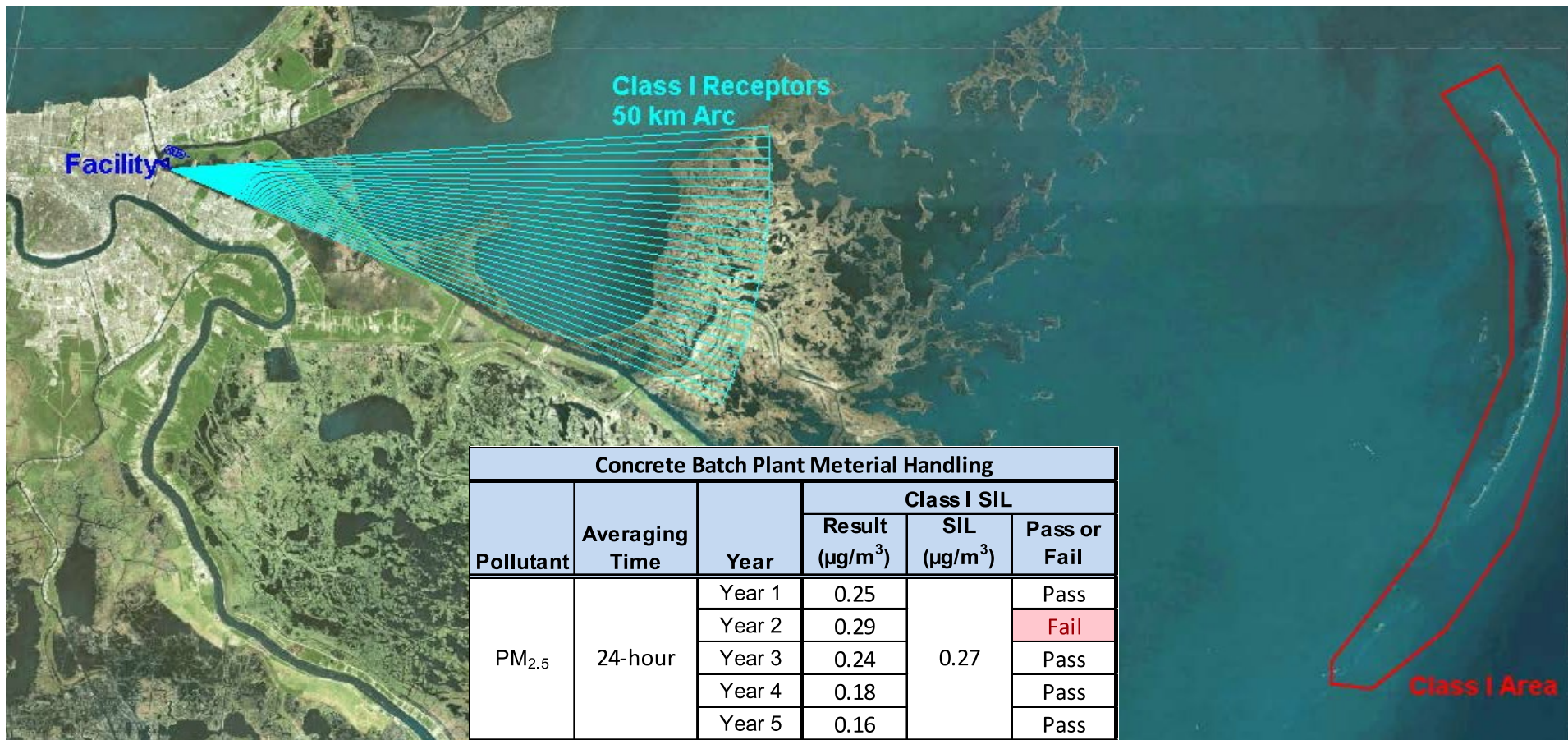
VOLUME AND AREA SOURCES:

SOURCE ID	RCPT NO.	FINAL PLUME HT. (m)	DIST. FINAL PL. HT (m)	WDIR HT. (deg)	Effect. FINAL WSPD (m/s)	3600* ueff (m/s)	<----- DISTANCE TO RECEIPT (m)	-----> MEAND. PLUME TYPE	EFFECT. SIGMA_V (m/s)	EFFECT. SIGMA_W (m/s)	HOURLY CONC. (µg/m3)	AERVAL or VAL (µg/m3)	PANCAKE (µg/m3)	QTK	EMIFAC	
VOLUME01	<--- Source is not emitting during this hour															
V VOLUME02	1105	45.0	0.0	273.	2.669	9610.1	14473.7	DIR	0.083	0.200	0.052	0.002	0.002	0.000	N.A.	N.A.
VOLUME03	<--- Source is not emitting during this hour															
V VOLUME04	1105	45.0	0.0	273.	2.669	9610.1	14255.1	DIR	0.082	0.200	0.052	0.002	0.002	0.000	N.A.	N.A.
VOLUME05	<--- Source is not emitting during this hour															
V VOLUME06	328	5.0	0.0	273.	0.929	3344.9	3055.8	DIR	0.222	0.200	0.079	0.507	0.648	0.017	N.A.	N.A.
VOLUME07	<--- Source is not emitting during this hour															
V VOLUME08	1090	35.0	0.0	273.	2.539	9141.4	14347.0	DIR	0.114	0.200	0.054	0.025	0.029	0.001	N.A.	N.A.
VOLUME09	<--- Source is not emitting during this hour															
V VOLUME10	324	5.0	0.0	273.	0.929	3344.9	2681.8	DIR	0.217	0.200	0.079	0.634	0.804	0.021	N.A.	N.A.
A AREA01	325	10.0	0.0	273.	1.347	4848.7	3427.0	DIR	N.A.	0.200	0.074	236.915	0.237E+00	N.A.	0.1E-02	0.1E+07

*DISTANCE-DEBUG assisted in the discovery of the AREACIRC issue associated with version 16216*

# DISTANCE-DEBUG: Low-wind case

A case involving AERMOD 24-hour  $PM_{2.5}$  modeling for the Class I PSD Increment SIL of 2 material handling transfer points at a concrete batch plant



# DISTANCE-DEBUG: Low-wind Case

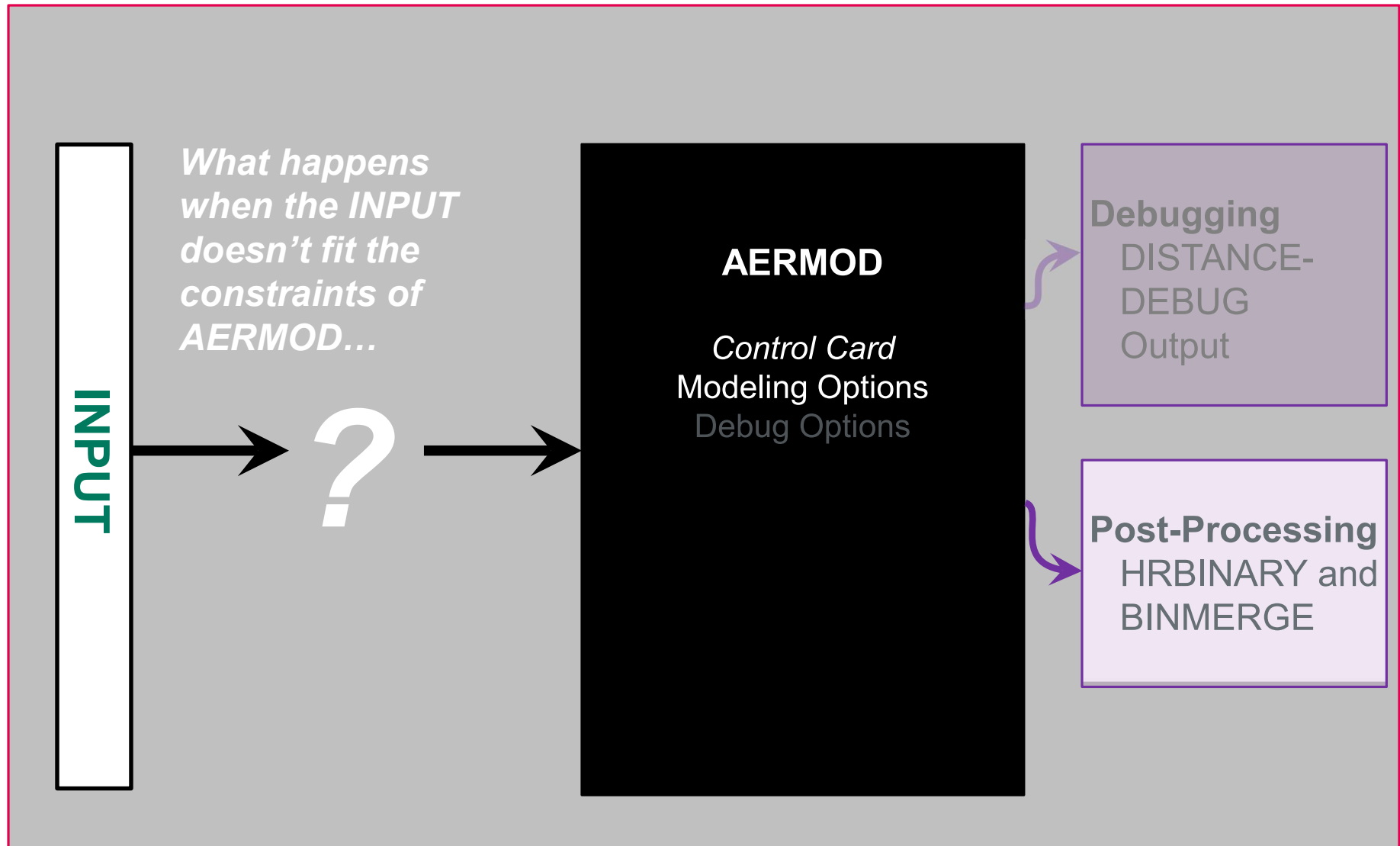
Point Sources	$Q_s$	$H_s$	$T_s$	$V_s$	$D_s$
	(g/s)	(m)	(K)	(m/s)	(m)
Turbine 1	1.0	30.0	810.0	37.0	4.5
Turbine 2	1.0	30.0	810.0	37.0	4.5
Volume Sources	$Q_s$	$H_s$	$\sigma_y$	$\sigma_z$	
	(g/s)	(m)	(m)	(m)	
Conveyor Loading	0.4	2	1.2	0.5	
Conveyor Unloading	0.4	2	1.2	0.5	

Case run using default meteorology

Hour	Source	$u^*$	$u_{eff}$	1-hour Transit Distance	Conc
		(m/s)	(m/s)	(m)	$\mu\text{g}/\text{m}^3$
4	Turb1	0.04	1.4	4,888	0.001
	Turb2		1.4	4,888	0.001
	Load		0.5	1,795	0.591
	Unload		0.5	1,795	0.644
5	Turb1	0.02	0.7	2,412	0.001
	Turb2		0.7	2,412	0.001
	Load		0.5	1,767	1.426
	Unload		0.5	1,767	1.631
6	Turb1	0.07	0.8	2,924	0.062
	Turb2		0.8	2,924	0.062
	Load		0.7	2,634	1.692
	Unload		0.7	2,634	1.816

3 low wind speed hours result in questionably high impacts 50 km out (from two gravel drop points)

# The AERMOD BlackBox



# HRBINARY Post-processor

---

- “HRBINARY” allows for the import of an AERMOD unformatted 1-hour binary file to be added to any modeling run in order to perform the averaging of ranked highs for all currently evaluated averaging periods.
- Hence HRBINARY can allow output from multiple AERMOD runs of different sources to be merged, on an hour-by-hour, receptor-by-receptor basis
- When would this be necessary?

# HRBINARY Example Case

---

- A steel mill with both stack and fugitive emission releases. Fugitive releases are represented by volume sources, area sources, and buoyant line sources (BLP). The BLP algorithms have been incorporated into AERMOD Version 16216r.
- The Plant operates 3 buoyant line sources.
- However, AERMOD v16216r allows only one set of average BLP parameters to be entered per run, these include the thermal buoyancy for line source and the associated downwash.
  
- Step 1:  
BINMERGE sums the separate AERMOD binary files for each different source groups. Each was modeled on the exact same grid.
- Step 2:  
AERMOD is re-run using the HRBINARY option. HRBINARY option takes the single merged binary file (from BINMERGE) and performs the pollutant and averaging time specific statistical ranking and averaging normally performed by AERMOD.
  
- Hence through this two-step method, very different sets of BLP source parameters can be more accurately represented in the modeling.

# Further work

---

## **DISTANCE-DEBUG**

- Does not currently support LINE, FLARE, BUOYLINE or OPENPIT sources
- Issue with reporting downwash contributions for impacts dominated by the “penetrated” plume type
- Provide an option for spreadsheet ready output

## **HRBINARY**

- Allow for the acceptance of multiple binary files (thus eliminating the need for BINMERGE)
- For exploratory purposes, add an option to linearly scale concentrations in binary files for a weighted analysis between the binary files

# Contact Information

---

**Carlos Szembek , ERM**  
Senior Air Quality Meteorologist  
New Orleans, LA  
+1 504 846 9236  
[carlos.szembek@erm.com](mailto:carlos.szembek@erm.com)

**Robert Paine, AECOM**  
Assoc. Vice President, Environment  
Chelmsford, MA  
+1 978 905 2352  
[bob.paine@aecom.com](mailto:bob.paine@aecom.com)

**Milena Borissova, ERM**  
Senior Air Quality Meteorologist  
Boston, MA  
+1 617 646 7892  
[milena.borissova@erm.com](mailto:milena.borissova@erm.com)

**Mark Garrison, ERM**  
Air Quality Technical Fellow  
Philadelphia, PA  
+1 484 913 0369  
[mark.garrison@erm.com](mailto:mark.garrison@erm.com)



# Review of models for dispersion of tall stack plumes at Collie: AERMOD questions

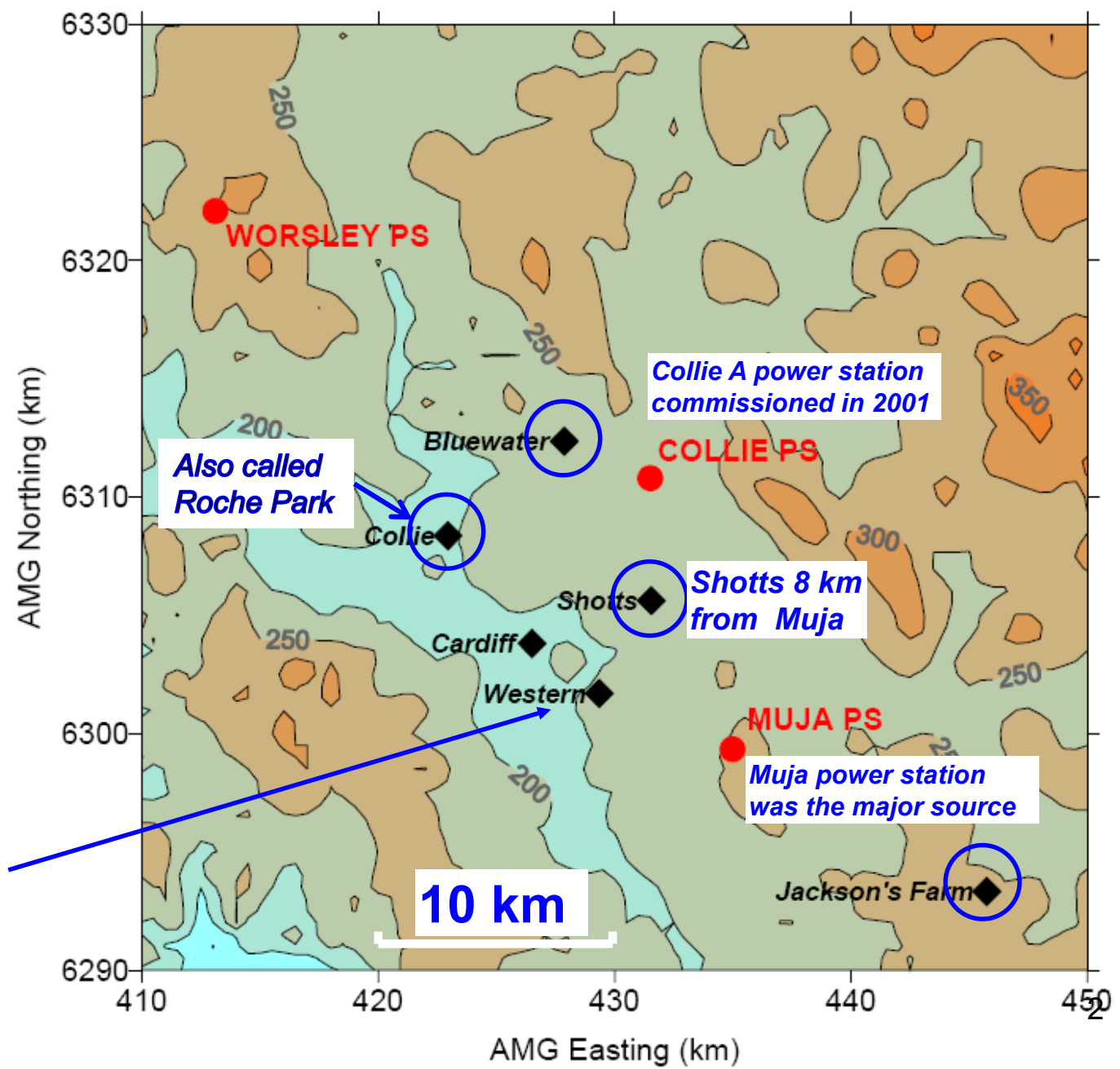
Ken Rayner  
Department of Environment and Conservation  
Western Australia  
2013



# Western Power monitoring program 1996 - 2001

SO<sub>2</sub> monitoring Western Power 1998, 2001

Western 2 (W2) meteorological station



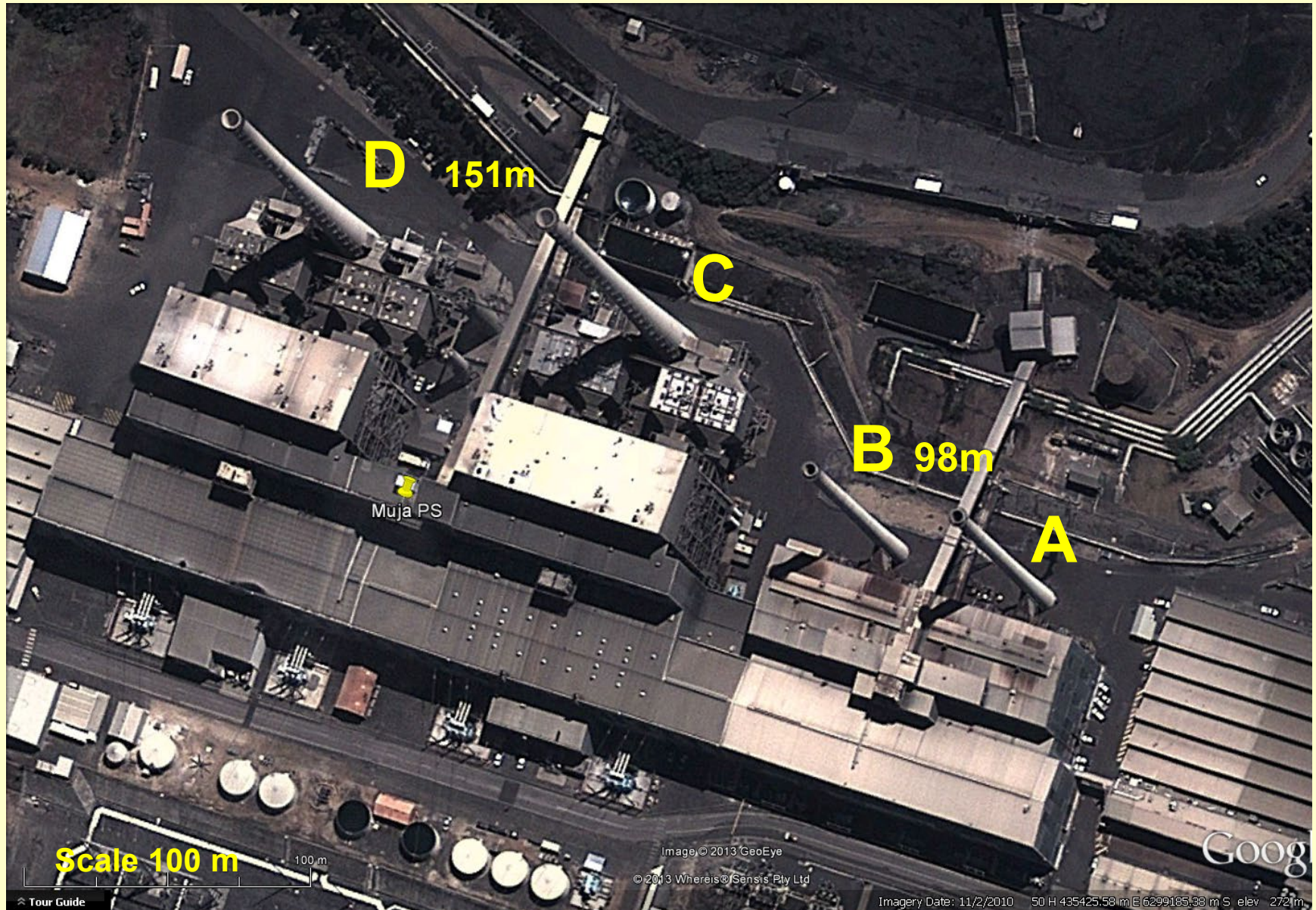
# Emissions parameters (indicative)

In 1998, the year used for modelling below, only Muja and Worsley power stations were operating

Table 1. Emission parameters for existing and proposed sources as modelled by Environ (2007) based on estimates by SKM (2005).

Source (stack)	Stack Height (m)	Stack tip diameter (m)	Exit temp. (deg C)	Exit velocity (m s <sup>-1</sup> )	SO <sub>2</sub> (g s <sup>-1</sup> )	Power out
Muja A	98	3.94	200	19.0	269	120 MW
Muja B	98	3.94	200	19.0	269	120 MW
Muja C	151	5.91	133	20.4	779	400 MW
Muja D	151	5.91	133	19.0	779	400 MW
Collie A	170	5.23	152	24.4	515	300 MW
Worsley PS	76	4.00	130	23.7	315	
Worsley boiler xtn	105	2.50	130	24.5	71	
Bluewaters I	100	4.00	131	25.5	230	200 MW
Bluewaters II	100	4.00	131	25.5	230	200 MW

# Muja Power Station



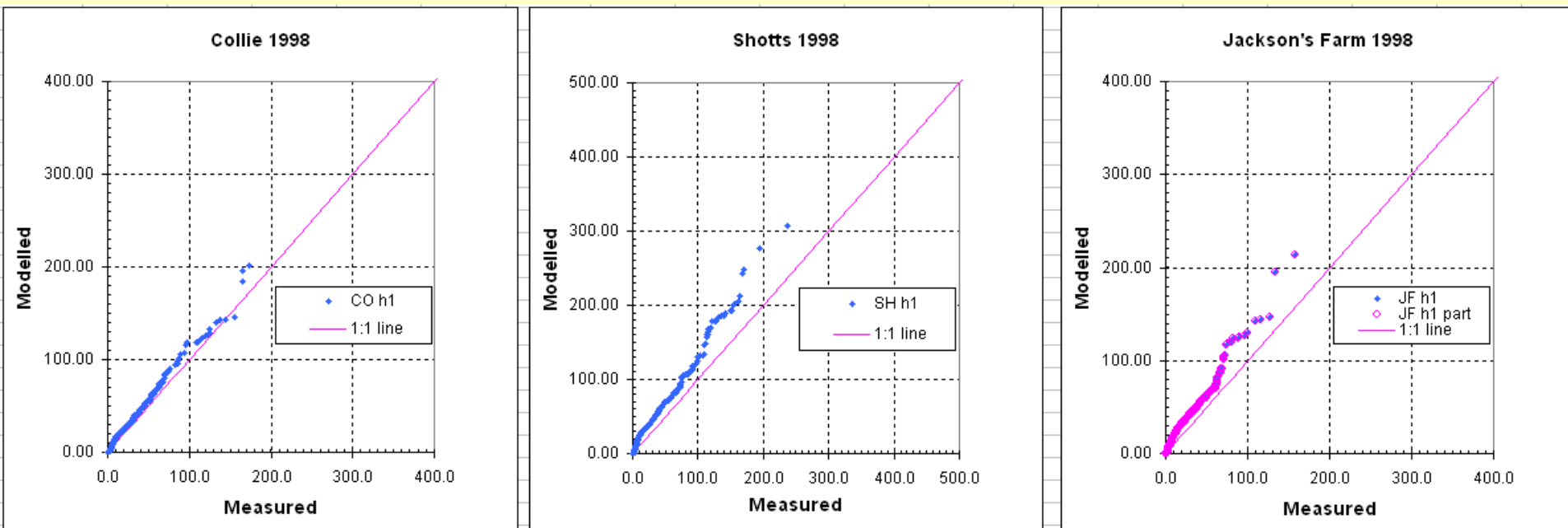
# Inputs for AERMET/AERMOD – limitations of historical data (1998, 2001)

- No radiosondes near Collie.
  - Temperature profiles from TAPM were used;
  - AERMET also run with radiosonde data from Perth Airport, 160 km NNW, to test sensitivity.
- The only nearby cloud observations were from Donnybrook, 40 km SW of Collie on the coastal plain (possibly unrepresentative since Collie is at 200 m altitude, east of the Darling Escarpment). These observations were only twice daily (9 am, 3 pm). TAPM-generated cloud estimates (questionable quality) were tested.
- AERMOD results (QQ plots) did not show much sensitivity to the different data options described above.
- Modelling described in these notes will be limited to 1998. Emissions from Muja power station were dominant. Emissions from the power station at the Worsley alumina refinery were relatively small and remote.

# AERMOD run h1 (1998)

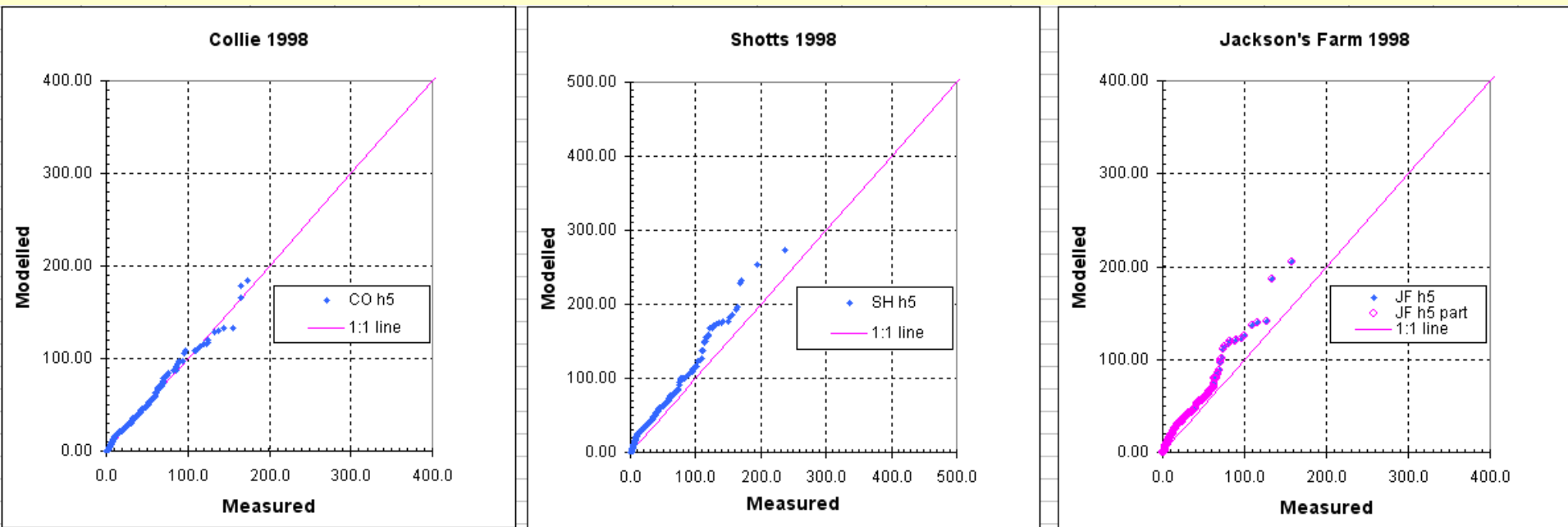
- measured met from W2 36m over forest, calculated solar radiation
- cloud from D'brook, temp profile (2 per day) from TAPM v403
- albedo = 0.1, Bowen = 1.0,  $z_0 = 1.0\text{m}$

*All Q-Q plots are for individual monitoring stations, i.e. predictions and observations paired in space but not time. Linear scales are used to better display the important higher concentrations.*



# AERMOD h5

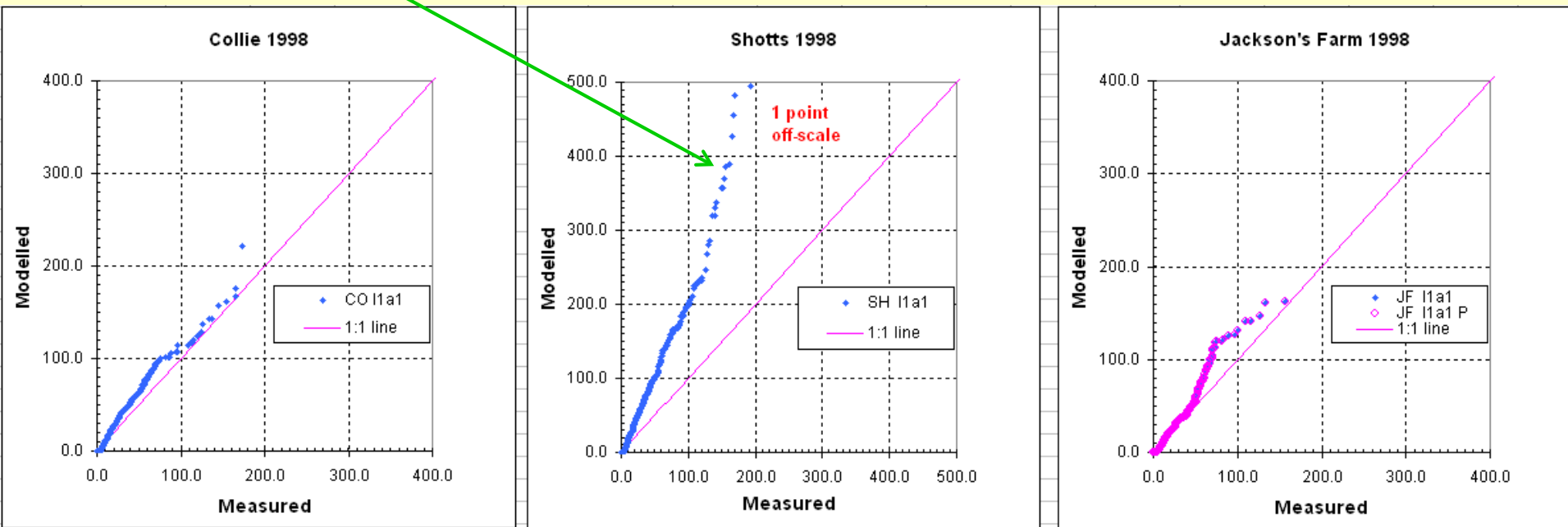
- as per h1 but topography modelled (Lakes software):  
concentrations reduced a little – probably due to Muja elevation.



# CALPUFF I1a1 (as per j1a1)

- measured met from W2 36m over forest, wind extrapolated (biases -1)
- cld from D'brook, geo and temp profile (24/day) from TAPM v403

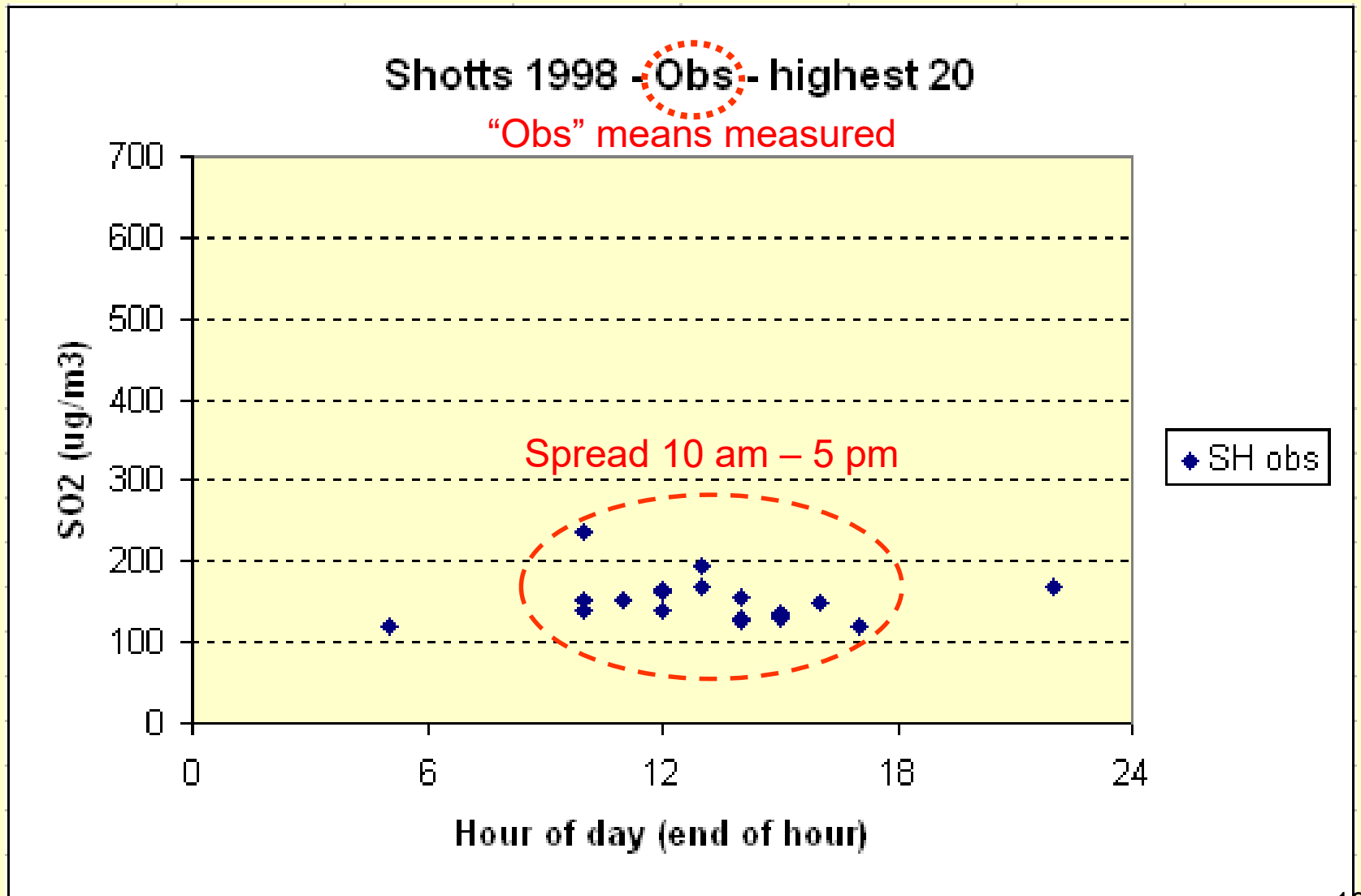
*This slide included for interest – CALPUFF overestimates at the closest monitor Shotts (about 8 km from Muja Power Station).*



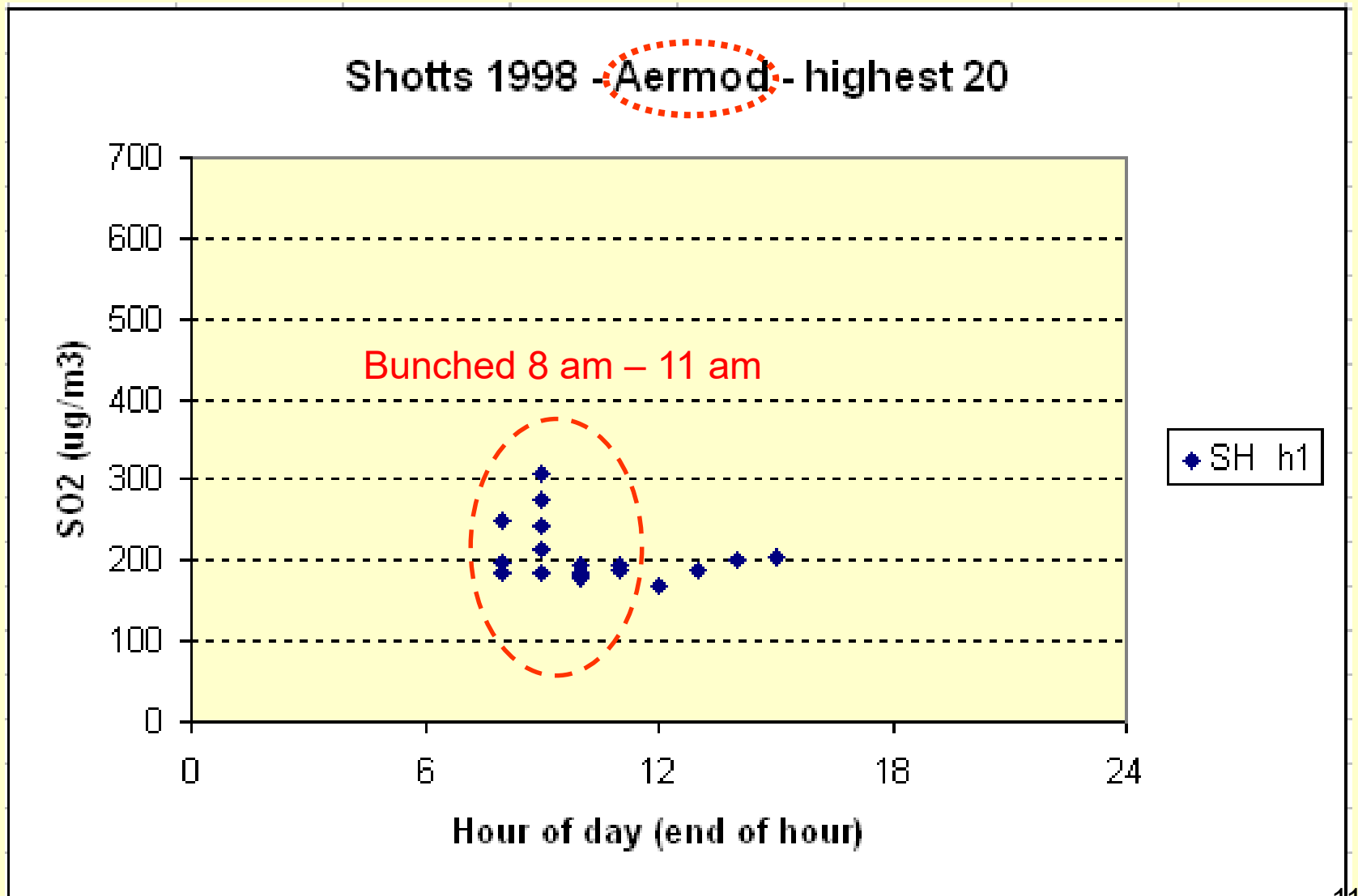
# Analysis of conditions associated with top 20 concentrations at Shotts

- both AERMOD and CALPUFF give highest concentrations mid-morning under light wind unstable conditions. AERMOD tends towards very light winds and low mixing heights
- measured highest concentrations are centred on midday and occur under light – moderate winds. AERMET results for the times of these measurements indicate significantly higher values of  $w_*$  and convective mixing height than those associated with AERMOD or CALPUFF modelled peak concentrations.
- See the following graphs, alternating between measurements (“obs”) and AERMOD run h1 results

# Analyses of top 20 concentrations

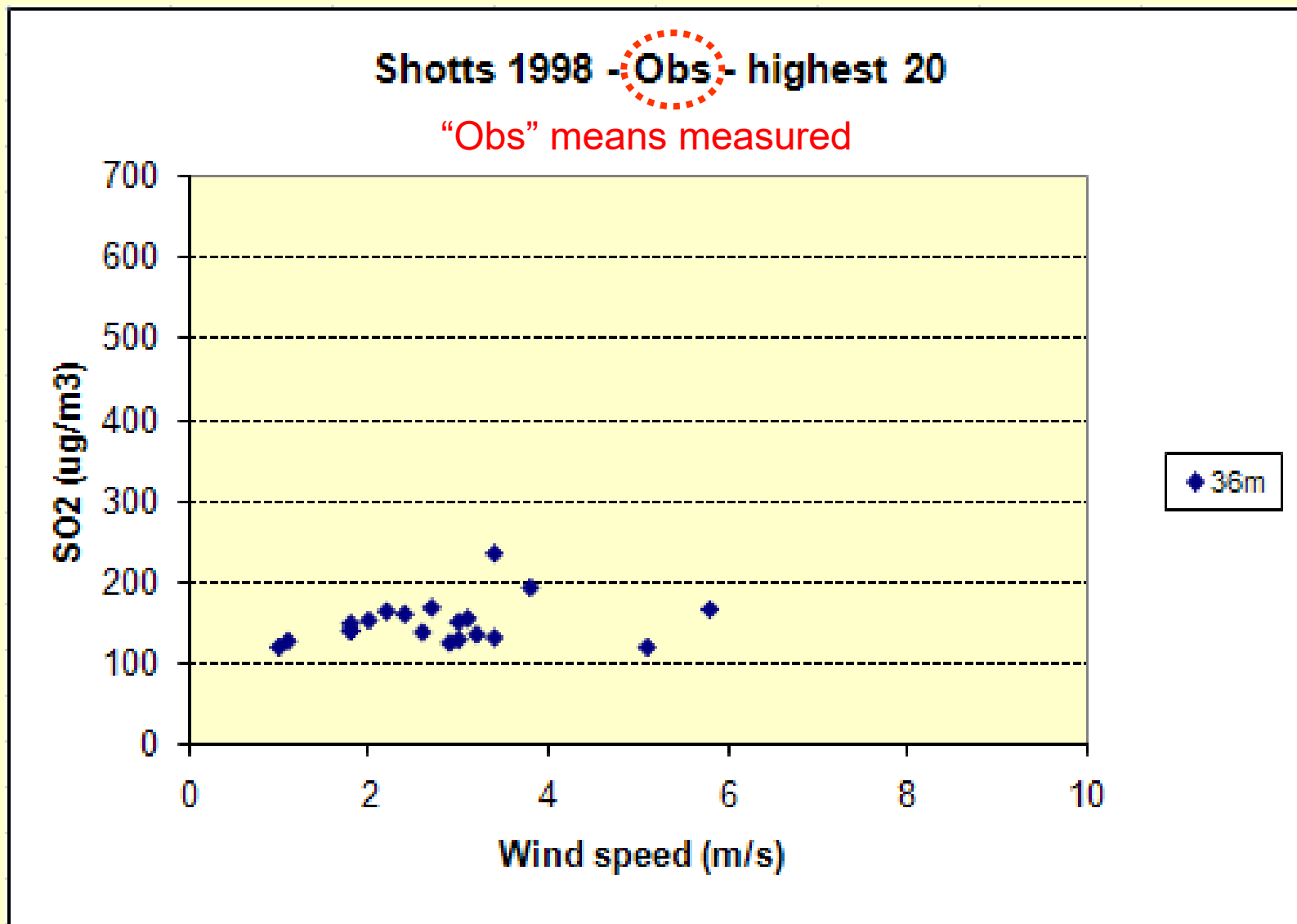


# Analyses of top 20 concentrations

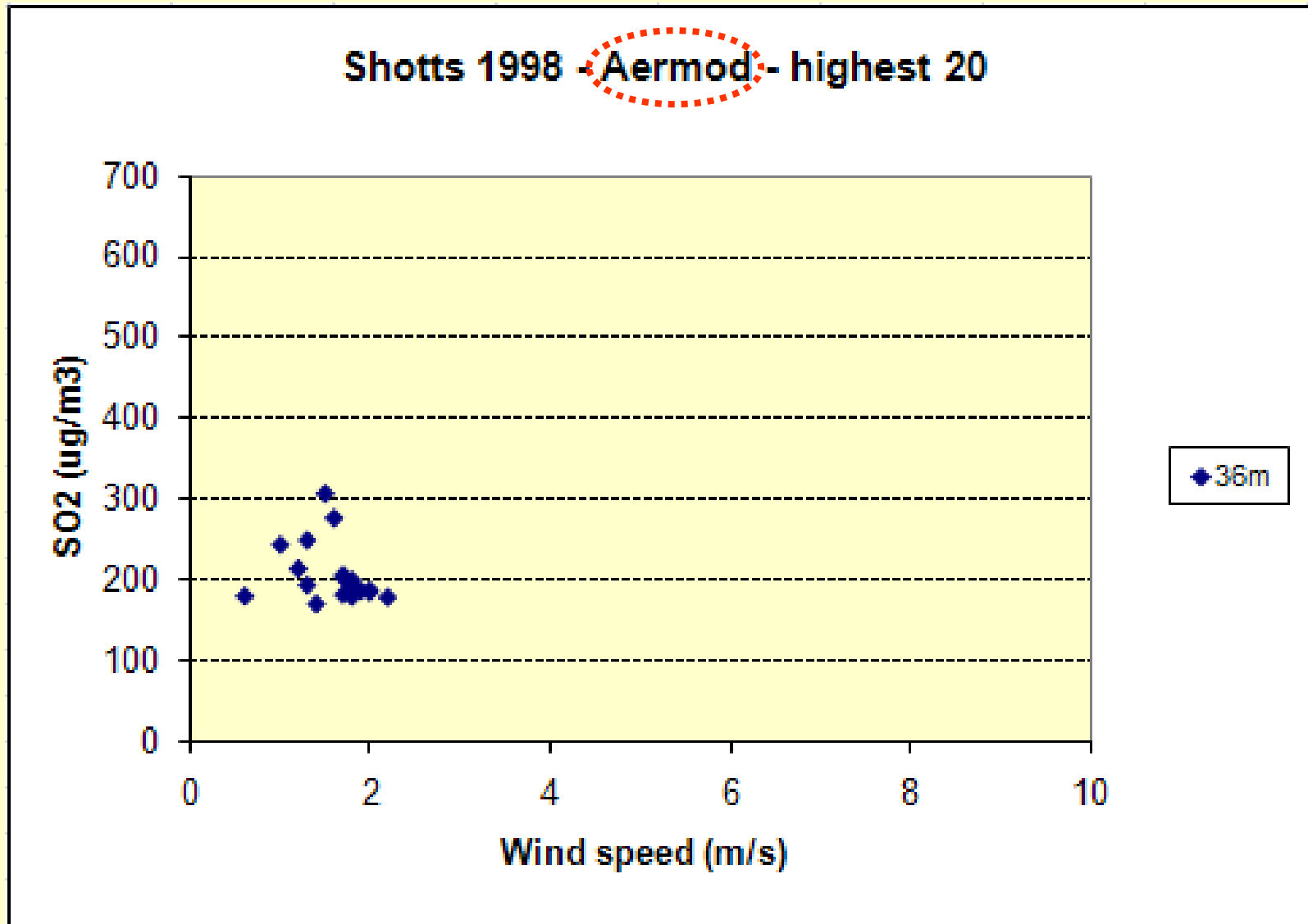


# Analyses of top 20 concentrations

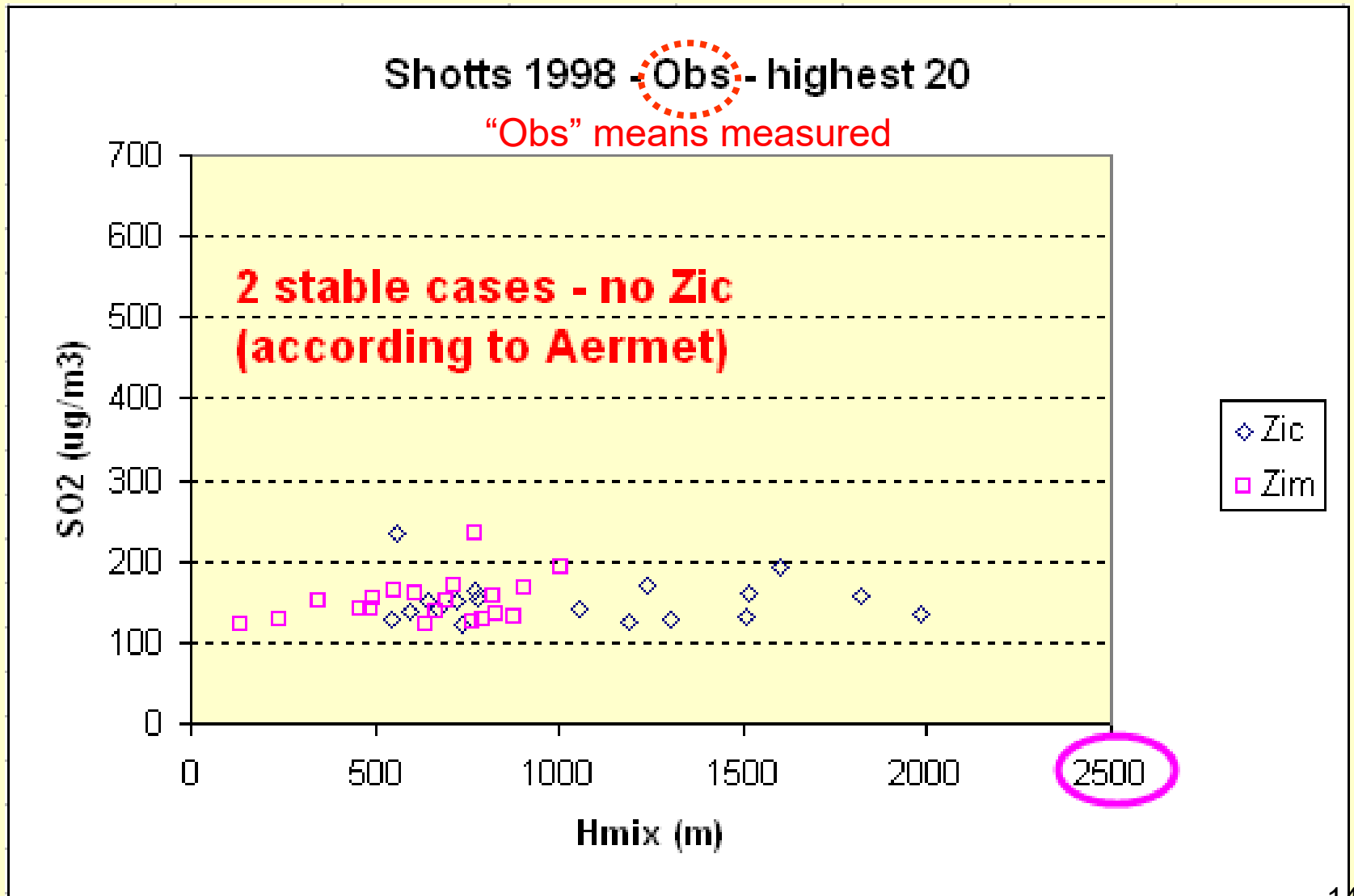
*winds measured at 36 metres*



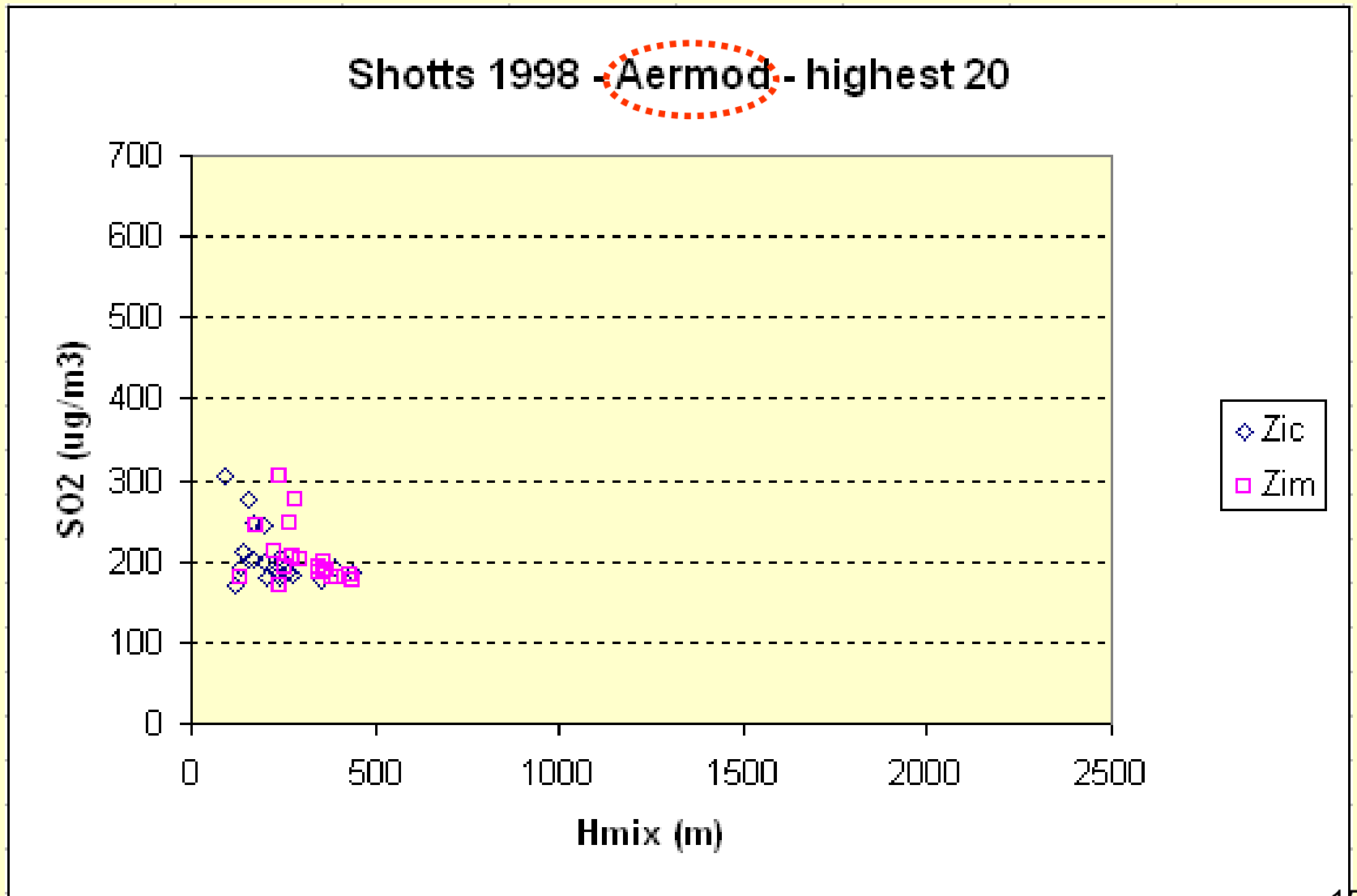
# Analyses of top 20 concentrations



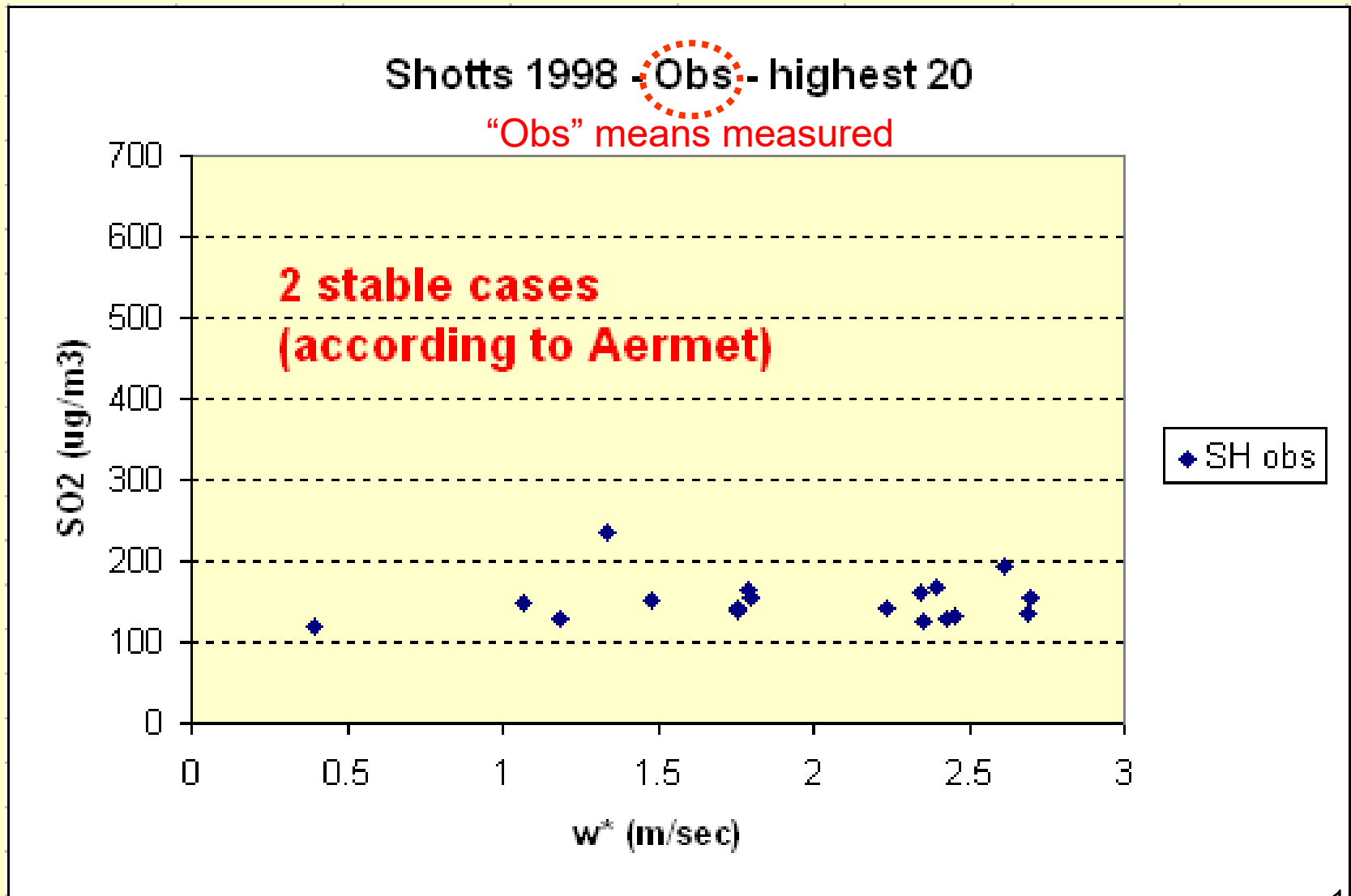
# Analyses of top 20 concentrations



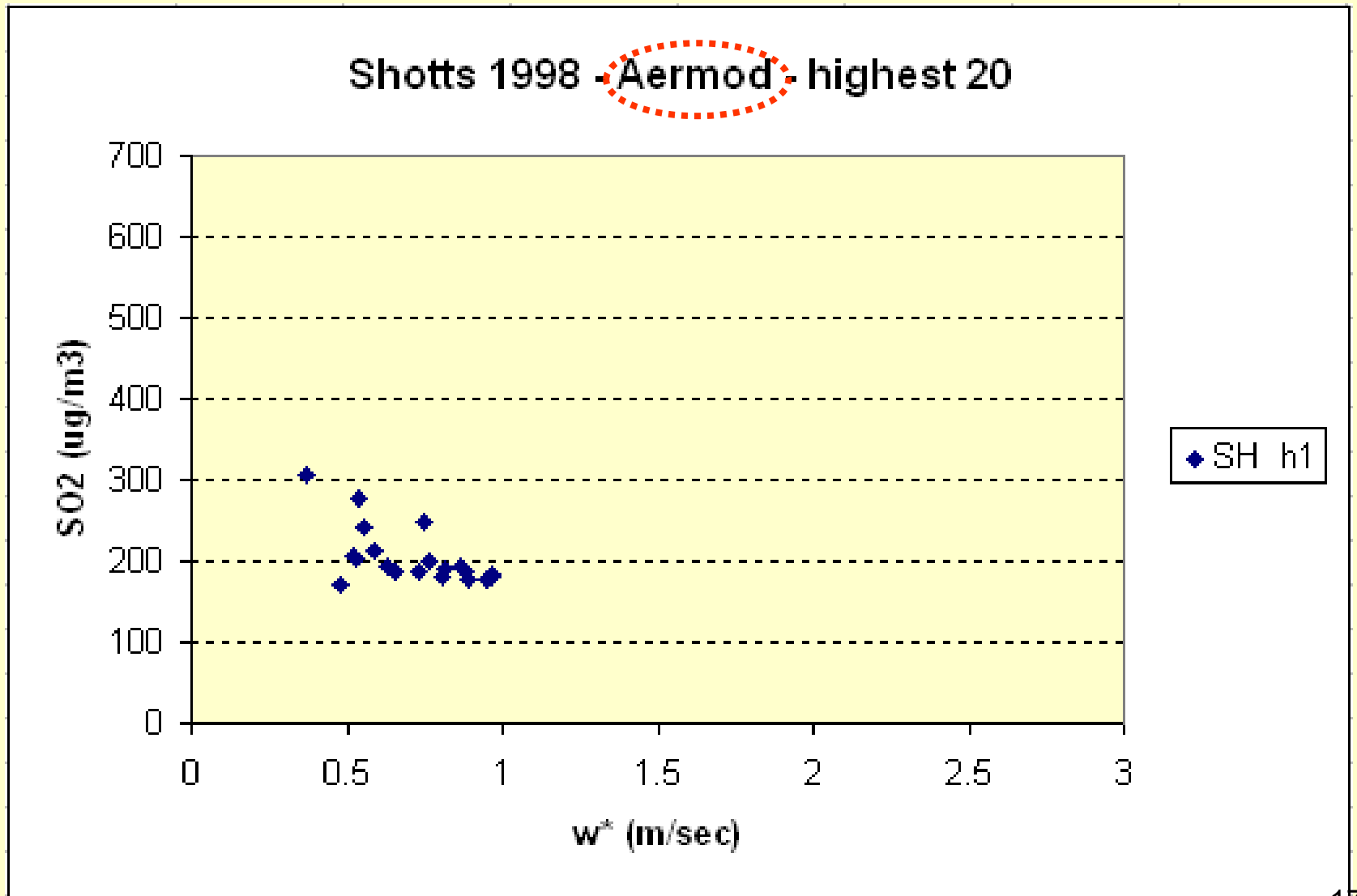
# Analyses of top 20 concentrations



# Analyses of top 20 concentrations



# Analyses of top 20 concentrations

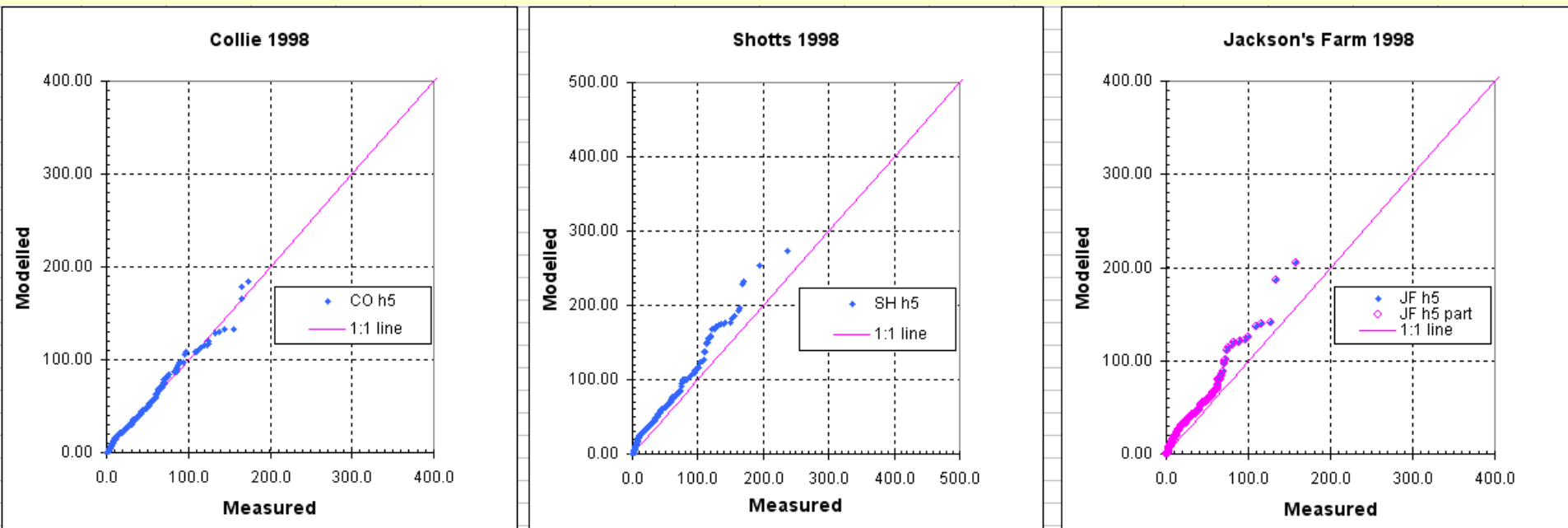


# Further assessment of conditions associated with highest concentrations at Collie.

- The series of slides below show QQ plots, firstly for run h5 (see above) for all hours of 1998 and then, in subsequent slides, re-plotted for subsets of the modelled and measured concentrations obtained by separately filtering these concentrations for specified ranges of parameter(s) in the coincident AERMET records, as labeled on each slide.
- *(Note – I have persisted with QQ plots, paired in space but not in time. Comments on method welcome.)*

# AERMOD run h5 (1998) (repeated)

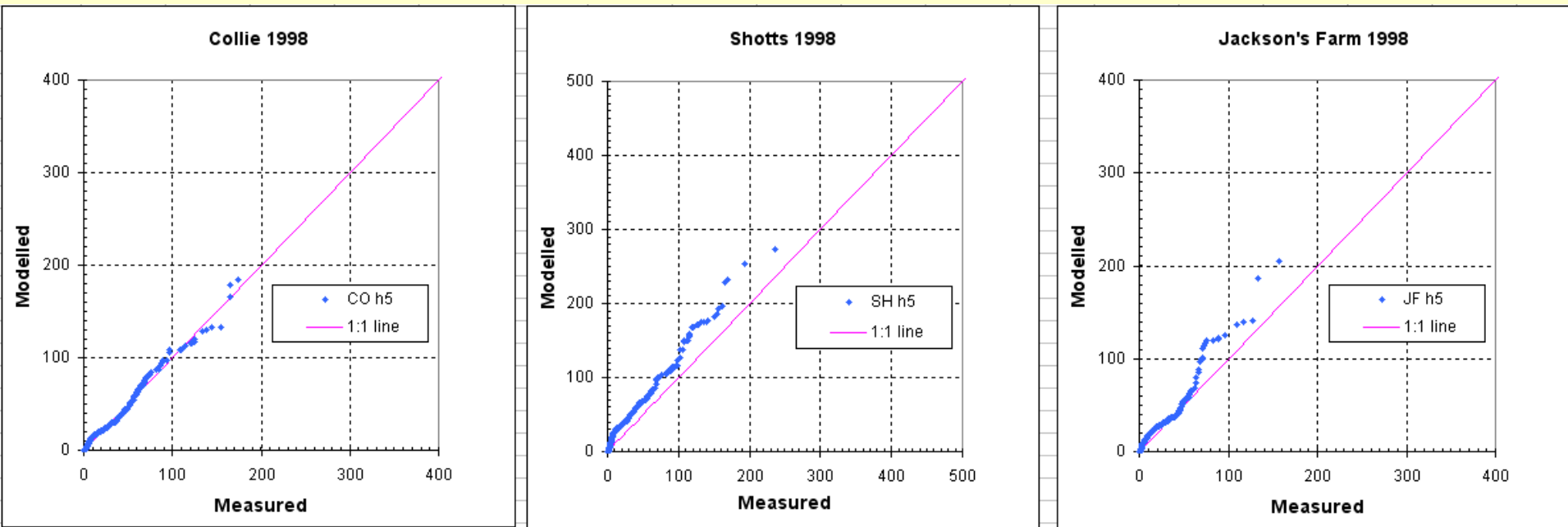
- measured meteorology (36m over forest), calculated solar radiation
- observed cloud from remote site, temperature profiles from TAPM (prognostic model)
- SRTM terrain data (terrain effects minor at Collie; stack height > 2 x terrain variation)
- all hours (no filtering for particular conditions)



*Is this apparently good model/measurement comparison for “all hours” a product of compensating under/over-estimates in particular conditions?  
See following slides.*

# AERMOD run h5 (1998)

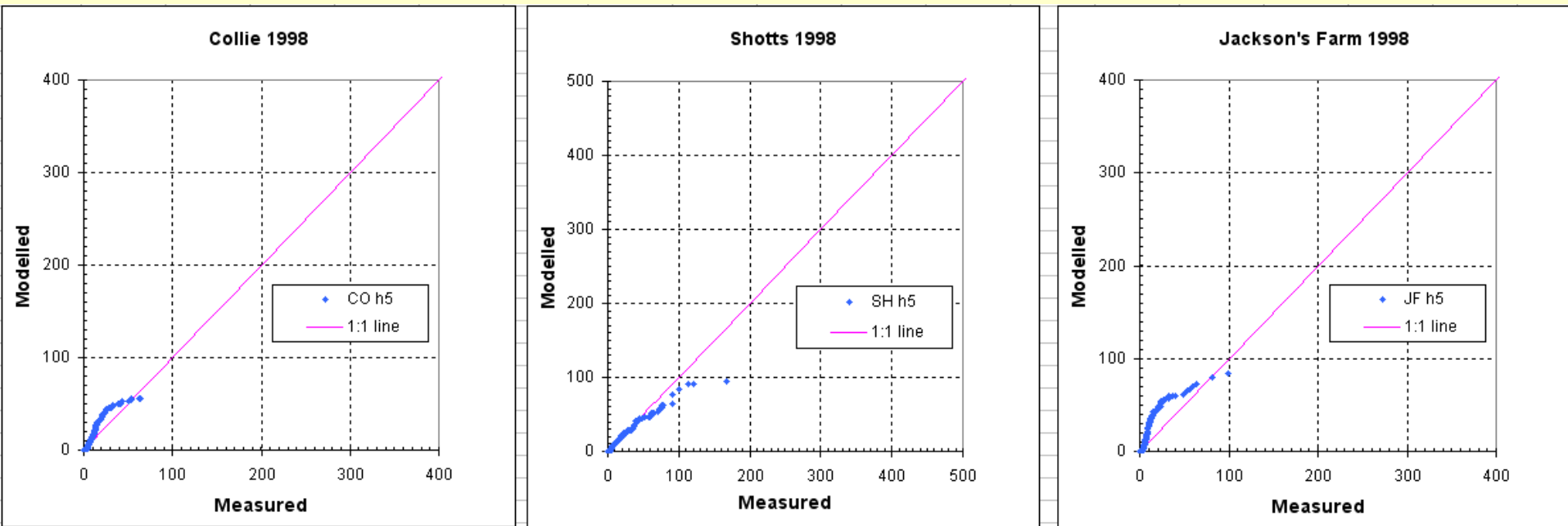
- unstable conditions



*Very similar for high concentrations to “all hours”. Highest concentrations clearly occur under unstable conditions (see next plot).*

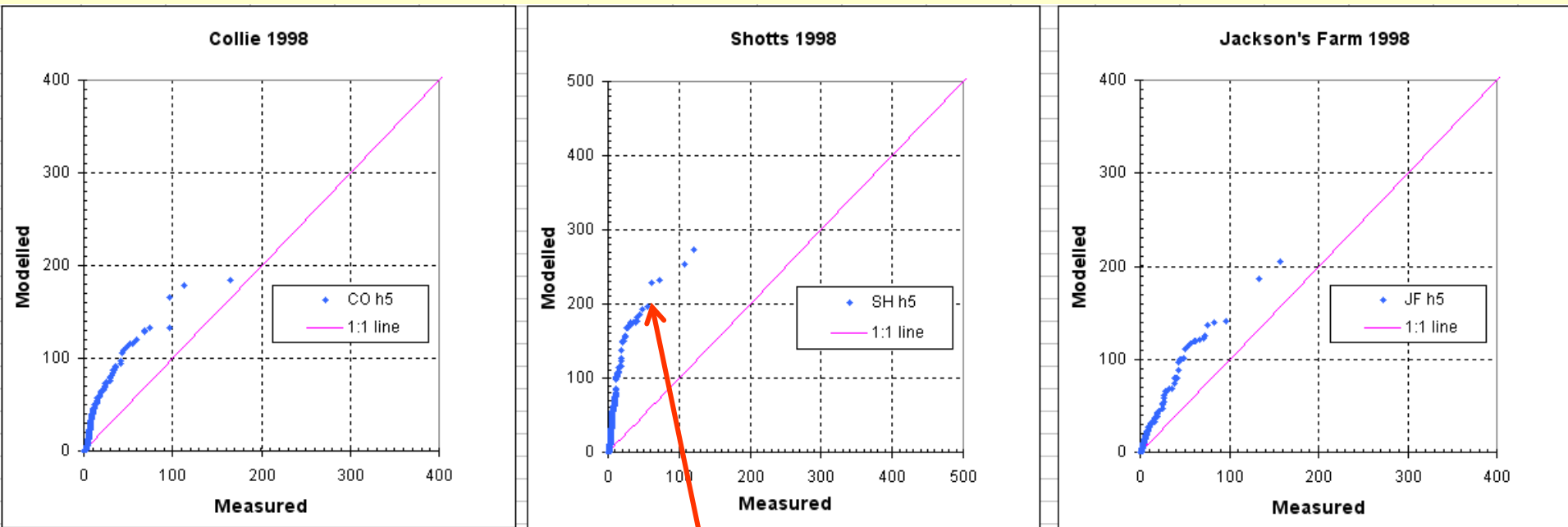
# AERMOD run h5 (1998)

- stable conditions



# AERMOD run h5 (1998)

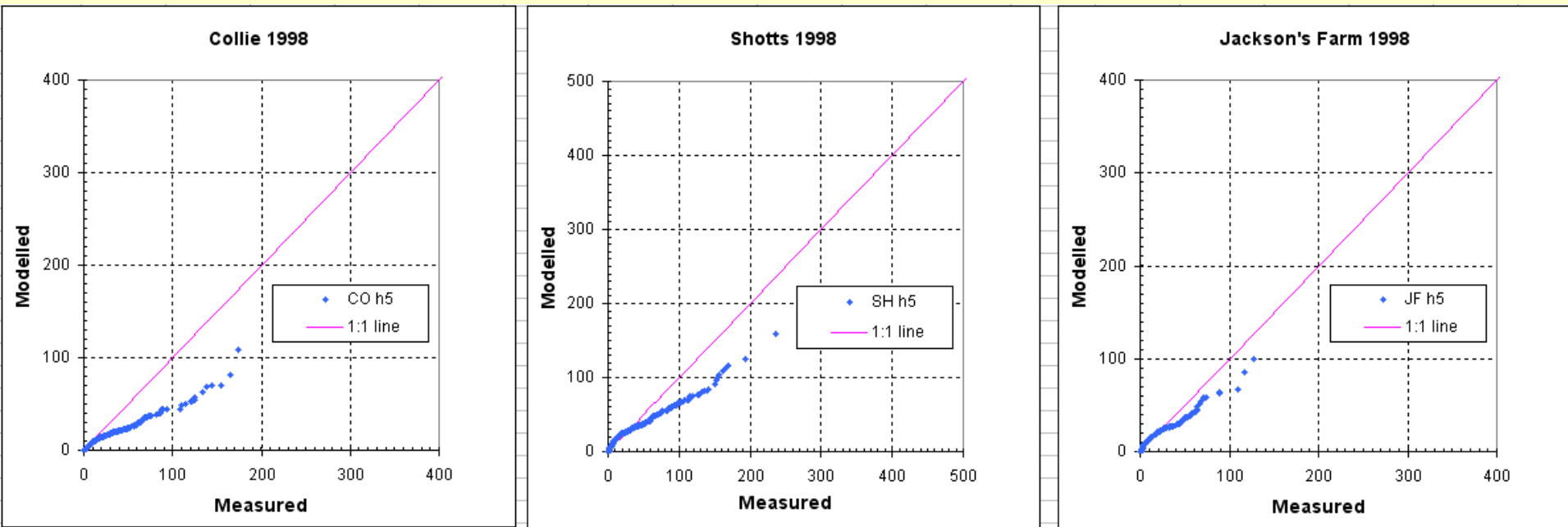
- convective mixing is mild ( $0 < w^* < 1$ )



*Model over-estimation, notably at Shotts*

# AERMOD run h5 (1998)

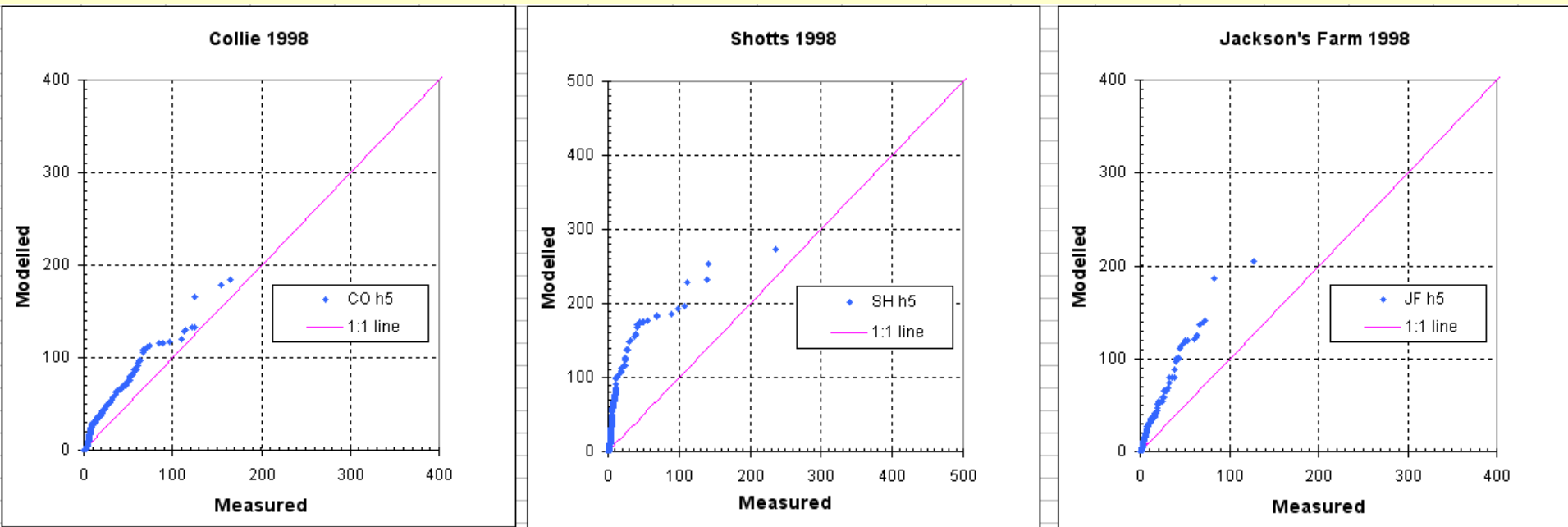
- convective mixing is moderate to strong ( $w^* > 1$ )



*Model under-estimation*

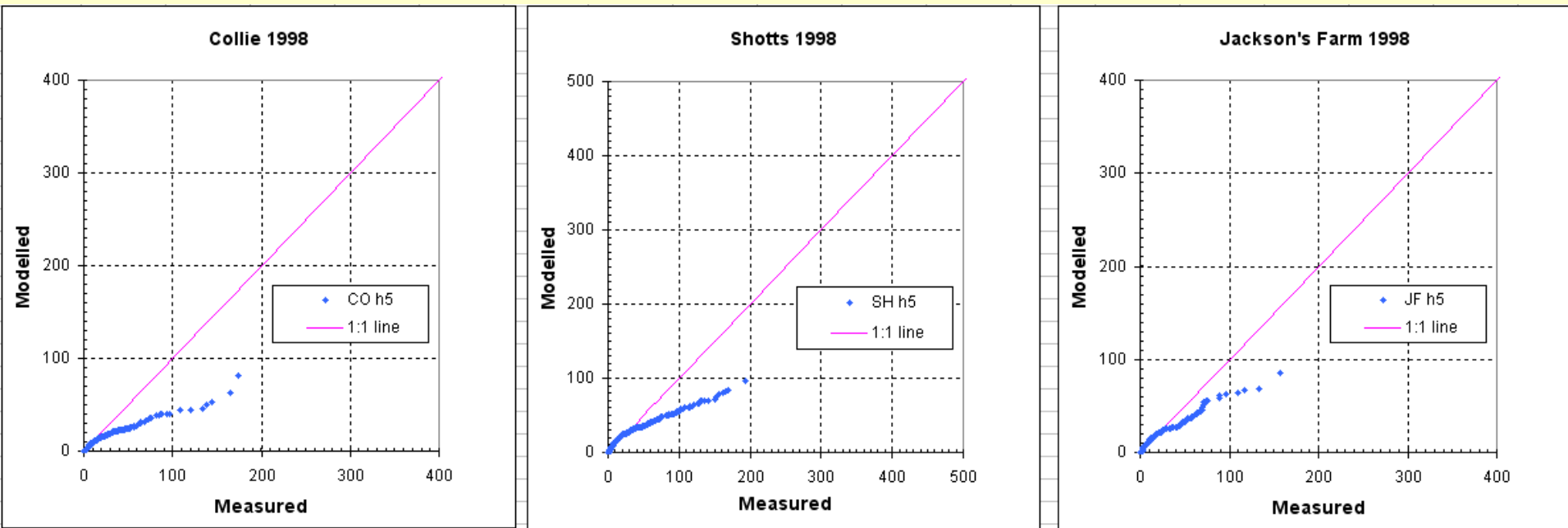
# AERMOD run h5 (1998)

- convective mixing height  $Z_{ic}$  between 0 and 600 m (*related to  $w_*$* )



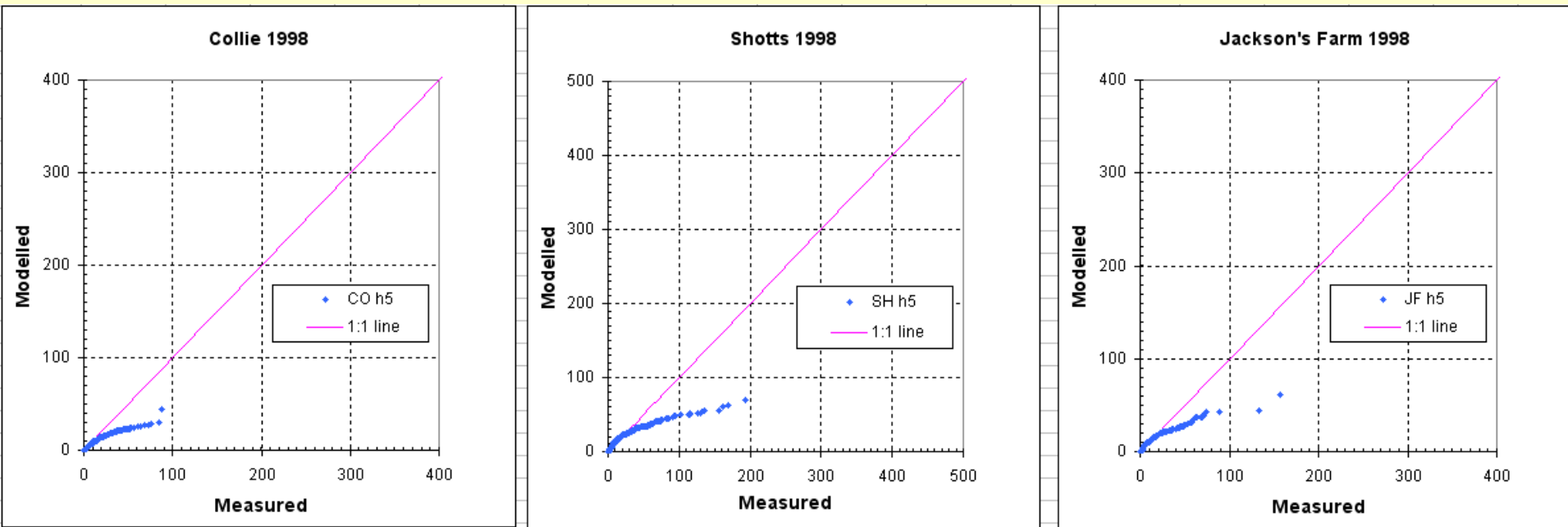
# AERMOD run h5 (1998)

- convective mixing height  $Z_{ic}$  greater than 600 m



# AERMOD run h5 (1998)

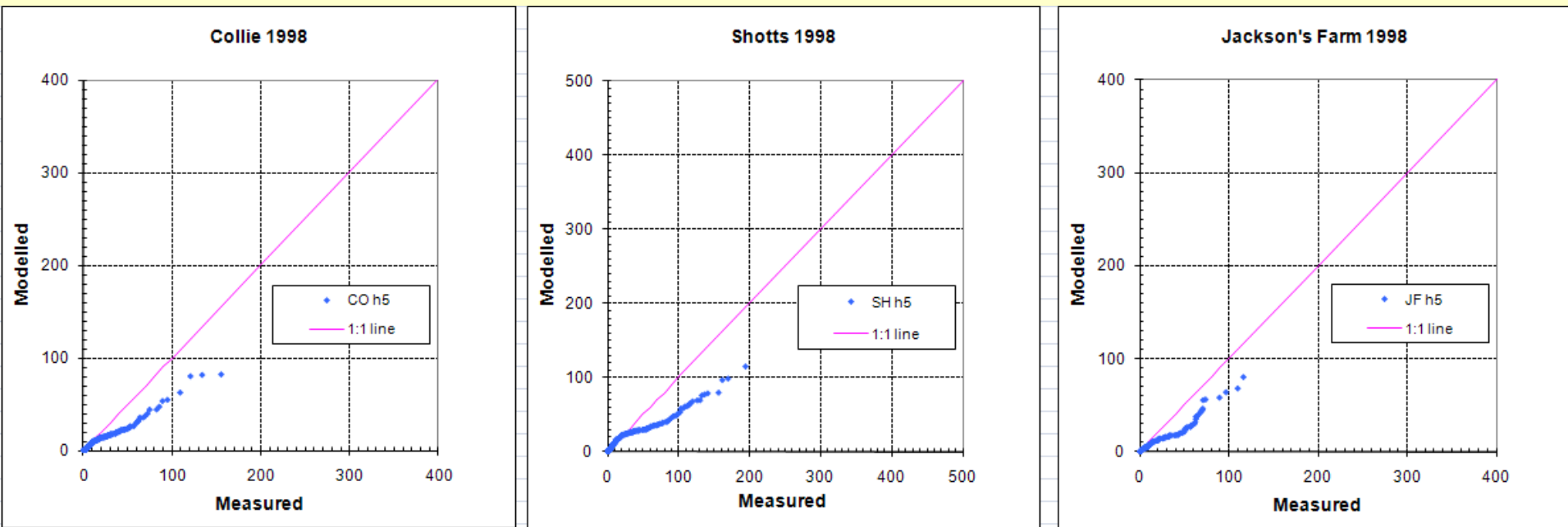
- convective mixing height  $Z_{ic}$  greater than 900 m



*Under-estimation occurring when mixing height is large, which should be relatively simple conditions for AERMOD. Has this been seen in other studies?*

# AERMOD run h5 (1998)

- hours ending 11 to 17 inclusive, air temperature > 20°C



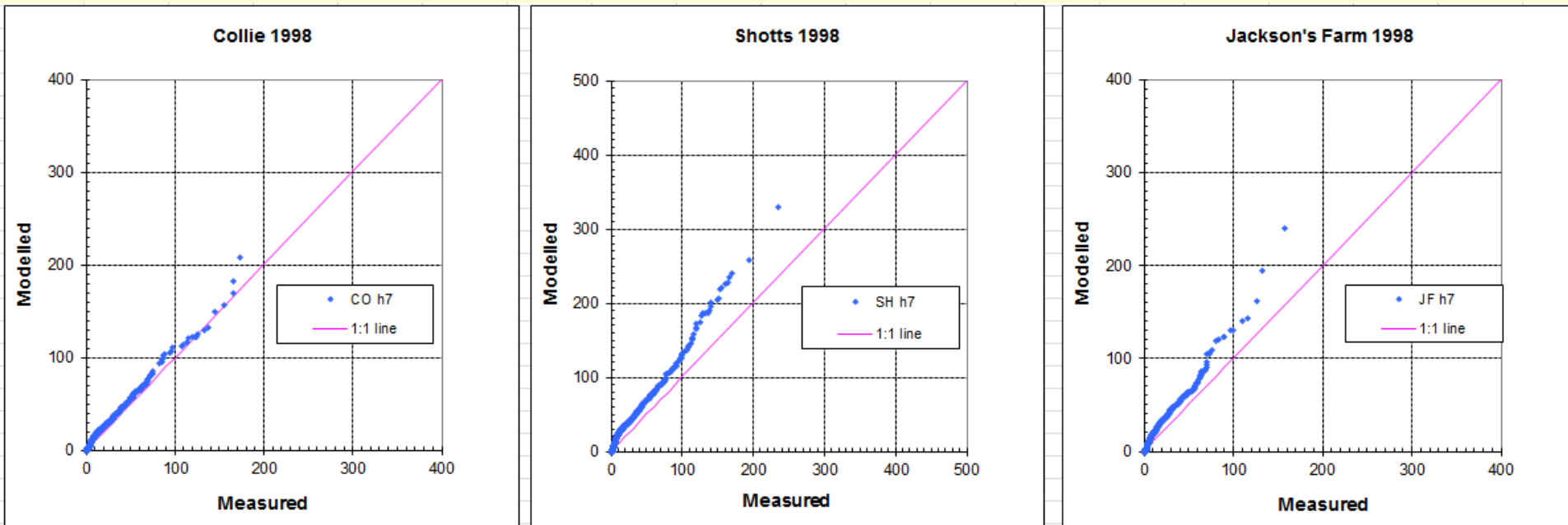
*Filtering here is for simple parameters (time, temperature), not using AERMET-calculated parameters. Confirms under-prediction in what should be straight-forward conditions for dispersion modelling (warm day, late morning to afternoon).*

# Sensitivity of the foregoing filtering results to meteorological data used in AERMET / AERMOD

- Historical Collie data do not include cloud cover or temperature soundings.
- The foregoing model run h5 used questionable cloud observations and temperature profiles from the prognostic model TAPM.
- AERMET / AERMOD were re-run using:
  - All measurements:- as per h5 but with [temperature soundings from Perth airport](#), 160 km NNW. QQ plots for all hours were very similar to the foregoing run h5.
  - All TAPM-generated input:- ([TAPM produces AERMET-format files](#) for direct input to AERMOD, bypassing AERMET). QQ plots for all hours showed moderated over-estimation.
- QQ plots for filtered cases from these additional two AERMOD runs showed the [same patterns of over and under-estimation for variations in  \$w\_\*\$ , etc.](#) (*Selected plots included below*).
- Suggests the behavior is characteristic of AERMOD (a resilient issue).

# AERMOD run h7 (1998)

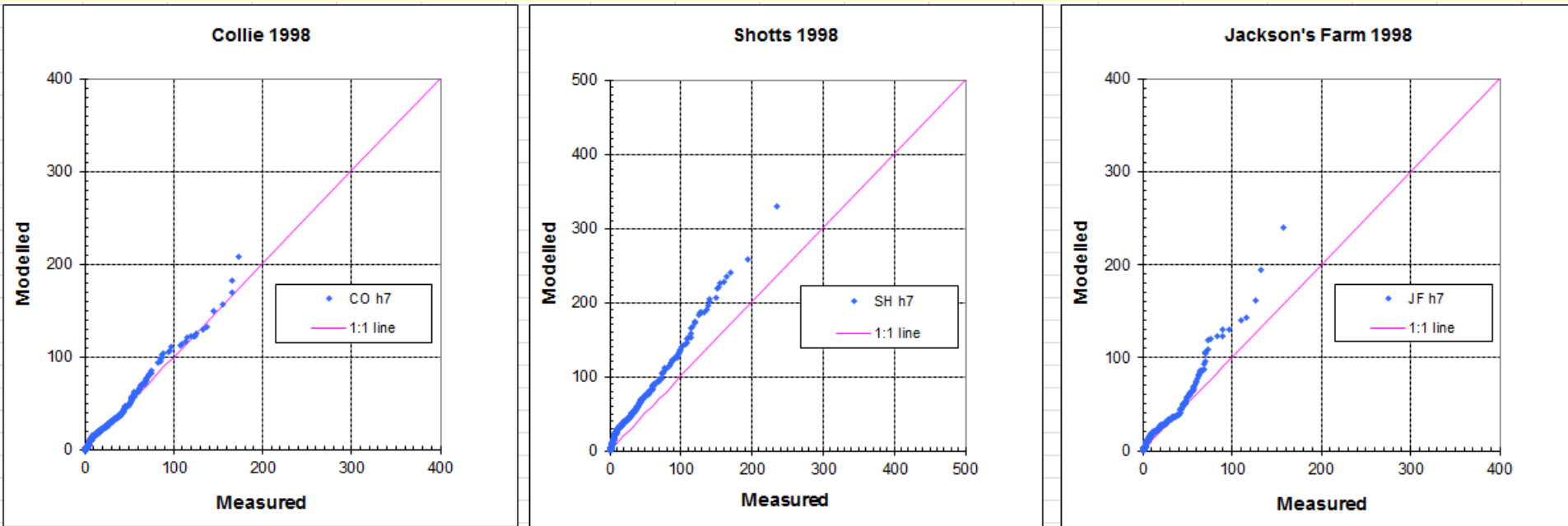
- measured meteorology (36m over forest), calculated solar radiation
- observed cloud from remote site, temperature soundings Perth Airport 160 km NNW
- terrain not included (minor factor)
- all hours (no filtering for particular conditions)



*Very similar to H5 all hours, despite using remote sounding data.*

# AERMOD run h7 (1998)

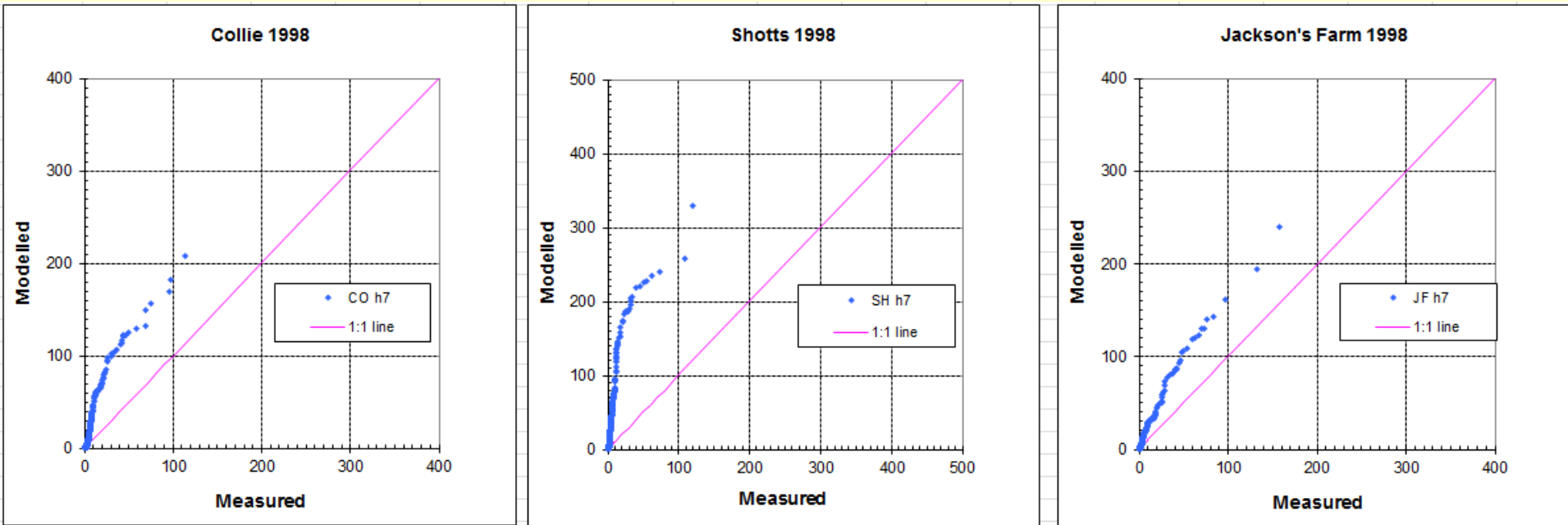
- unstable conditions



*c.f. h7 all hours - unstable conditions dominate high concentrations*

# AERMOD run h7 (1998)

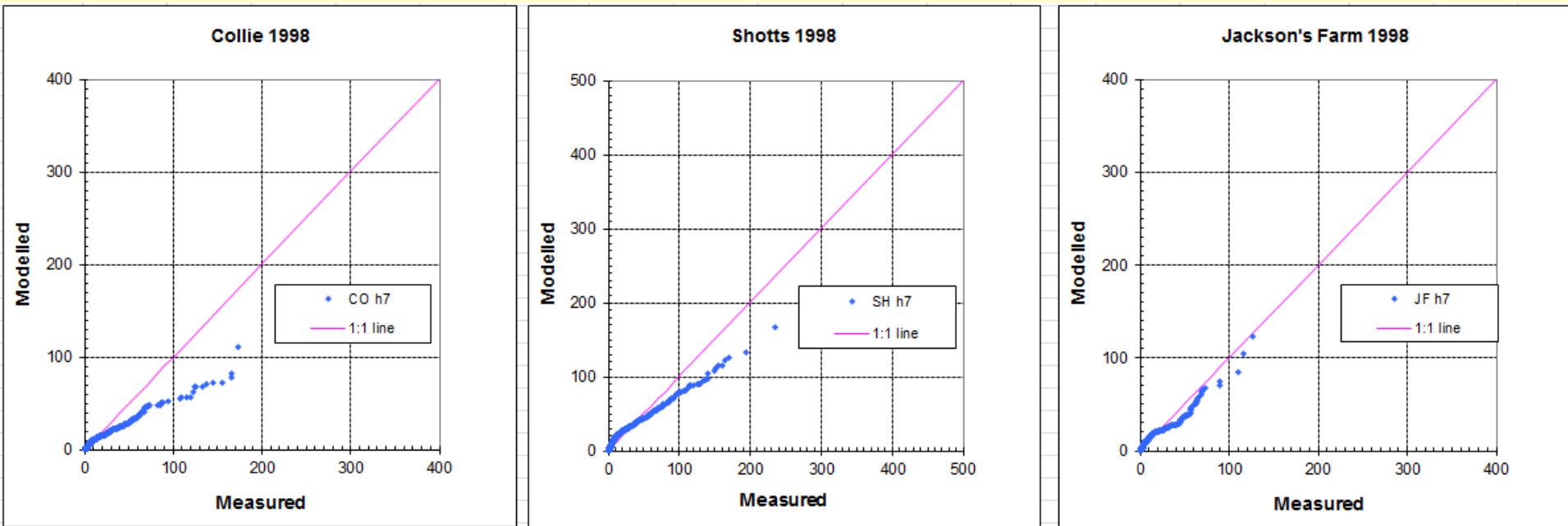
- convective mixing is mild ( $0 < w^* < 1$ )



*model over-estimation in mildly convective conditions, notably at Shotts*

# AERMOD run h7 (1998)

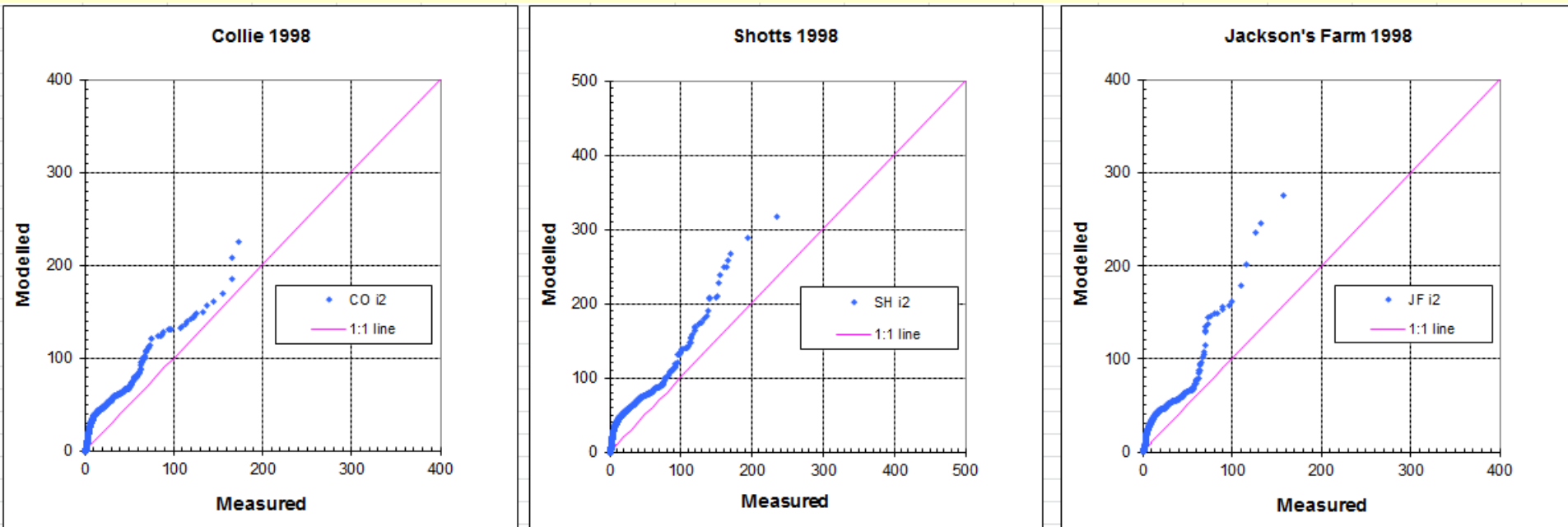
- convective mixing is moderate to strong ( $w^* > 1$ )



*model under-estimation*

# AERMOD run i2 (1998)

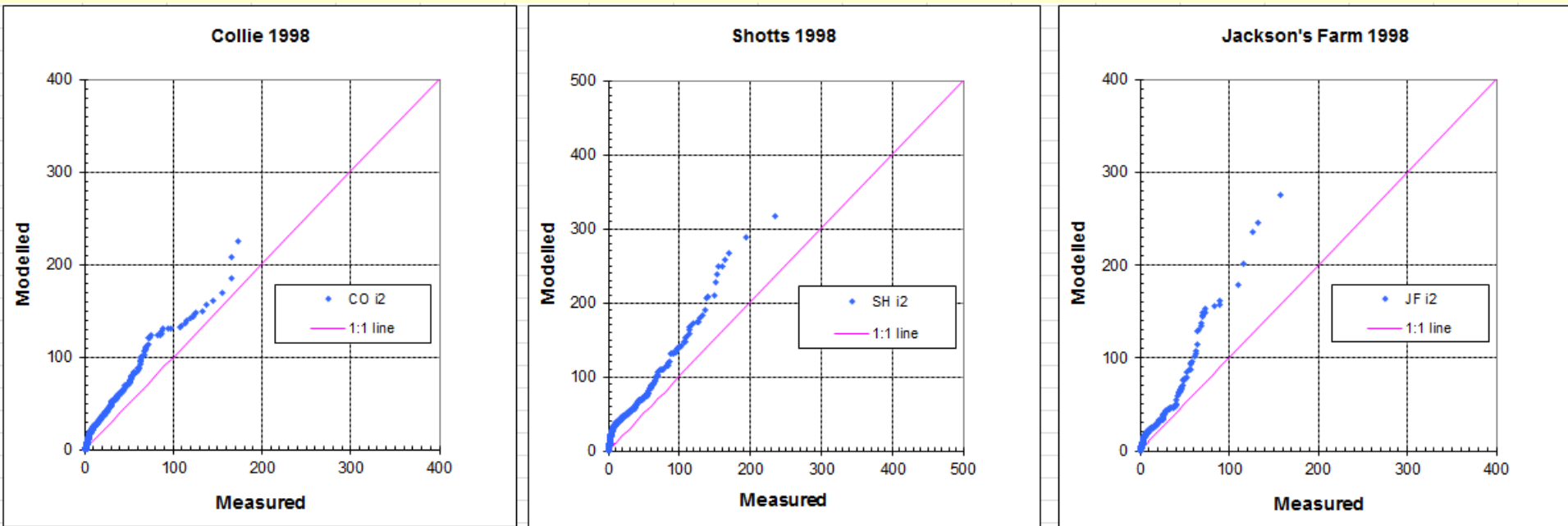
- mesoscale model TAPM meteorology (no measurements)
- TAPM produces AERMET-format .sfc and .pfl files
- .pfl file reduced to surface level wind and temperature only (no upper levels, no turb.)
- all hours (no filtering for particular conditions)



*moderate over-estimation c.f. runs h5 and h7.*

# AERMOD run i2 (1998)

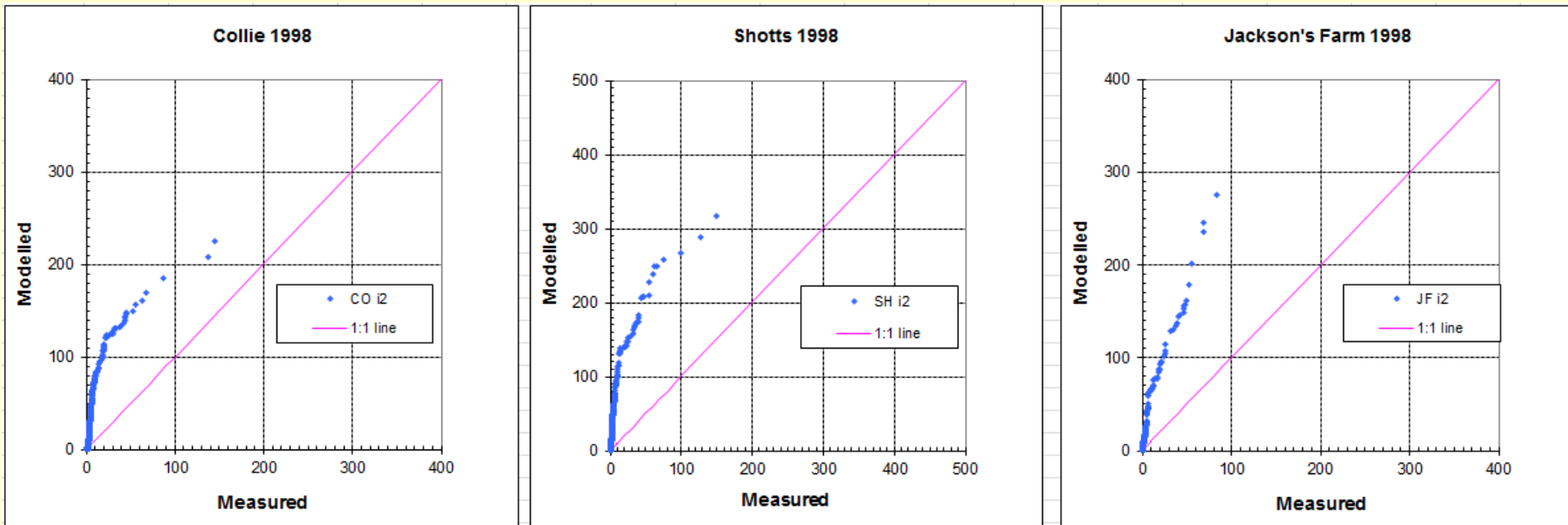
- unstable conditions



*c.f. i2 all hours - unstable conditions dominate high concentrations*

# AERMOD run i2 (1998)

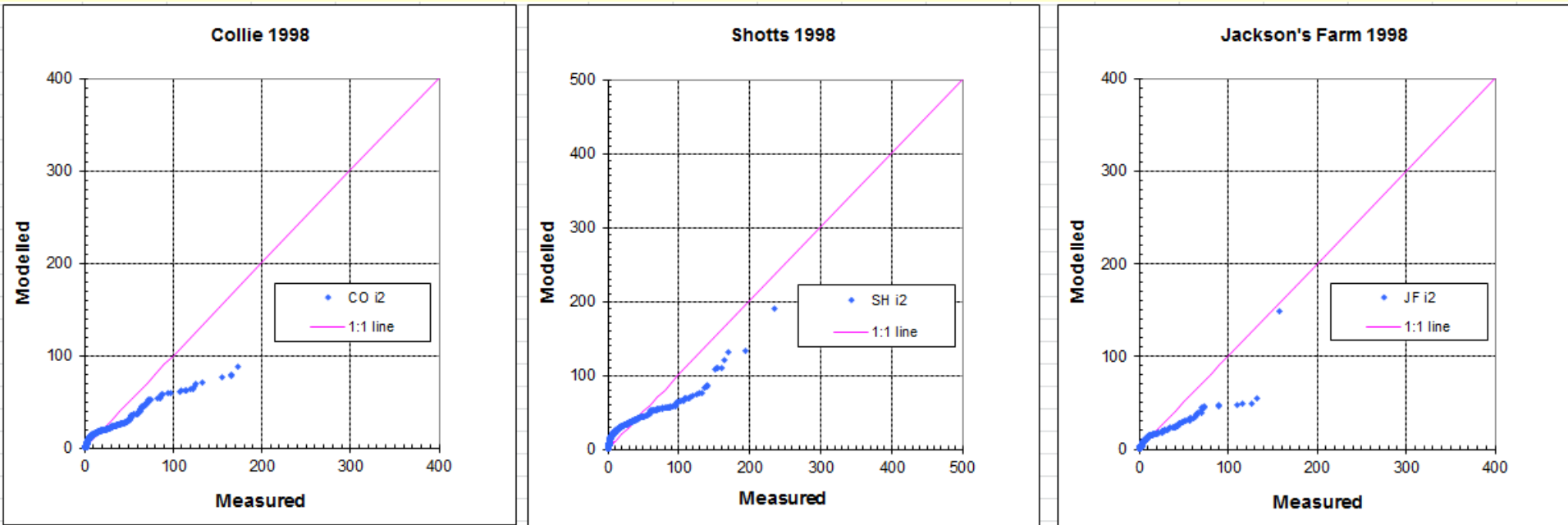
- convective mixing is mild ( $0 < w^* < 1$ )



*model over-estimation in mildly convective conditions at all monitoring sites*

# AERMOD run i2 (1998)

- convective mixing is moderate to strong ( $w^* > 1$ )



*model under-estimation despite over-estimation for all hours and unstable hours*

# AERMOD's three plume scheme

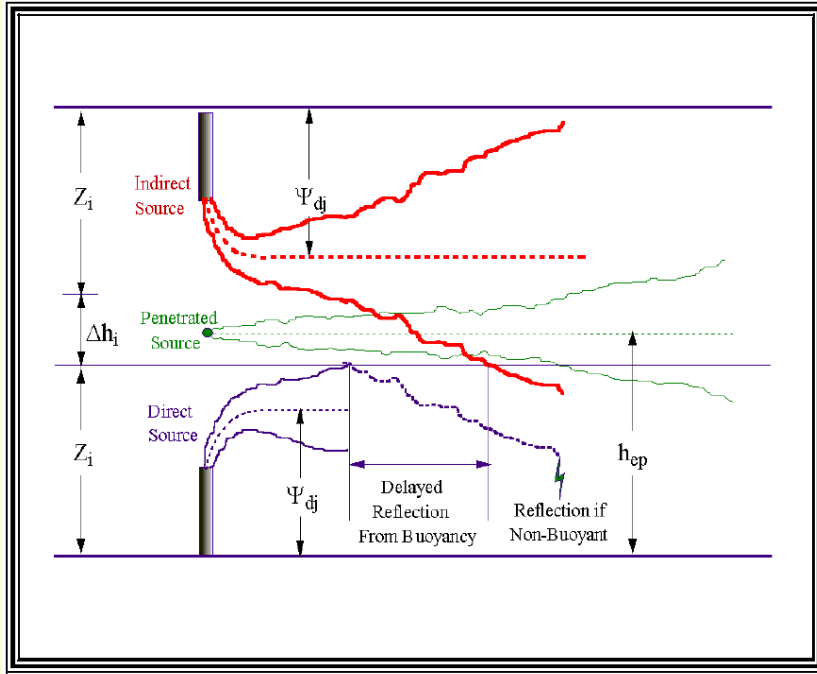


Figure 14: AERMOD's Three Plume Treatment of the CBL

- AERMOD's penetrated plume has been found (from debug output) to be a dominant cause of highest concentrations at Collie and Caversham (further evidence follows);
- AERMOD has no memory from one hour to the next;
- must calculate the concentration from a penetrated plume in the hour it penetrates even though it may not mix to ground in that hour;
- in reality, by the time it mixes to ground, the meteorology would be different, notably the turbulent mixing would be greater;
- the scheme must therefore be "tuned" to give a representative magnitude of concentrations, recognising that the time of occurrence will not be generally correct.
- How well has it been tested? Might it become unreliable for various ranges of met conditions, plume buoyancy, distance-time, etc?

# AERMOD's three plume scheme cont...

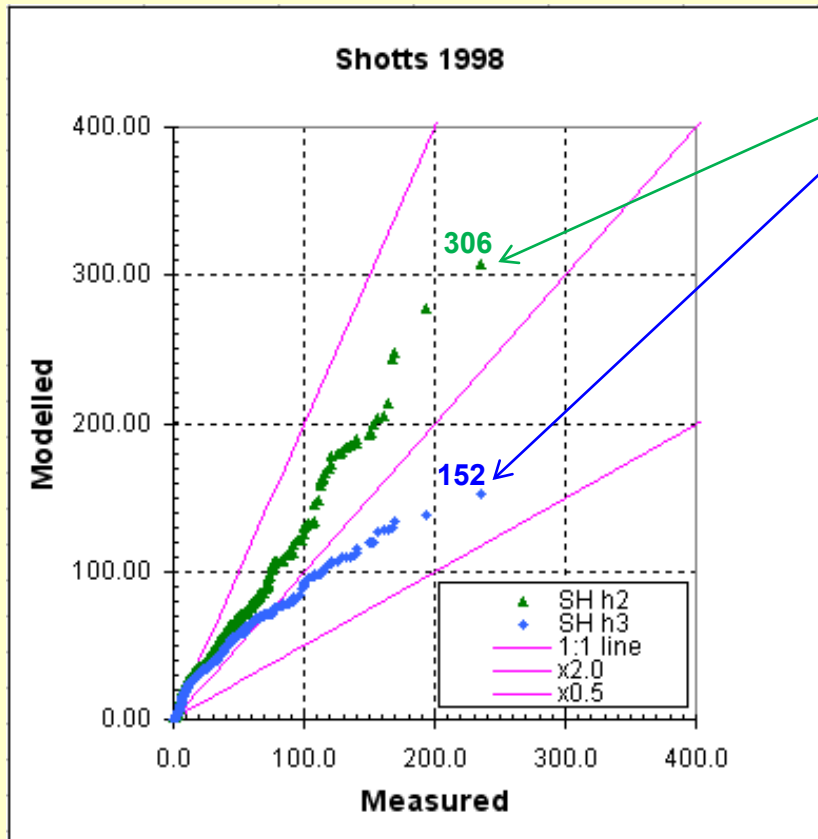
*The AERMOD MFD discussion of dispersion in the CBL references Weil Corio and Brower (1997). It is not clear whether the penetrated plume dispersion scheme came from that reference, but Jeff Weil referred to the paper in an email 23 June 2012 to Steve Hanna, forwarded to Paine and Rayner.*

*WC&B (1997) has a dispersion formulation for the penetrated plume (eq. 30) that uses the convective PDF model, whereas the AERMOD Model Formulation Document eq. 66 is Gaussian in the vertical.*

- Is it likely that a Gaussian plume formulation for vertical dispersion into a growing CBL will be generally reliable?*
- Is the penetrated plume formulation (eq. 66 and the formulae for  $\sigma_y$  and  $\sigma_{zp}$  described in MFD p59-62) unique to AERMOD or does it have another origin and how has it been evaluated?*

# Effect of turning off the penetrated plume.

run h2 is ~ identical to h1 (Zic calculation corrected as in v12345 – negligible difference);  
run h3 is as per h2 but with the concentration contribution from the penetrated plume set to zero in the code;  
the penetrated plume dominates the highest modelled concentrations at the Shotts monitoring site (8 km from the power station).



*The following slides use debug output to examine these highest concentrations in h2 and h3, to demonstrate that these concentrations occur on different occasions when different phases of dispersion are dominant (plume penetration-fumigation c.f. plume trapping) and that the penetration-fumigation process that gave rise to the h2 maximum was very dominant, contributing much almost 90% of the total concentration for that hour at Shotts. AERMET records associated with the highest hours are included on the following slides.*

# Highest concentration in run h2, hour 98072309:

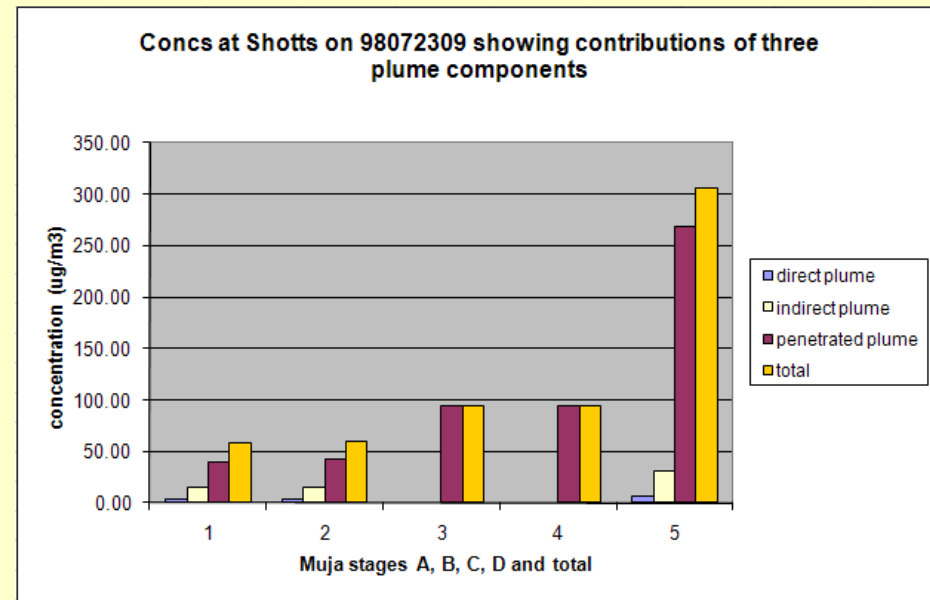
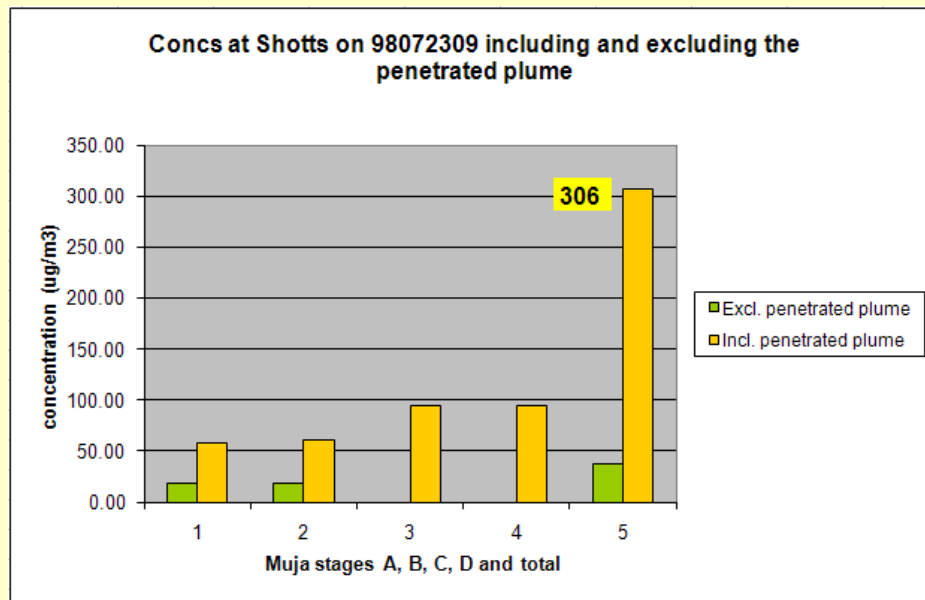
The first graph shows concentrations from each stage (stack) at Muja PS, including and excluding the contribution of the penetrated plume, and the totals from all stacks. The second graph shows plume components. Values were obtained from debug output.

Only the smaller A & B plumes are not fully penetrated.

Penetrated plumes cause 88% of the total concentration at Shotts from Muja.

The contribution from the alumina refinery is negligible

yr	mo	dy	jd	hr	Hs	u*	w*	VPTG	Zic	Zim	L	z0	B0	r	Ws	Wd	Zref	Temp	Ztemp
98	7	23	204	9	18.7	0.221	0.369	0.011	96	239	-51.8	1	1	0.27	1.5	147	36	280.4	36

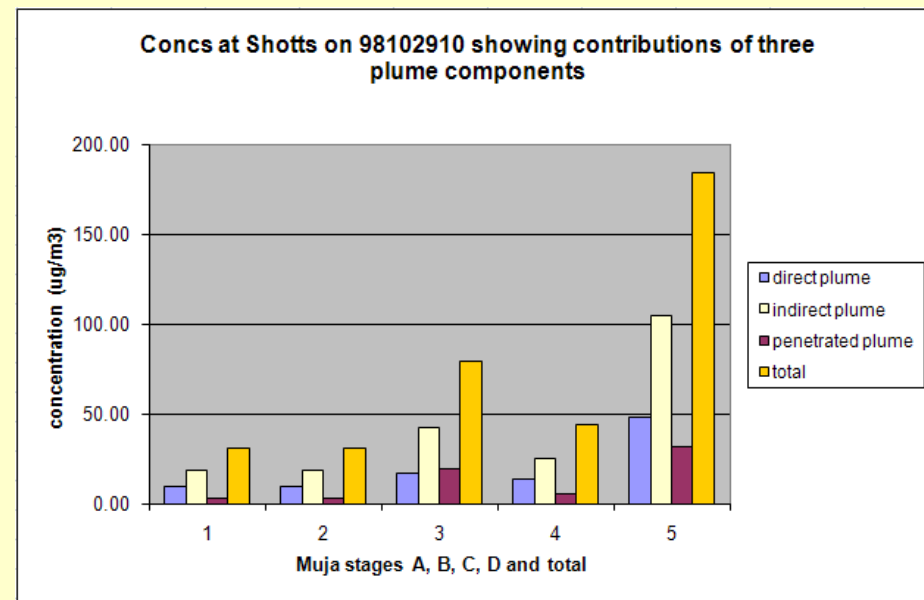
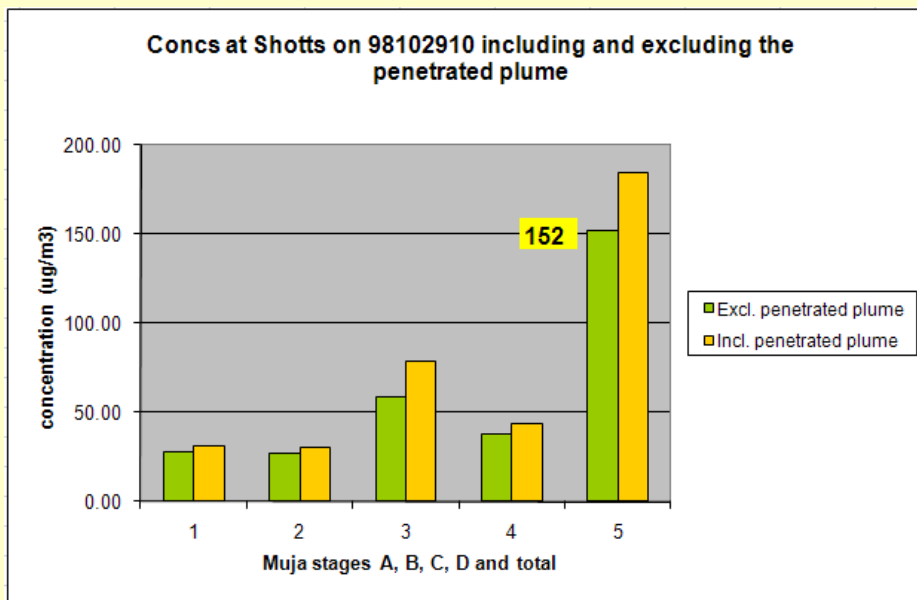


# Highest concentration in run h3, hour 98102910:

Compare to the foregoing graph for run h2 - penetrated plumes make a relatively minor contribution at Shotts for all Muja stacks, so that exclusion of the penetrated plumes reduces the total concentration by a relatively small amount, from 184 to 152 (152 is the value on the QQ plot for h3 above).

The indirect plume is the major component for each plume, due to a high fraction of trapping for all plumes within the 442m convective mixed layer. The contribution from the alumina refinery is negligible.

yr	mo	dy	jd	hr	Hs	u*	w*	VPTG	Zic	Zim	L	z0	B0	r	Ws	Wd	Zref	Temp	Ztemp
98	10	29	302	10	55.4	0.291	0.882	0.01	442	361	-39.7	1	1	0.1	1.9	147	36	288.8	36



# Penetration and dispersion - AERMOD's plume c.f. CALPUFF's puff

- NOTE – the following are Ken Rayner's observations – comments welcome.
- A **plume** penetrates and disperses within a 1-hour timestep. Dispersion of a penetrated **puff** may occur an hour or more later (an obvious point but it can make a big difference to concentrations).
- A partly trapped “indirect” **plume** disperses via a convective PDF formulation. A partly trapped **puff** does not (CALPUFF uses a Gaussian distribution in the vertical for this case).
- On the other hand, a penetrated **plume** disperses via a vertical Gaussian formula, not convective PDF. Because penetrated **puffs** typically have very small  $\sigma_z$ , they are typically fully entrained in a single timestep by a growing mixed layer, and dispersion of a fully entrained **puff** is via convective PDF, hence relatively rapid vertical dispersion, relatively large concentrations. *(And this could occur if the mixing height had been set to  $Z_{im}$ , despite convective turbulence not being fully developed in the upper portion of  $Z_{im}$ ).*
- Note – comments on CALPUFF's behavior are based on other work provided to Bob Paine for review, available on request.

# Aspects of AERMOD formulation that may warrant review.

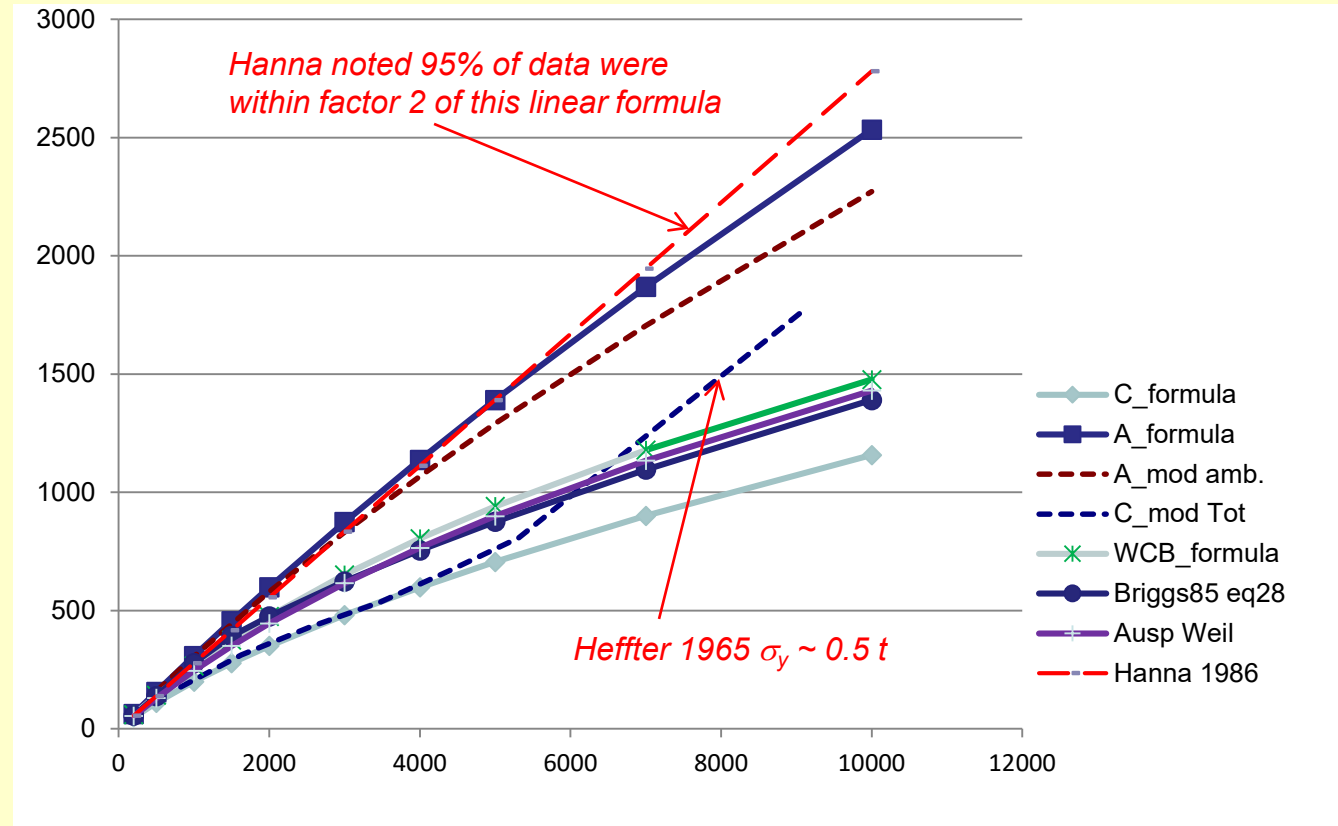
- Slides 26, 27 show apparent AERMOD underestimation in well developed convective conditions at distances of 8 km and greater (tentative finding). Reasons considered to date:
  - Lateral dispersion formulation under unstable conditions;
  - Meandering plume.
- Initial examination and questions in the following slides.

# AERMOD lateral dispersion formulation c.f. others.

- See in the next slide a graph of various  $\sigma_y$  formulae for Muja A using AERMET results printed above the graph. Convection is developing in this mid-morning hour. See the spreadsheet *Sigma Y formulae.xls* for AERMET data and  $\sigma_y$  calculations.
- AERMOD and CALPUFF curves are calculated from tech. documents and also extracted from debug output. Agreement is quite close in each case (noting that guesstimates were made for height in CBL and  $u_{\text{eff}}$ ).
- AERMOD  $\sigma_y$  is close to linear for a 100 m stack – much larger  $\sigma_y$  values than others (except a linear option noted by Hanna 1986). Has this difference been examined and confirmed, noting sensitivity of AERMOD's formula to source height? If based on field observations, how important was shear, topographic effects? What scales of motion are large enough to give near-linear growth far from the source? Is there any “double counting” of plume meander by the  $\sigma_y$  formula and the meandering plume formulation?
- The CALPUFF formulation, including Heffter (1965), is quite different to all others. The Heffter formula gives a fixed growth rate of 1.8 km per hour, irrespective of stability or anything else, after reaching a user-selectable handover value of  $\sigma_y$ . Is this reliable?

# Various $\sigma_y$ formulae – convective dispersion

AERMET data used to derive the $\sigma_y$ curves:							
hour	u-	w-	Zic	Zim	L	z0	speed
10	0.279	1.483	1001	339	-16.6	0.25	2



C\_formula: CALPUFF UG eq 2-65  
 A\_formula: Aermod MFD  
 A\_mod amb.: AERMOD debug  $\sigma_y$  ambient  
 C\_mod Tot: CALPUFF debug  $\sigma_y$  + Heffter

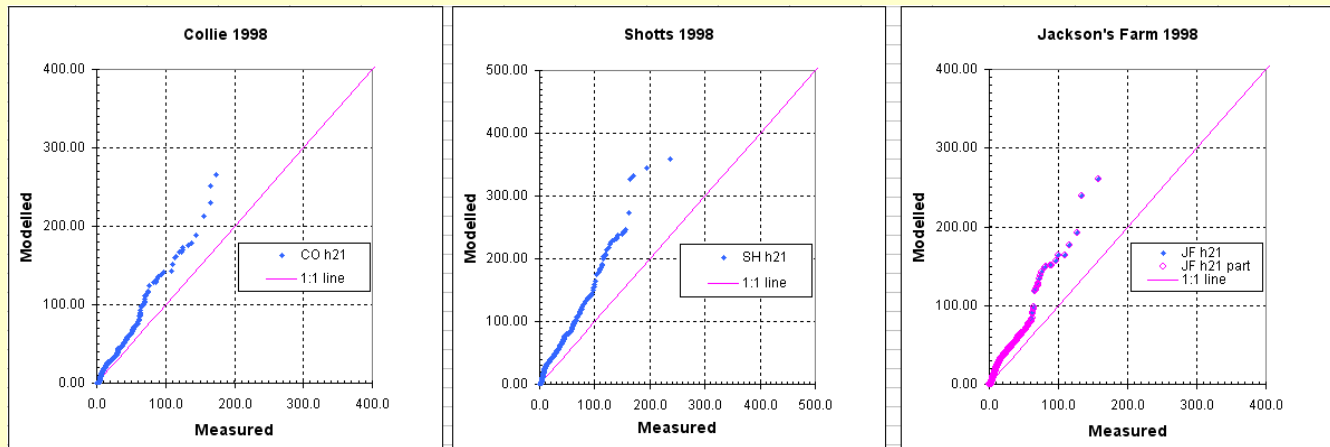
WCB\_formula: Weil et al. 1997  
 Briggs85 eq28: J Clim & Appl Met p 1167  
 Ausplume Weil (not sure of ref.)  
 Hanna 1986: J Clim & Appl Met p1426

# Forcing AERMOD and CALPUFF a little closer.....

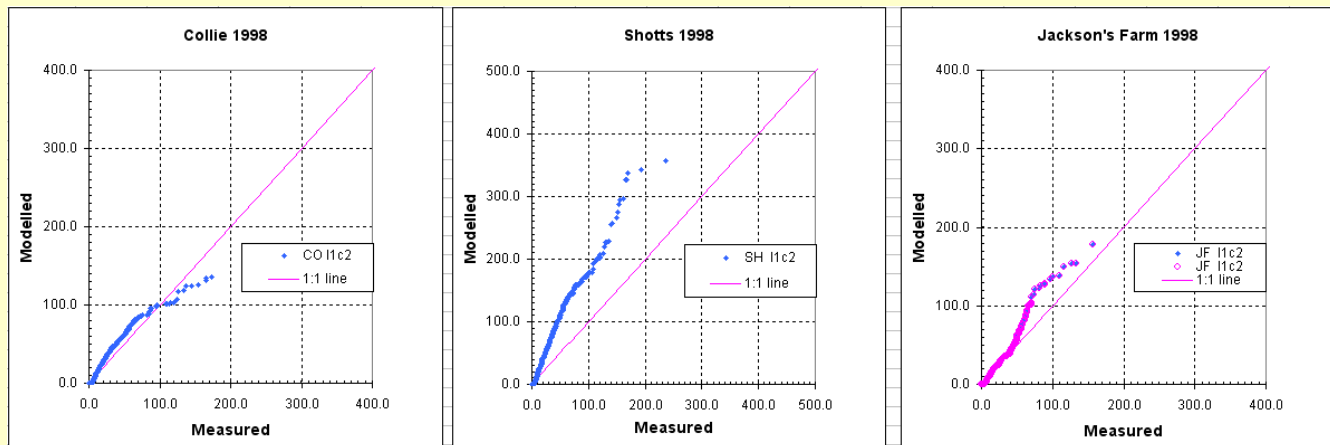
Interesting to note that disabling the meandering plume in AERMOD while making CALPUFF's  $\sigma_y$  linear from the source, like AERMOD, gives closer agreement at Shotts (closest monitor) while making CALPUFF values lower at more distant monitors.

*Not suggesting that these model changes have merit!*

AERMOD h1/h2  
(slide 6) with  
meandering  
plume disabled



CALPUFF I1a1  
(slide 8) with  
Heffter linear  $\sigma_y$   
starting at  
source



## Other AERMOD questions.

- AERMOD uses  $Z_i = \text{MAX}(Z_{im}, Z_{ic})$  in unstable conditions.  $Z_{im}$  is calculated from the formula of Venkatram (1980), which is valid if the temperature scale  $T_*$  is approximately constant in stable conditions. But  $T_*$  changes sign and magnitude from night to day (unstable) so how can the formula be validly used in unstable conditions? Should an alternative neutral-conditions formula be used?
- A smoothing formula is applied to  $Z_{im}$ . It gives rapid growth but slower decline which can result in long post-sunrise transition periods while  $Z_{ic}$  catches up to  $Z_{im}$ . Realistic?
- Isn't the fixed depth (500 metres) of the layer above  $Z_{ic}$ , over which the  $d\theta/dz$  is calculated, sometimes excessive, e.g. after sunrise,  $Z_{ic}$  low and growing, plume penetration-dispersion dominant? The actual  $d\theta/dz$  that determines plume leveling height could easily be greater than that over 500m for other than very buoyant plumes.

## Other AERMOD questions cont....

- Most met parameters, measured or calculated, are hourly averages whereas Zic is an end-of-hour integrated value – this affects  $w^*$  too. May cause under-estimation of concentrations – has this been considered?
- Modeling studies using TAPM indicates that plume enhancement from adjacent stacks may be significant for Muja power station. The Briggs 1975 plume enhancement method produces a 10 to 25% reduction in the predicted concentrations. Is there some standard practice for considering plume enhancement from adjacent stacks in the US?
- Appropriate model performance measures? (For a few far-flung monitoring stations, QQ plots and residual plot analyses seem appropriate.)
- Comments on important meteorological measurement welcome, e.g. wind and temperature profiles (RASS Sodar?), turbulence – what parameters and heights?

# Evaluation of AERMOD SO<sub>2</sub> Predictions for a Research-Grade Field Experiment

**Paper # MO10**

**Presented at the**

**Guideline on Air Quality Models: Planning Ahead**

**March 19-21, 2019**

**Durham, NC**

**Jeff Connors, Christopher Warren, and Robert Paine**

AECOM, 250 Apollo Drive, Chelmsford, MA 01453

## **ABSTRACT**

The Collie region in Western Australia has a number of significant sources of atmospheric emissions associated with mining, electricity generation and alumina refining. The major sources of air pollution include 3 coal-fired power plants and an alumina refinery. Due to the extent of the emission sources in the area, the Western Australia Department of Environmental Conservation (WA DEC) has overseen ambient measurement studies and air dispersion modeling studies for this area. The need for a Collie Airshed Study (CAS) has been addressed by the installation of a comprehensive network of 12 SO<sub>2</sub> monitoring stations, several meteorological measurements, and collection of hourly emissions information.

This paper reports on the results of an AERMOD<sup>1</sup> model evaluation study involving the initial 6 months of a 2-year model evaluation study. Due to the relatively flat terrain and tall stacks for the major sources, the peak concentrations are observed to occur during convective conditions, especially on low wind speed days in the summer. The evaluation exercise involves a number of AERMOD variations in order to determine the best performing model, including options with the ALPHA LOWWIND keyword exercised. The results of the evaluation have been used to recommend enhancements in the ongoing measurement program as well as additional areas of model review.

## **INTRODUCTION**

The Collie region has a number of significant sources of atmospheric emissions (SO<sub>2</sub>) associated with mining, electricity generation and alumina refining. The major sources of air emissions include:

- Muja Power Station,
- Collie Power Station,
- Bluewaters Power Station, and
- Worsley Alumina Refinery.

Due to the extent of the emission sources in the area, the Western Australia Department of Environmental Conservation (WA DEC) has overseen several ambient measurement and air dispersion modeling studies for this area.

The industrialized sources in the Collie Region have generally accepted the merits of developing an airshed management strategy, supported by reliable modeling and adequate monitoring. Despite the existence in the past of a significant monitoring program (1996-2001), the WA DEC requires a comprehensive, integrated monitoring program to be undertaken to demonstrate the reliability of a model (or models), in light of:

- limitations in the previous monitoring program;
- major emissions sources added since the previous monitoring study concluded (2001),
- the potential for higher sulfur content in coal to be used by the plants in the future, creating the potential for ambient SO<sub>2</sub> criteria to be approached;
- lack of reliable data on actual emissions for all sources for model input; and
- WA DEC's preference that any airshed management strategy be based on a model proven to be reliable using comprehensive and reliable data on emissions, ambient concentrations and meteorology.

## **COLLIE AIRSHED STUDY OVERVIEW**

The need for the Collie Airshed Study (CAS) has been addressed by the installation of a comprehensive network of SO<sub>2</sub> monitoring stations, meteorological measurements, and collection of hourly emissions information. Figure 1 shows the entire region for the emission sources and the monitoring network, consisting of 12 SO<sub>2</sub> monitoring stations.

Additional model evaluation exercises for the CAS will be conducted once a more complete database is available. The focus of this initial model validation exercise, utilizing the initial 6 months of data, is to meet the following objectives:

1. To evaluate the performance of the preferred model (AERMOD) in predicting ground-level concentrations at the monitoring sites.
2. To determine if any potential improvements can be made to the measurement program or to the dispersion model for the remaining period of the monitoring study.

To carry out these objectives, a basic evaluation of the meteorological data was performed followed by the actual model evaluation.

The meteorological data evaluation involved a preliminary evaluation of the 6 months of meteorological data collected early in the program (November 2017 – April 2018) to evaluate the quality of the data and assess the performance of the meteorological pre-processor to AERMOD, AERMET.

A review of the emissions, meteorological, and monitoring data indicates a database with a high data capture that is very useful for the initial model evaluation study. The monitoring data indicates that, as expected, most of the peak SO<sub>2</sub> concentrations occur during the daytime hours (with the majority occurring during the late morning to early afternoon). This understanding helped to focus the review of the meteorological conditions upon daytime hours and the growth of the convective mixing layer.

A considerable effort was made to review data from the various meteorological towers and Sound Detection and Ranging (SODAR) instruments to determine the best set of meteorological data to be used for input into AERMOD. The data capture and detection range from the main Scintec SODAR and Radio Acoustic Sounding System (RASS; collocated with the 80-m tall meteorological tower) were low during the six months reviewed for this study due to site-specific issues. With the installation of additional acoustic material at the base of the SODAR, there has been a significant improvement (at least 90% data capture) in the performance of that instrument since May 2018.

The importance of the daytime hours guided the meteorological analysis toward a review and evaluation of the heat flux and soil measurements and use of that information to determine the allocation of net radiation toward the major components of sensible and latent heat flux. The growth of the convective boundary layer predicted by AERMET was tested during a period of multiple radiosonde launches that occurred from March 6-15, 2018. This testing is described in detail in a companion paper<sup>2</sup> and will not be repeated here.

The actual model evaluation evaluated AERMOD's predicted ground-level concentrations for each monitoring site by modeling all of the major sources listed above. The evaluation was conducted for two heat flux approaches; a Base and Alternative Case, along with variations in the turbulence data used as well as "LOWWIND" options (minimum sigma-v values) available in AERMOD. A screening evaluation utilizing several model options was used to narrow the list of best performing models for a larger set of statistical tests.

AERMOD's predicted ground-level concentrations at each of the 12 monitoring sites was evaluated by modeling all sources (i.e., no discrimination by source). The evaluation was conducted for the following 6 cases, as requested by WA DEC:

- All observations;
- Convective mixing height < 600 meters;
- Convective mixing height > 900 meters;
- Convective velocity scale < 1 m/s;
- Convective velocity scale > and = 1 m/s; and
- For hours between 11 and 17 WST with the ambient temperature greater than 20°C.

For each of the above listed cases, several statistical analysis techniques were used for these evaluations, including quantile-quantile ("Q-Q") plots and statistical measures such as the European Environmental Agency Relative Mean Error and the Robust Highest Concentration, meteorological conditions for the top 5 1-hour concentrations at each monitor, and residual plots of concentration versus distance.

## **FIELD STUDY MEASUREMENT PROGRAM**

The CAS includes four major SO<sub>2</sub> emission facilities consisting of eight stacks; the Muja Power Station (2 stacks), Collie Power Station (1 stack), Bluewaters Power Station (2 stacks) and Worsley Alumina (3 stacks). Table 1 lists the stack parameters with the location of the sources. One of the stacks from the Worsley Alumina facility has 3 separate flues contained within a single stack. Hourly SO<sub>2</sub> emissions were tracked using continuous emission monitoring systems (CEMS) for all sources during the 6-month initial study period with the exception of the Worsley Alumina Boilers 1-3. Temporary CEMS were installed in February 2018 for Worsley Alumina sources. Prior to that step, parametric monitoring was used to estimate the emissions for these boilers. Figure 2 provides hourly time-series plots for all sources to be modeled as part of the study.

Figure 1: Collie Airshed SO<sub>2</sub> Sources, Monitoring Network and Meteorological Sites

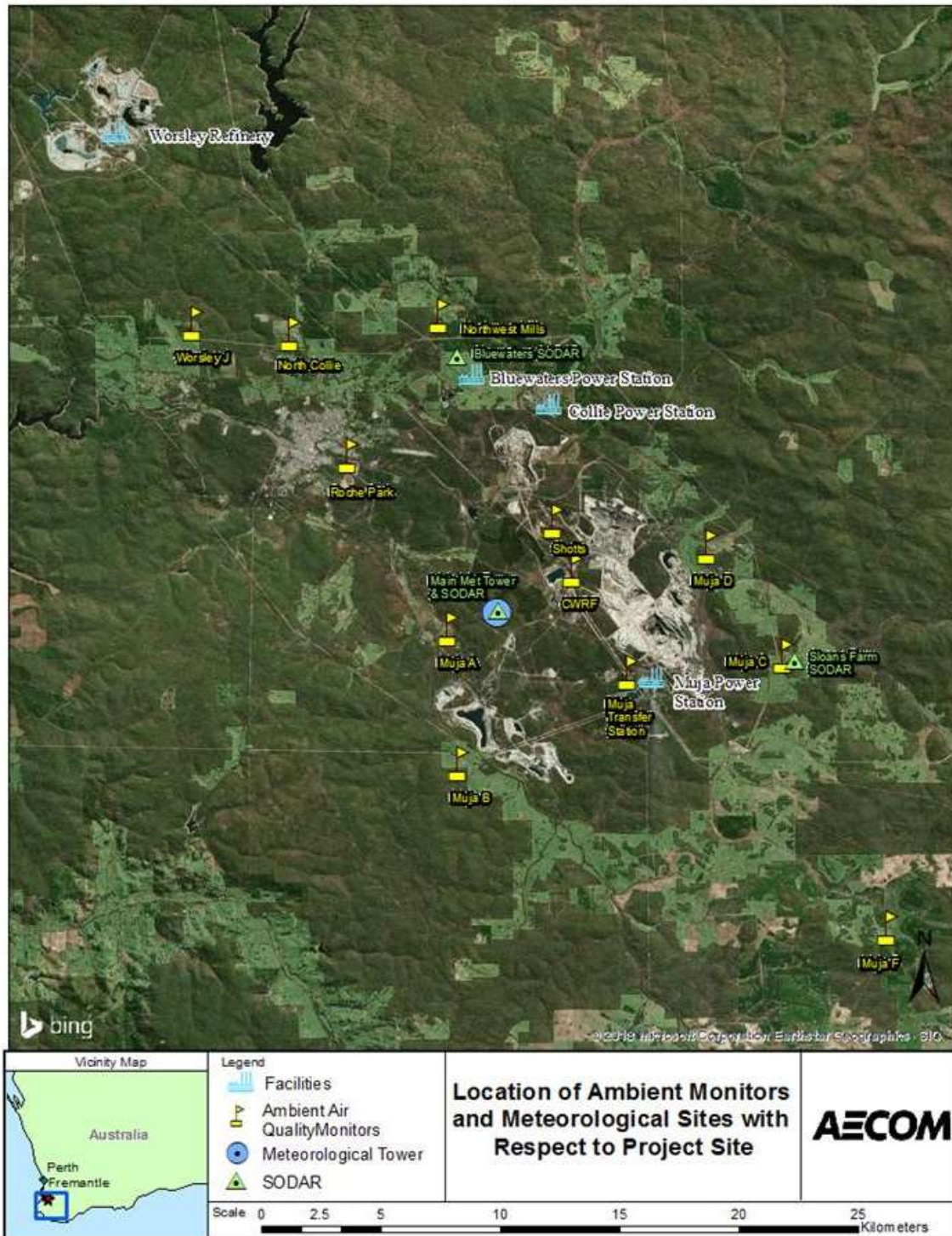


**Table 1: SO<sub>2</sub> Source Locations and Stack Parameters**

Source	Easting (m) MGA94	Northing (m) MGA94	Stack Height (m)	Stack Diameter (m)
Muja Unit C	435636	6299074	151	5.91
Muja Unit D	435525	6299109	151	5.91
Collie Unit A	431227	6310439	170	5.23
Bluewaters Unit 1	428126	6311651	100	4.00
Bluewaters Unit 2	428202	6311609	100	4.00
Worsley Boilers 1-3	413242	6322257	76	2.30
Worsley MFC 5	412750	6322140	90	2.50
Worsley MFC 6	412750	6322074	90	2.50

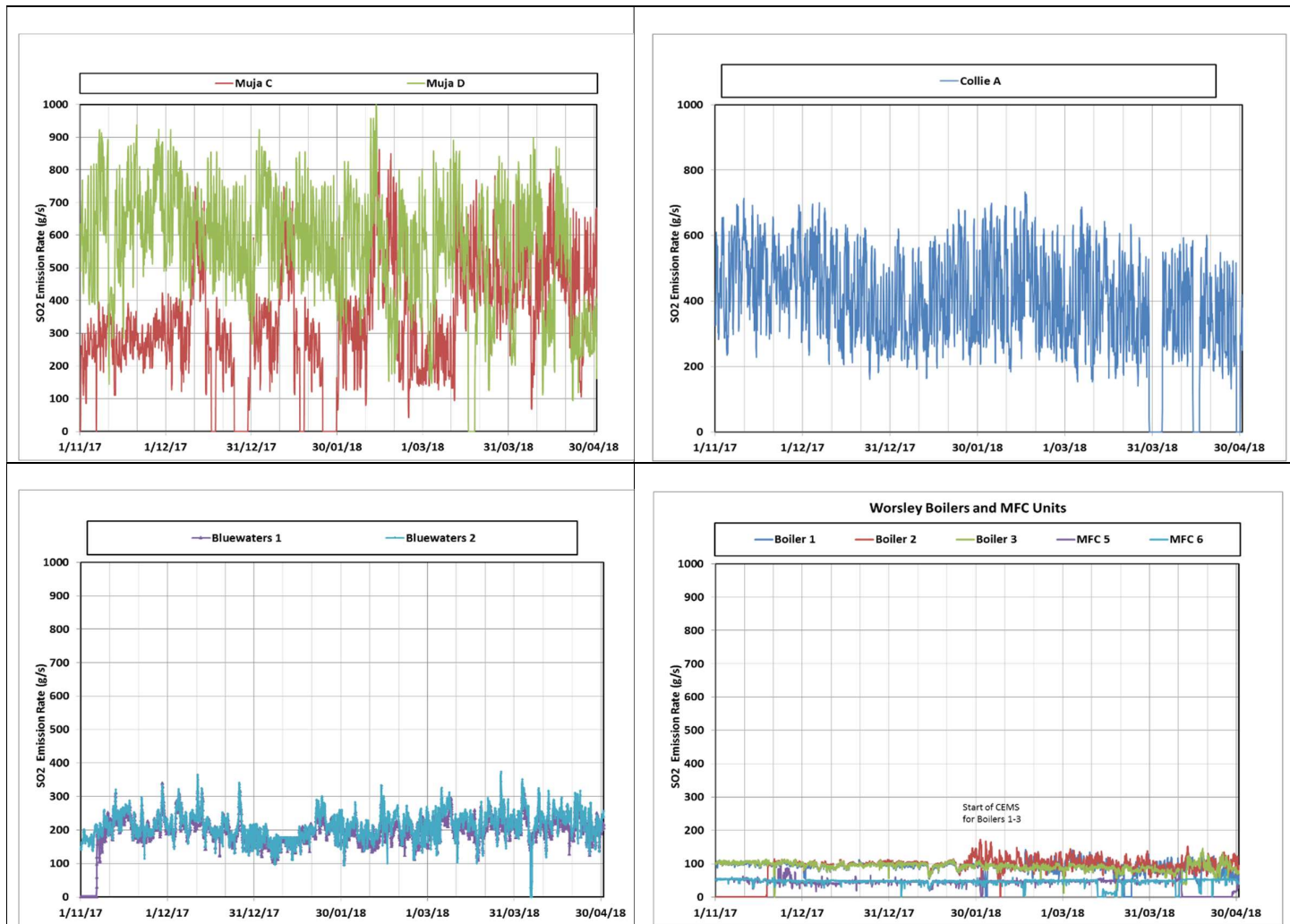
The “raw” SO<sub>2</sub> monitoring data were 5-minute average values; 1-hour averages were computed from this information. Applicable SO<sub>2</sub> ambient standards<sup>3</sup> for Australia are: a 1-hour standard of 200 ppb (can be exceeded on only 1 day per year), a daily standard of 80 ppb (can be exceeded on only 1 day per year), and an annual standard of 20 ppb. A summary of the maximum 1-hour SO<sub>2</sub> value for each month and over the entire 6-month study period is plotted in Figure 3. The highest hourly SO<sub>2</sub> observed concentrations generally occurred during the summer months of January through March.

The design of the meteorological monitoring program for the CAS had the goal of providing a vertical profile of several levels of wind, temperature, and turbulence data for input to dispersion models such as AERMOD. In addition, with the expectation that the daytime hours with convective mixing would be very important in the modeling analysis, measurements of heat flux components were included in the measurement program.

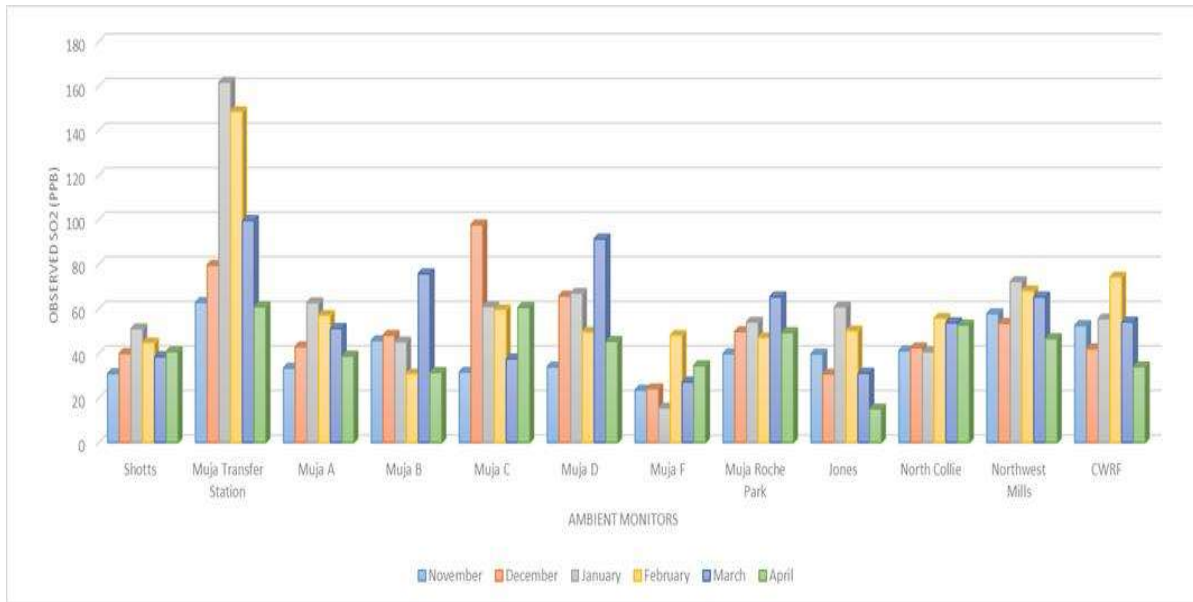
AERMOD uses measured or parametrized estimates of horizontal and vertical atmospheric turbulence to estimate plume spreading rates. These turbulence parameters are typically measured from the standard deviation of the crosswind wind speed in the horizontal, or  $\sigma_v$ , and the standard deviation of the wind speed in the vertical, or  $\sigma_w$ . In the absence of observed turbulence measurements, AERMOD will parameterize these variables. In general, we would expect the AERMOD model performance to be optimized with the use of the measured turbulence data, but there are some applications where this is not necessarily the case. Therefore, for the model evaluation study, we conducted modeling tests with the turbulence data omitted for the initial modeling runs of the base and alternative meteorological dataset cases, and then included turbulence data for subsequent modeling runs.

Table 2 summarizes the recommended meteorological data from the November 1, 2017 – April 30, 2018 period selected for use in the model evaluation of the Collie Airshed Study.

Figure 2: Hourly Emission Time Series for Major SO<sub>2</sub> Sources within the Collie Airshed (November 2017 – April 2018)



**Figure 3: Monthly Distribution of the Maximum Hourly SO<sub>2</sub> Ambient Measurements November 2017 to April 2018**



**Table 2: Meteorological Data Supplied to AERMET for CAS Model Evaluation**

Measurement	Height Above Ground (m)
Wind Speed	30, 50, 80
Wind Direction	30, 50, 80
Vertical Winds	30, 80
Ambient Temperature	2, 10, 30, 50, 80
Relative Humidity	2
Pressure	2
Net Radiation	80
Precipitation	2
Ceilometer	0 to 7,600
Eddy Covariance	35
Bluewaters SODAR (Wind Speed, Direction)	100 to 300 (10-m intervals)
Surface Roughness	1.08 <sup>1</sup>
Bowen Ratio	Varies <sup>2</sup>
Upper-Air Radiosonde	On-Site (Perth used Nov 1-5, 2017)
1 Composite roughness length based on average of twelve 30° sectors around the Consortium tall tower.	
2 Daily and Monthly average Bowen ratios used.	

## MODEL EVALUATION RESULTS

The initial phase of the modeling evaluation considered several candidate AERMOD approaches with limited statistical tests to determine the best candidates for more extensive testing and evaluation. The first set of modeling runs assessed the model performance between the two meteorological datasets. The primary difference between the two datasets is that the Base Case uses an approach that derives sensible heat flux values from daily-varying Bowen ratios, while the Alternative Case forces the predicted sensible heat flux in convective conditions to be equal to the measured flux data. All observational hours over the duration of the 6-month initial study period were included as part of this initial evaluation phase.

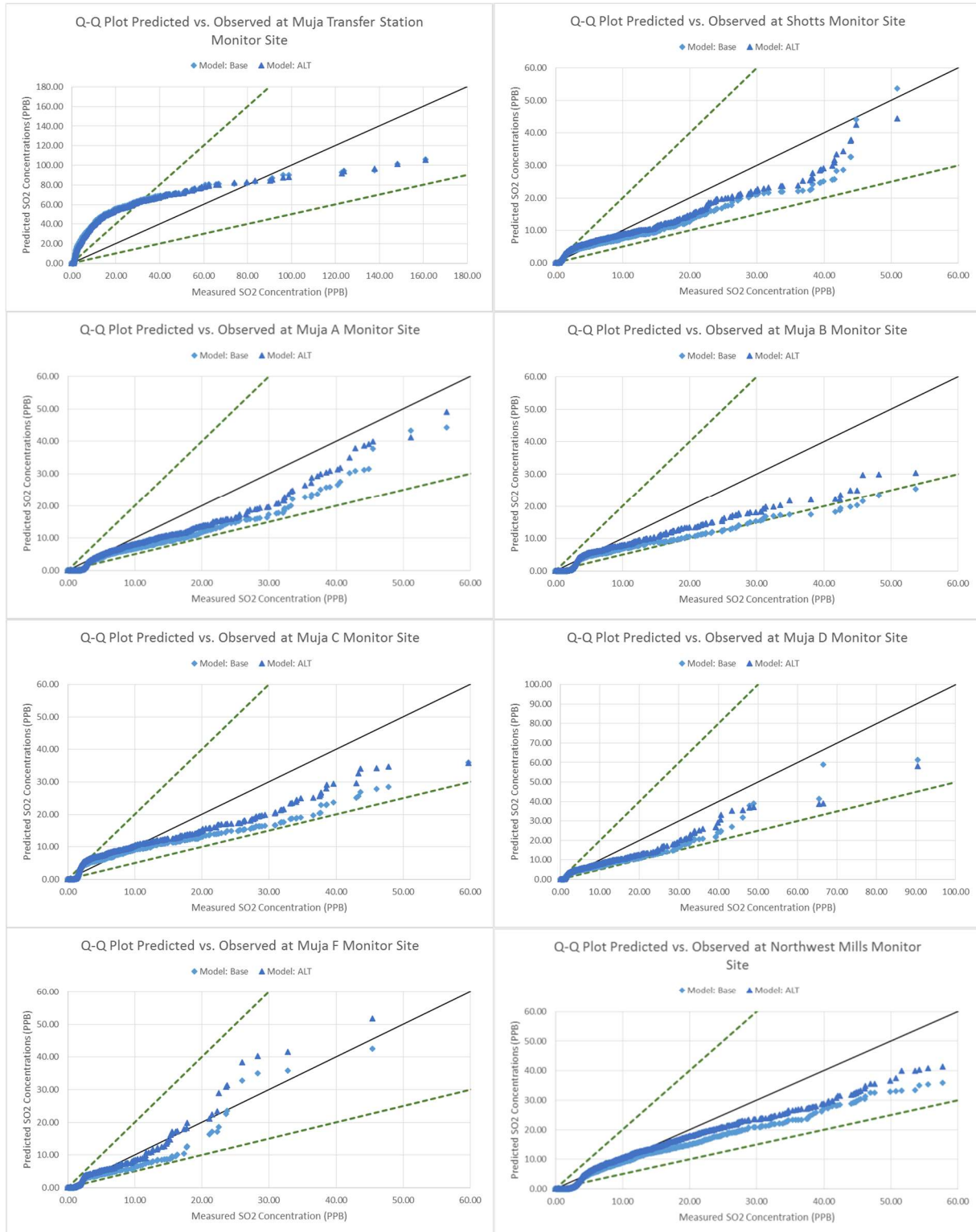
In general, the difference between the ranked hourly predicted concentrations between the Base and Alternative Case runs without turbulence were less than 20%. Overall, the Base Case runs demonstrated better performance than the Alternative Case. Q-Q plots for each of the monitor locations are provided in Figure 4 for modeling runs without turbulence data.

When the ranked-paired concentrations did exhibit larger differences (i.e., greater than 20%), the Base Case showed improved performance to the observed data over the Alternative Case dataset. The outliers consisted of Muja D and CWRF sites where a few ranked pairs differed by as much as 50%. For example, at CWRF, the highest ranked concentration for the Base Case run was  $81.2 \mu\text{g}/\text{m}^3$ , while it was only  $54.1 \mu\text{g}/\text{m}^3$  for the Alternative Case. With the highest observed hourly concentration reported at CWRF being  $73.8 \mu\text{g}/\text{m}^3$ , this is the difference between the Base Case model slightly over-predicting versus the Alternative Case model under-predicting.

One notable difference was seen at the Muja F monitoring site location (representing a relatively large distance between the source and monitor) where the Alternative Case dataset shows an over-prediction by the model for the highest predicted versus observed concentration, compared to an under-prediction by the model from the Base Case. Further review revealed that in both of the models' peak-predicted concentration events, the key plume component was from the penetrated plume (that is, the plume initially rose to a level above the convective mixing height). It is noteworthy that some AERMOD peak predictions can occur with the penetrated plume component, while others occur due to a direct plume component in which the plume is emitted within the convective boundary layer. For inversion breakup conditions, the time difference between these two types of events can be as short as a single hour.

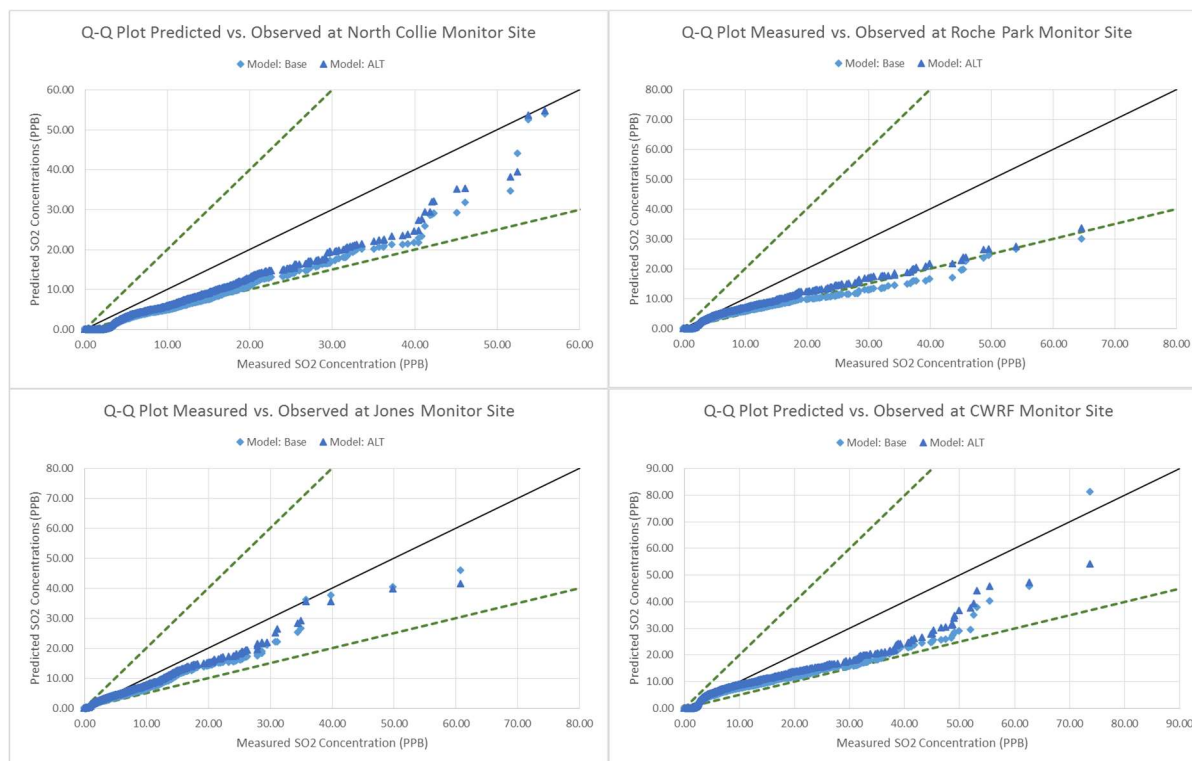
A key monitor is the Muja Transfer Station, which is only about 1 km from the Muja Station. At that monitor, the peak observations may be under-predicted due to stagnation events associated with inversion breakup conditions at mid-day. For these events, multiple hours of emissions can accumulate, and AERMOD has no memory of previous hours' emissions. The over-predictions for a large portion of the ranked concentration distribution is likely due to the plume penetration formulation, which results in plumes mixing to the ground too quickly in most cases (when the mixing height is still below the plume level). This issue is likely due to AERMOD's omission of a stable component of the sigma-w formulation, leading to values of sigma-w that are too high in most cases. The recommended correction is to test within AERMOD for cases where the mixing height would intercept the plume within the hour, and then allow for the high sigma-w values only then.

**Figure 4: Q-Q Plots for No Turbulence Base and Alternative Case Runs**



Note: Dashed lines represent 1-to-2 and 2-to-1 measure-to-predicted ratios.

**Figure 4: Q-Q Plots for No Turbulence Base and Alternative Case Runs, continued**



Note: Dashed lines represent 1-to-2 and 2-to-1 measure-to-predicted ratios.

At several of the monitors, a model under-prediction tendency is noted. These monitors range from about 5-10 km from one or more sources. Therefore, this issue will be further investigated with a full grid of receptors, as well as sensitivity testing for the roughness length used (currently about 1 meter). Due to the fact that only a 6-month period has been tested, the model evaluation will be extended to a longer period in a planned effort for the future. Other means of determining possible causes of AERMOD under-prediction will be the use of model sensitivity plots with the predicted-to-observed ratio plotted on the y-axis versus a variable such as mixing height, wind speed, etc.

Additional model performance evaluations were conducted prior to the selection of a “best model performing dataset” for the Collie Airshed, including the following model options:

- Inclusion of sigma-theta component of turbulence data,
- inclusion of sigma-theta and sigma-w components of turbulence data, and
- use of AERMOD’s LOWWIND alpha option.

The Robust Highest Concentration (RHC)<sup>4</sup> was computed for several modeling options at each monitor; the results are plotted in Figure 5. The runs that include sigma-w nearly always show ratios well below 1.0 (under-predictions). The only exception is at CWRP, where the ratios for the sigma-w options are comparable to the other runs. It should be noted that sigma-theta and sigma-w inputs to the model were only obtained from the 80-m tall tower. Given the recent improvements in SODAR data returns, future work is anticipated to involve assessing the use of the turbulence data from this instrument. Otherwise, the options using sigma-theta and sigma-theta with LOW\_WIND perform the best overall.

**Figure 5: Ratio of the Robust Highest Concentration (RHC) for N=10 for Sigma-theta and Sigma-theta with LOW\_WIND Runs at Each Monitoring Site**



Low RHC ratios are seen at three specific monitors: Muja B, Muja C and Roche Park, indicating the model is under-predicting at those monitors by more than 30%. Under-predictions at three other monitors range between 10 and 30%, while predictions at two monitors are within 10% of being unbiased. Four monitors have over-predictions of more than 10%. The overall model performance over the monitors other than the three with the largest under-predictions with the use of sigma-theta and sigma-theta with the LOWWIND option is encouraging, with a geometric mean predicted-to-observed RHC ratio of 1.02 for the sigma-theta option and 0.97 for the sigma-theta with LOWWIND option for the Base Case modeling runs.

Although the extent of the monitors deployed (12 in total) is quite extensive, the concentration pattern over the entire area has not yet been reviewed. It is also unclear by just modeling at these discrete locations whether the plume predicted by the model is directly impacting these locations, partially hitting or completely missing. While a model run using a nested receptor grid that would cover the entire Airshed domain (i.e., 40 km by 40 km) would likely provide valuable

insight into this uncertainty, a review of whether the model is performing well at various distances based on the data points currently being used is a useful evaluation test.

Figures 6, 7, and 8 show the maximum, 5<sup>th</sup> and 10<sup>th</sup> highest concentrations for observed and predicted (Base and Alternative Cases without turbulence) for monitors grouped by distances from the Muja Power Station. The near-field distance group is represented by the Muja Transfer Station monitor, which is located approximately 1 km from the station. The intermediate distance group consists of monitors located between 5 and 9 km from Muja and include; Muja A, B, C, D and CWRF. The far-field distance group includes Muja F, located approximately 14 km to the southwest of Muja. These monitors were selected as the dominant SO<sub>2</sub> source is the Muja Power Station, which allows for a “cleaner” evaluation rather than needing to account for multiple sources as varying distances.

One important finding from this distance-from-source analysis is, as expected, that the concentration decreases as the distance from the source increases for both monitored and predicted concentrations. A second finding is that the analysis suggests that AERMOD is under-predicting at closer distances from the source and trending to over-prediction at the far-field (i.e., Muja F). This is the case for the maximum and 5<sup>th</sup> highest values, but for the 10<sup>th</sup> highest value, the model and observations in the near-field appear to be almost identical. AERMOD under-predictions at the closer distances need further attention, with some future sensitivity analyses planned for roughness length variations and the meander fraction used in AERMOD.

An additional finding is that when the monitors around Muja Power Station are grouped by distance and the ratio of the predicted-to-observed RHC is calculated, the result suggests that AERMOD handles the concentrations in the intermediate range relatively well, within about 20-25%, as shown in Table 3. Figure 9 illustrates this using a scatter plot. These percentages fall within the typical mean biases of air quality models (20 to 40%) as suggested by Hanna<sup>5</sup>.

## **SUMMARY AND CONCLUSIONS**

AECOM has conducted a preliminary review of 6 months of meteorological, emissions, and SO<sub>2</sub> monitoring data in order to develop a reliable site-specific dispersion model for the Collie Airshed in Western Australia. This preliminary study provides an assessment of a candidate dispersion model, AERMOD, for use in the Collie Airshed management.

Two meteorological datasets (Base and an Alternative Case) were prepared and evaluated using AERMOD on the 6-months of Collie Airshed data. The Base Case estimated the sensible heat flux and convective mixing height through the use of measured net radiation, daily-averaged Bowen ratios (derived from measured sensible and latent heat flux data), and cloud cover data. The Alternative Case used AERMET to predict the measured sensible heat flux by modifying the input of net radiation and holding the Bowen ratio constant. In both cases, the initial modeling runs excluded the use of turbulence data. The results of this initial modeling indicated that the Base Case meteorological dataset appeared to perform slightly better than the Alternative Case. Further evaluations included testing these datasets with available turbulence data from the tall tower and using AERMOD’s low wind option (“LOW\_WIND”). Two clear frontrunners emerged based on these analyses, the sigma-theta and sigma-theta using LOW\_WIND from the Base Case meteorological dataset.

**Figure 6: Maximum 1-hour Model Concentrations vs. Distance from Muja Power Station**

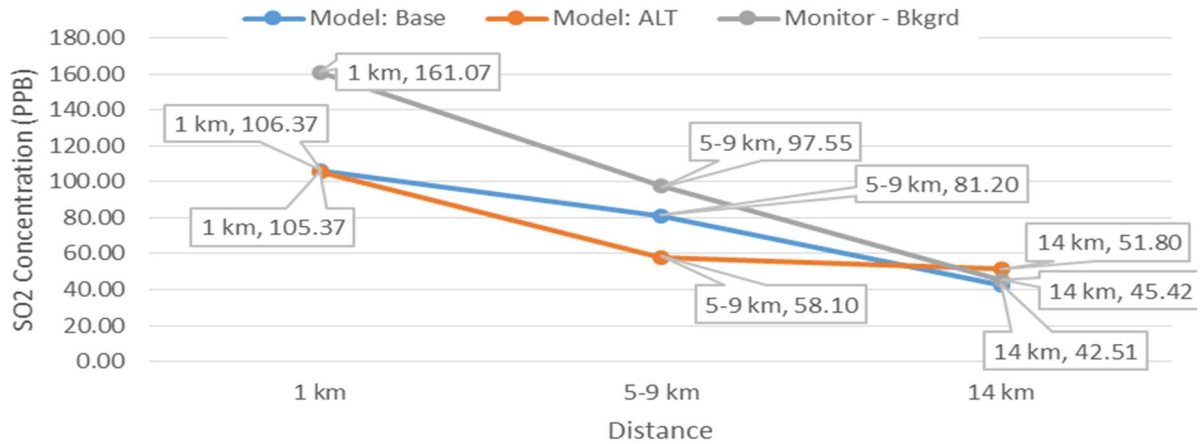


**Figure 7: 5th Highest 1-hour Model Concentrations vs. Distance from Muja Power Station**

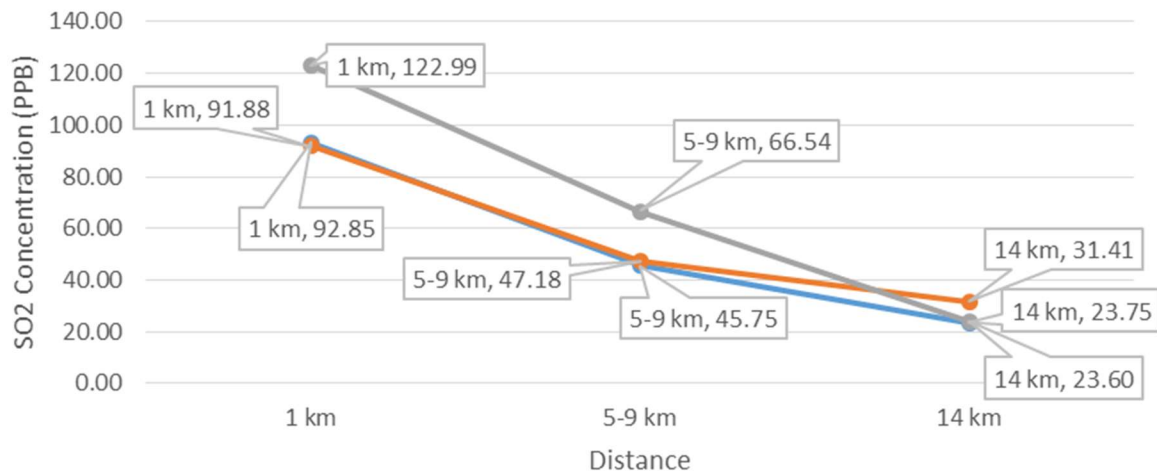


**Figure 8: 10th Highest 1-hour Model Concentrations Compared to Distance from Muja Power Station**

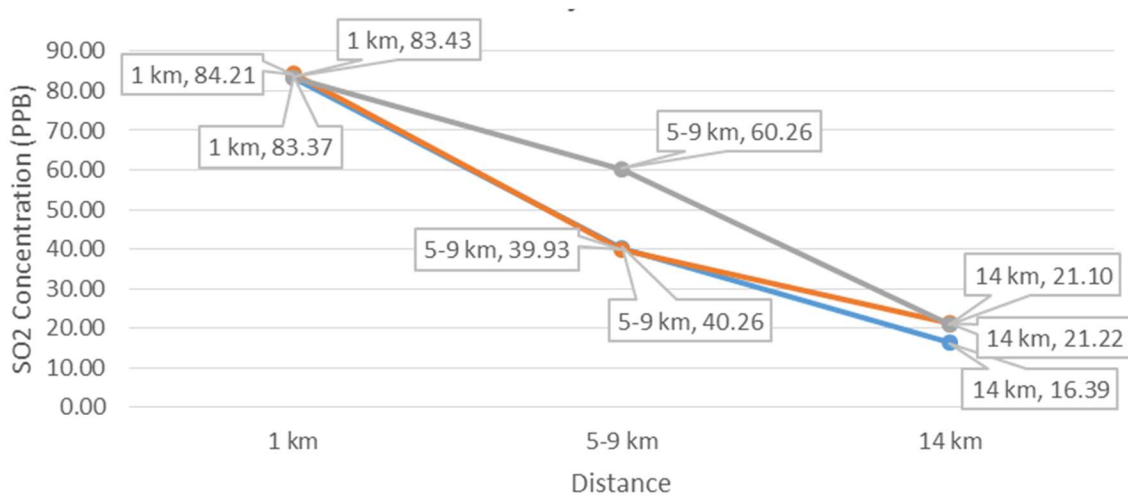
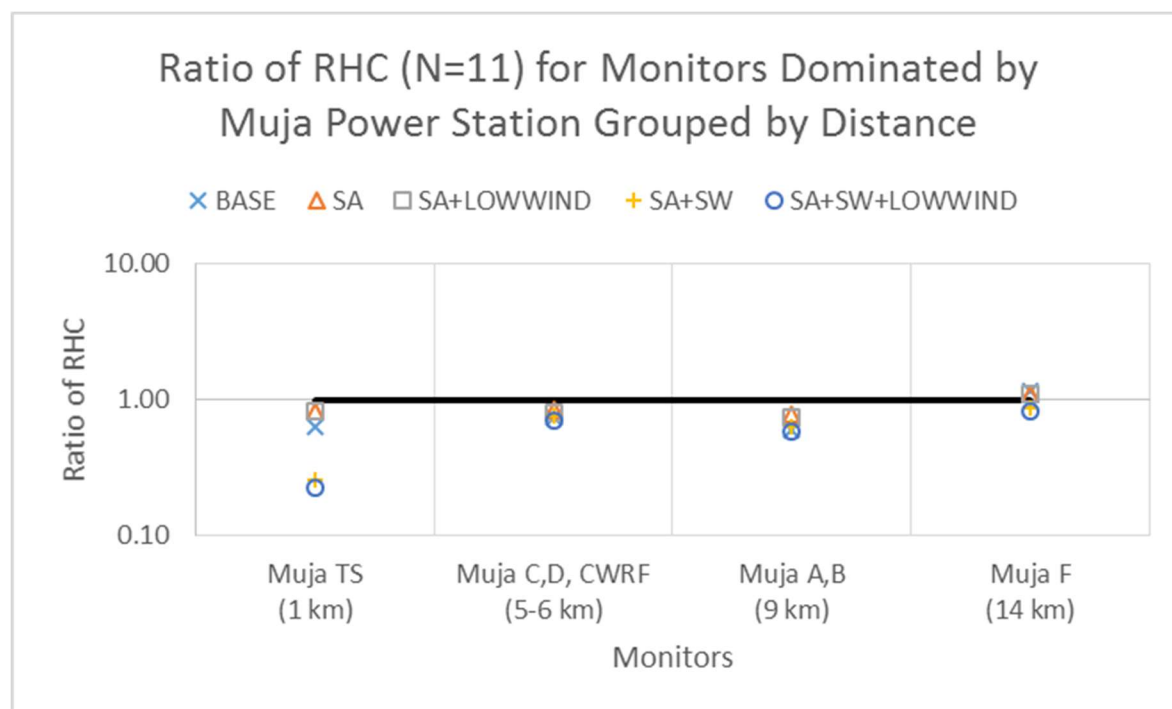


**Table 3: Ratio of the Robust Highest Concentration (RHC) for N=10 Using Base Case Meteorological Dataset by Monitors Grouped by Distance from Muja Power Station**

Model Run	Muja TS (1 km)	Muja C,D, CWRP (5-6 km)	Muja A,B (9 km)	Muja F (14 km)
BASE	0.63	0.74	0.60	1.17
SA	0.82	0.85	0.78	1.12
SA+LOWWIND	0.82	0.80	0.74	1.10
SA+SW	0.26	0.76	0.64	0.86
SA+SW+LOWWIND	0.23	0.71	0.59	0.82

Notes: OBS = observations, BASE = Base Case without turbulence, SA = sigma-theta, SA+LOW\_WIND = sigma-theta with LOW\_WIND option, SA+SW = sigma-theta and sigma-w, SA+SW+LOW\_WIND = sigma-theta and sigma-w with LOW\_WIND option.

**Figure 9: Ratio of the Robust Highest Concentration (RHC) for N=10 Using Base Case Meteorological Dataset by Monitors Grouped by Distance from Muja Power Station**



One area that appears to be a consistent feature from earlier AERMOD evaluations is that the peak concentrations predicted by AERMOD occur earlier in the daytime period than the peak observed concentrations (also in the daytime). This is due, in part, to AERMOD’s “anticipation” that the plume that rises into the stable layer above the convective boundary layer (the “penetrated plume”) eventually mixes down to the ground, but AERMOD predicts this to happen earlier than it actually does. The observed peak concentrations are delayed until the time (in an

event typically lasting about an hour) when the convective mixing layer actually intercepts the penetrated plume and mixes it to the ground.

More work is needed to fully diagnose and correct this AERMOD model behavior, but one area of scrutiny is the parameterization of the penetrated plume vertical spreading (sigma-z). Note that AERMOD simulates three plume components in convective conditions: the “direct” plume that reaches the ground in a convective downdraft, the “indirect” plume that reaches the top of the boundary layer in a convective updraft, and the “penetrated plume” that has sufficient buoyancy to reach the stable layer aloft (or gets directly injected into that layer if the stack height is higher than the convective mixing height). AERMOD’s formulation computes a vertically-integrated value of parameters such as sigma-w between the plume centerline and the receptor at the ground, even for the penetrated plume component. However, this calculation will substantially overstate the vertical plume growth if the actual plume behavior shows it not escaping from the stable layer aloft (and this has been observed in Bull Run lidar data<sup>6</sup>), while AERMOD presumes that the plume spreads to the ground. Once the vertical integration involves a significant depth within the convective boundary layer, the plume spreading will be greatly exaggerated due to the large turbulent eddies in the convective boundary layer. The plume spreading for the penetrated plume all the way to the ground is only appropriate for the hour when the convective mixing height rises to overtake the plume. Otherwise, the computation of the effective turbulence values for the penetrated plume should be limited to a layer that is smaller, such as to the top of the convective mixed layer until that layer rises to overtake the plume and mix it to the ground. This altered treatment would mix the penetrated plume all the way to the ground just for the hour during which the convective mixing height starts below the plume level and then rises to a level above it for the next hour.

Treatment of the penetrated plume issue is currently a “second tier” area for AERMOD development. It should be elevated to a first-tier status and be given a higher priority for being addressed.

There are a few caveats and limitations with the dataset tested so far:

- Only 6 months of data have been tested, with limitations in SODAR data and the inability to utilize the Scintec SODAR and RASS dataset;
- the maximum detection range for the SODAR and RASS instruments are nearly always too low (SODAR range 600-800 meters) to capture the top of the boundary layer (typically 800-1,200 meters from balloon launch data) (even with recent improvements at the Consortium SODAR site);
- the evolution of the inversion breakup and effects on plume transport (including fumigation) are not well captured with current upper-air data collection (i.e., a single near sunrise weather balloon launch), and the AERMOD model treatment needs improvement;
- AERMOD under-predictions at the intermediate distances need further attention, with some sensitivity analyses planned for roughness length length variations and the meander fraction used in the model.

## ACKNOWLEDGEMENTS

The Collie Airshed Study is funded by a consortium of Synergy, Bluewaters Power, and South 32 Worsley Alumina Pty Ltd with support from the WA Department of Water and Environmental Regulations. The authors greatly appreciate the support and access to this study.

## REFERENCES

1. U. S. Environmental Protection Agency, 2018. AERMOD modeling system. Available at [http://www.epa.gov/ttn/scram/dispersion\\_prefrec.htm#aermod](http://www.epa.gov/ttn/scram/dispersion_prefrec.htm#aermod).
2. Warren, C., R. Paine, and J. Connors, 2019. Performance Evaluation of AERMET's Convective Mixing Height Estimation Procedure. Paper #MO16, presented at the Air & Waste Management Association Specialty Conference (Guideline on Air Quality Models: Planning Ahead), March 19-21, 2019, Durham, NC.
3. Australian Government Department of the Environment and Energy, 2005. National standards for criteria air pollutants in Australia. <http://www.environment.gov.au/protection/publications/factsheet-national-standards-criteria-air-pollutants-australia>.
4. Cox, W.M. and J.A. Tikvart, 1990. A statistical procedure for determining the best performing air quality simulation model. *Atm. Env.*, 24A(9): 2387–2395.
5. Hanna, S. R., 1991. Uncertainties in Air Quality Model Predictions, 1993. *Boundary-Layer Meteorology*, 62(1):3-20.
6. Paine, R., J. Connors, and C. Warren, 2019. Peak Observed and AERMOD-Predicted SO<sub>2</sub> Concentrations and AERMOD's Skill in Simulating These Events. Paper #593805, presented at 112<sup>th</sup> Annual Conference and Exhibition of the Air & Waste Management Association, Québec City, Québec, Canada. June 25-28, 2019.

## **ATTACHMENT 2**

**MODELING PROTOCOL FOR ALTERNATIVE MODEL APPROVAL DEMONSTRATION  
FOR THE RUSK-PANOLA ATTAINMENT DEMONSTRATION STATE  
IMPLEMENTATION PLAN REVISION FOR THE 2010 SULFUR DIOXIDE (SO<sub>2</sub>)  
NATIONAL AMBIENT AIR QUALITY STANDARD**

Prepared for:

Texas Commission on Environmental Quality  
12100 Park 35 Circle MC 164  
Austin, TX 78753

Prepared by:

Ramboll US Corporation  
19020 33<sup>rd</sup> Ave W, Suite 580  
Lynnwood, WA, 98036

May 18, 2021

**MODELING PROTOCOL FOR ALTERNATIVE MODEL APPROVAL  
DEMONSTRATION FOR THE ATTAINMENT DEMONSTRATION STATE  
IMPLEMENTATION PLAN REVISION FOR THE 2010 SULFUR DIOXIDE (SO<sub>2</sub>)  
NATIONAL AMBIENT AIR QUALITY STANDARD**

PREPARED UNDER A CONTRACT FROM THE  
TEXAS COMMISSION ON ENVIRONMENTAL QUALITY

*The preparation of this document was financed through a contract from the State of Texas through the Texas Commission on Environmental Quality.*

*The content, findings, opinions and conclusions are the work of the author(s) and do not necessarily represent findings, opinions or conclusions of the TCEQ.*

## CONTENTS

Contents	2
<b>1. Introduction</b>	<b>3</b>
<b>2. Dispersion Model Setup</b>	<b>5</b>
2.1 Source Parameters and Emissions	5
2.2 Meteorology	5
2.3 Terrain Data and Receptor Grid	8
2.4 Onsite Structures and Building Downwash Effects	9
2.5 Modeling Procedures	11
<b>3. Graphical Evaluation</b>	<b>11</b>
<b>4. Cox-Tikvart Analysis</b>	<b>11</b>
4.1 Screening Test	11
4.2 Statistical Test	12
4.3 Cox-Tikvart Scenario Description	14
<b>5. Comparison to EPA Model Evaluations</b>	<b>14</b>
<b>6. References</b>	<b>17</b>

## 1. Introduction

Portions of Rusk and Panola Counties in Texas have been designated as a nonattainment area<sup>1</sup> (NAA) for the 2010 sulfur dioxide (SO<sub>2</sub>) National Ambient Air Quality Standard (NAAQS). The Martin Lake Electric Plant (referred to as Martin Lake Generating Facility), owned and operated by Vistra Energy Corporation (referred to as Vistra), is the primary source of SO<sub>2</sub> emissions in the Rusk-Panola NAA.

Initial dispersion modeling performed by Vistra's consultant AECOM using AERMOD version 19191 showed that AERMOD is conservative, and overpredicts strongly compared to SO<sub>2</sub> observations. AECOM has identified a detail in AERMOD's formulation related to its treatment of penetrated plumes as contributing to overpredictions in certain conditions, and suggested the use of an alternative formulation of AERMOD to better characterize dispersion when penetrated plumes are present.

Weil et al., (1997) first suggested the alternate formulation, the Highly-buoyant Plume Model (HIPMOD), for the treatment of penetrated plumes and more fully described it in Weil (2020) and Paine et al. (2020). The term "HIPMOD" as used by Weil et al., (1997) and Weil (2020) refers to a model formulation that adds important features that are not present in AERMOD. However, the computer code supplied by AECOM does not include all features described by Weil. The alternative model provided by AECOM refers to a variant of AERMOD that only has a different treatment of the penetrated plume component and is referred to as AERMOD-HBP.

The Texas Commission on Environmental Quality (TCEQ) contracted with Ramboll US Consulting, Inc. (Ramboll) to evaluate the model performance of AERMOD and AERMOD-HBP. The goal of the evaluation is to determine if an alternate model approval (AMA) demonstration can be made for the use of AERMOD-HBP under section 3.2 of Appendix W<sup>2</sup>, *Guideline on Air Quality Models*, for use in the attainment demonstration state implementation plan (SIP) revision for the Rusk-Panola NAA.

This document describes the proposed model set up and evaluation procedures that will be applied to determine if AERMOD-HBP could be used for the attainment demonstration modeling required for the Rusk-Panola NAA SIP revision. The evaluation follows established statistical procedures described in *Protocol for Determining the Best Performing Model* (EPA, 1992).

Model evaluation will be performed based on SO<sub>2</sub> concentrations observed at two monitoring stations, Tatum CR 2181d Martin Creek Lake (referred to as Martin Creek) and Longview. The location of each monitor relative to the Martin Lake Generating facility is shown in **Figure 1-1**, and given in **Table 1-1**.

<sup>1</sup> [https://www3.epa.gov/airquality/greenbook/tnp.html#SO2.2010.Rusk\\_Panola\\_Cos](https://www3.epa.gov/airquality/greenbook/tnp.html#SO2.2010.Rusk_Panola_Cos)

<sup>2</sup> [https://www.epa.gov/sites/production/files/2020-09/documents/appw\\_17.pdf](https://www.epa.gov/sites/production/files/2020-09/documents/appw_17.pdf)

**Table 1-1. Coordinates of Martin Lake Generating Facility, and Longview and Martin Creek SO<sub>2</sub> Monitors**

Location	AQS Code	UTM Easting (m, Zone 15)	UTM Northing (m, Zone 15)	Bearing to Martin Lake Generating Facility (deg)	Distance to Martin Lake Generating Facility (km)
Martin Lake Generating Facility	-	352004	3570225	-	-
Martin Creek Monitor	484011082	352066	3572325	179°	2
Longview Monitor	481830001	338968	3583699	135°	19



**Figure 1-1. Location of Martin Lake Generating Facility, and Longview and Martin Creek SO<sub>2</sub> Monitors**

## 2. Dispersion Model Setup

This section describes the model setup that will be used to run AERMOD-HBP and AERMOD.

### 2.1 Source Parameters and Emissions

For the performance comparison, the TCEQ proposes to run both AERMOD and AERMOD-HBP with sources at the Martin Lake Generating Facility. Variable hourly actual emission rates, stack exhaust temperatures, and stack exit gas velocities were provided by Vistra on 25 January, 2021. Emission rates and stack parameters were based on 40 CFR Part 75 monitoring.

The Martin Lake Generating Facility contains three primary stacks that account for the bulk of SO<sub>2</sub> emissions. These sources were included in the models as point sources, with the locations provided in **Table 2-1**. Also provided are the elevation, height, and diameter of each stack. The location of each source is shown in **Figure 2-3**.

**Table 2-1. Martin Lake Generating Facility Stack Locations and Source Parameters**

Source ID	UTM Easting (m, Zone 15)	UTM Northing (m, Zone 15)	Elevation (m)	Stack Height (m)	Stack Diameter (m)
S1	351999	3570400	95.0	137.8	7.0
S2	352041	3570309	95.0	137.8	7.0
S3	352084	3570217	95.0	137.8	7.0

### 2.2 Meteorology

Meteorological input files created by TCEQ will be used for the evaluation. The meteorological data set was created by the TCEQ spanning the period of 2016 to 2020. Surface data was obtained from the National Weather Service (NWS) station at the East Texas Regional Airport (KGGG), located 19 km northwest of the Martin Lake Generating Facility, and collocated with the Longview monitor. Despite the 19 km distance, KGGG should be representative of conditions at the Martin Lake Generating Facility, due to the relatively flat surrounding terrain. To complete the five-year data set, regional data for 2016-2020 were downloaded for the NWS upper air station located at the Shreveport, Louisiana Regional Airport.

AERSURFACE (Version 20060) was used to develop surface characteristics for KGGG. NLCD 2016 TIFs of landuse, percent impervious, and tree canopy coverage for eastern Texas were used according to the updated guidance in the latest AERSURFACE User's Guide<sup>3</sup>.

<sup>3</sup> [https://gaftp.epa.gov/Air/aqmg/SCRAM/models/related/aersurface/aersurface\\_uq\\_v20060.pdf](https://gaftp.epa.gov/Air/aqmg/SCRAM/models/related/aersurface/aersurface_uq_v20060.pdf)

AERMET (Version 19191) was used with regulatory default options to process surface data, landuse outputs from AERSURFACE, and the NWS upper air data. No onsite meteorological data was available for inclusion in AERMET. In the absence of on-site differential temperature measurements, the default Holtslag method was used for the stable boundary layer. The Adjust U\* option was included to adjust friction velocities during low wind speed hours.

A wind rose showing the distribution of wind speeds and directions for the resulting 5-year data set is shown in **Figure 2-1**. The mean wind speed during the 5-year period was calculated to be 3.5 m/s. Winds are predominantly southerly, with few hours from the west. There are sufficient hours in the dataset with winds blowing towards the Martin Creek and Longview monitors to achieve statistically significant results.

The same AERMET-produced SFC and PFL files will be used to run both AERMOD and AERMOD-HBP. The models will be run separately for each monitor for the duration of available SO<sub>2</sub> concentration data; 2016 – 2020 at Longview, and 2018 – 2020 at Martin Creek.

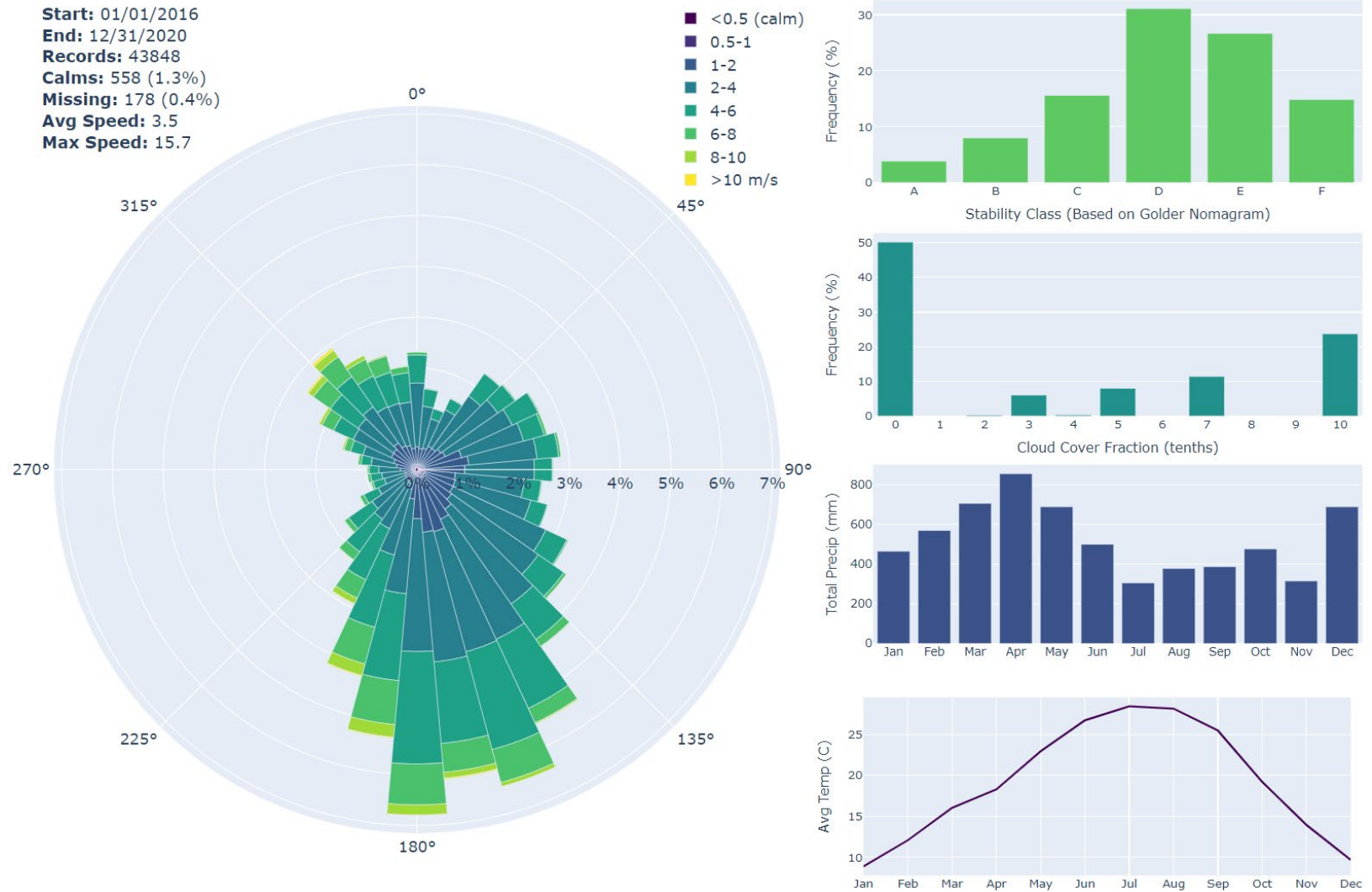


**Figure 2-1. Wind Rose and Meteorological Values for KGGG 2016 - 2020**

### 2.3 Terrain Data and Receptor Grid

The evaluation of AERMOD-HBP and AERMOD will be done by placing a receptor at the location of the Martin Creek and Longview monitors. In addition, to account for known uncertainties in replicating spatiotemporal patterns in dispersion models, and to allow for more in-depth analyses, a “microgrid” of receptors was created. This grid was selected to span a 2° arc downwind from the Martin Lake Generating Facility to each monitor. **Figure 2-2** shows the microgrids at the Longview and Martin Creek monitors.

The 2° arc was selected to account for errors in wind direction measurements. As an example, the Gill WindSonic Anemometer User’s Manual<sup>4</sup> lists an accuracy in wind direction readings of  $\pm 2^\circ$ . At a downwind distance of 19 km (the distance of the Longview monitor from the Martin Lake generating facility), a 2° difference in wind direction translates to a 650 m difference in location of the maximum.

The spacing of the receptors is as follows:

- Longview
  - 30 degree spacing for radius of 20 m;
  - 24 degree spacing for radius of 60 m; and
  - 15 degree spacing for radii of 150 m, 250 m, and 500 m.
- Martin Creek
  - 30 degree spacing for radius of 20 m; and
  - 15 degree spacing for radius of 60 m.

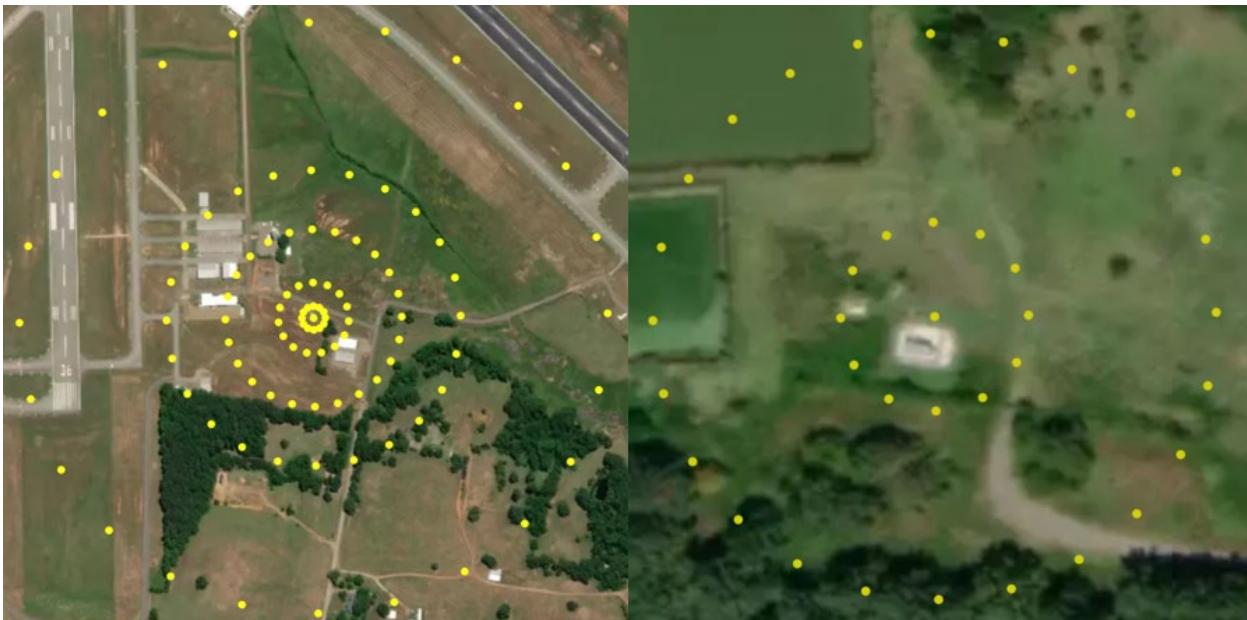


**Figure 2-2. “Microgrid” centered on the Longview (left) and Martin Creek (right) Monitors**

<sup>4</sup> <http://gillinstruments.com/data/manuals/windsonic-manual.pdf?iss=22.20151201>

Receptor heights were processed using the AERMAP terrain processor (Version 18081) with elevation data from the National Elevation Dataset (NED), developed by the United States Geological Survey (USGS). The same receptor grid will be used to run both AERMOD and AERMOD-HBP.

## 2.4 Onsite Structures and Building Downwash Effects

Potential downwash effects on emissions plumes will be accounted for in the model by using building dimensions and locations (locations of building corners, base elevation, and building heights). Dimensions and orientation of onsite structures, as shown in **Figure 2-3**, will be input to the Building Profile Input Program for the Plume Rise Model Enhancements (BPIP-PRIME) v04274 program to calculate direction-specific dimensions and Good Engineering Practice (GEP) stack height information for input to AERMOD. A listing of the onsite structures to be included in the analysis, along with their heights above grade, base elevation, and the number of tiers included is provided in **Table 2-2**.

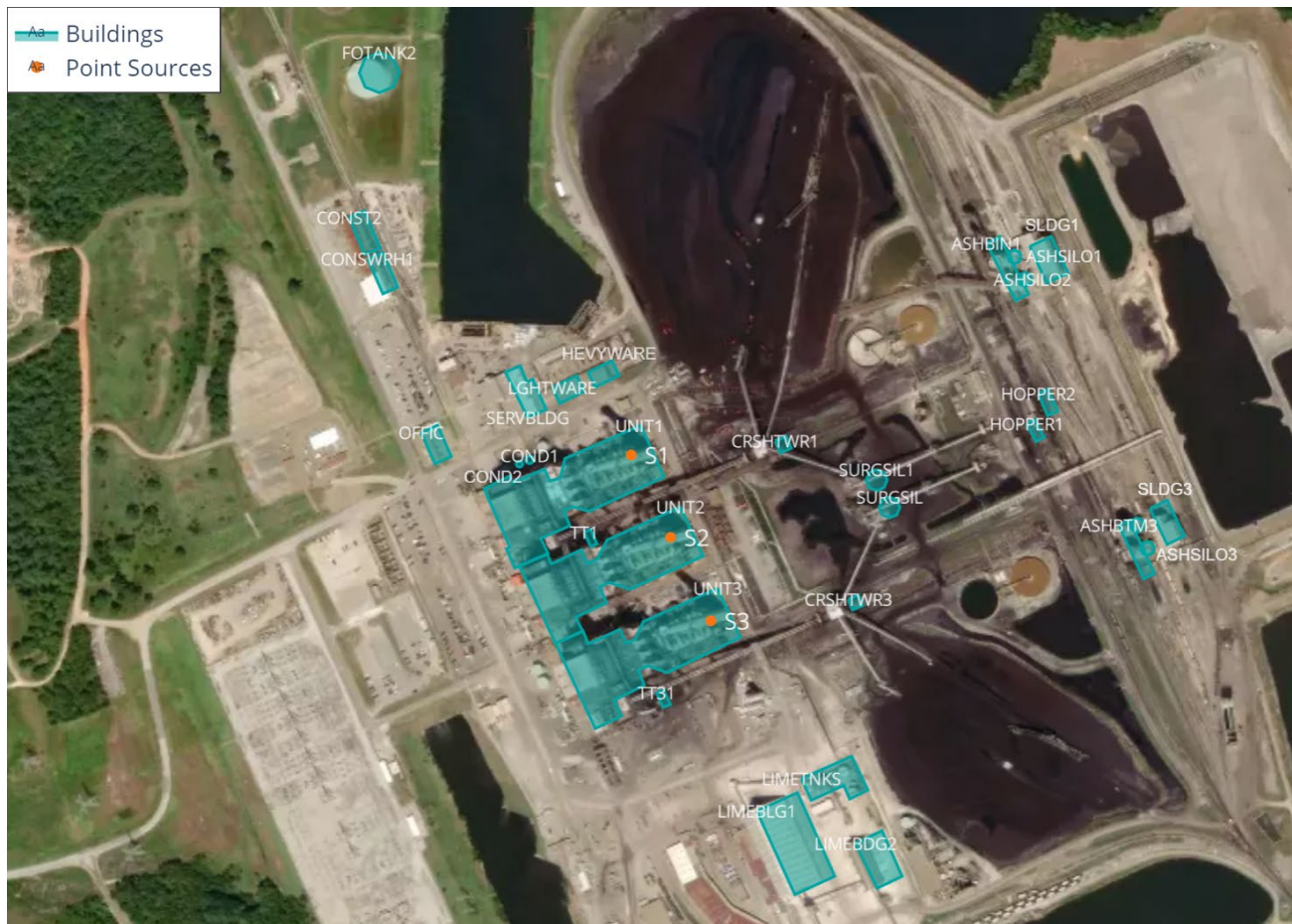


**Figure 2-3. Martin Lake Generating Facility Source and Building Layout**

**Table 2-2. Martin Lake Generating Facility Building Parameters**

<b>Building ID</b>	<b>Elevation (m)</b>	<b>Height (m)</b>	<b>Number of Tiers</b>
UNIT1	95.11	78.64 <sup>5</sup>	8
UNIT2	95.11	78.64 <sup>5</sup>	8
UNIT3	94.63	78.64 <sup>5</sup>	8
TT1	95.04	60.96	1
CRSHTWR3	95.09	31.70	1
SURGSIL1	93.64	44.20	1
SURGSIL	91.29	44.20	1
ASHBIN1	94.46	24.38	1
ASHSILO1	94.45	42.67	1
ASHSILO2	94.45	42.67	1
SLDG1	94.71	18.29	1
ASHBTM3	96.16	24.38	1
ASHSILO3	96.47	42.67	1
ASHSILO4	96.47	42.67	1
SLDG3	96.90	18.29	1
LIMEBLG1	95.47	15.24	1
LIMEBDG2	97.36	6.10	1
LIMETNKS	96.10	6.10	1
FOTANK1	96.70	6.10	1
FOTANK2	96.21	12.19	1
LGHTWARE	94.86	6.10	1
HEVYWARE	94.61	6.10	1
SERVBLDG	95.34	6.10	1
OFFIC	96.60	6.10	1
CONSWRH1	96.16	6.10	1
CONST2	96.50	6.10	1
COND1	95.74	12.19	1
COND2	95.84	12.19	1
HOPPER1	91.47	6.10	1
HOPPER2	91.05	6.10	1
TT31	95.07	60.96	1

<sup>5</sup> Height of highest tier

## **2.5 Modeling Procedures**

AERMOD and AERMOD-HBP will be run to produce hourly post files using the input data described above. These files produce an hourly time series of concentrations at each modeled receptor. All statistical calculations and inputs to further analyses will be performed using these hourly post files – no statistical calculations will be performed by the models.

## **3. Graphical Evaluation**

While AERMOD and AERMOD-HBP share much of the same formulation, there are key situations in which they produce different concentrations. Dispersion in AERMOD-HBP is treated differently than AERMOD only when using the convective boundary layer. Therefore, concentrations only differ for those hours where the mixed layer height is between the bottom of the plume and the center of the plume. Both models are expected to produce identical results during stable (night-time) conditions; for hours when the entire plume is above the mixed layer (i.e., when the mixed layer height is shallow, early in the morning); and for those hours where the mixed layer height exceeds the plume height (i.e., when mixed layer is high, late in the day).

To ensure differences between the two models are as expected, daily trends in concentrations will be compared using plots of concentration grouped by hour of the day at Longview and Martin Creek monitors. Plots will be created for 90<sup>th</sup>, 95<sup>th</sup>, 99<sup>th</sup>, and 100<sup>th</sup> percentile concentrations.

Plots will compare observed and modeled (AERMOD and AERMOD-HBP) concentrations over the date of the n<sup>th</sup> percentile observed values, as well as modeled concentrations during nth-percentile days. This means that daily concentration trends will be compared based on the statistic (e.g. 95<sup>th</sup> percentile daily max value) in addition to presenting comparisons paired in time. Since AERMOD and AERMOD-HBP are statistical models, they do not excel at pairing concentrations in space and time, but do a good job of replicating the statistical distribution of observed concentrations datasets. Statistics are what should be compared between observations and predictions.

To further understand model performance across the distribution of observed and modeled values unpaired in time, quantile-quantile (QQ) plots that compare ranked hourly concentrations, with observations along the X axis, and model predictions along the Y axis will be created for the Longview and Martin Creek monitors by year.

## **4. Cox-Tikvart Analysis**

As described in 3.2.2(d) of Appendix W, for alternate model approvals established statistical performance evaluation procedures should be used. The Cox-Tikvart method (EPA, 1992) has been used extensively for evaluating models. For the AERMOD-HBP evaluation, the Cox-Tikvart method was used to compare the model performance of AERMOD and AERMOD-HBP at the Martin Creek and Longview monitors.

### **4.1 Screening Test**

As an initial screening step, the fractional bias of the average and standard deviation is used as a metric. For each station (Longview and Martin Creek) the SO<sub>2</sub> concentrations will be pooled by year and sorted by

averaging period. From this data, the 25 highest observed concentrations unpaired in space or time, are used to calculate a mean and standard deviation. The same procedure is applied to the predicted concentrations obtained from the air dispersion models AERMOD and AERMOD-HBP, using the highest value over the receptor sets for each hour. Using these top 25 values, the fractional bias of the average and of the standard deviation are determined for each model for 1-hour, 3-hour and 24-hour averages. Fractional bias is calculated using Equation 1.

$$FB = 2 \cdot \frac{(Mean_{OBS} - Mean_{PRD})}{(Mean_{OBS} + Mean_{PRD})} \quad (1)$$

It is important to note that the above equation will result in a *negative* bias when the model *overpredicts*, and a *positive* bias when the model *underpredicts*. A positively biased standard deviation indicates that there is less variance in the top 25 predicted values compared to observations.

Fractional biases will be calculated for 1-hour, 3-hour and 24-hour averaged concentrations. If fractional biases for most periods, years, and sites are within a factor of two (0.5 – 2), the model demonstrates adequate performance to proceed to more in-depth analyses.

## 4.2 Statistical Test

If AERMOD-HBP and AERMOD pass the screening test they will be subjected to a more comprehensive statistical comparison. The performance of AERMOD will be compared with the performance of AERMOD-HBP using a composite statistical measure that combines the performance of the scientific component (1-hour averages) and the operational component (3-hour and 24-hour averages).

The scientific component assesses the 1-hr averages during 6 specific meteorological conditions. The meteorological conditions are unique combinations of unstable (class A, B, C), neutral (class D), or stable (class E, F) conditions and wind speeds above or below 3 m/s. The 50<sup>th</sup> percentile of observed wind speeds is just over 3 m/s, so this cut-off value sorts the data approximately in half.

The Golder (1972) nomogram method will be used to convert AERMET's Monin-Obukhov length and roughness length to stability class, using Fortran code taken from the Mesoscale Model Interface Program (MMIF<sup>6</sup>).

The robust highest concentration (RHC) is a comparison of modeled and observed concentrations at the upper end of a frequency distribution and is calculated using Equation 2 where  $n=26$ ,  $c_n$  is the  $n^{\text{th}}$  highest concentration and  $\bar{c}$  is the average of the  $(n-1)$  highest concentrations.

$$RHC = c_n + (\bar{c} - c_n) \ln\left(\frac{3n-1}{2}\right) \quad (2)$$

<sup>6</sup> See <https://www.epa.gov/scram/air-quality-dispersion-modeling-related-model-support-programs#mmif>

For each meteorological condition, the RHC is calculated for both the observed and modeled dataset and the fractional bias (FB) and absolute fractional bias (AFB) between the modeled and measured RHC are calculated using Equation 3 and Equation 4, respectively.

$$FB = 2 \cdot \frac{(RHC_{measured} - RHC_{modeled})}{(RHC_{measured} + RHC_{modeled})} \quad (3)$$

$$AFB = \left| 2 \cdot \frac{(RHC_{measured} - RHC_{modeled})}{(RHC_{measured} + RHC_{modeled})} \right| \quad (4)$$

The operational component evaluates the peak 3-hour and 24-hour averages independent of meteorology or spatial location. The absolute fractional bias between measured and modeled RHC is calculated in a similar manner, except that the data is grouped into 3-hour and 24-hour averages, respectively.

A composite performance metric (CPM) combines the 1-hr, 3-hr, and 24-hr absolute fractional biases in RHC for both the scientific and operational components, as shown in Equation 5.

$$CPM = \frac{(average(AFB(i,j)) + AFB(3) + AFB(24))}{3} \quad (5)$$

where AFB(i,j) is the absolute fractional bias for each meteorological condition and each station, AFB(3) is the absolute fractional bias for 3-hour averages, and AFB(24) is the absolute fractional bias for 24-hour averages.

The CPM is lowest when there is a good agreement between measured and modeled RHC values. Comparing the magnitudes of the CPM values from different models using the same observational data quantizes performance of each dispersion model.

To improve the robustness of data used for model comparison, a statistical technique known as bootstrapping will be used to generate a probability distribution of outcomes. The bootstrap method resamples the available data into three-day blocks. These blocks are grouped by season (regardless of year), then sampled with replacement until a full season of data is created. After 1,000 iterations of this process, the standard deviation of generated runs is used as the standard error for model comparison. The Python script used to run the bootstrap analysis is available upon request.

To highlight differences between models, and to determine which model performs better, the Model Comparison Measure (MCM) is used. This is simply the difference in CPM between two models, as described by Equation 6.

$$MCM = CPM(a) - CPM(b) \quad (6)$$

A positive MCM indicates better performance from model b than model a, and vice-versa.

### 4.3 Cox-Tikvart Scenario Description

To provide deeper insights into differences between the models, the Cox-Tikvart method will be performed for three scenarios:

1. **Standard Methodology** - One modeled receptor placed at the location of the monitor, with concentrations from both sites pooled.
2. **Single Receptor** - One modeled receptor placed at the location of the monitor, with concentrations from each site treated separately.
3. **2° Microgrid** - Max hourly concentrations from a microgrid of modeled receptors centered on the monitor, with concentrations from each site treated separately.

Option 1 is consistent with the standard Cox-Tikvart methodology (EPA, 1992). However, options 2 and 3 will provide more insights into the differences between the dispersion models and as an assessment of their use for regulatory purposes.

Since the RHC is calculated using the top 25 values, and concentrations at a receptor 2 km downwind will generally be much higher than those at 19 km, if sites are pooled, RHC values will be dominated by near-field concentrations. Evaluating each site independently will highlight model performance at a range of distances.

Evaluating model performance at a single receptor is not representative of regulatory use cases for dispersion models – they are almost always run with a grid of receptors covering the entire modeling domain. Using the maximum across a grid of receptors will allow for comparison during hours when errors in wind direction readings might cause a plume to “miss” a receptor. The use of a 2° microgrid – derived from the error range of modern wind sensors is proposed.

## 5. Comparison to EPA Model Evaluations

To contextualize the Cox-Tikvart results of the comparison of AERMOD-HBP and AERMOD an examination of EPA’s Model Evaluation Databases<sup>7</sup> and their discussion in EPA’s 2003 paper “*AERMOD: Latest Features and Evaluation Results*”<sup>8</sup> is proposed. EPA’s 2003 paper primarily evaluates model performance by examining the ratio of the model-predicted RHC to observed RHC. The various tracer studies were used for model formulation and/or validation. A summary of these studies and their results is provided in **Table 5-1**. This table also summarizes the study duration, whether the model was used for development or independent validation, the distance to the nearest and farthest monitors/receptors, whether the model over or under predicted, and the ratio of the predicted RHC to observed RHC.

<sup>7</sup> See <https://www.epa.gov/scram/air-quality-dispersion-modeling-preferred-and-recommended-models>

<sup>8</sup> See [https://gaftp.epa.gov/Air/aqmg/SCRAM/models/preferred/aermod/aermod\\_mep.pdf](https://gaftp.epa.gov/Air/aqmg/SCRAM/models/preferred/aermod/aermod_mep.pdf) (454-R-03-003)

For the purposes of this study, the independent datasets are the most relevant, as this analysis is independent of any sort of model formulation. While the development studies showed a mix of over and underprediction, all but one of the independent studies resulted in an RHC ratio above 1 (overprediction), (not including the Lee Power Plant Wind Tunnel study under neutral conditions - maximum concentrations generally occur under stable conditions). However, RHC values were calculated using the top 25 values for the entire dataset, irrespective of space and time (like the proposed "Standard Methodology" for this study). These 25 values almost certainly occur at one of the closest receptors. Since many of these studies' closest receptors are around the same range as the distance to the Martin Creek monitor, these results are directly comparable.

The Longview monitor, however, is 19 km from the Martin Lake Generating Facility. The farthest receptor in the Kincaid study was 20 km from the source. However, this study was used for model development. The independent study with receptors farthest from the source, at 15 km, is the Clifty Creek study<sup>9</sup>, which ran for a full year. To observe performance at various distances from the source 1-hour RHC values at each receptor was calculated independently using AERMOD Post files and records of observations. These values are provided in **Table 5-2**.

<sup>9</sup> AERMOD inputs/outputs and observed concentrations from the Clifty Creek study are available for download at [https://gaftp.epa.gov/Air/aqmg/SCRAM/models/preferred/aermod/eval\\_databases/clifty.zip](https://gaftp.epa.gov/Air/aqmg/SCRAM/models/preferred/aermod/eval_databases/clifty.zip)

Table 5-1: Summary of EPA AERMOD Model Evaluation Studies

Name	Duration	Model Development/ Independent	Min Source to Receptor Distance (m)	Max Source to Receptor Distance (m)	1hr or 3hr MOD/OBS RHC Ratio	Under/Over Prediction
Kincaid	2 x 6 weeks	Development	450	20000	0.77	Under
Kincaid	6 months	Development	2000	20000	0.98	Under
Lovett	1 year	Development	2000	3650	1.03	Over
Alaska North Slope Tracer Study	44 hours	Development	17	3399	1.06	Over
Millstone	36 hours	Development	350	1500	0.44	Under
Duane Arnold Energy Center	12 + 16 + 11 hours	Development	300	1000	0.69	Under
Prairie Grass	44 ten-min samples	Development	50	800	0.89	Under
Bowline	1 year	Development/ Independent	250	800	1.14	Over
Clifty Creek	1 year	Independent	3000	15000	1.05	Over
Baldwin	1 year	Independent	1300	10000	1.24	Over
Tracy	128 hours	Independent	3000	10000	1.04	Over
Martins Creek	1 year	Independent	3000	8000	1.12	Over
Indianapolis	700 hours	Independent	300	6000	1.11	Over
Westvaco	1 year	Independent	780	1500	1.06	Over
Lee Power Plant wind tunnel study	78 hours	Independent	450	900	0.51 (neutral) 2.50 (stable)	Under
Experimental Organic Cooler Reactor	22 hours	Independent	800	800	1.72	Over
American Gas Association	63 hours	Independent	200	200	0.92	Under
Westar NO <sub>2</sub>	6 weeks	Not used	55	125	--	--

**Table 5-2. Clifty Creek Model Evaluation RHC Ratios by Receptor**

UTM Easting (m)	UTM Northing (m)	1 Hour Predicted RHC	1 Hour Observed RHC	1 Hour RHC Ratio (Prd/Obs)	Distance from Source (km)
646890	4300090	767	1149	0.67	15.0
641970	4299200	909	1422	0.64	11.6
645150	4287350	987	542	1.82	8.0
643380	4292740	1061	1012	1.05	7.4
638490	4292930	1535	948	1.62	4.5
637570	4285520	1152	892	1.29	3.1

The RHC ratio for the Longview and Martin Creek monitors will be calculated to allow comparison to the Clifty Creek study. If RHC ratios produced by AERMOD-HBP over the Martin Lake modeling domain indicate better performance than those shown in previous EPA studies, it can be said that in this specific use case, AERMOD-HBP meets model performance requirements for regulatory evaluations.

## 6. References

1. Environmental Protection Agency, 1992. Protocol for Determining the Best Performing Model (EPA-454/R-92-025). U.S. Environmental Protection Agency, Research Triangle Park, NC.
2. Golder, 1972. Relations among stability parameters in the surface layer. *Boundary-Layer Meteorology*, 3:56.
3. Gill Instruments Limited, 2015. WindSonic Ultrasonic Anemometer User’s Guide. Available at <http://gillinstruments.com/data/manuals/windsonic-manual.pdf?iss=22.20151201>
4. Weil, J.C., L.A. Corio, and R.P. Brower, 1997: A PDF dispersion model for buoyant plumes in the convective boundary layer. *J. Appl. Meteor.*, 36, 982–1003.
5. Weil, J.C., 2020. New Dispersion Model for Highly-Buoyant Plumes in the Convective Boundary Layer. Preliminary Draft V4.
6. User’s Guide for the Industrial Source Complex (ISC3) Dispersion Models, Volume II – Description of Model Algorithms. USEPA/OAQPS, EPA-454/B-95-003b, September 1995. Available at <https://gaftp.epa.gov/Air/aqmg/SCRAM/models/other/isc3/isc3v2.pdf>
7. Paine, R., C. Szembek, and C. Warren, 2020. Overview of the Highly-buoyant Plume (HIPMOD) Model. October 15, 2020.